MIT-2344-2
MITNE-53

STUDIES OF EPITHERMAL NEUTRONS IN URANIUM, HEAVY WATER LATTICES

by

W. H. D'Ardenne, T. J. Thompson, D. D. Lanning, I. Kaplan

Contract AT(30-1)2344
U. S. ATOMIC ENERGY COMMISSION

August 24, 1964

Department of Nuclear Engineering
Massachusetts Institute of Technology
Cambridge, Massachusetts

MASSACHUSETTS INSTITUTE OF TECHNOLOGY

DEPARTMENT OF NUCLEAR ENGINEERING

Cambridge 39, Massachusetts

STUDIES OF EPITHERMAL NEUTRONS IN URANIUM, HEAVY WATER LATTICES

by

W. H. D'Ardenne, T. J. Thompson, D. D. Lanning, I. Kaplan

August 24, 1964

MIT-2344-2 (MITNE-53)

AEC Research and Development Report

UC-34 Physics

(TID-4500, 31st Edition)

Contract AT(30-1)2344

U. S. Atomic Energy Commission

The contents of this report have been submitted by Mr. Walter H. D'Ardenne to the Massachusetts Institute of Technology in partial fulfillment of the requirements for the degree of Doctor of Philosophy.

ERRATA FOR MITNE-53

Page(s)	Line(s)	Change
4,5,6	9,21,10	(H4) to (H6)
12,15	5,4,7,16	n/cm^2 to n/cm^2 sec
21	Eq. 2.2.15	D_N^{FP} to D_H^{FP}
81	Replace with Fig. 3.2.17 attached	
82	3	"3.2.17 and 3.2.19" to "3.2.15 through 3.2.17"
93	footnote (e)	(H8) to (H1)
119	13	(K4) to (K3)
120	6 from bottom	0.258...0.264 to 0.266...0.274
121	Eq. 5.4.2	Σ_{sc}^{28} to Σ_{sc}^{H}
137	Eq. 6.1.15	in numerator "absorbed" to "captured"
149	11	0.894 to 0.897

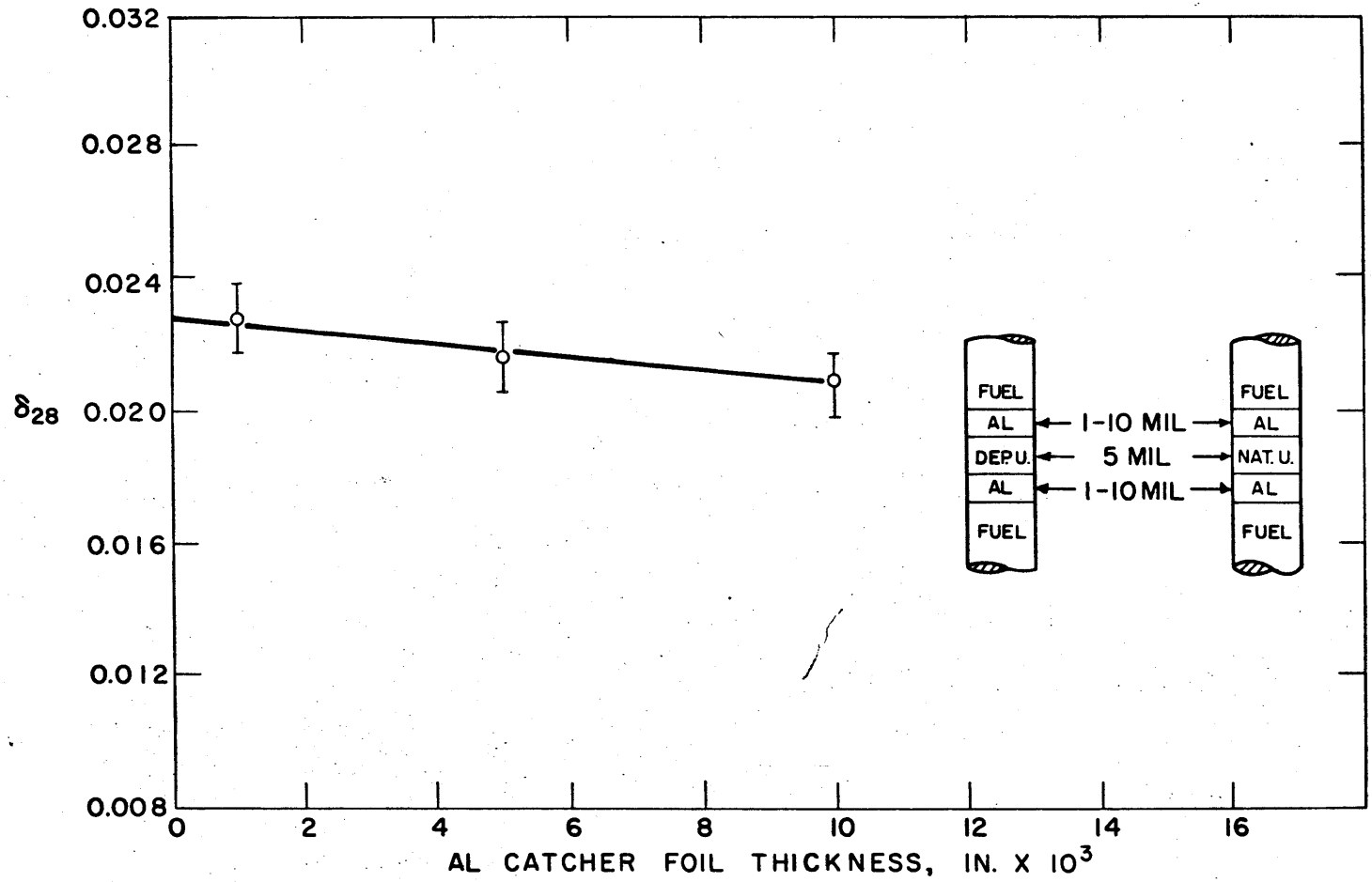

δ_{28} VERSUS ALUMINUM CATCHER FOIL THICKNESS

FIG. 3.2.17

DISTRIBUTION

MIT-2344-2 (MITNE-53)
AEC Research and Development Report
UC - 34 Physics
(TID - 4500, 31st Edition)

1. USAEC, New York Operations Office (D. Richtmann)
2. USAEC, Division of Reactor Development (P. Hemmig)
3. USAEC, New York Patents Office (H. Potter)
4. USAEC, Division of Reactor Development, Reports and Statistics Branch
5. USAEC, Maritime Reactors Branch
6. USAEC, Civilian Reactors Branch
7. USAEC, Army Reactors Branch
8. USAEC, Naval Reactors Branch
9. Advisory Committee on Reactor Physics (E. R. Cohen)
10. ACRP (G. Dessauer)
11. ACRP (D. de Bloisblanc)
12. ACRP (M. Edlund)
13. ACRP (R. Ehrlich)
14. ACRP (I. Kaplan)
15. ACRP (J. Chernick)
16. ACRP (F. C. Maienschein)
17. ACRP (C. R. Avery)
18. ACRP (P. F. Zweifel)
19. ACRP (P. Gast)
20. ACRP (G. Hansen)
21. ACRP (S. Krasik)
22. ACRP (L. W. Nordheim)
23. ACRP (T. M. Snyder)
24. ACRP (J. J. Taylor)
25. - 27. O. T. I. E., Oak Ridge, for Standard Distribution, UC - 34, TID - 4500 (31st Edition)
28. - 49. W. H. D'Ardenne
50. - 100. Internal Distribution

ABSTRACT

Measurements related to reactor physics parameters were made in three heavy water lattices. The three lattices studied consisted of 0.250-inch-diameter, 1.03 w/o U^{235} uranium fuel rods arranged in triangular arrays and spaced at 1.25, 1.75, and 2.50 inches. The following quantities were measured in each of the three lattices studied: the ratio of the average epicadmium U^{238} capture rate in the fuel rod to the average subcadmium U^{238} capture rate in the fuel rod (ρ_{28}); the ratio of the average epicadmium U^{235} fission rate in the fuel rod to the average subcadmium U^{235} fission rate in the fuel rod (δ_{25}); the ratio of the average U^{238} capture rate in the fuel rod to the average U^{235} fission rate in the fuel rod (C^*); the ratio of the average U^{238} fission rate in the fuel rod to the average U^{235} fission rate in the fuel rod (δ_{28}); and the effective resonance integral of U^{238} in a fuel rod (ERI^{28}). The results of an investigation of systematic errors associated with these measurements have led to many changes and adjustments in the experimental techniques and procedure which have improved the general precision of the experimental results.

A new method was developed to measure the ratio C^* which simplified the experiment, significantly reduced the experimental uncertainty associated with the measurement, and avoided systematic errors inherent in the method used to measure C^* in earlier work.

The value of ERI^{28} was also measured by a new method in which the results of measurements made in an epithermal flux which had a 1/E energy dependence are combined with the results of measurements made in a lattice.

The experimental results were combined with theoretical results obtained from the computer programs THERMOS and GAM-I to determine the following reactor physics parameters for each of the three lattices studied: the resonance escape probability, p; the fast fission factor, ϵ; the multiplication factor for an infinite system, k_∞; and the initial conversion ratio, C.

Methods were developed to measure that portion of the activity of a foil which is due to neutron captures in the resonances in the activation cross section of the foil material. The resonance escape probability was determined by a new method, using the resonance activation date, in which the use of cadmium is not necessary.

ACKNOWLEDGMENTS

Many individuals and groups have contributed to the success of the M.I.T. Heavy Water Lattice Project. The results of this report are primarily due to the work of the principal author, Walter Herbert D'Ardenne, who has submitted substantially this same report in partial fulfillment for the requirements of the Ph.D. degree at M.I.T. He has been assisted by other students working on the project as well as by those mentioned specifically below.

Over-all direction of the project and its research is shared by Professors I. Kaplan, T. J. Thompson, and D. D. Lanning. Messrs. Joseph Barch and Albert Supple have been of invaluable assistance in the setting up and performing of experiments. Miss Barbara Kelley has been of assistance in procuring materials, preparing and counting foils, reducing data, and in many other ways.

The staffs of the M.I.T. Reactor, the Reactor Machine Shop, the Reactor Electronics Shop, and the Radiation Protection Office have provided much assistance and advice during the experimental portion of this work. The data reduction was done in part at the M.I.T. Computation Center. Mrs. W. D'Ardenne and Mrs. M. Bosco have given invaluable assistance in the preparation and typing of this report.

Mr. Henry Bliss, who worked closely with the principal author, has also made a significant contribution to the work on which this report is based. He has provided considerable assistance in many phases of this endeavor.

All of these individuals and groups were essential to the completion of this work.

TABLE OF CONTENTS

TABLE OF CONTENTS (continued)

TABLE OF CONTENTS (continued)

LIST OF FIGURES

LIST OF FIGURES (continued)

LIST OF FIGURES (continued)

LIST OF FIGURES (continued)

LIST OF TABLES

LIST OF TABLES (continued)

CHAPTER I
INTRODUCTION

Introduction

The Nuclear Engineering Department of M.I.T. is conducting a research program, the Heavy Water Lattice Project, under the sponsorship of the United States Atomic Energy Commission. The general objective of this project is to carry out experimental and theoretical investigations of the physics of subcritical lattices of partially enriched uranium rods in heavy water. Several reports describing the results of previous investigations associated with this project have been published (B2, H2, H3, H4, M1, M3, P1, P2, S1, W1, W2).

1.1 Area of Interest and General Scope of the Present Work

As a part of the general program of the Lattice Project, the work to be described in this report deals primarily with processes involving neutrons in the epithermal portion of the neutron energy spectrum. A parameter that is often used to serve as an index of the physical properties of a multiplying medium is the multiplication factor, k_∞, for an infinite assembly. The definition of k_∞ is the ratio of the rate at which neutrons are produced to the rate at which neutrons are consumed in an assembly large enough so that the loss of neutrons by leakage is negligible. The value of k_∞ can depend appreciably on the ratio of the number of epithermal neutron processes to the number of thermal neutron processes. The epithermal energy region can be subdivided into the fast energy region and the resonance energy region, each of which is distinguished by particular neutron reactions limited to that region. The fast energy region is characterized by those neutrons whose energies are great enough to cause the fission of U^{238}, and the resonance energy region is characterized by neutron capture in the many resonances in U^{238} absorption cross section. The upper limit of the fast region is

usually taken as 10 Mev, and the lower limit of the fast region is usually set equal to the threshold energy, about 1 Mev, for the U^{238} fission process. The resonance region extends from the lower limit of the fast region to the cadmium-cutoff energy, about 0.4 ev, which is usually chosen as the upper limit of the thermal energy region. Because the neutron energy spectrum can be divided into these few distinctive regions, the analysis of the physics of reactors is often made on the basis of these energy groupings.

In the familiar four-factor expression for k_∞:

$$k_\infty = \eta f \epsilon p , \qquad (1.1.1)$$

the fast fission factor ϵ, if appropriately determined, can account for reactions which occur in the fast region; the resonance escape probability p accounts for neutron captures in the resonance region, and the combination ηf accounts for reactions in the thermal region. The fast fission factor, ϵ, and the resonance escape probability, p, are the factors which are of primary interest in the present work since they characterize the epithermal neutron processes. Another reactor physics parameter which is strongly dependent on the epithermal reaction rates relative to the thermal reaction rates is the initial conversion ratio, C, defined as the ratio of the rate at which Pu^{239} is produced to the rate at which U^{235} is destroyed. The value of k_∞ is closely related to the critical size and mass of a thermal reactor, and the value of C is related to the lifetime of the fuel.

1.2 Experimental Methods

None of the parameters, k_∞, p, ϵ, and C, which are sensitive to the epithermal reactions, can be measured directly, but they can be related to quantities which are measurable. The measurable quantities to be considered here are: the ratio of the epicadmium U^{238} capture rate to the subcadmium U^{238} capture rate, ρ_{28}; the ratio of the U^{238} fission rate to the U^{235} fission rate, δ_{28}; the ratio of the epicadmium U^{235} fission rate to the subcadmium U^{235} fission rate, δ_{25}; and the ratio of the total U^{238} capture rate to the U^{235} fission rate, C^*. The fast fission factor, ϵ, can be related to the fast fission ratio, δ_{28}, as follows:

$$\epsilon = 1 + \delta_{28}\left(\frac{\nu_{28}-1-\alpha_{28}}{\nu_{25}}\right), \qquad (1.2.1)$$

where ν_{28} and ν_{25} are the average numbers of neutrons produced per U^{238} and U^{235} fission, respectively, and α_{28} is the ratio of the U^{238} capture rate to the U^{238} fission rate in the fast region. The resonance escape probability, p, can be expressed in terms of the measured microscopic parameter ρ_{28} by means of the following simple relation:

$$p = \frac{1}{1 + \rho_{28} fG}, \qquad (1.2.2)$$

where f is the thermal utilization factor and G is the ratio of the subcadmium U^{238} capture rate to the total "thermal" absorption rate in the fuel. (The term "thermal" is set in quotation marks because the exact neutron reaction rates included in this term are not uniquely determined; see Section 6.1.) Equation 1.2.2 represents a very simple approach and yields a very approximate value of p. More sophisticated (and complicated) expressions for p usually involve not only ρ_{28} but also δ_{25} and δ_{28}. The definition and thus the particular expression used for p must be consistent with the definitions used for k_∞ and the other factors, η, f, and ϵ.

The multiplication factor, k_∞, can also be expressed directly in terms of measured quantities. One such expression, which is derived in Section 6.1, is:

$$k_\infty = \frac{\nu_{25} + \delta_{28}(\nu_{28}-1-\alpha_{28})}{(1+\alpha_{25}) + C^* \ell_{C^*} + \left(\frac{1}{f} - 1\right)\left(\frac{1}{1-G}\right)\left(1+\alpha_{25}\right) - \delta_{28}\alpha_{28}}, \qquad (1.2.3)$$

where α_{25} is the ratio of the U^{235} capture rate to the U^{235} fission rate, and ℓ_{C^*} is a leakage correction factor to convert the measured value of C^* to the value which would be obtained in an infinite system. Again, care must be exercised to ensure that the formulation used embodies a definition consistent with other formulations of the same parameter and with formulations of other parameters. If capture by U^{239} or Np^{239} is neglected, the initial conversion ratio, C, may be be related to the

measured microscopic parameter C^*:

$$C = C^*(1+\alpha_{25})^{-1} \quad . \tag{1.2.4}$$

Experimental determinations of reactor physics parameters have two purposes. First, they provide data to which theoretical results may be compared and thus provide a test of the theoretical treatment. Second, they can provide data and results in areas in which theory is not sufficiently developed to produce results of sufficient accuracy. An example of the first case is the thermal energy region where theoretical treatments such as THERMOS (H4) can produce results which can be considered equal to or better than experimental results (B2, S1). An example of the second case is the epithermal energy region in which only Monte Carlo treatments yield adequate space and energy dependent neutron distributions.

1.3 Objectives and General Program of This Work

With the above considerations in mind, the general objectives of the research to be described in this report were as follows:

1. To measure quantities which can be used to characterize the lattices studied and, in particular, the epithermal portion of the neutron spectrum.
2. To reduce the experimental errors associated with the measurements of these quantities by improving the experimental methods and techniques.
3. To eliminate or correct for systematic errors associated with the experimental methods and techniques.
4. To seek new measurements to make and new methods of making existing measurements in the area of interest.
5. To analyze the experimental results for consistency and compare them to the results of other investigations.

To accomplish these objectives, the microscopic parameters ρ_{28}, C^*, δ_{25}, and δ_{28} were measured in three different lattices which were studied during the course of the present work. The method used to measure C^*

was modified extensively, and many experimental details associated with irradiation and counting techniques were improved. An extensive investigation of systematic errors was carried out. As a result of this investigation, the experimental foil arrangements were modified to eliminate the effects of some sources of systematic error, and, where the effects could not be removed, correction factors were developed to compensate for the effects. To aid in the understanding, interpretation, and analysis of the experimental results, additional measurements were made, such as the determination of the microscopic parameters as a function of position within the lattice and the measurement of the intracellular activation distributions of Np^{239} and Cu^{64}. The investigation of the resonance energy region was extended by measuring the resonance activity of several nuclides irradiated in one of the lattices studied. The results of this investigation indicate that the methods presented can provide valuable data to which sophisticated theoretical treatments of the resonance energy region may be compared. In addition, the new methods provide new approaches to the experimental determination of the resonance escape probability, p, and the effective resonance integral of U^{238} in the fuel rods, ERI^{28}. To aid in the interpretation and analysis of the experimental results, analytical results obtained by means of the computer codes THERMOS (H4) and GAM-I (J1) were used. Since experimental results for similar systems are not available, and since differences between the results obtained for other systems, e.g., water-moderated assemblies, and the three lattices studied cannot be readily studied, the results of the present work were examined mainly for self-consistency and compared to the results of measurements by Peak et al. (P2) made in a miniature lattice assembly at M.I.T. The assembly by Peak et al. was experimental and exploratory in nature, and the resulting measurements required corrections as large as 25 or 30 per cent in some cases to compensate for the effects of neutron leakage from the small assembly. Thus the present results actually provide a test for the results of Peak et al. rather than vice versa.

1.4 Contents of Report

The experimental facilities, equipment and methods used to make the experiments are presented in Chapter II. In Chapter III, the investigation into systematic errors is described and discussed, and any correction factors which become necessary as a result of the investigation are derived. The experimental results of the measurements described in Chapter II are presented in Chapter IV together with a discussion of their associated errors. The general methods used for data reduction are also described in Chapter IV. The results of the theoretical calculations obtained by means of the two computer programs, THERMOS (H4) and GAM-I (J1), are presented and discussed in Chapter V. The experimental results are analyzed, with the aid of the theoretical results, and discussed in Chapter VI. The conclusions drawn from the results of this research and recommendations for future work are given in Chapter VII. The nomenclature is given in Appendix A. The references are given in Appendix B. The computer codes written to aid in the data reduction are described and listed in Appendix C. The input data for the THERMOS and GAM-I programs are presented in Appendix D. In Appendix E, the fraction of the epicadmium activity, of a uranium foil irradiated in a lattice, caused by fast neutrons is derived.

CHAPTER II
EXPERIMENTAL FACILITIES AND METHODS

Introduction

This chapter deals with the facilities, equipment and methods used to make the experiments. Chapter III describes and discusses the investigations of possible systematic errors associated with the methods used. In Chapter IV, the experimental results will be given for the actual quantities measured and for the parameters derived from them for the various lattices studied.

2.1 Experimental Facilities

The primary source of neutrons for all the experimental work was the M.I.T. Reactor (MITR) which is moderated by D_2O, contains MTR-type fuel elements and operates at a nominal power level of 2 Mw (L1). Figure 2.1.1 is an isometric view of the MITR and its experimental facilities. Figure 2.1.2 is a plan view. The facilities used in the work to be described were the lattice facility, the beam port of the Medical Therapy Room, the pneumatic sample tubes, and an in-core sample thimble.

2.1.1 The M.I.T. Lattice Facility

Most of the experiments were made in the lattice facility which uses the MITR thermal column as a source of thermal neutrons. Figures 2.1.3 and 2.1.4 are cross-section views of the lattice facility which has been described in detail in earlier reports (H2, M1, P1).

An exponential tank is supported above a graphite-lined cavity or "hohlraum." Neutrons from the thermal column enter the cavity and are effectively reflected through 90 degrees into the bottom of the tank. An experimental and theoretical design study of the cavity was done by Dr. J. T. Madell and is described in detail in Ref. (M1). A graphite

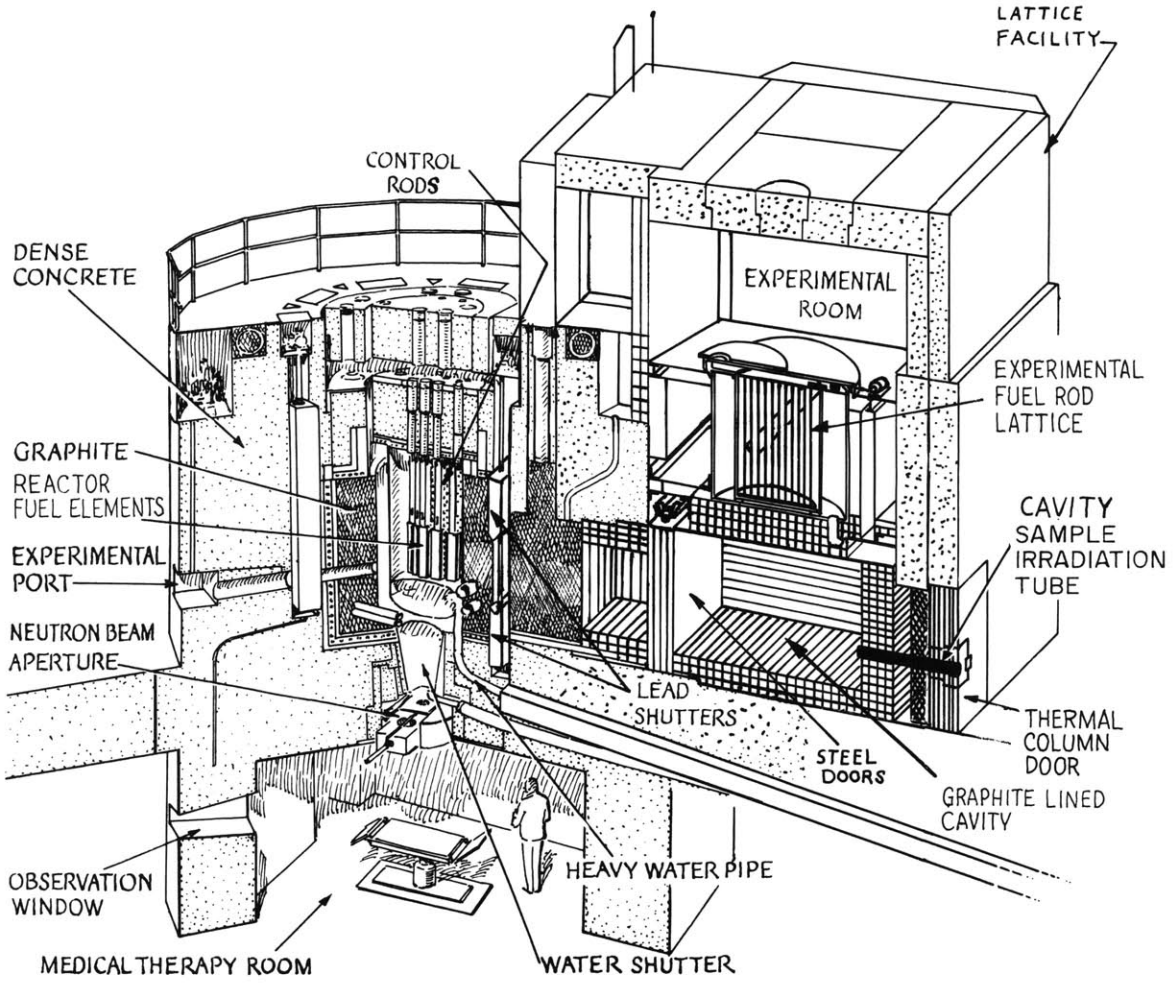

FIG. 2.1.1
CUT-AWAY VIEW OF THE MIT RESEARCH REACTOR

IRRADIATION FACILITIES

Facility	No. Available	Size	Estimated Thermal Flux at 2 MW n/cm^2-sec	Special Features
Horizontal Beam Ports 4" 6" 12"	 6 4 1	 $4\frac{1}{16}$" i.d. $6\frac{5}{8}$" i.d. $12\frac{1}{16}$" i.d.	 at tank wall 8×10^{12}	All ports have readily available the following services: 1. Demineralized cooling water 2. 110 V AC 3. Access to basement 4. Access to reactor top 5. Inert gas system 6. Off gas system 7. Waste drain. In addition the 6" and 12" ports have shutters useful for changing experiments
Rotary Horizontal Ports 6"	 2	 $6\frac{5}{8}$" i.d.	 at tank wall, 8×10^{12}	
Horizontal Thru Ports 6" 4" *	 1 1	 $6\frac{5}{8}$" i.d. $4\frac{1}{2}$" i.d.	 8×10^{12} at point closest to tank	
Vertical Thimbles Graphite $3\frac{1}{2}$" * In-tank 1" (in reflector) * In-tank 1" (in core)	 6 up to 10 up to 3	 $3\frac{5}{16}$" i.d. - up to 12" long 1" i.d. - up to 24" long same size	 $0.6 - 1.0 \times 10^{13}$ 2×10^{13} 3×10^{13}	Fast flux up to 5×10^{13} available in in-tank thimbles (also gammas up to 3×10^{8} r./hr.
Thermal Column	1	Holes up to 14" × 14" extend into thermal column. Larger holes can be made if needed	$10^{9} - 10^{12}$	The therman column has lead and cadmium shutters
Pneumatic Rabbit Tubes	4	Space for sample 1" dia. × $2\frac{3}{8}$" long	8×10^{12}	"In" to "out" travel time is 0.5 sec.
Medical Therapy Facility	1	---	Thermal 10^{10} Fast 10^{7}	Opens into operating room beneath reactor
Gamma Facility	Many	Flexible	$10^{4} - 10^{5}$ r./hr.	Spent fuel storage

* Note: Some of these facilities have sample changers to permit insertion and removal of samples during reactor operation at full power. They use standard aluminum cans as outside containers ($\frac{13}{16}$" i.d. × $1\frac{1}{4}$" or $2\frac{1}{4}$" long).

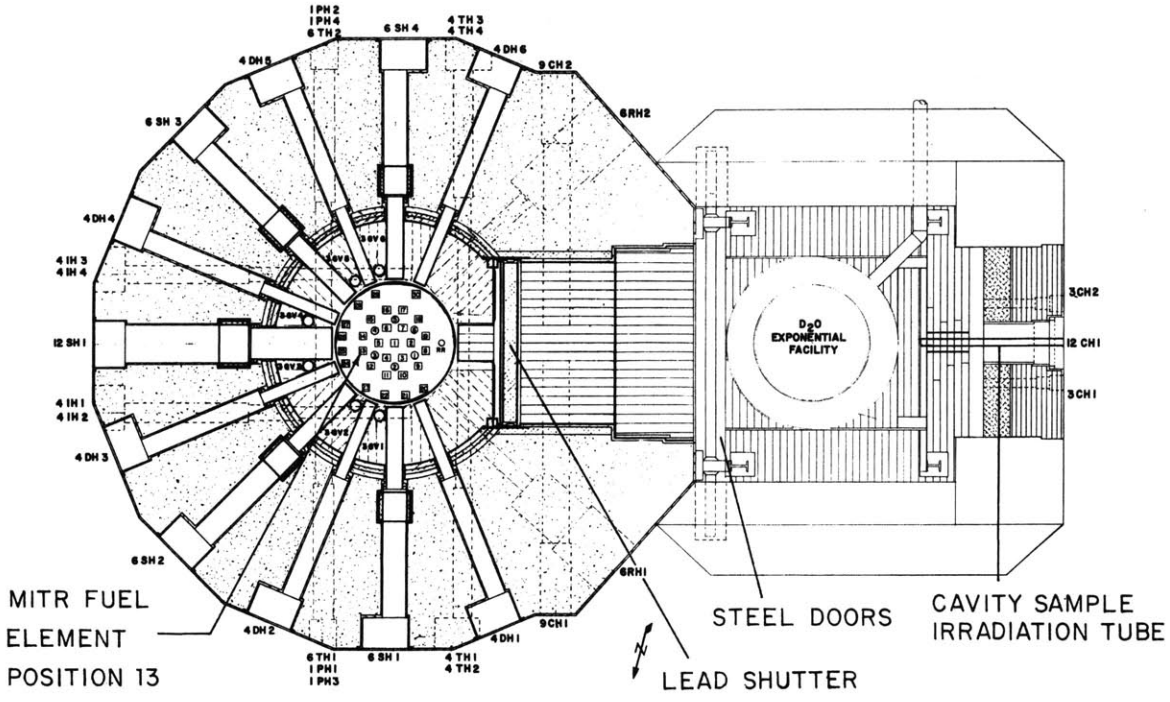

HORIZONTAL SECTION THROUGH REACTOR AND EXPONENTIAL FACILITY

FIG. 2.1.2

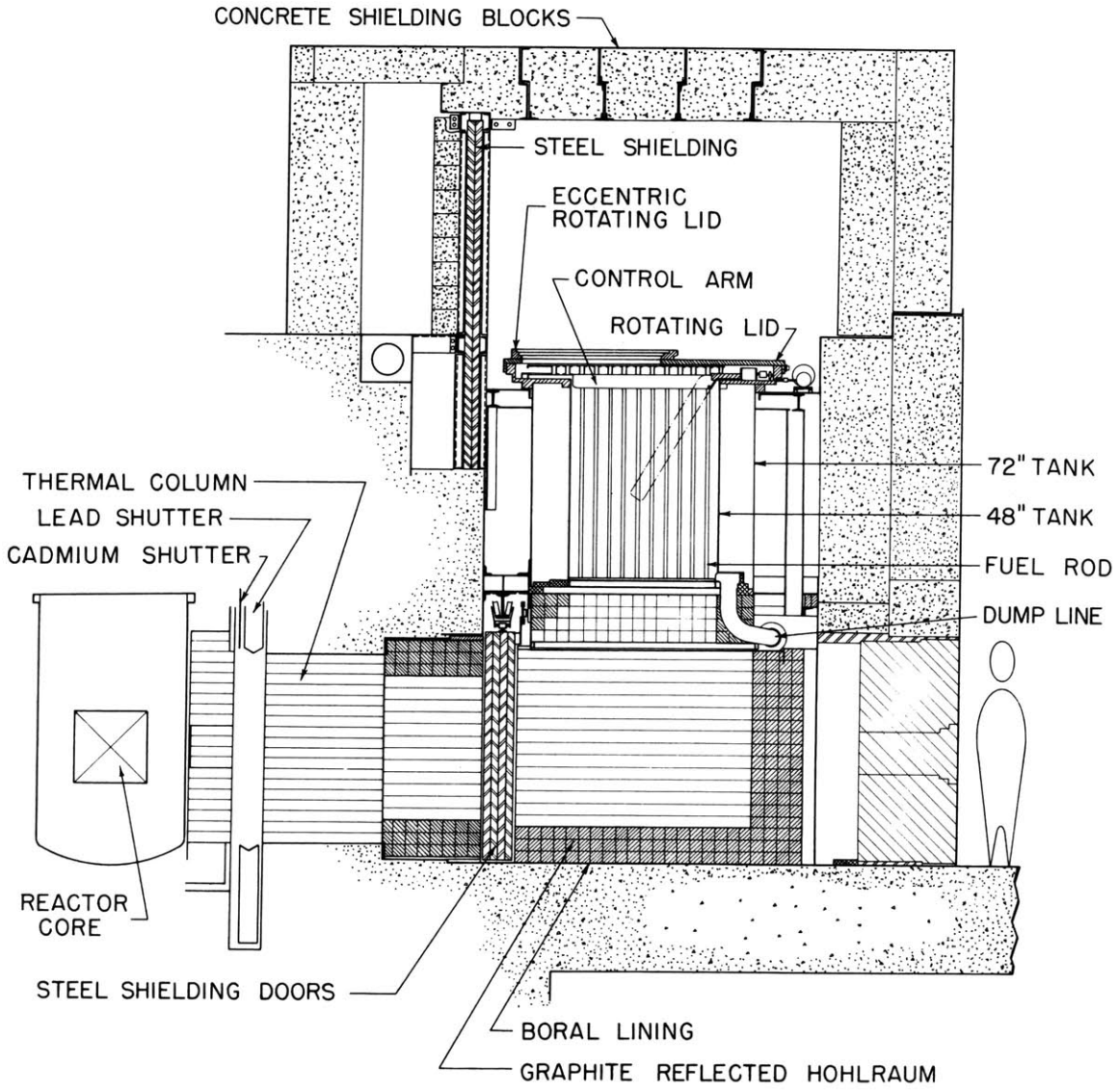

VERTICAL SECTION OF THE SUBCRITICAL ASSEMBLY

FIG. 2.1.3

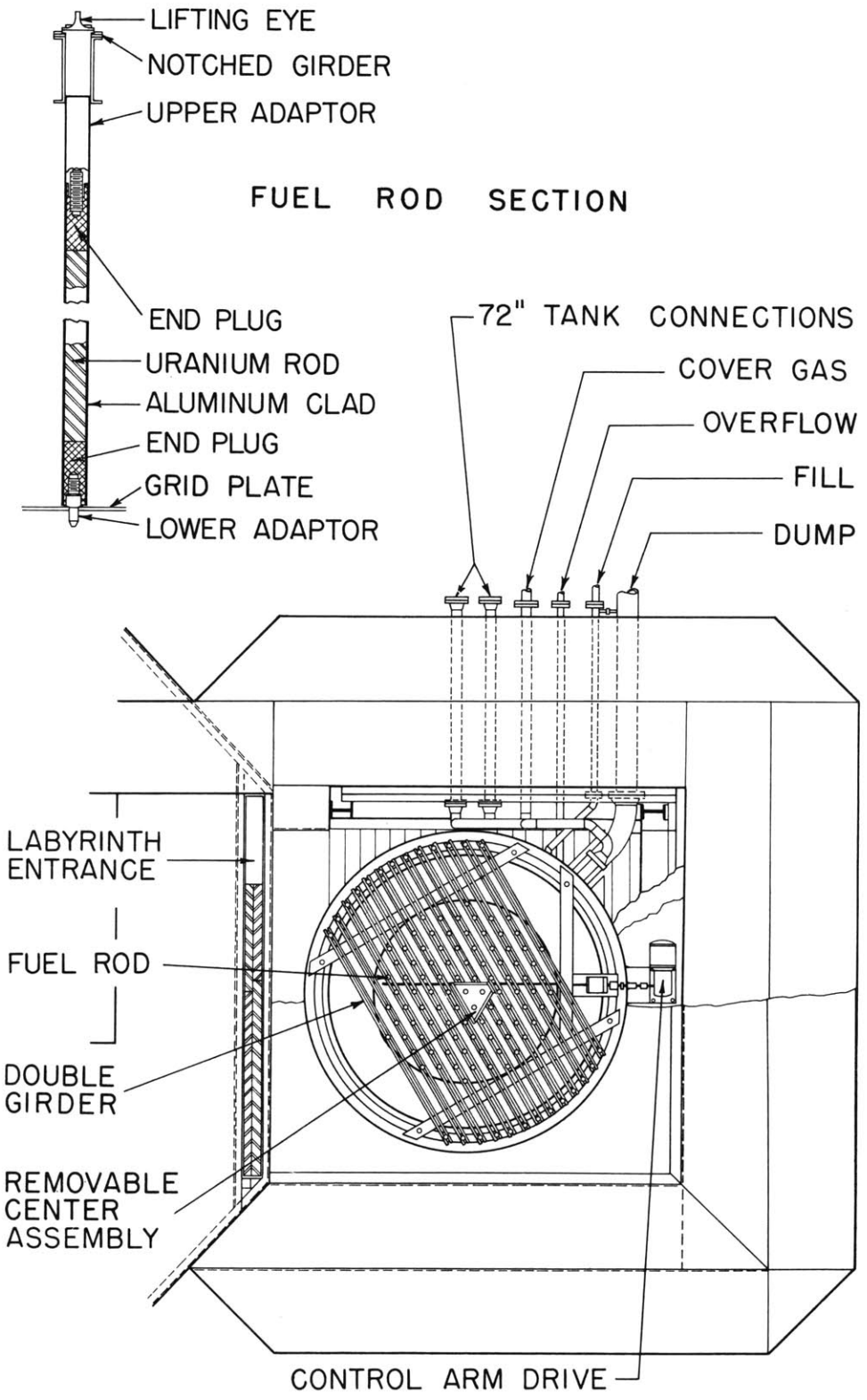

PLAN VIEW OF THE SUBCRITICAL ASSEMBLY

FIG. 2.1.4

pedestal located immediately below the tank shapes the entering flux to approximately a J_o radial distribution. The design of the pedestal was the result of work by Dr. P. F. Palmedo and is described in Ref. (P1). With the MITR operating at 1.8 Mw, the flux entering the bottom of the tank is about 10^{10} n/cm^2 (P1).

A sample tube is located in the graphite wall of the cavity directly opposite the thermal column. Boral-lined steel doors between the thermal column and the cavity reduce the neutron flux entering the cavity by a factor of at least 10^3 (P1). Irradiations in both the exponential tank and the cavity sample tube were started or ended by the opening or closing, respectively, of the steel doors.

The exponential tank is removable so that different sized tanks may be used, and tanks 48 inches and 36 inches in diameter have been used. The sides of the tanks are covered with 0.020-inch-thick cadmium to approximate bare, i.e., unreflected, thermal systems. The exponential tank is contained in a 72-inch-diameter outer tank. The space between the exponential tank and the outer tank can be filled to permit the use of radial reflectors or external poison regions if necessary; this has so far not been done. The tanks are 67-1/4 inches high.

The fuel rods are suspended from double girders at the top of the tank. The spacing of the fuel rods is determined by the relative spacing of the girders and by notches on top of each girder. Tabs of the upper adapters of the fuel rods fit into these notches. The lower adapters of the fuel rods fit into positioning holes of a grid plate situated at the bottom of the exponential tank. Usually each lattice had a removable central cluster consisting of the central fuel rod and two adjacent rods of the inner hexagon. The lattices are normally assembled on the floor of the reactor building and placed in the exponential tank by means of a crane, after removing the tank lid.

The tank lid contains a smaller eccentric lid; the two lids may be rotated independently of each other. The smaller lid has an eccentric 10-inch hole with a transparent plastic shutter. By proper positioning of the two lids, any portion of the exponential or outer tanks is accessible. The 10-inch hole is fitted with a removable glove box which has a plastic bag attached. The plastic bag and glove box permit fuel rods and

experimental apparatus to be inserted or removed from the lattice tank while preventing the degradation of D_2O in the system by atmospheric H_2O. If necessary, pieces of apparatus can be placed in the lattice before the lattice is put into the exponential tank.

Before the tank lid is removed, the D_2O is drained from the exponential tank into a storage tank. The exponential tank is dried before D_2O is reintroduced into it. During operation of the system, the D_2O is circulated through an ion exchange column and two heat exchangers, one for heating the D_2O and one for cooling it. The temperature of the D_2O during irradiations was usually between 75°F and 85°F, and the maximum temperature change during these irradiations was about 10°F.

During the present work, three lattices were studied. Each lattice had 0.250-inch-diameter, 48-inch-long uranium fuel rods containing 1.027% U^{235} by weight. The cladding was 0.028-inch-thick, Type 1100 aluminum with an outside diameter of 0.318 inch. A 0.005-inch-thick air gap separated the fuel and cladding. Aluminum end plugs, three inches long, were inserted into the cladding which extended three inches beyond the fuel at each end. Both end plugs were drilled and taped so that upper and lower adapters could be fitted to the fuel rods. In the lattices, the fuel rods were arranged in triangular arrays with rod-to-rod spacings of 1.25, 1.75 and 2.50 inches, respectively.

Figure 2.1.5 shows a cross-sectional view of the cavity sample tube and its neutron flux distribution. The flux in the cavity is well thermalized and it is assumed that spectrally averaged thermal cross sections such as those of Westcott (W2) can be used to calculate thermal reaction rates in this flux. A Westcott "r" value of less than 10^{-4} was determined from the gold-cadmium ratio of 800 for 0.008-inch-thick gold foils. The gold-cadmium ratio was the same with or without a lattice in the exponential tank. Thus the cavity sample tube provides a standard irradiation position in a Maxwellian flux which can be used simultaneously with the lattice.

The sample tube is 5/8 inch in diameter and samples were introduced by attaching them to a 1/2-inch-diameter, 6-foot-long polyethylene rod. The polyethylene rod had no effect on the flux distribution in the sample tube (P4).

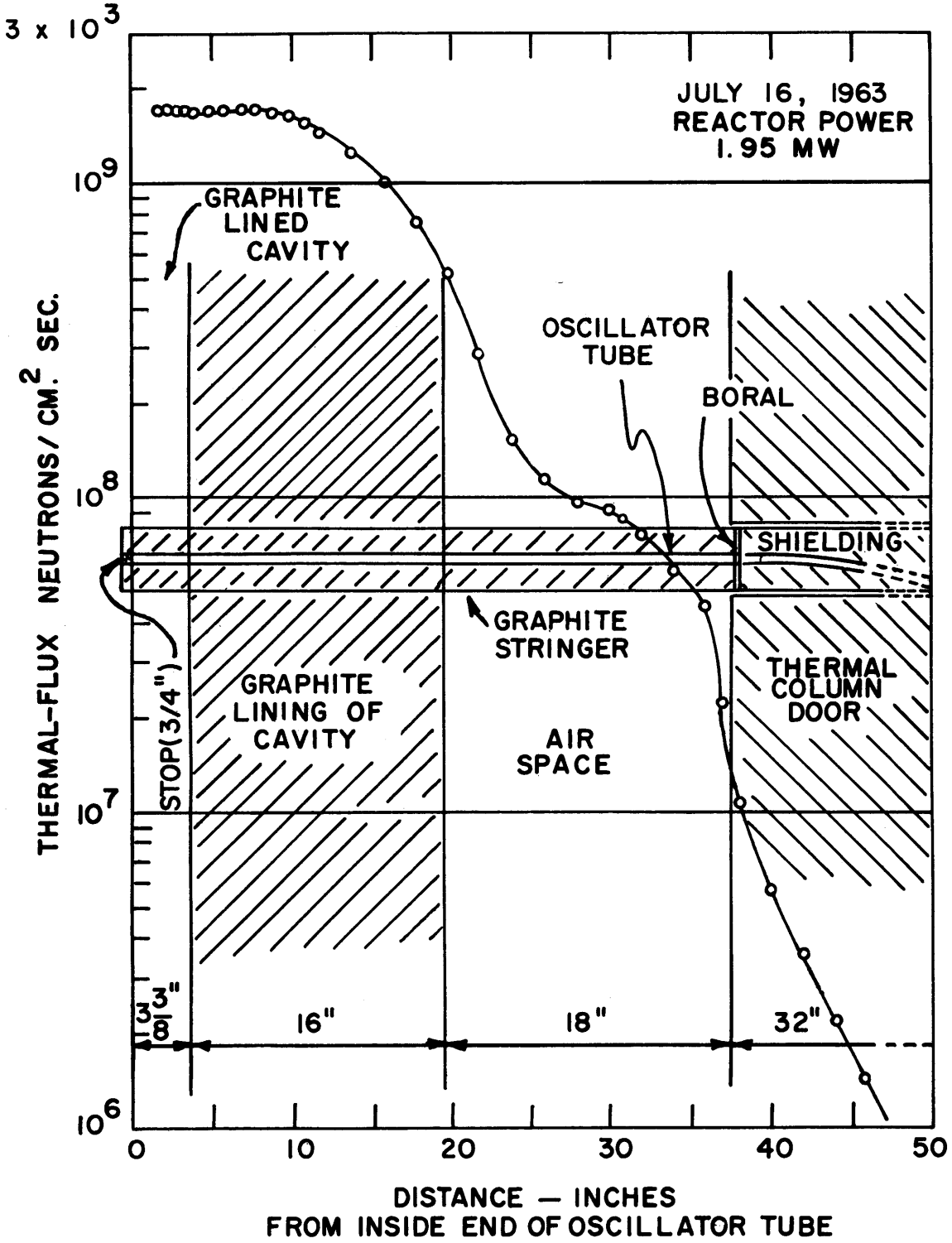

VERTICAL SECTION OF THE CAVITY SAMPLE TUBE WITH THE NEUTRON FLUX DISTRIBUTION MEASURED BY CLARK (CI) SUPERIMPOSED

FIG. 2.1.5

2.1.2 Other Facilities

The other facilities of the MITR which were used in the present work were the Medical Therapy Room beam port (P2), the pneumatic sample tubes, and an in-core sample thimble. The neutron flux in the Medical Therapy Room beam is about 10^{10} n/cm^2 with a Westcott "r" value of about 0.01 (R2). This provides a facility with a well thermalized neutron flux which is independent of the lattice facility. The pneumatic sample tubes have a thermal neutron flux of about 8×10^{12} n/cm^2 with an epithermal "tail" which has been found to vary as $\frac{1}{E}$ (A3). The tubes are good for short irradiations of small samples.

The MITR fuel element position 13 shown in Fig. 2.1.2 contains a partially loaded fuel element. The fuel element has no central fuel plates, and a sample thimble extends down through the element. On the basis of fast chopper results (A3) and the absence of strong resonance absorption, the epithermal component of the neutron spectrum is assumed to vary as $\frac{1}{E}$ at this position. This facility provides a thermal flux of about 3×10^{13} n/cm^2 with a relatively large "$\frac{1}{E}$ tail."

2.2 Measurements of the Microscopic Parameters

The four microscopic parameters, ρ_{28}, C^*, δ_{25} and δ_{28}, which will be defined below, were measured in each of the three lattices studied. In addition, since one of the objectives of the present work was to obtain results of higher precision, improvements have been made in the methods and techniques which are used to measure the four parameters. The measurement of each parameter had at least two detector foils in common with at least one other measurement; in fact, one detector foil was common to all four parameter measurements. Hence, all four of the microscopic parameters were usually measured in the course of one experiment. After outlining the method used to measure each parameter, the experimental details and techniques will be described for all the parameter measurements together.

2.2.1 Methods of Measuring the Microscopic Parameters

2.2.1.1 ρ_{28}

The microscopic parameter ρ_{28} is related to the cadmium ratio of the average U^{238} capture rate in the fuel, R_{28}:

$$\rho_{28} = \frac{1}{R_{28} - 1} = \left(\frac{\text{average epicadmium } U^{238} \text{ capture rate in the fuel}}{\text{average subcadmium } U^{238} \text{ capture rate in the fuel}} \right). \tag{2.2.1}$$

The value of R_{28}, the U^{238} cadmium ratio, was measured by irradiating two identical uranium foils, depleted in U^{235} content to 18 parts per million, in equivalent positions (positions of equal height and radius) inside fuel rods in the exponential tank with one foil surrounded by cadmium. By "identical" is meant two foils with the same U^{235} content and with the same diameter, weight, and thickness to within a fraction of one per cent. The Np^{239} activity of each foil was measured and then the cadmium ratio, R_{28}, was obtained from the ratio:

$$R_{28} = \frac{D_b^{39}}{D_c^{39}}, \tag{2.2.2}$$

where D refers to a measured activity of a depleted uranium foil, the superscript 39 means that the Np^{239} activity was the measured activity and the subscripts b and c refer to bare and cadmium-covered detector foils, respectively.

2.2.1.2 δ_{28}

The fast fission ratio, δ_{28}, is defined by the following relation:

$$\delta_{28} = \left(\frac{\text{average total } U^{238} \text{ fission rate in the fuel}}{\text{average total } U^{235} \text{ fission rate in the fuel}} \right); \tag{2.2.3}$$

it may be rewritten (W3):

$$\delta_{28} = P(t)F(t) = P(t)\left[\frac{EC \cdot a \cdot \gamma(t) - S}{1 - a \cdot \gamma(t)} \right]. \tag{2.2.4}$$

The terms in Eq. 2.2.4 are defined as follows:

P(t) is the ratio of measured fission product activity per U^{235} fission to the measured fission product activity per U^{238} fission.

$\gamma(t)$ is the ratio of measured fission product activity of a foil depleted in U^{235} content to the fission product activity of a foil of natural uranium (or from a foil of fuel material if such material is available) when both foils have been irradiated in the same neutron flux.

a is the ratio $\left(\frac{W_N}{W_D}\right)\left(\frac{N_N}{N_D}\right)^{28}$ where the W's represent detector foil weights and the N's represent numbers of atoms per cubic centimeter; the subscripts D and N refer to the depleted uranium detector foil, and the natural uranium detector foil, respectively.

EC is the ratio $\left(\frac{N_N}{N_F}\right)^{25}\left(\frac{N_F}{N_N}\right)^{28}$, an enrichment correction; the subscript F refers to the fuel material.

S is the ratio $\left(\frac{N_D}{N_F}\right)^{25}\left(\frac{N_F}{N_D}\right)^{28}$.

The derivation of Eq. 2.2.4 from Eq. 2.2.3 is given in Refs. (W3) and (B1).

To determine δ_{28}, both P(t) and $\gamma(t)$ in Eq. 2.2.4 must be measured. In all the methods used so far, this requires two experiments. First, a reference value of the fast fission ratio, δ^*_{28}, is determined for a particular lattice configuration by using the La^{140} counting technique discussed in Section 2.2.5. Then the quantity $\gamma(t)$ is measured in the same lattice, and the quantity P(t) is determined by using Eq. 2.2.4 combined with the measured values of $\gamma(t)$ and δ^*_{28}. Once P(t) has been determined, it will remain the same for the different lattices with the same fuel rods, providing the counting arrangement remains unchanged. Hence, further determinations of δ_{28} require only the measurement of $\gamma(t)$ which, when inserted in the expression F(t) and multiplied by P(t), yields δ_{28}.

The quantity $\gamma(t)$ was measured by irradiating two uranium foils,

one foil depleted in U^{235} content and one natural uranium foil, at the same position inside a fuel rod in a lattice in the exponential tank. The gross fission product activity of each foil was measured and $\gamma(t)$ calculated:

$$\gamma(t) = \frac{D_b^{FP}}{N_b^{FP}}, \tag{2.2.5}$$

where N refers to a measured activity of a natural uranium detector foil and the superscript FP means that the gross fission product activity was the measured activity, and the subscript b indicates that bare foils were irradiated.

2.2.1.3 δ_{25}

The ratio δ_{25} is defined by the relation:

$$\delta_{25} = \left(\frac{\text{average epicadmium } U^{235} \text{ fission rate in the fuel}}{\text{average subcadmium } U^{235} \text{ fission rate in the fuel}} \right), \tag{2.2.6}$$

or,

$$\delta_{25} = \frac{A_{EC}^{25}}{A_{SC}^{25}}. \tag{2.2.7}$$

As shown in Refs. (B1) and (H4):

$$\delta_{25} = \frac{\left[N_c^{FP} - \left(\frac{1-\epsilon_N}{1-\epsilon_D} \right) D_c^{FP} \right]}{\left[N_b^{FP} - \left(\frac{1-\epsilon_N}{1-\epsilon_D} \right) D_b^{FP} \right] - \left[N_c^{FP} - \left(\frac{1-\epsilon_N}{1-\epsilon_D} \right) D_c^{FP} \right]}, \tag{2.2.8}$$

where ϵ_N is the atom fraction of U^{235} in the natural uranium and ϵ_D is the atom fraction of U^{235} in the depleted uranium. All activities in Eq. 2.2.8 are to be determined at the same time after simultaneous irradiation. This formulation of δ_{25} is more general than an earlier one given in Ref. (W3) which was restricted to lattices containing natural uranium fuel studied in earlier work at M.I.T.

The value of δ_{25} was determined by irradiating two sets of foils in equivalent positions inside fuel rods in a lattice in the exponential tank with one set of foils surrounded by cadmium. Each set of foils consisted of one depleted uranium foil and one natural uranium foil. After the relative fission product activity of each foil was measured, δ_{25} was calculated from Eq. 2.2.8.

The value of δ_{25} can also be related to the average gold-cadmium ratio in the fuel, R_{Au}, by means of the following equation (K3):

$$\delta_{25} = \frac{\text{constant}}{(R_{Au} - 1)} = \text{constant } \rho_{Au} \, . \tag{2.2.9}$$

2.2.1.4 $\underline{C^*}$

The ratio C^* is defined by the relation:

$$C^* = \left(\frac{\text{average total } U^{238} \text{ capture rate in the fuel}}{\text{average total } U^{235} \text{ fission rate in the fuel}} \right) . \tag{2.2.10}$$

To determine this ratio experimentally, Eq. 2.2.10 is rewritten:

$$C^* = \left(\frac{U^{238} \text{ capture rate of fuel material in a Maxwellian flux}}{U^{235} \text{ fission rate of fuel material in a Maxwellian flux}} \right)_{\text{calculated}}$$

$$\times \left(\frac{U^{235} \text{ fission product activity of fuel material irradiated in a Maxwellian flux}}{Np^{239} \text{ activity of fuel material irradiated in a Maxwellian flux}} \right)_{\text{measured}}$$

$$\times \left(\frac{\text{average } Np^{239} \text{ activity of fuel irradiated in the lattice}}{\text{average } U^{235} \text{ fission product activity of fuel irradiated in the lattice}} \right)_{\text{measured}}$$

or,

$$C^* = C^*_M \left(\frac{A^{25}_M}{A^{39}_M} \right) \left(\frac{A^{39}_b}{A^{25}_b} \right) . \tag{2.2.11}$$

In earlier work at M.I.T., (W1), Eq. 2.2.11 was written:

$$C^* = C^*_M\left(\frac{A^{25}_M}{A^{39}_M}\right)\left(\frac{A^{39}_b}{A^{25}_b}\right) = C^*_{STD}\left(\frac{1}{R_{STD}(t)}\right)\left(R_{LAT}(t)\right) . \tag{2.2.12}$$

The value of C^*_{STD} was calculated with the aid of Westcott's method of averaging cross sections and with the known atom concentrations of the fuel. Both $R_{LAT}(t)$ and $R_{STD}(t)$ were measured in the exponential tank with and without a lattice, respectively. This procedure required that the determination of the two ratios be separated by as much as several months. The irradiation times for both experiments should be the same to ensure that the two ratios have the same time dependence. The ratios are functions of time after irradiation because the U^{235} fission product activity and the Np^{239} activity do not decay with the same time dependence. For both ratios, aluminum alloy foils containing 9.8% uranium by weight enriched to 93.17 atom per cent U^{235} and depleted uranium foils were used to measure the U^{235} fission product activity and the Np^{239} activity, respectively.

The method of measuring C^* has been modified extensively to simplify the experiment, achieve higher precision, and avoid systematic errors associated with the use of aluminum alloys inside the fuel rods (see Section 3.2.3.1). By using the well thermalized flux in the cavity sample tube instead of the exponential tank filled only with D_2O, the four activities in Eq. 2.2.11 can be measured simultaneously. Regrouping the terms in Eq. 2.2.11:

$$C^* = C^*_M\left(\frac{A^{25}_M}{A^{25}_b}\right)\left(\frac{A^{39}_b}{A^{39}_M}\right) = C^*_{STD}\left(\frac{1}{R_F}\right)\left(R_N\right) . \tag{2.2.13}$$

The ratio C^*_{STD} is calculated as described after Eq. 2.1.12. The new experimental ratios, which are not functions of time after irradiation and do not require a specific irradiation time, permit much more latitude in planning and performing the experiment.

The ratios were measured by irradiating a natural uranium foil and a depleted uranium foil back-to-back inside a fuel rod in the

exponential tank, and a natural uranium foil and a depleted uranium foil back-to-back in the cavity sample tube. The Np^{239} activity of the depleted uranium foils and the gross fission product activity of both the depleted and the natural uranium foils are measured. Then the two ratios are:

$$R_N = \frac{D_b^{39}}{D_H^{39}}, \tag{2.2.14}$$

and

$$R_F = \frac{N_b^{FP} - \left(\frac{1-\epsilon_N}{1-\epsilon_D}\right) D_b^{FP}}{N_H^{FP} - \left(\frac{1-\epsilon_N}{1-\epsilon_D}\right) D_N^{FP}}, \tag{2.2.15}$$

where the subscript H refers to the cavity or "hohlraum" sample tube.

The value of C^* can also be obtained from the measured values of ρ_{28} and δ_{25} via the following relation (W1):

$$C^* = \left(\frac{1+\rho_{28}}{1+\delta_{25}}\right)\left(\frac{\Sigma_a^{28}}{\Sigma_f^{25}}\right)_{SC}, \tag{2.2.16}$$

where $\left(\frac{\Sigma_a^{28}}{\Sigma_f^{25}}\right)_{SC}$ is the ratio of the U^{238} capture rate in the fuel to the U^{235} fission rate in the fuel below the cadmium cutoff of about 0.4 ev.

2.2.2 Foil and Fuel Slug Fabrication

The foils used were made of 0.250-inch-diameter, 0.005-inch-thick, natural and depleted uranium, respectively. The depleted uranium had a measured atom concentration of 18 U^{235} atoms per million U^{238} atoms (W3). Both the natural and the depleted uranium, obtained from the Oak Ridge National Laboratory, were of high purity and no observable activities due to impurities were produced during irradiation. Foils of both U^{235} concentrations were fabricated in the same manner.

The materials from which the foils were made had a nominal thickness of 0.005 inch. Foils of each enrichment were all punched from the same original piece of uranium. The thickness of the foil material was carefully measured with a micrometer and areas of the material used to make detector foils were selected so that they were free of fissures and surface defects and were of uniform thickness.

The foils were made with a modified commercial punch and die set. The diameter of the foils should match the diameter of the fuel as closely as possible. The punch was ordered slightly oversize; the die, slightly undersize. The diameter of the punch was precision-ground to match the diameter of the fuel. Then the die was opened up by means of a tapered brass rod and lapping compound until a press fit between the die and the punch was obtained. The uranium foils made with this "zero clearance" punch and die set had no detectable burr. As a foil was punched, it was clamped between the punch and a steel rod extending through the die so that the foil would not become crowned or dished by the punching process.

Each foil was weighed with an accuracy of about ± 0.02% on a high-precision balance. The measured foil weights were plotted against the measured foil thickness. The variation in foil weight was found to be directly proportional to the variation in foil thickness. The foils were arranged according to weight and placed in a plastic foil holder. The foils were reweighed periodically because their weights gradually decreased owing to the formation and loss of the oxide coating.

A set of fuel slugs with lengths varying from 0.020 inch to 10 inches was made. The slugs were precision-cut with an alundum grinding wheel from 0.250-inch-diameter, 1.027% U^{235} by weight, uranium rod. By means of an appropriate combination of the fuel slugs and 0.005-inch-thick, natural uranium shim foils, detector foils could be located at any height, within 0.005 inch, inside a fuel rod. The variation of the flux for a change in height of 0.006 inch is about 0.05% for the lattice with the shortest relaxation length.

2.2.3 Foil Arrangements

The microscopic parameters were measured by irradiating, simultaneously, three sets of uranium detector foils. Each set consisted of a natural uranium foil and a depleted uranium foil. Two of the foil sets were irradiated in the exponential tank and one set was irradiated in the cavity sample tube. In the exponential tank, one of the foil sets was surrounded by 0.020-inch-thick cadmium.

A foil packet was made up for each set of foils placed in the exponential tank. Each detector foil was sandwiched between two uranium "catcher" foils, identical to the detector foil. The catcher foils prevent U^{235} fission products produced in uranium of a differing enrichment from reaching the detector foils. The three depleted uranium foils and the three natural uranium foils were placed back-to-back between two 0.060-inch-thick fuel slugs or "buttons." The diameters of all of the foils and the fuel buttons were matched as closely as possible. The foils and fuel buttons were placed inside an 0.125-inch-long Teflon sleeve with a wall thickness of 0.005 inch. At each end of this packet was placed a 0.020-inch-thick "holder" foil to keep the Teflon sleeve in position. The holder foils were made of Type 1100 aluminum for the bare detector foil packet and of cadmium for the cadmium-covered detector foil packet. The holder foils were 0.258 inch in diameter, 0.008 inch larger than the diameter of the fuel or uranium foils, and 0.004 inch smaller than the internal diameter of the aluminum cladding of the fuel rod. In some of the experiments, the Teflon sleeves were replaced by sleeves of Mylar tape and the 0.020-inch-thick aluminum holder foils were replaced by 0.020-inch-thick fuel buttons. The use of the two different sleeves produced no detectable differences in the results.

The foil assemblies were placed between two fuel slugs in a lattice fuel rod. In the case of the cadmium-covered detector foil assembly, a cadmium sleeve was positioned outside the 0.028-inch-thick aluminum cladding of the fuel rod so that the mid-point of the cadmium sleeve was located at the same height as the mid-point of the foil packet. The cadmium sleeve was formed by wrapping 0.001-inch-thick, 1-inch-wide cadmium around the outside of the cladding twenty times to form a

sleeve 0.020 inch thick and one inch long. A compressive force was applied to the fuel inside the fuel rod to ensure that the foils were kept tightly together. A schematic drawing of the foil arrangements in the lattice is shown in Fig. 2.2.1.

The bare detector foils and the cadmium-covered detector foils were usually irradiated at a height of 20 inches from the bottom of the fuel region (the length of the fuel region was 48 inches) and in two diametrically opposite fuel rods adjacent to the central fuel rod of the lattice. Bare gold foils were placed in each fuel rod about 10 inches above the uranium foil packets so that the flux at the uranium detector foil locations could be monitored and normalized if necessary. The gold monitor foils, prepared as described in Section 2.2.2, were 0.250 inch in diameter and 0.008 inch in thickness. Figure 2.2.2 shows the fuel rod arrangements and detector foil locations.

The set of foils irradiated in the cavity sample tube had each detector foil sandwiched between two foils identical to the detector foil. The three depleted uranium foils and the three natural uranium foils were placed back-to-back inside an aluminum sleeve 0.125 inch long with a 0.005-inch-thick wall. The aluminum sleeve kept the foils aligned. A 0.250-inch-diameter, 0.250-inch-long piece of polyethylene was placed on each side of the foil stack. This foil packet was inserted into a 0.250-inch-diameter hole drilled through a 0.500-inch-diameter, 6-foot-long polyethylene rod. The packet was held in place by Mylar tape. The hole in the rod was located so that, when the rod was fully inserted into the sample tube, the foils would be 18 inches from the cavity end of the tube. Figure 2.2.3 shows the foil arrangement.

2.2.4 Counting Methods

The depleted uranium detector foils were gamma counted for both fission product activity and Np^{239} activity. The natural uranium foils were gamma counted for fission product activity only. The counting was done in an air-conditioned counting laboratory which had an electrical circuit independent of the rest of the building to minimize the electrical noise reaching the counting equipment.

The foils were fission product counted by the integral gamma-ray

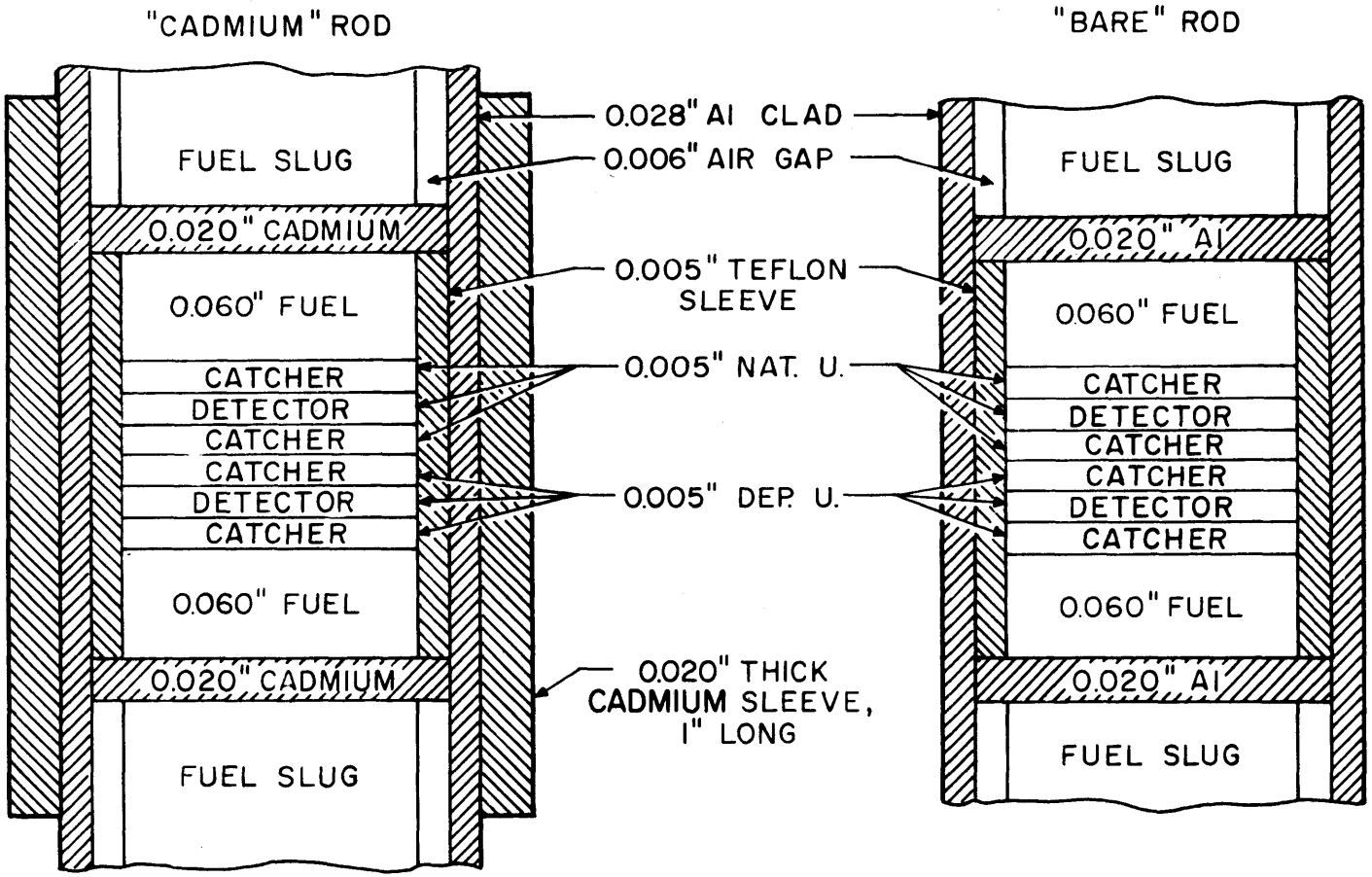

URANIUM FOIL ARRANGEMENTS IN THE FUEL RODS FOR THE MICROSCOPIC PARAMETER MEASUREMENTS

FIG. 2.2.1

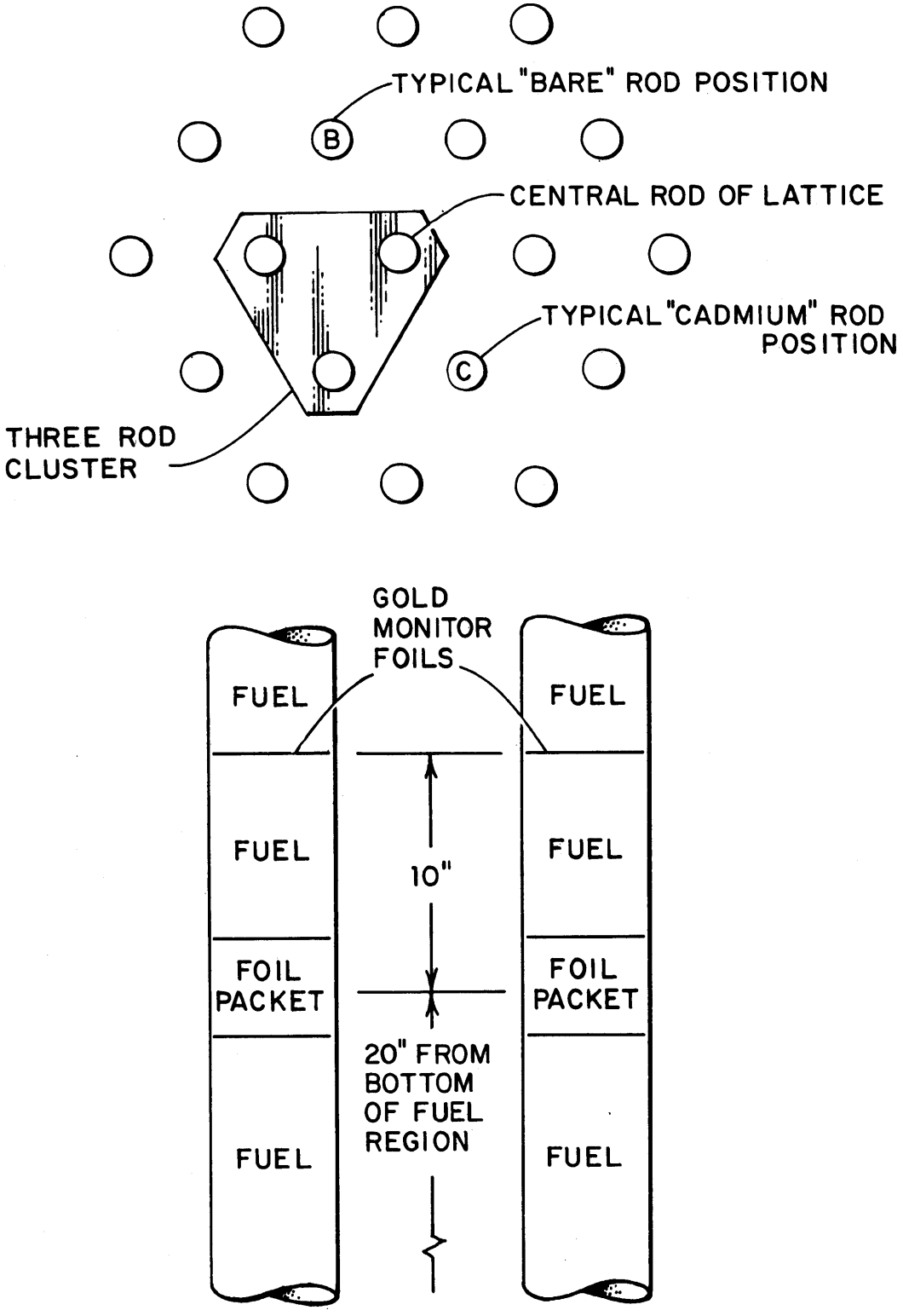

FUEL ROD ARRANGEMENT AND FOIL PACKET LOCATIONS FOR THE MICROSCOPIC PARAMETER MEASUREMENTS

FIG. 2.2.2

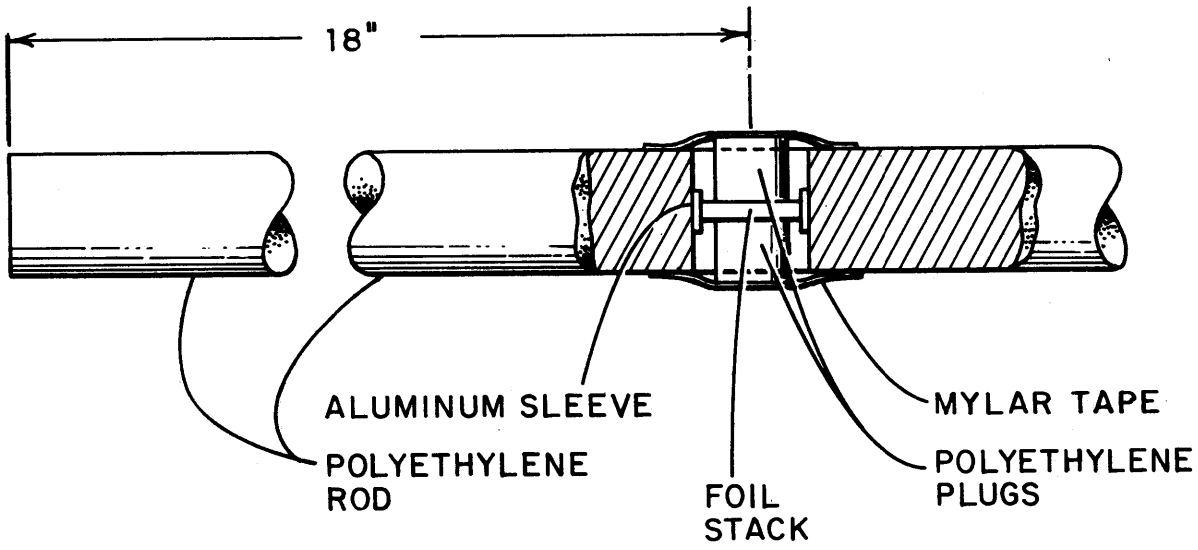

FOIL ARRANGEMENT IN THE CAVITY SAMPLE TUBE FOR THE MICROSCOPIC PARAMETER MEASUREMENTS

FIG. 2.2.3

counting technique with a baseline equivalent to 0.72 Mev. Before being counted, the foils were allowed to cool for about four hours so that the 23-minute U^{239} activity formed could decay almost completely to Np^{239}. In its decay process, U^{239} emits a 1.2-Mev β ray. The cooling period avoids the possible inclusion in the fission product counting of bremsstrahlung radiation associated with the 1.2-Mev β ray. The baseline of 0.72 Mev avoided the bremsstrahlung radiation arising from the 0.72-Mev β ray emitted during the decay of Np^{239}. The equipment used to count the fission product activity of the uranium foils consisted of a Baird Atomic Model 815BL scintillation probe, a Baird Atomic Model 312A high voltage supply, a Baird Atomic Model 215 linear amplifier, a Baird Atomic Model 134 scaler, and a Baird Atomic Model 960 timer. The scintillation probe contained a 1-3/4-inch-thick, 2-inch-diameter NaI(Tl) crystal, an RCA 6342A photomultiplier tube, and a preamplifier. A schematic diagram of the counting system is shown in Fig. 2.2.4. The counting system was calibrated with the 0.47-Mev, 0.66-Mev and 0.84-Mev gamma rays of Ir^{192}, Cs^{137} and Mn^{54}, respectively. Each time the foils were counted, the system was calibrated before and after counting to check for drift in the electronics. The foils were counted between 4 and 12 hours after irradiation was completed. After 12 hours, the activity of the depleted uranium foils was generally too low to obtain statistically meaningful counting results.

Before the depleted uranium foils were counted for Np^{239} activity, the foils were permitted to "cool" for at least four hours after completion of irradiation to allow the U^{239} formed to decay into Np^{239}. Therefore the depleted uranium foils were Np^{239} counted for the first time after the fission product counting had been completed. The 103-Kev peak in the gamma-ray and X-ray spectrum of the Np^{239} was counted; this peak is the result of a 106-Kev γ ray of Np^{239} and the 99- and 100-Kev X rays of Pu^{239} arising from the internal conversion of higher energy γ rays of Np^{239}. The γ-ray and X-ray spectrum of Np^{239} is shown in Fig. 2.2.5. The counting system consisted of an integral detector unit containing a 1/2-inch-thick, 1-1/2-inch-diameter NaI(Tl) crystal and an RCA 6342A photomultiplier, a preamplifier constructed by Mr. D. Gwinn, a Technical Measurement Corporation Model HV-4A high voltage supply, and a

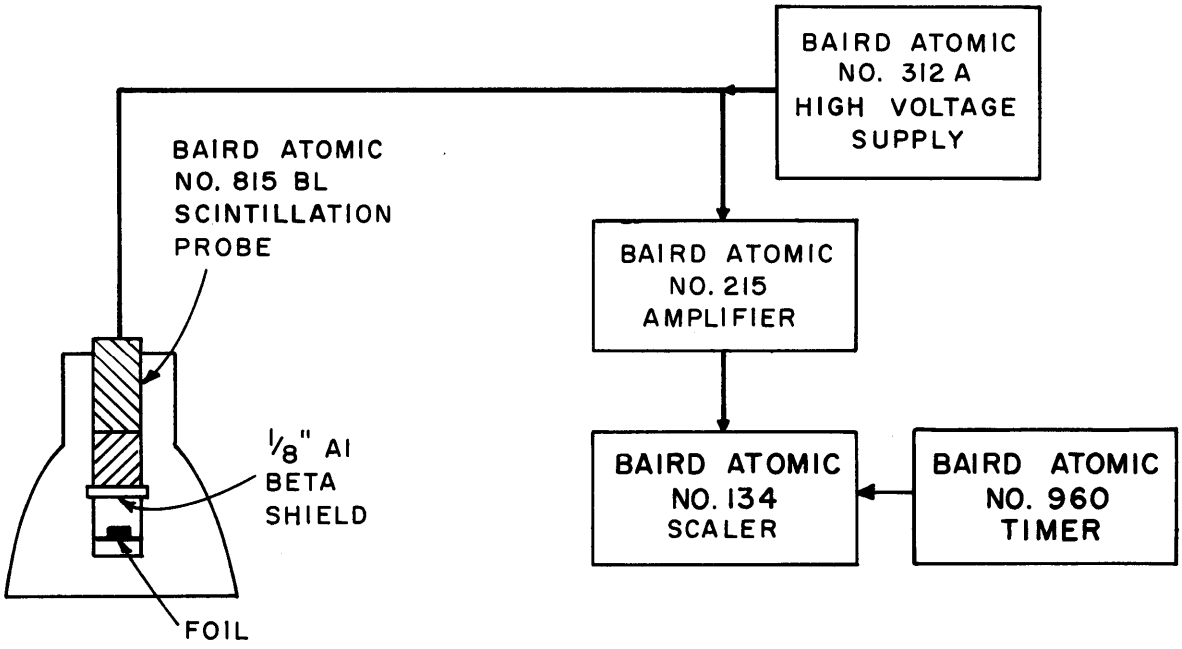

COUNTING SYSTEM USED TO MEASURE THE GROSS FISSION PRODUCT ACTIVITY OF THE NATURAL AND DEPLETED URANIUM FOILS

FIG. 2.2.4

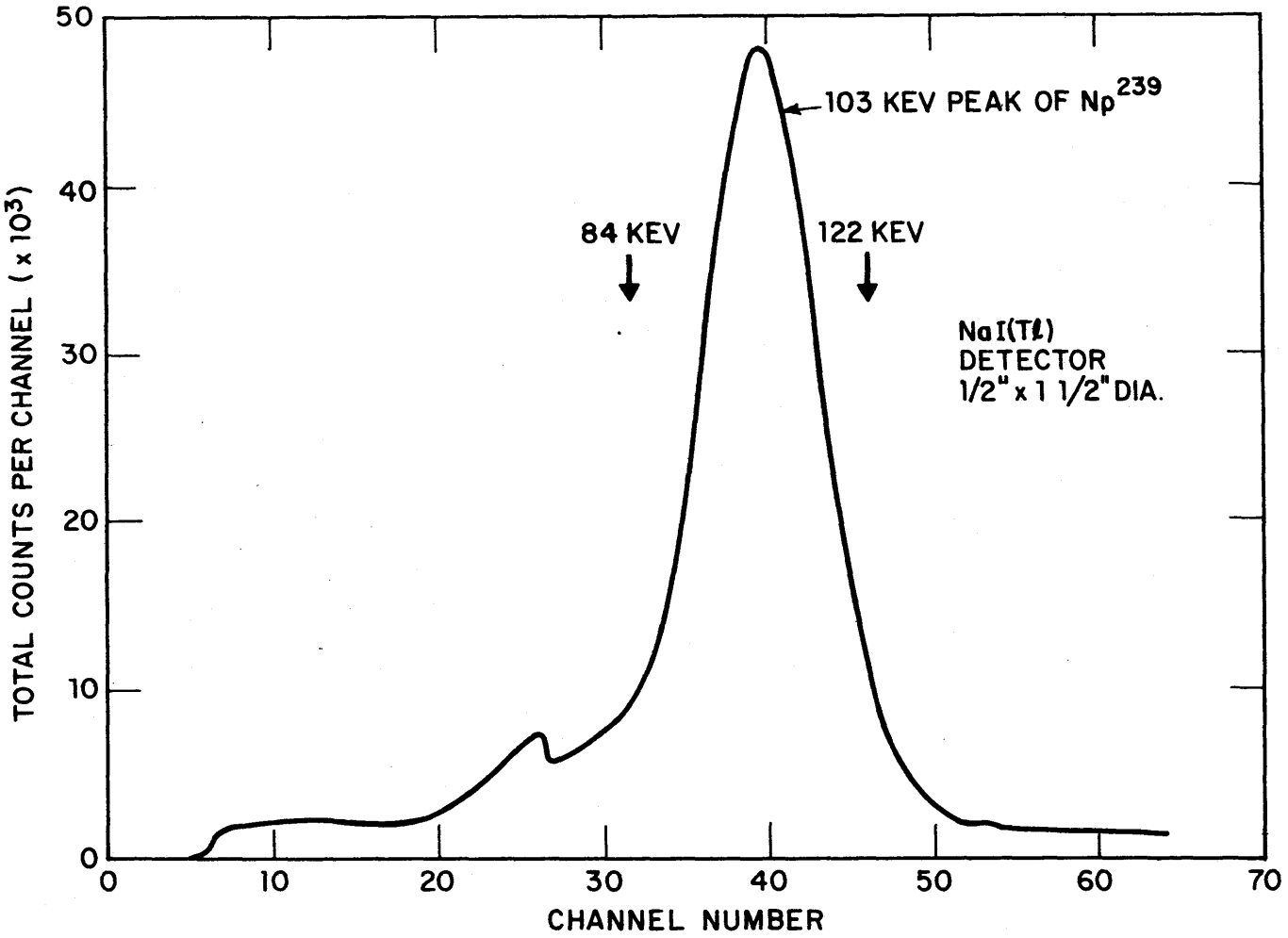

THE GAMMA RAY SPECTRUM OF A DEPLETED URANIUM FOIL SHOWING THE 103-KEV PEAK FROM Np^{239}

FIG. 2.2.5

Radiation Instrument Development Laboratory (RIDL) single-channel spectrometer. The spectrometer consisted of an RIDL Model 30-19 amplifier, an RIDL Model 33-10 single-channel analyzer, and an RIDL Model 49-25 combination scaler-timer, all mounted in an RIDL Model 29-1 chassis. Figure 2.2.6 is a schematic drawing of the counting system. The lower limit of the analyzer window was set at an equivalent energy of 84 Kev; the upper limit at 122 Kev. The 84-Kev gamma ray of Tm^{170} and the 122-Kev gamma ray of Co^{57} were used to calibrate the window settings each time the system was used. In addition, the Tm^{170} and Co^{57} γ rays, along with the 103-Kev peak in the γ- and X-ray spectrum of Gd^{153}, were used to give a sensitive indication of any drift during each counting session. Each set of foils was counted in at least four counting sessions.

Either the Np^{239} counting system or the fission product counting system, whichever was convenient, was used to measure the activity of the gold monitor foils. When the Np^{239} system was used, the 411-Kev peak in the γ-ray spectrum of Au^{198} was straddled with a window width of approximately 60 Kev. When the fission product system was used, the foils were integral counted with the base line set at the minimum between the 411-Kev peak and its Compton edge. Figure 2.2.7 shows the γ-ray spectrum of Au^{198}.

2.2.5 Experimental Procedure

For each experiment performed to measure the microscopic parameters, ρ_{28}, C^*, δ_{25} and δ_{28}, the following procedure was used. The uranium detector foils to be irradiated were chosen so as to have minimum weight differences among themselves. The foils were cleaned with acetone and mounted on aluminum planchets. The two counting systems, the Np^{239} counting system and the fission product counting system, were calibrated as described in Section 2.2.4. The natural uranium foils were background counted on the fission product counting system, and the depleted uranium foils were background counted on both the fission product counting system and the Np^{239} counting system to determine the natural and residual activities of the foils. An additional natural uranium foil and an additional depleted uranium foil, both of

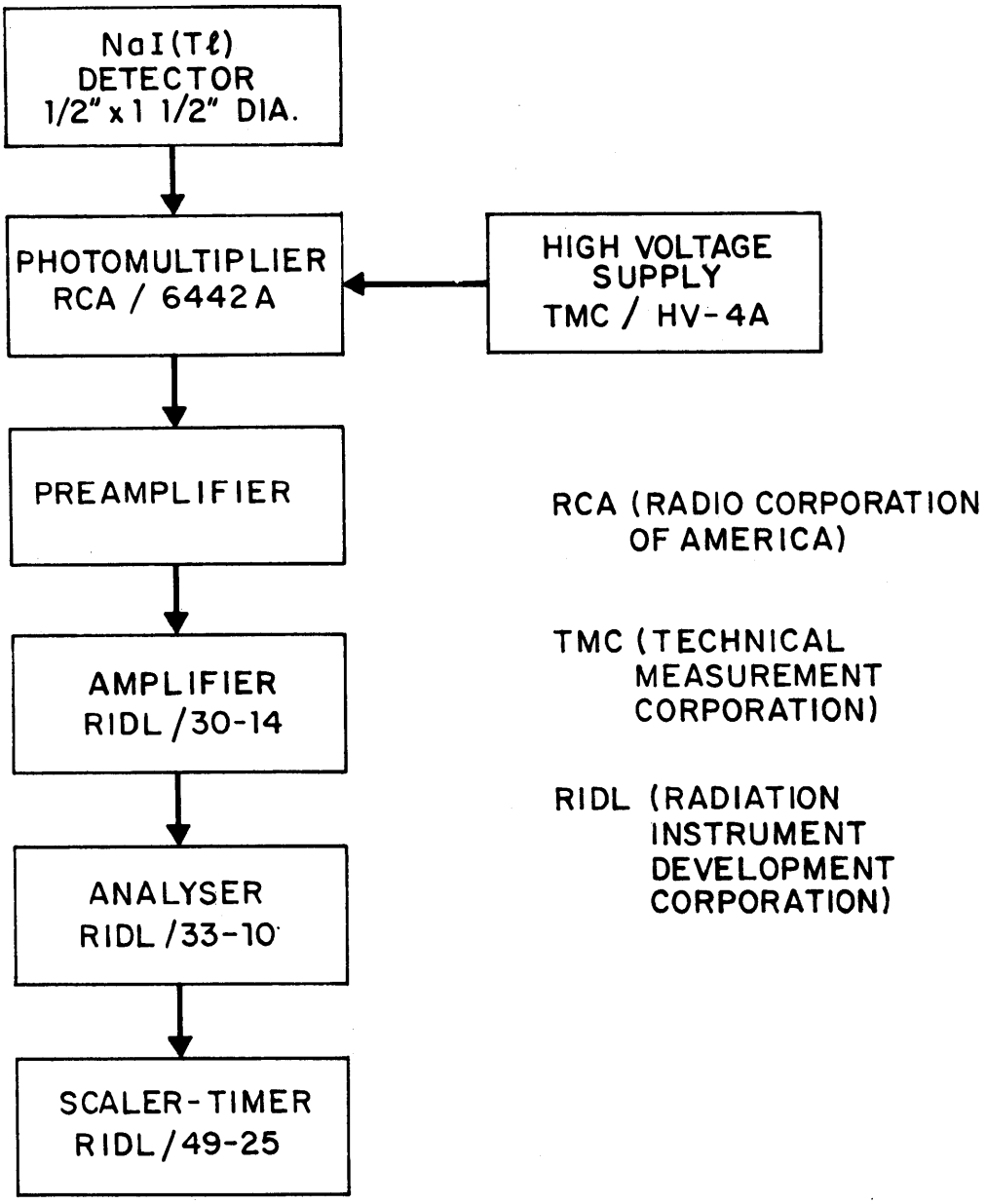

COUNTING SYSTEM USED TO MEASURE THE Np^{239} ACTIVITY OF THE DEPLETED URANIUM FOILS

FIG. 2.2.6

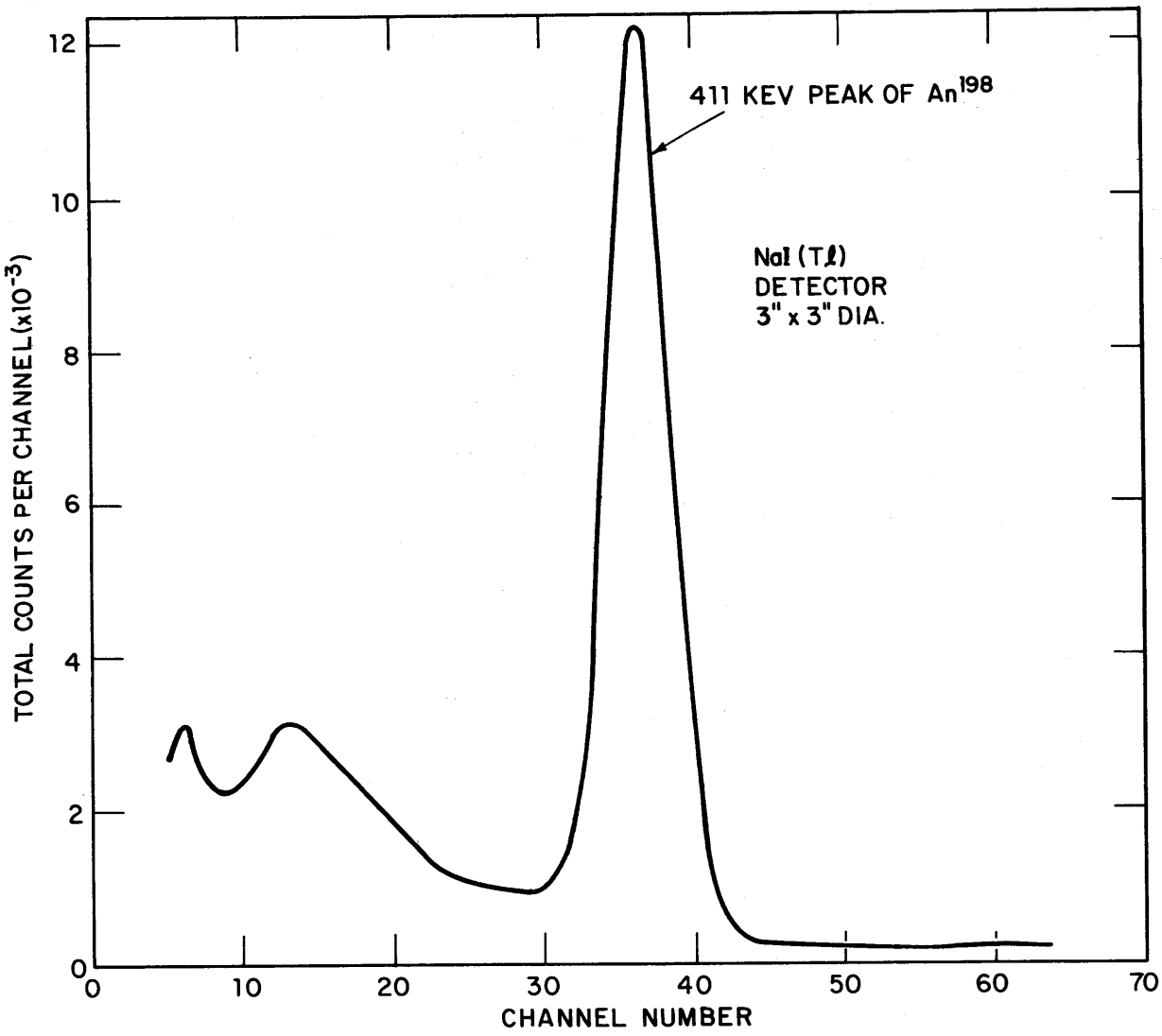

THE GAMMA RAY SPECTRUM OF Au^{198}

FIG. 2.2.7

which had irradiation histories similar to those of the detector foils, were also background counted. These additional foils were not irradiated and were counted with the detector foils each time they were counted after irradiation. This procedure provided a means of correlating the measured natural and residual activities of the uranium detector foils between the time the foils were background counted and the times they were counted after irradiation.

The uranium detector foils together with the necessary gold monitor foils were then loaded into the lattice fuel rods and the polyethylene rod for the cavity sample tube as described in Section 2.2.2. The polyethylene rod was inserted into the sample tube; the lattice fuel rods were washed with acetone, rinsed with D_2O and introduced into the exponential tank through the glove box arrangement described in Section 2.1. As a standard practice, twelve-hour irradiations were used when a measurement of δ_{28} was included in the experiment, because P(t) in the experimental formulation of δ_{28}, Eq. 2.2.4, is a function of the irradiation time. If δ_{28} was not measured, the irradiation times used varied from four hours to more than 24 hours, as was convenient for the particular experiment. After the irradiation was completed, the lattice was allowed to cool at least four hours before the fuel rods were removed. This cooling period, which was necessary before the foils were counted, also permitted the dose rates at the surface of the fuel rods to decay to an acceptable level for handling purposes (about 1r per hour). After the fuel rods and the polyethylene rod were removed from the exponential tank and the cavity sample tube, the detector foils were unloaded and cleaned with acetone; then each foil was remounted on the same aluminum planchet used to background count it before irradiation.

The fission product counting system was calibrated and all the uranium detector foils were fission product counted from about six hours to about 12 hours after completion of irradiation. The room background of the counting system and the unirradiated control background foils were counted several times during this period. The counting system was recalibrated after the counting session was completed to check for drift in the electronics.

The depleted uranium foils were Np^{239} counted as described in

Section 2.2.4 once or twice a day for several days after irradiation. The foils of each experiment were counted at least four times. Each time the foils were counted, the room background of the counting system and the control background foils were also counted.

The gold monitor foils were counted as described in Section 2.2.4. The activities of the gold monitor foils were always within the experimental error so that corrections to the uranium foil activities for differences in flux were not necessary.

2.2.6 Measurement of δ_{28}^* by La^{140} Counting

The reference value of the fast fission ratio, δ_{28}^*, used to determine the function P(t), was measured by means of the La^{140} counting technique developed by Wolberg et al. (W3). The experimental formulation for δ_{28}^*, derived in Ref. (W3), is:

$$\delta_{28}^* = \left(\frac{\beta^{25}}{\beta^{28}}\right)\left[\frac{EC \cdot a \cdot \Gamma - S}{1 - a \cdot \Gamma}\right], \tag{2.2.17}$$

where β^{25} and β^{28} are the yields of La^{140} from the fission of U^{235} and U^{238}, respectively, and

$$\Gamma = \frac{D_b^{140}}{N_b^{140}}. \tag{2.2.18}$$

The superscript 140 indicates that La^{140} activity was the measured activity.

To measure the value of Γ, bare foil packets were constructed and placed inside fuel rods in the exponential tank as described in Section 2.2.3. Typical positions for the foils were near the central rod radially and four to eight inches above the bottom of the fuel region axially so that the foils would be irradiated in a relatively high neutron flux. The foils were irradiated for about 100 hours and then allowed to cool for about a week. This cooling period allowed the La^{140}, which has a 40.2-hour half-life, to come into equilibrium with its precursor Ba^{140}, which has a 12.8-day half-life, and also permitted other fission product activity competing with the 1.60-Mev La^{140} gamma ray to decay (W3).

The La^{140} activity of the depleted and natural uranium foils was measured by counting the 1.60-Mev gamma ray with a system which consisted of an integral detector unit containing a 3-inch-thick, 3-inch-diameter NaI(Tl) crystal and photomultiplier tube, a preamplifier constructed by Mr. J. Renner, a Baird Atomic Model 312A high voltage supply, a Baird Atomic Model 215 linear amplifier and a Technical Measurements Corporation Model CN-110 256 channel pulse height analyzer containing a Model 210 plug-in unit. A diagram of the counting arrangement is shown in Fig. 2.2.8. A small sample of $La(NO_3)_3$, which was periodically irradiated in one of the pneumatic sample tubes of the MITR to produce 40.2-hour La^{140}, was used to calibrate the system.

The detector foils were counted between one week and five weeks after irradiation. It was found that 30-minute counting times for the natural uranium foil and 300-minute counting times for the depleted foils produced enough counts for acceptable counting statistics (10,000 or more total counts per foil). Before irradiation, both the depleted and natural detector foils were background counted along with an additional depleted uranium foil and an additional natural uranium foil, both of which had irradiation histories similar to those of the detector foils. These additional or "control background" foils were not irradiated and were counted each time the detector foils were counted after irradiation. This procedure provided a means of correlating the measured natural and residual activities of the uranium detector foils between the time they were background counted and the times they were counted after irradiation.

The relative La^{140} activity of the depleted uranium detector foil and the natural uranium detector foil were used to determine a value of δ^*_{28} via Eq. 2.2.17. Three of the nine determinations of δ^*_{28} were performed by Mr. H. Bliss (B1). An identical set of detector foils in an identical foil arrangement was irradiated in the same position as was used to measure δ^*_{28} to obtain a value of $\gamma(t)$ for that position. Then the function P(t) was determined via Eq. 2.2.5. Once P(t) had been evaluated, subsequent values of δ_{28} were determined by measuring $\gamma(t)$ and calculating δ_{28} from Eq. 2.2.4.

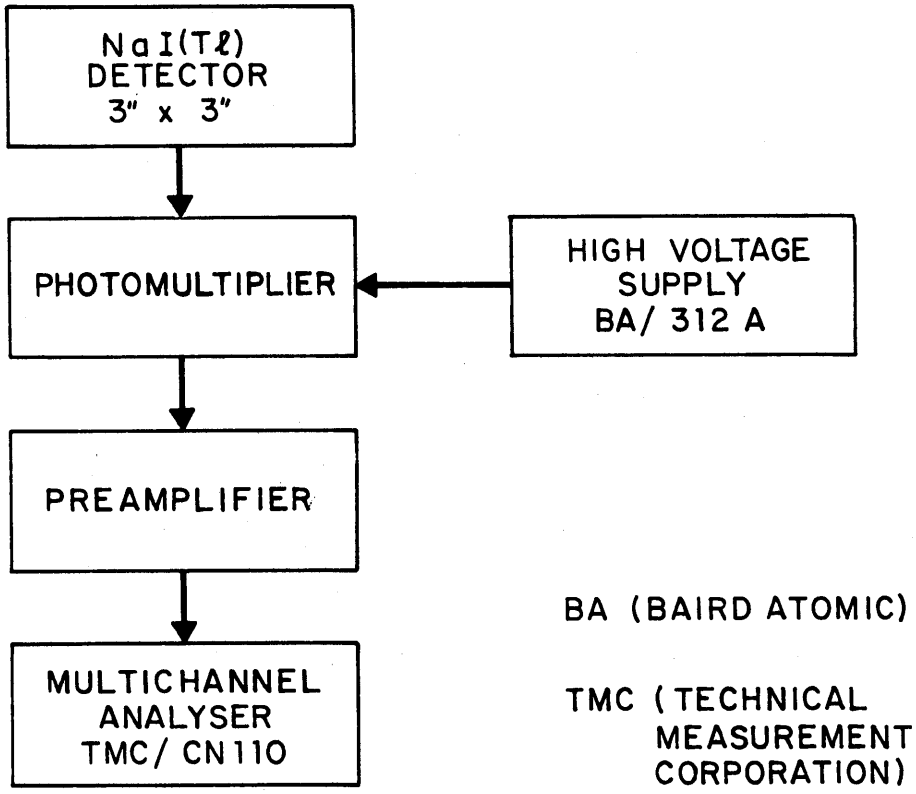

COUNTING EQUIPMENT USED TO MEASURE LA^{140} ACTIVITY

FIG. 2.2.8

2.2.7 Measurement of R_{Au} in the Fuel

The average gold-cadmium ratio in the fuel, R_{Au}, was measured in the three lattices studied. The same foil arrangement as described in Section 2.2.3 was used except that in each foil packet the uranium foils were replaced with three 0.005-inch-thick, 0.250-inch-diameter lead alloy foils containing 13.6% gold by weight. These Pb-Au foils whose absorption and scattering properties closely matched those of the fuel were prepared as described in Section 2.2.2. Inside the fuel rods, the foil packets containing the Pb-Au foils were placed adjacent to the foil packets containing the uranium foils for the microscopic parameter measurements. The Pb-Au foils were counted with the gold monitor foils as described in Section 2.2.4. The experimental procedure outlined in Section 2.2.5 was followed.

2.2.8 ρ_{28} and R_{Au} of a Single Rod in a $\frac{1}{E}$ Flux

Both ρ_{28} and R_{Au} were measured for a single fuel rod irradiated in the $\frac{1}{E}$ epithermal flux of position 13 of the MITR (see Section 2.1). A 3-inch-long section of a lattice fuel rod was placed in a standard MITR sample can and irradiated in the in-core sample thimble of position 13. Both bare and cadmium-covered foil arrangements, which were the same as those described in Sections 2.2.3 and 2.2.7, were located in the middle of the fuel rod sections. Figure 2.2.9 is a schematic drawing of the sample can showing the foil packet and fuel arrangement. To ascertain that both samples were irradiated in the same neutron flux, separate irradiations were made with the samples in the same position. For each run, a gold monitor foil was placed about three inches away from the sample to provide a means of intercalibrating the neutron dose between runs. The methods and experimental procedures for ρ_{28} and R_{Au} described in the preceding sections were used.

2.3 Measurement of the Intracellular Activation Distributions

The intracellular flux distribution was measured by using depleted uranium foils, irradiated both bare and cadmium-covered, and by using copper foils, both bare and cadmium-covered. The depleted uranium was

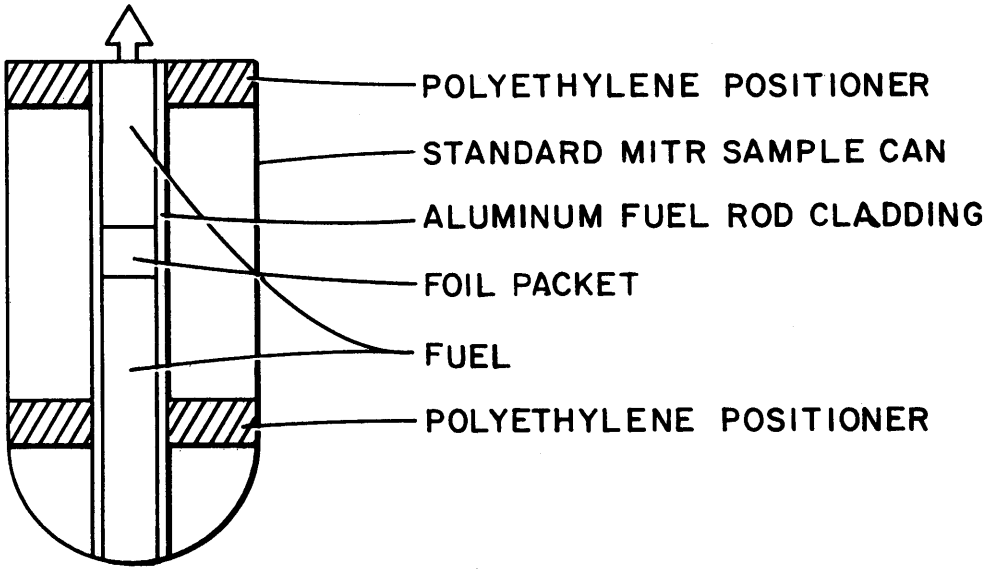

FUEL ROD AND FOIL PACKET ARRANGEMENTS FOR THE SINGLE ROD MEASUREMENTS IN THE MITR

FIG. 2.2.9

used to determine the intracellular distribution of the neutron flux captured by the U^{238}; the copper was used to estimate the neutron flux captured by the $\frac{1}{v}$ portion of the U^{238} cross section.

Both the depleted uranium foils and the copper foils were 0.005 inch thick and 1/16 inch in diameter. All foils of one element were punched from the same sheet of material with the same punch and die. The foils were weighed with an accuracy of about ±0.1% on a high-precision balance. The foils were arranged according to weight and placed in a plastic foil holder. Foils for a particular experiment were chosen so that the weight differences among them would be as small as possible.

The experimental methods for intracellular traverses developed by Brown et al. (B2) and Simms et al. (S1) were used. Inside the central fuel rod, the detector foils were placed in 1/16-inch-diameter, 0.012-inch-deep holes milled into the ends of 0.060-inch-thick fuel slugs. The foils were shielded with 0.001-inch-thick aluminum or 0.002-inch-thick Mylar tape to prevent the pickup of fission products. In the moderator, 0.012-inch-thick, aluminum foil holders were used for both the bare and cadmium-covered foils. A typical holder is shown in Fig. 2.3.1. The moderator holders were attached as shown in Fig. 2.3.2 to the three fuel rods of the removable central cluster. Figure 2.3.3 is a schematic diagram of the arrangement of the foil holders.

The activities of both the depleted uranium foils and the copper foils were measured with a gamma-counting system coupled with a Nuclear Chicago automatic sample changer, Model C-110B. The counting system consisted of an integral detector unit containing a 1/2-inch-thick, 1-1/2-inch-diameter NaI(Tl) crystal and an RCA 6342A photomultiplier tube, a Baird Atomic Model 312A high voltage supply, a Baird Atomic Model 215 linear amplifier, a Baird Atomic Model 510 single channel analyzer, a Nuclear Chicago Model 186 scaler, and a Nuclear Chicago Model 111B printing timer. A block diagram of the system is shown in Fig. 2.3.4. The copper foils were counted by straddling the 510-Kev peak in the γ-ray spectrum of Cu^{64} with a window width of 60 Kev.

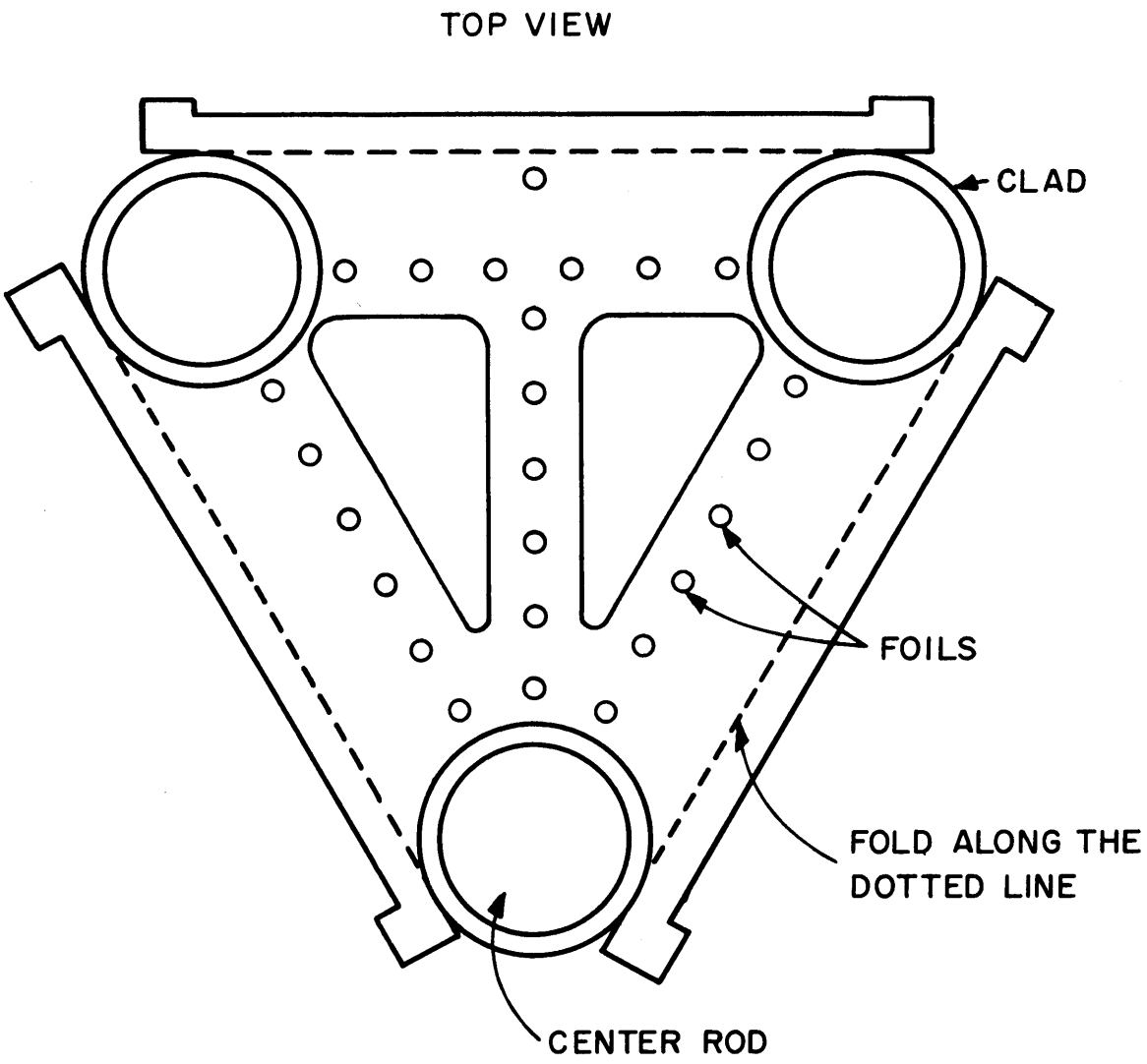

MODERATOR FOIL HOLDER FOR THE
INTRACELLULAR TRAVERSES

FIG. 2.3.1

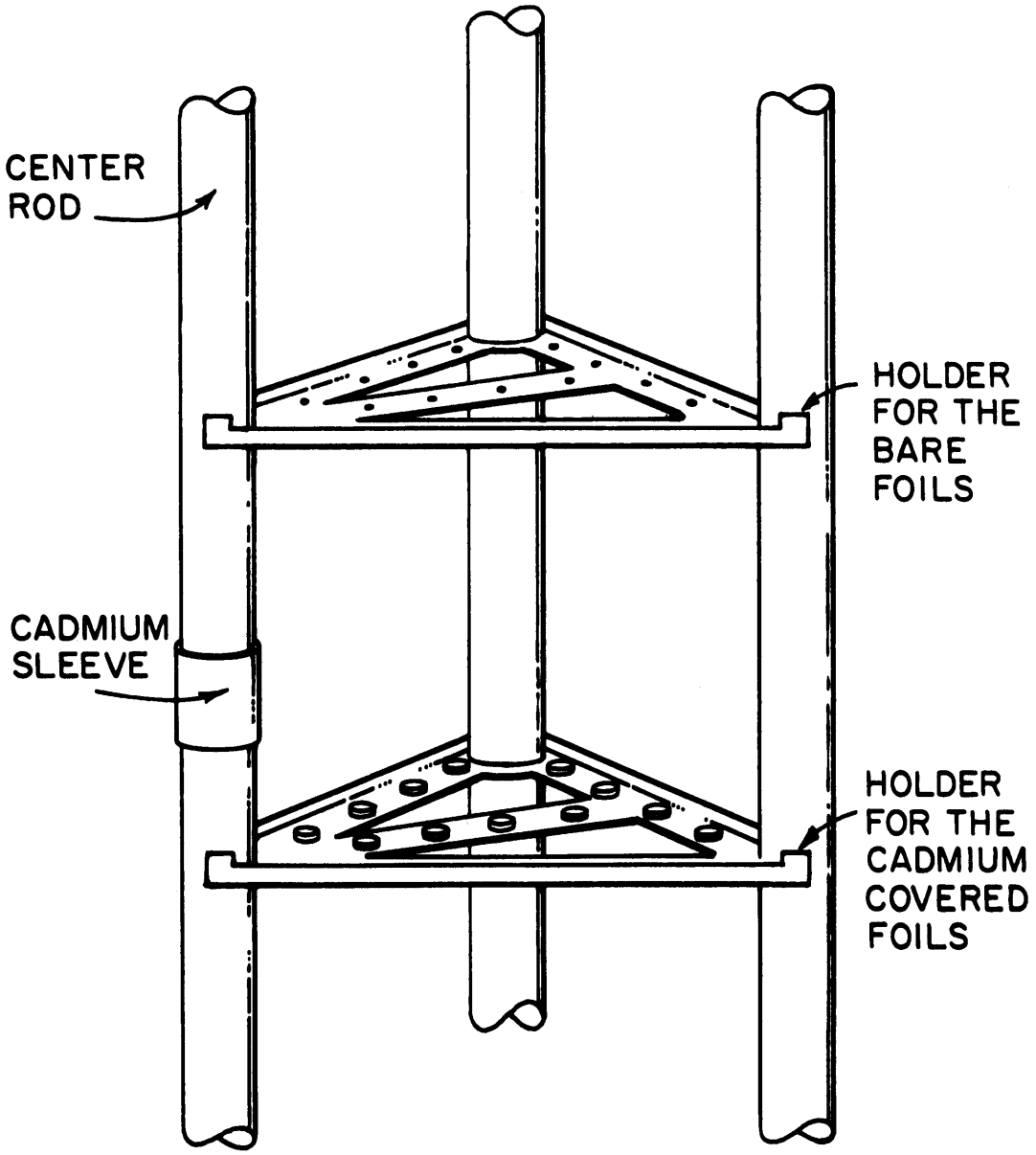

REMOVABLE THREE ROD CLUSTER
ARRANGEMENT FOR THE INTRACELLULAR
TRAVERSES

FIG. 2.3.2

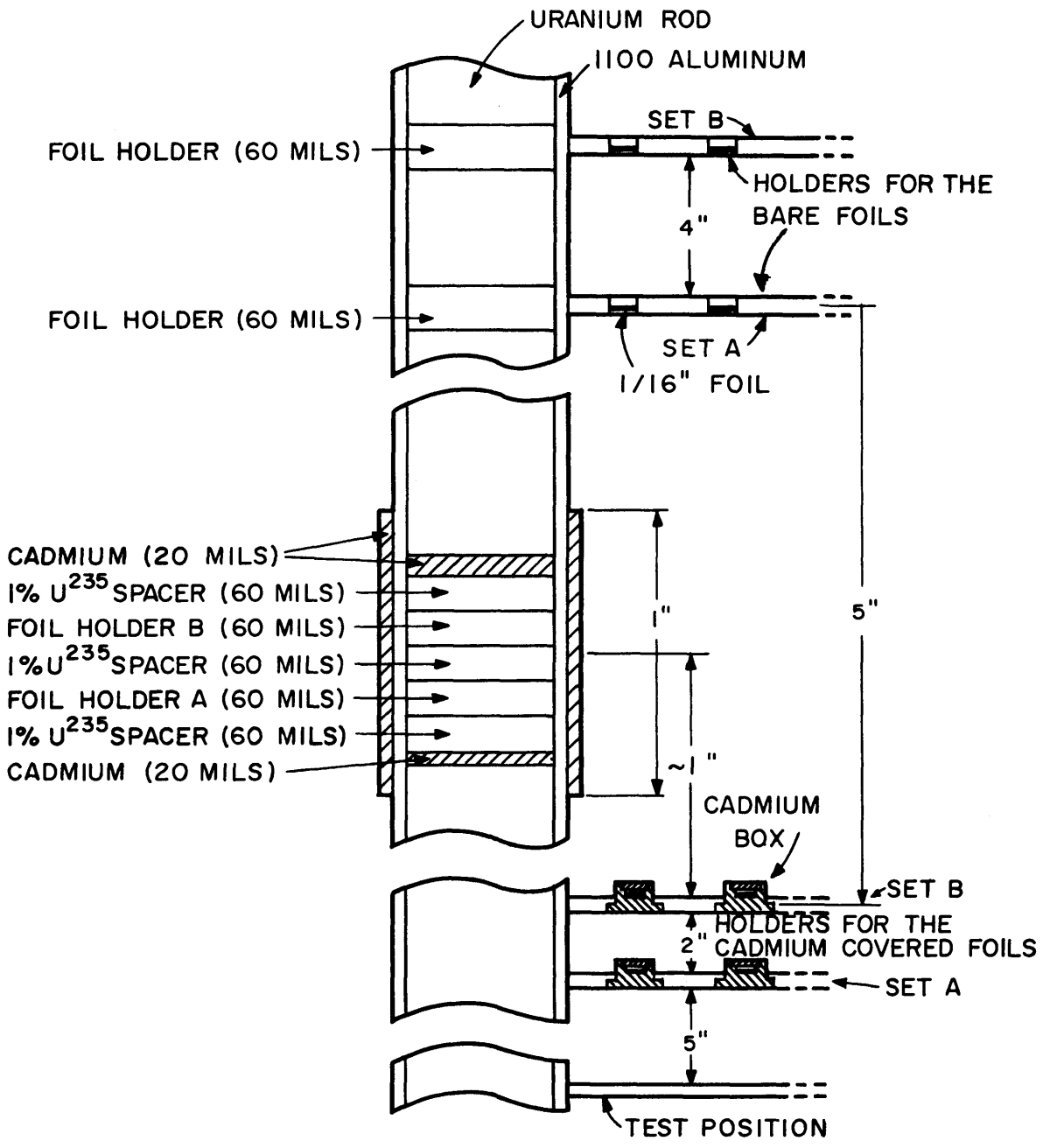

FOIL HOLDER ARRANGEMENTS FOR THE INTRACELLULAR TRAVERSES

FIG. 2.3.3

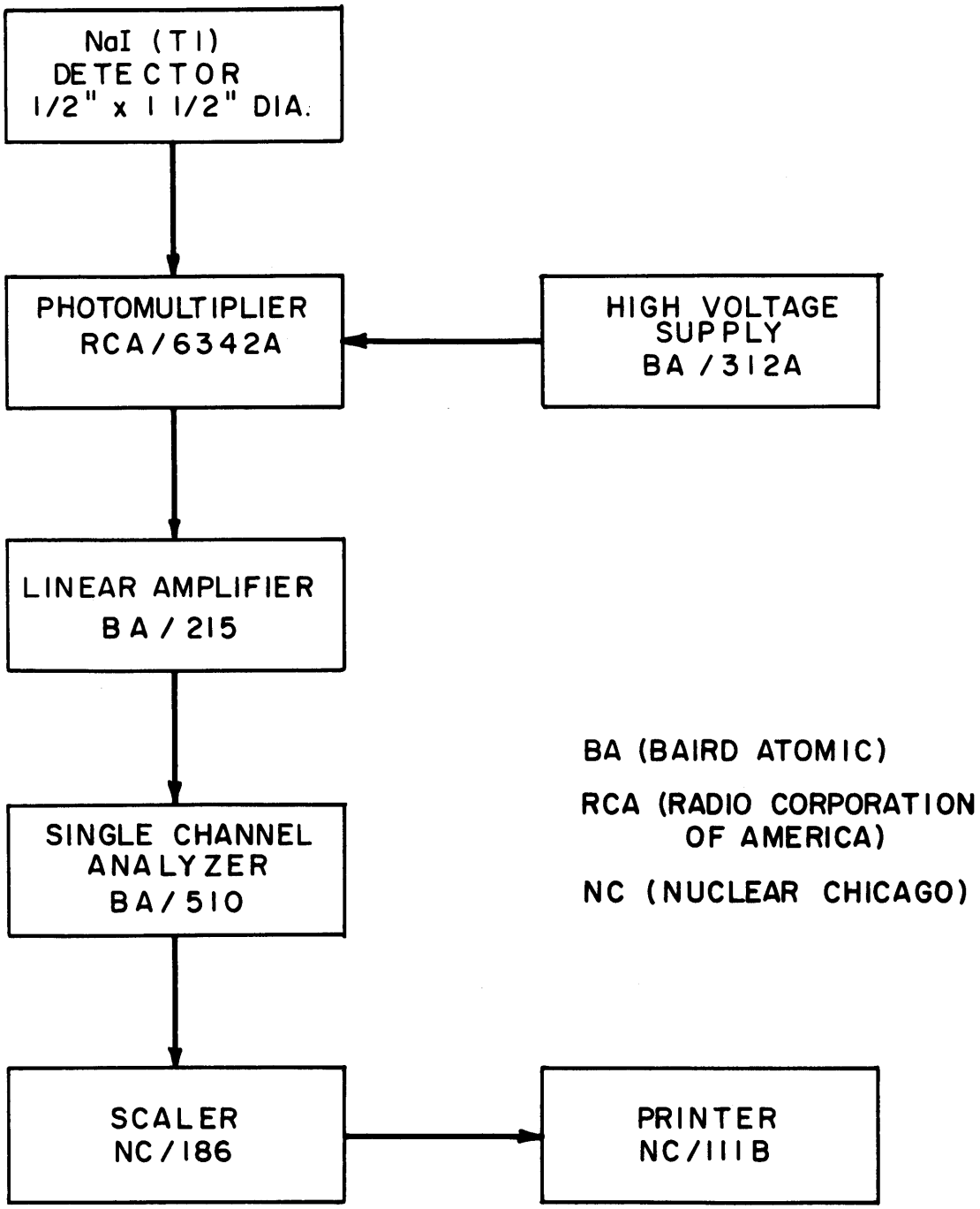

COUNTING SYSTEM USED TO MEASURE Cu^{64} AND Np^{239} ACTIVITIES FOR THE INTRACELLULAR TRAVERSES.

FIG. 2.3.4

The depleted uranium foils were counted, as described in Section 2.2.4, by straddling the 103-Kev peak in the Np^{239} γ-ray spectrum with the lower and upper limits of the analyzer window set at 84 Kev and 122 Kev, respectively.

2.4 Methods of Measuring Resonance Activation

In connection with one of the objectives of this work, which was to seek new measurements to make and new methods of making existing measurements in the area of interest, the investigation of the resonance energy region was extended by irradiating several nuclides, which have large resonance integrals, in the moderator of the 1.75-inch lattice and measuring the resonance activity of these nuclides. The resonance activity of a nuclide is that portion of its activity due to neutrons captured by resonances in the activation cross section of the nuclide. In Chapter VI the resonance activities of these nuclides will be related to the slowing-down density in the moderator which will then, in turn, be used in a new approach to the calculation of the resonance escape probability, p. Other potential uses of the resonance activities, including the determination of the effective resonance integral of U^{238}, will also be discussed in Chapter VI.

The measured activity of a nuclide, a, may be expressed as follows:

$$A^a = \varepsilon^a \int_{E_o}^{\infty} \sigma^a_{res}(E)\, \phi(E)\, dE + \varepsilon^a \int_{E_o}^{\infty} \sigma^a_{1/v}(E)\, \phi(E)\, dE\,, \tag{2.4.1}$$

or

$$A^a = A^a_{res} + A^a_{1/v} = \varepsilon^a \left[RI^a \phi^a_{res} + \sigma^a_o \phi_{1/v} \right], \tag{2.4.2}$$

where

$$RI^a \phi^a_{res} = \int_{E_o}^{\infty} \sigma^a_{res}(E)\, \phi(E)\, dE\,, \tag{2.4.3}$$

$$\sigma^a_o \phi_{1/v} = \int_{E_o}^{\infty} \sigma^a_{1/v}(E)\, \phi(E)\, dE\,, \tag{2.4.4}$$

and ε^a is a factor containing the counting efficiency, nuclide concentration, etc.; the subscripts res and $\frac{1}{v}$ refer to the resonance and $\frac{1}{v}$ portions

of the activation; σ_o is the 2200 meter per second activation cross section; and the superscript, a, refers to the nuclide. The lower limit E_o on the integrals in Eq. 2.4.1 will be zero in the case of a bare foil and approximately 0.4 ev in the case of a cadmium-covered foil. Now, if a second nuclide, b, which closely approximates a pure $\frac{1}{v}$ absorber so that its resonance activity is negligible, is irradiated in an equivalent position, then:

$$A^b = A^b_{1/v} = \epsilon^b \sigma^b_o \phi_{1/v} , \tag{2.4.5}$$

and, using Eqs. 2.4.4 and 2.4.5:

$$A^a_{res} = A^a - A^a_{1/v} = A^a - \frac{A^a_{1/v}}{A^b_{1/v}} A^b = A^a - \alpha A^b . \tag{2.4.6}$$

If A^a_{res} is negligible below about 0.1 ev, then the proportionality constant α can be determined by irradiating the nuclides a and b in a pure Maxwellian neutron flux.

Since it is difficult to measure accurately the absolute activity of a nuclide, it is desirable to perform the irradiations in such a way that only ratios of the relative activities for a particular nuclide need be measured. This can be done by means of cadmium ratio measurements or by making use of an auxiliary irradiation position. For irradiations performed in the lattice in the exponential tank, the cavity sample tube provided an ideal auxiliary position for the following reasons:

1. Both facilities (the exponential tank and the cavity sample tube) have the same source of neutrons, and thus the ratio of the neutron flux levels in the two facilities will be a constant for all irradiations performed for a particular lattice.
2. Irradiations in both facilities are begun at the same time and ended at the same time.
3. The energy spectrum in the cavity sample tube closely approximates a Maxwellian spectrum; the cavity sample tube can, therefore, be used both for making the relative measurements mentioned above and for determining the proportionality constant α.

4. The flux levels in the exponential tank and the cavity sample tube are of the same order of magnitude so that activities of the same order of magnitude will be obtained from simultaneous irradiations.

The activities of nuclides a and b irradiated in the exponential tank and in the cavity sample tube can be expressed as follows:

$$A_b^a = \varepsilon^a\left(RI^a \phi_{res}^a + \sigma_o^a \phi_{1/v}\right) ; \tag{2.4.7}$$

$$A_b^b = \varepsilon^b \sigma_o^b \phi_{1/v} ; \tag{2.4.8}$$

$$A_H^a = \varepsilon^a \sigma_o^a \phi_H ; \tag{2.4.9}$$

$$A_H^b = \varepsilon^b \sigma_o^b \phi_H ; \tag{2.4.10}$$

where the subscript H refers to the cavity or "hohlraum" sample tube and the subscript b refers to an irradiation of bare foils in the exponential tank. Using Eqs. 2.4.7 to 2.4.10, we obtain:

$$R_b^a = \frac{A_b^a}{A_H^a} = \frac{\left(\frac{RI}{\sigma_o}\right)^a \phi_{res}^a + \phi_{1/v}}{\phi_H} ; \tag{2.4.11}$$

$$R_b^b = \frac{A_b^b}{A_H^b} = \frac{\phi_{1/v}}{\phi_H} ; \tag{2.4.12}$$

$$R_b^a - R_b^b = R_{res}^a = \frac{A_{res}^a}{A_H^a} = \left(\frac{RI}{\sigma_o}\right)^a \frac{\phi_{res}^a}{\phi_H} ; \tag{2.4.13}$$

and thus:

$$\frac{\phi_{res}^a}{\phi_H} = \frac{R_{res}^a}{\left(\frac{RI}{\sigma_o}\right)^a} = \frac{R_b^a - R_b^b}{\left(\frac{RI}{\sigma_o}\right)^a} . \tag{2.4.14}$$

If we now assume that the resonance integral of nuclide a is due to one large narrow resonance at energy E_a, then we can assume that:

$$\phi^a_{res} = \phi(E_a) \ , \tag{2.4.15}$$

and Eq. 2.4.14 is then a measure of the neutron flux at energy E_a in the lattice relative to the flux in the cavity sample tube. By irradiating nuclides a and b in the exponential tank with cadmium covers and assuming A^a_{res} is zero below the cadmium cutoff, we get an expression analogous to Eq. 2.4.14:

$$\frac{\phi^a_{res}}{\phi_H} = \frac{\left[\frac{A^a_c}{A^a_H} - \frac{A^b_c}{A^b_H}\right]}{\left(\frac{RI}{\sigma_o}\right)^a} = \frac{R^a_{res}}{\left(\frac{RI}{\sigma_o}\right)^a} = \frac{R^a_c - R^b_c}{\left(\frac{RI}{\sigma_o}\right)^a} \ , \tag{2.4.16}$$

where the subscript c refers to an irradiation of cadmium-covered foils in the exponential tank. The cadmium ratios of nuclides a and b in the exponential tank furnish a third approach to attain ϕ^a_{res}. The cadmium ratio of a in the exponential tank, R^a_L, is:

$$R^a_L = \frac{A^a_b}{A^a_c} = \frac{RI^a\phi^a_{res} + \sigma^a_o\phi_{1/v,SC} + \sigma^a_o\phi_{1/v,EC}}{RI^a\phi^a_{res} + \sigma^a_o\phi_{1/v,EC}} \ , \tag{2.4.17}$$

where the subscripts SC and EC refer to the subcadmium and epicadmium portions of the spectrum. On rearranging terms, Eq. 2.4.17 becomes:

$$\rho^a = \left(R^a_L - 1\right)^{-1} = \frac{\left(\frac{RI}{\sigma_o}\right)^a \phi^a_{res} + \phi_{1/v,EC}}{\phi_{1/v,SC}} \ . \tag{2.4.18}$$

Analogously we can obtain the following expression for nuclide b:

$$\rho^b = \left(R^b_L - 1\right)^{-1} = \frac{\phi_{1/v,EC}}{\phi_{1/v,SC}} \ , \tag{2.4.19}$$

and, combining Eqs. 2.4.18 and 2.4.19:

$$\rho^a - \rho^b = \left(\frac{RI}{\sigma_o}\right)^a \frac{\phi^a_{res}}{\phi_{1/v,SC}} \ , \tag{2.4.20}$$

or

$$\frac{\phi^{a}_{res}}{\phi_{1/v,SC}} = \frac{\left(\rho^{a}-\rho^{b}\right)}{\left(\frac{RI}{\sigma_o}\right)^{a}} . \qquad (2.4.21)$$

Thus Eqs. 2.4.14, 2.4.16, and 2.4.21 provide three methods to obtain the relative resonance energy neutron flux at various energies which can then be related to the slowing-down density at those energies, or, knowing the relative flux, any of the three equations can be used to determine the ratio $\left(\frac{RI}{\sigma_o}\right)$ which suggests a method of determining the effective resonance integral of U^{238} in a lattice.

Both bare and cadmium-covered resonance detector foils were irradiated in the moderator of the lattice in the exponential tank and, simultaneously, identical foils were irradiated in the cavity sample tube to provide a means of normalizing between runs and between different foil materials. Since the epithermal flux spectrum in the in-core sample thimble at position 13 of the MITR varies very nearly as $\frac{1}{E}$, both bare and cadmium-covered foils were irradiated at that position to serve as references to which measurements in the lattice could be compared. From these irradiations, four ratios were measured for each nuclide: the cadmium ratio, R_R, in position 13 of the MITR; the cadmium ratio, R_L, in the moderator of the lattice; the ratio, R_b, of the bare foil in the lattice to the activity of the foil in the cavity sample tube; and the ratio, R_c, of the activity of the cadmium-covered foil in the lattice to the activity of the foil in the cavity sample tube.

In selecting suitable nuclides as resonance detectors to carry out these resonance activation measurements, the following characteristics were sought:

1. The ratio of the activation resonance integral to the activation cross section at 2200 meters per second, $\frac{RI}{\sigma_o}$, should be large to maximize the resonance activity relative to the $\frac{1}{v}$ activation. (If $\frac{RI}{\sigma_o}$ is 0.5, then the resonance activation will be equal to the epicadmium $\frac{1}{v}$ activation.)

2. The resonance activation should be due almost entirely to a single dominant resonance.
3. The resonance integral and the resonance cross section parameters should be known.
4. Other isotopes should not produce significant competing activities.
5. The half-life of the activity produced should be long enough (about 1/2 hour, depending on the cross section and the isotopic abundance) to allow time to remove the foils from the exponential tank and prepare them for counting before the activity has decayed to too low a level to obtain acceptable count rates.
6. The combination of cross section, isotopic abundance, and half-life should be such that sufficient activity can be produced in the exponential tank to obtain suitable count rates.

The initial selection of the nuclides was made on the basis of the characteristics 1 to 4. This group of nuclides was then irradiated in the lattice to determine which nuclides satisfied the conditions 5 and 6. If the dominant resonance of one or more acceptable nuclides had nearly the same energy as the dominant resonance of another nuclide, only one of the nuclides was selected. If the element containing a chosen nuclide was not available or not acceptable (because of some of the reasons listed below) in the uncombined form, compounds or alloys of the element were chosen on the following basis:

1. The combining elements, if any, should not produce significant competing activities.
2. The compound or alloy should not be harmful to the lattice facility.
3. The compound or alloy should not be soluble in water.
4. If possible, the material should be inexpensive and readily available.

The nuclides finally chosen for the measurements are listed with their properties in Table 2.4.1. Sodium, which is also listed in Table 2.4.1, has an extremely small resonance integral (only 3% of its epicadmium

TABLE 2.4.1

Properties of Resonance Detectors

Resonance Detector Nuclide	Chemical and Physical Form	Natural Elemental Abundance	2200 m/s Activation Cross Section, σ_o, barns	Ratio of Total Resonance Integral to σ_o, $\frac{TRI}{\sigma_o}$ [a]	Peak Energy of Dominant Resonance E_o, ev	Half-life $T_{1/2}$	Active Nuclide Produced
In^{115}	In powder	95.84%	155	12.8	1.457	54m	In^{116m}
Au^{197}	3 w/o Au in Al alloy	100%	98.8	15.8	4.906	2.7d	Au^{198}
W^{186}	W powder	28.7%	35	10	18.8	24h	W^{187}
I^{127}	NH_3I powder	100%	7.0	18.6	20.5	25m	I^{128}
As^{75}	As_2O_3 powder	100%	4.3	8.56	47	26.6h	As^{76}
Ga^{71}	Ga_2O powder	40%	5.1	2.94	95	14.2h	Ga^{72}
Br^{81}	NH_3Br powder	49.4%	3.3	18.7	101.2	35.9h	Br^{82}
Mn^{55}	MnO_2 powder	100%	13.2	1.17	337	2.58h	Mn^{56}
Cu^{63}	CuO powder	69.1%	4.5	0.98	580	12.8h	Cu^{64}
Na^{23}	Na_2CO_3 powder	100%	0.5	0.515	2850	15h	Na^{24}

[a] Data for the values of the total resonance integrals (which include the epicadmium 1/v contribution) were obtained from Refs. (M2) and (P3).

activity is due to resonance activation) and it was used to approximate a $\frac{1}{v}$ detector. Since the activity of main interest was the epicadmium activity, thin foils were used to minimize self-shielding and thus maximize the resonance activation relative to the $\frac{1}{v}$ activation.

2.4.1 Foil Preparation

Foils of the alloy of three weight per cent gold in aluminum, which were 0.0035 inch thick and 0.250 inch in diameter, were fabricated in the same manner as were the uranium detector foils described in Section 2.2.3.

Foils of the powdered materials were made by dipping 0.250-inch-diameter foils of Mylar tape in the powder to obtain a thin, uniform layer of powder clinging to the adhesive side of the tape. The powder was ground with a mortar and pestle to ensure that it was fine and uniform. This foil was then sandwiched between two 0.375-inch-diameter Mylar tape foils to seal in the powder. Figure 2.4.1 shows the construction of the powder foils.

2.4.2 Foil Arrangements

In the exponential tank, the foils were irradiated both bare and cadmium-covered. The cadmium box used for the cadmium-covered foils, shown in Fig. 2.4.2, was made of 0.020-inch-thick cadmium. The bare foils were contained in identical boxes made of 0.020-inch-thick Type 1100 aluminum. Both types of boxes were made watertight by sealing them around the edge with epoxy resin. The foils were positioned in the moderator by means of foil holders of 0.012-inch-thick Type 1100 aluminum. For each material, both the bare and cadmium-covered foils were irradiated at positions equidistant from the surrounding fuel rods, in equivalent positions in the exponential tank at least 16 inches above the bottom of the fuel region. Figure 2.4.3 shows the resonance detector foil arrangement in the exponential tank.

In the cavity sample tube, bare foils of each material were attached with Mylar tape to the polyethylene rod 18 inches from the end closest to the cavity.

Standard MITR irradiation sample cans were used for the

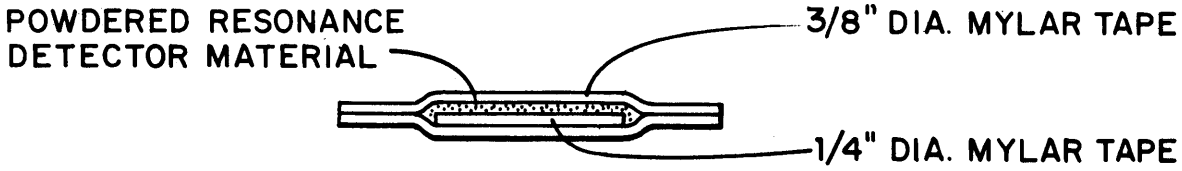

FIG. 2.4.1 CROSS SECTIONAL VIEW OF THE POWDER FOILS

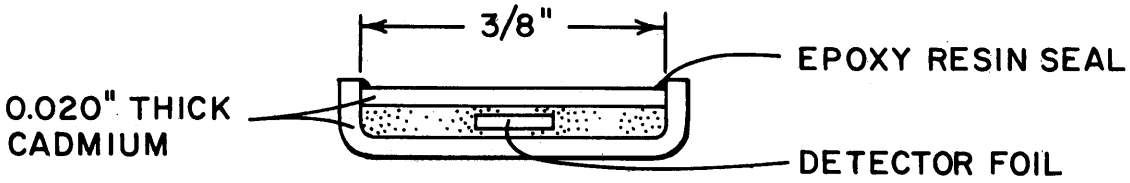

FIG. 2.4.2 CADMIUM BOX USED FOR RESONANCE DETECTOR FOILS

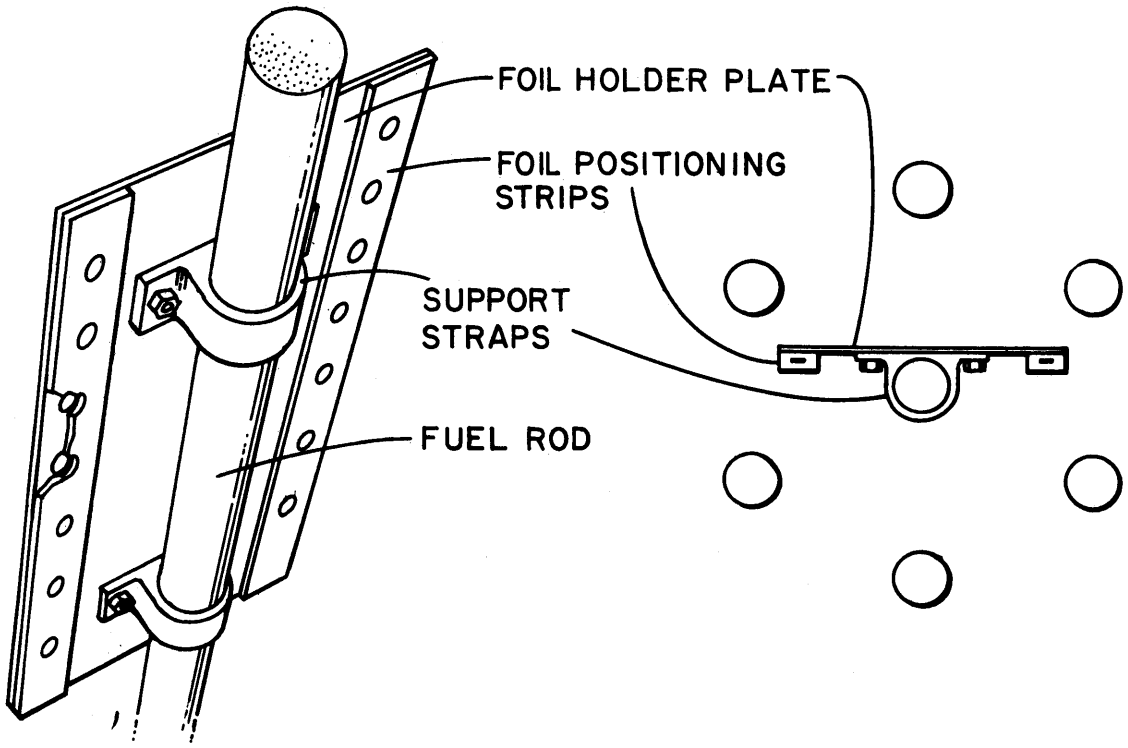

RESONANCE DETECTOR FOIL ARRANGEMENT IN THE EXPONENTIAL TANK

FIG. 2.4.3

measurements performed in position 13. Separate cans were used for the bare foils and the cadmium-covered foils; the can for the latter was lined with 0.020-inch-thick cadmium.

2.4.3 Counting Methods

After irradiation, the gamma activity of the foils was measured with the same counting setup, described in Section 2.2.6, used to measure La^{140} activity. Each foil was counted several times and the decay of the measured activity was checked to ensure that it had the proper half-life. The foils were intercalibrated by irradiating foils of each material simultaneously at the same position in the cavity sample tube and comparing the measured activities. The 256 channel analyzer of this system eliminated the need for doing a time-consuming calibration for each material and permitted examination of the gamma-ray spectra for the presence of competing activities. During each counting session, room background and a Co^{60} source were often counted; counting the Co^{60} provided a check for drift in the electronics.

2.4.4 Experimental Procedure

With the versatility, speed and ease of operation of the counting system permitted by the multichannel analyzer, much more latitude in planning and performing the experiments was permitted. Several nuclides with similar half-lives were irradiated in one run; the irradiation times ranged from about one hour for nuclides with short half-lives to one week for nuclides with very long half-lives. Extra care in handling the powder foils was exercised to keep them clean, since they could not be cleaned with acetone.

CHAPTER III
INVESTIGATION OF SYSTEMATIC ERRORS

Introduction

This chapter describes the investigations of systematic errors associated with the experimental methods (described in Chapter II) used to measure the microscopic parameters, ρ_{28}, C^*, δ_{25} and δ_{28}. First, the sources of systematic error are considered; then the methods used and results obtained in each investigation are given. Finally, the results of the error investigations are summarized and their relations to the experimental methods of Chapter II are discussed.

3.1 Sources of Systematic Error

Corrections to compensate for common sources of systematic error are made routinely. Such sources include counter dead time and pulse pile-up, variation of foil weights and foil thicknesses, exponential decay of activity, room background in the counting system, natural and residual activities of uranium foils, different foil positions during irradiations, etc. Other common sources of error, which cannot be corrected for easily, are avoided if possible; some examples are counter gain shift, photomultiplier fatigue, and variation in counting arrangement.

There are, however, some "uncommon" sources of error which are peculiar to the particular experiments being performed, and we shall be mostly concerned with these. First, these sources must be recognized. That this is not easy is indicated by the fact that "new" systematic errors can be uncovered in such "old" experiments as the measurements of ρ_{28} or δ_{28}. Systematic errors which were once neglected may become significant because of the higher precision resulting from improvements in the measurements, or because of modifications in the experiments such as changes in fuel rod size or U^{235}

concentration of the fuel.

Systematic errors associated with the measurement of the microscopic lattice parameters can be introduced by the following factors:

1. The measurements are not made in an equilibrium neutron spectrum.
2. The neutron flux is perturbed by the introduction of "foreign" experimental materials into the lattice.
3. The over-all counting efficiency varies from foil to foil.
4. Competing activities are present.

One of the aims of the present work has been to eliminate these errors or to establish appropriate corrections where the sources of error cannot be removed entirely.

3.2 Methods of Investigation

To determine which of the possible sources of error were significant, all of the error sources considered were investigated experimentally. When feasible, the effects due to factors that might introduce errors were observed directly; otherwise, the effects were determined indirectly. The investigation into the effect of the position in the lattice at which measurements were made is an example of direct observation, while the effect of a depression of the fast flux caused by the presence of cadmium on the values of δ_{25} and ρ_{28} is an example of an indirect determination.

3.2.1 Effect of Lattice Position

Values of microscopic parameters measured in an exponential assembly are to be related to the values of the parameters in a critical lattice. Although useful measurements can be made in neutron energy spectra which are not characteristic of the critical lattice (P2), the interpretation of the measurements is greatly simplified if they are made in a characteristic or "asymptotic" spectrum, that is, one free of source or edge effects.

The parameters, ρ_{28}, C^*, δ_{25}, and δ_{28}, were measured as functions of position in the lattice to see if they were independent of position over a significant portion of the lattice. The existence of a region of the lattice

in which such independence is found is taken to mean that a satisfactory approximation to an equilibrium or "asymptotic" neutron energy spectrum does indeed exist in the lattice. Axial and radial distributions of ρ_{28}, δ_{25}, and δ_{28} were determined in the 1.75-inch lattice and in the 2.50-inch lattice. The distributions of δ_{25} and δ_{28} were measured by Mr. H. Bliss (B1). The foil arrangements for these measurements were the same as those described in Section 2.2.3. For the axial distributions, foils were placed in two diametrically opposite rods adjacent to the central rod of the lattice. The foil packets were separated by 4-inch-long fuel slugs and were located at heights between 4 and 28 inches from the bottom of the fuel region. For the radial distributions, foils were placed at a height of 20 inches in rods adjacent to the central row of rods. Figure 3.2.1 shows the fuel rod and foil arrangements. The experimental procedure and the counting methods of Chapter II were followed.

The results of these measurements are shown in Figs. 3.2.2 to 3.2.7. The measured values of ρ_{28} and δ_{25} were constant axially between 16 and 28 inches from the bottom of the fuel region and radially from the center of the lattice to within four inches of the tank wall. The constancy of these parameters over a large fraction of the volume of the lattice indicates that the results may safely be assumed to be the same as those that would be obtained in a critical assembly or actual reactor. These results are consistent with the results of buckling measurements in which the same values of the radial and axial bucklings were obtained with different materials and with cadmium-covered foils (K2). The results also agree qualitatively with the theory of small assemblies developed by Peak et al. (P2) which predicted that the asymptotic region would begin at a height of about 16 inches. Figures 3.2.6 and 3.2.7 indicate that, within the experimental uncertainties, δ_{28} is independent of lattice position. This result is not surprising since δ_{28} is mainly a "local" effect; the spatial distribution of the fast neutron flux is nearly the same as the thermal neutron distribution because the distance which fast neutrons diffuse after originating from thermal fission is relatively short (two to five inches).

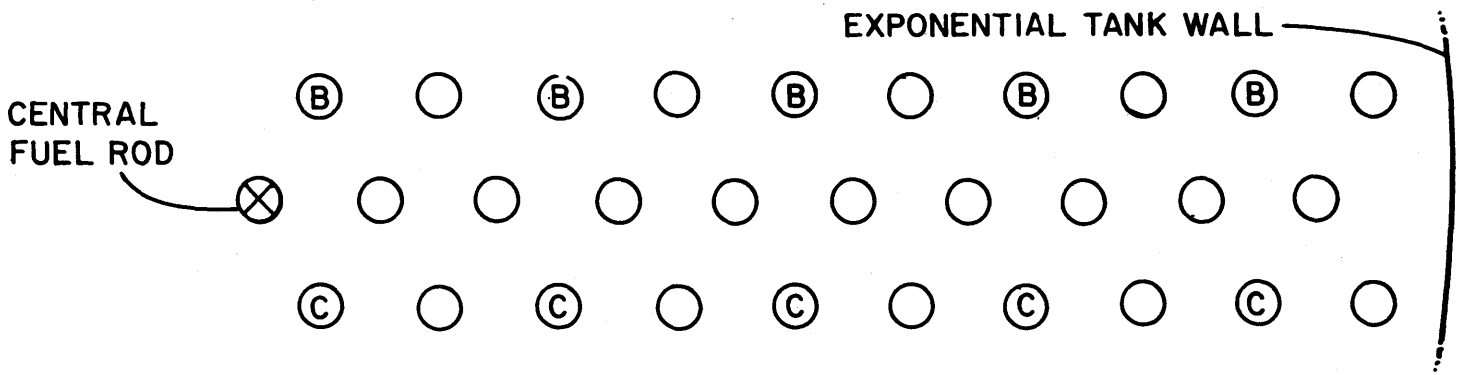

(a) FUEL ROD LOCATIONS FOR RADIAL DISTRIBUTIONS

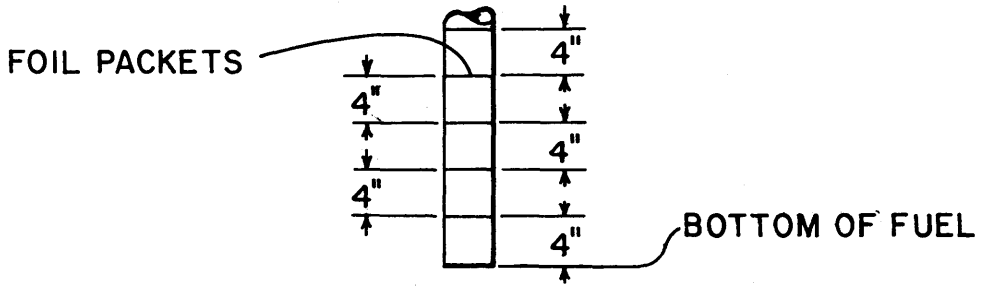

(b) FOIL PACKET LOCATIONS FOR AXIAL DISTRIBUTIONS

FUEL ROD AND FOIL PACKET ARRANGEMENTS FOR THE AXIAL AND RADIAL DISTRIBUTIONS OF THE MICROSCOPIC PARAMETERS

FIG. 3.2.1

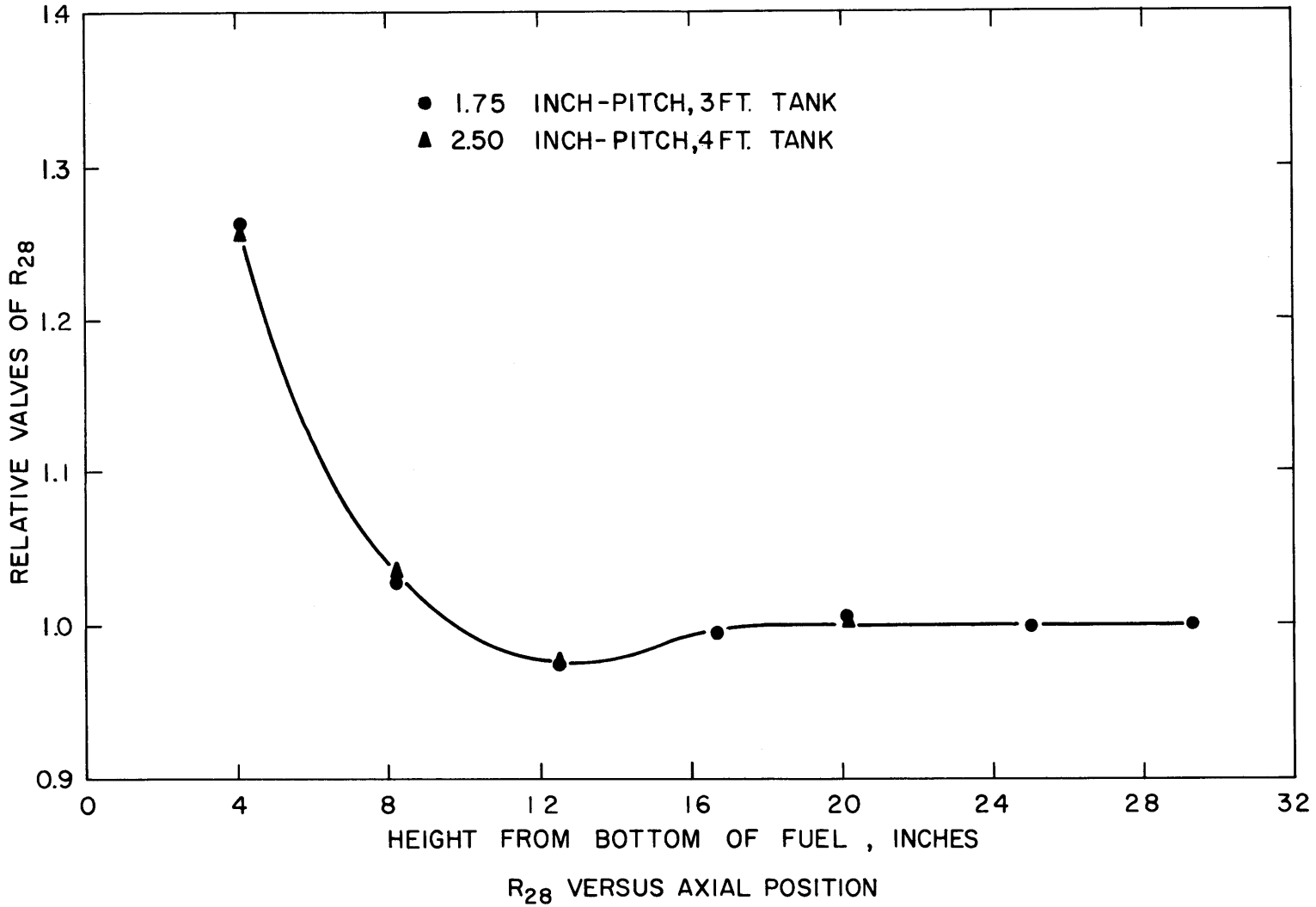
1.4
1.3
1.2
1.1
1.0
0.9
RELATIVE VALVES OF R_{28}
● 1.75 INCH-PITCH, 3FT. TANK
▲ 2.50 INCH-PITCH, 4FT. TANK
0
4
8
12
16
20
24
28
32
HEIGHT FROM BOTTOM OF FUEL , INCHES
R_{28} VERSUS AXIAL POSITION

FIG. 3.2.2

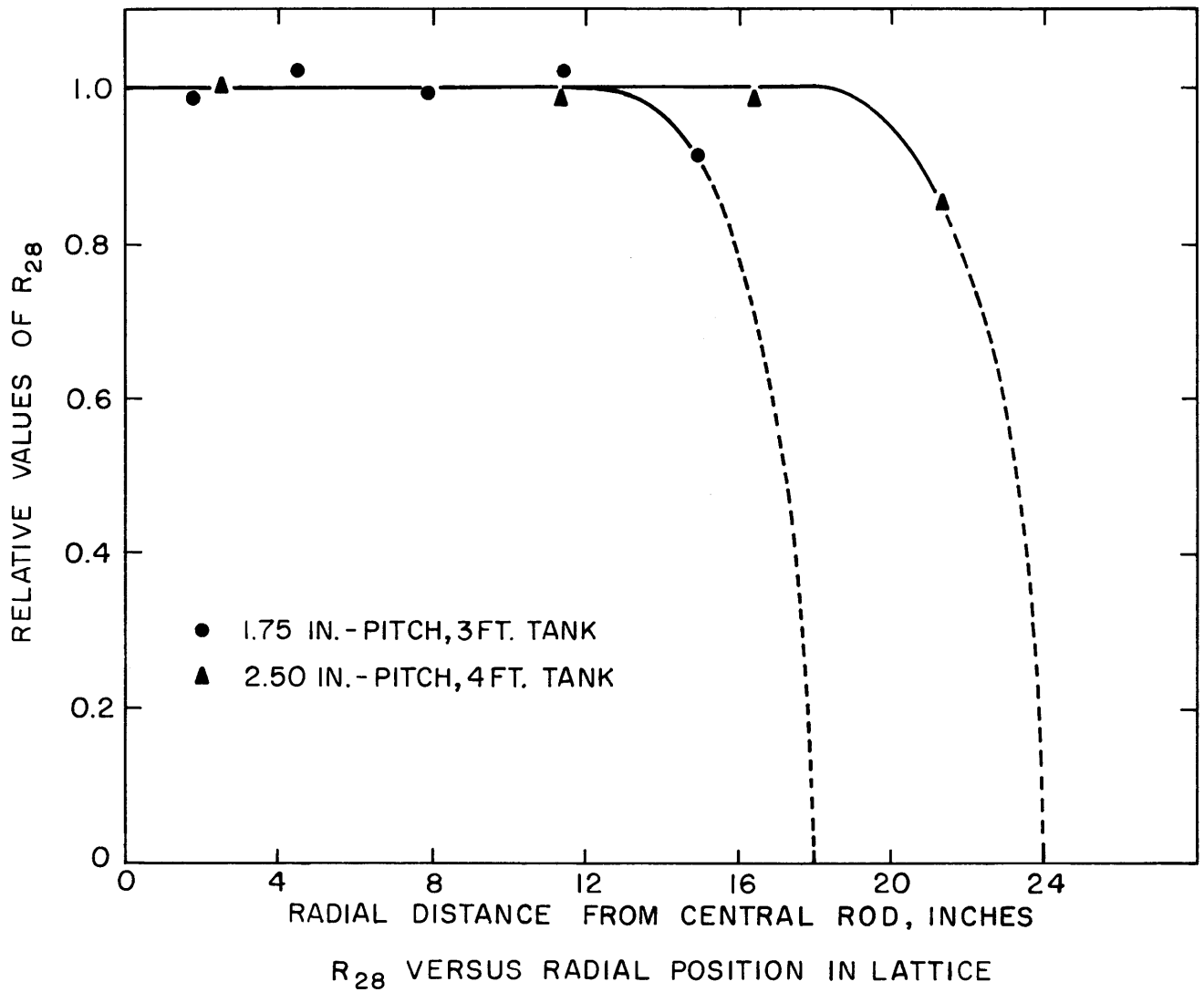

R_{28} VERSUS RADIAL POSITION IN LATTICE

FIG. 3.2.3

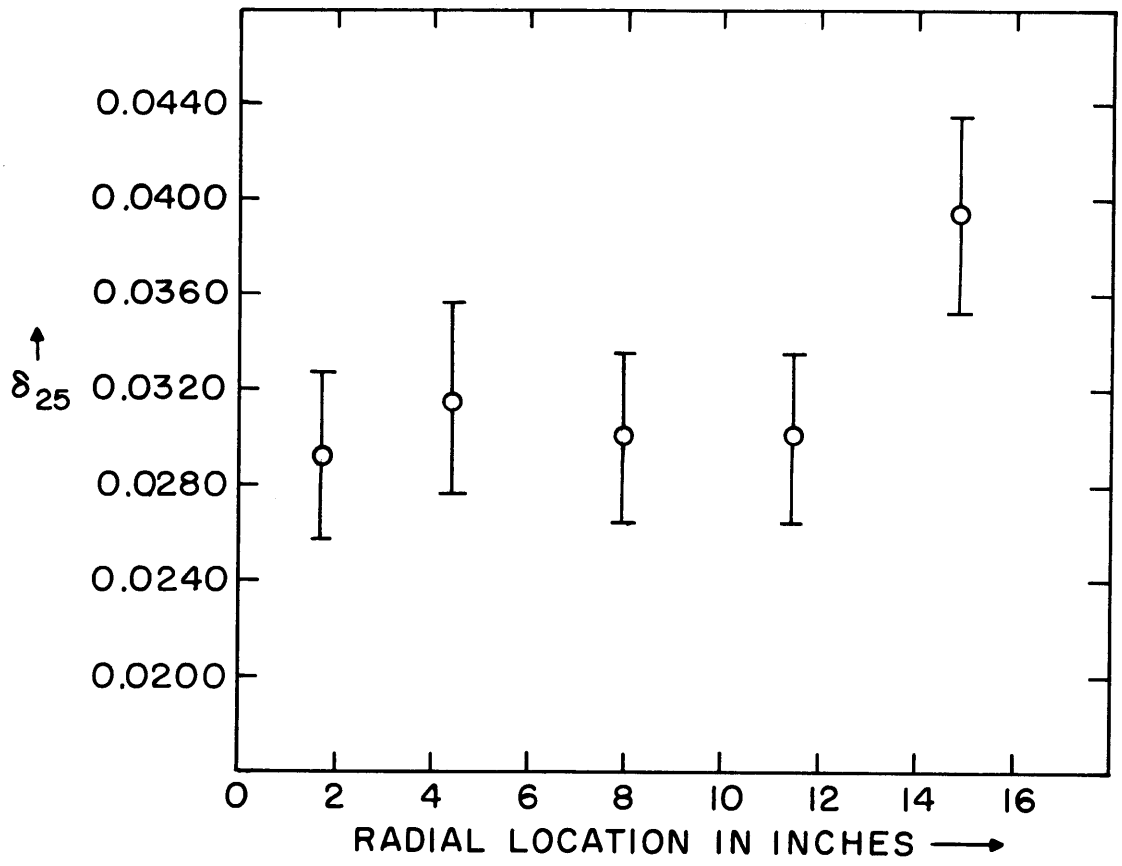

δ_{25} AS A FUNCTION OF RADIUS
AXIAL LOCATION - 20 INCHES,
1.75 INCH LATTICE

FIG. 3.2.4

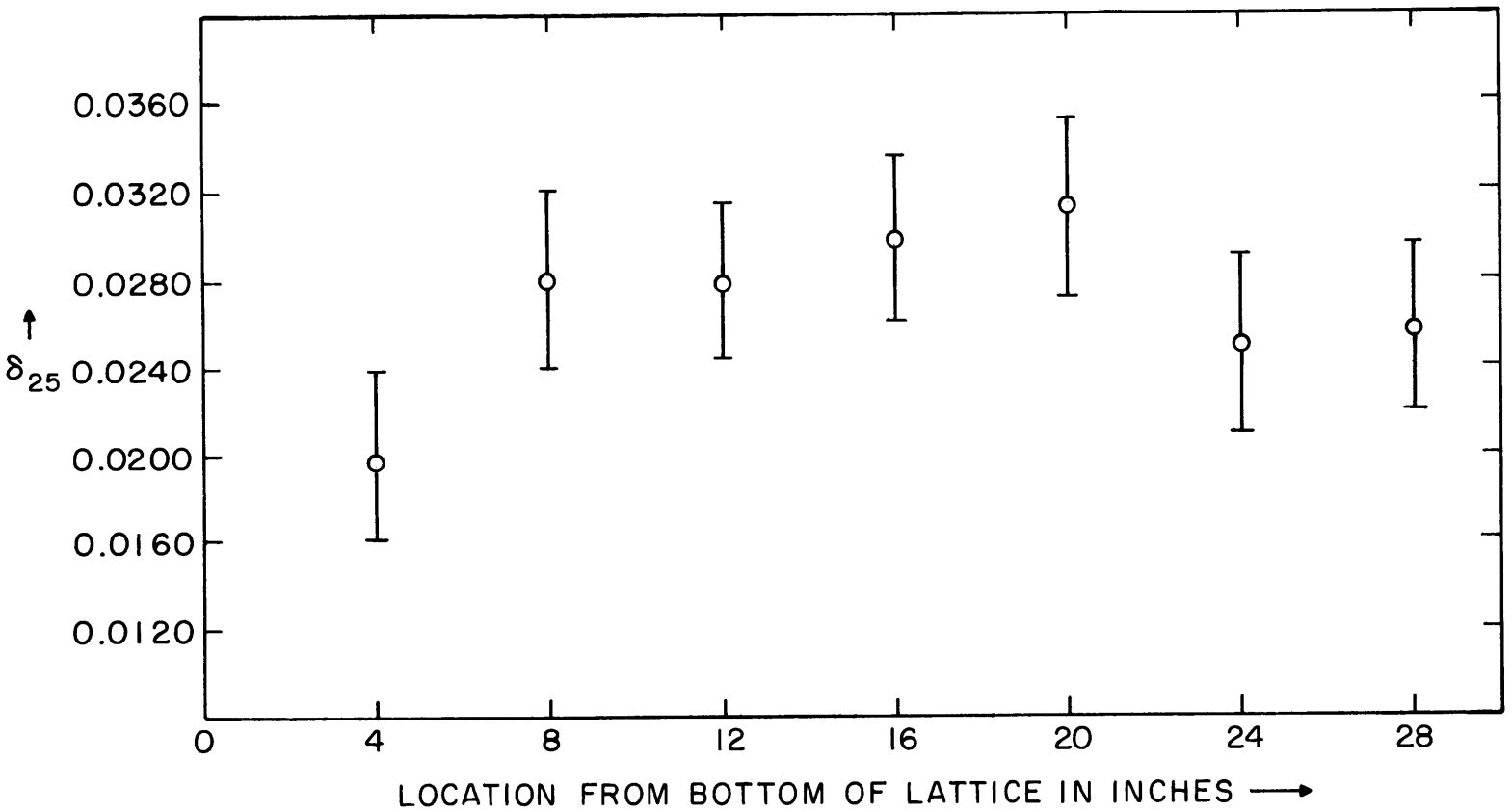

δ_{25} AS A FUNCTION OF HEIGHT
RADIAL LOCATION - 1.75 INCHES,
1.75 INCH LATTICE

FIG. 3.2.5

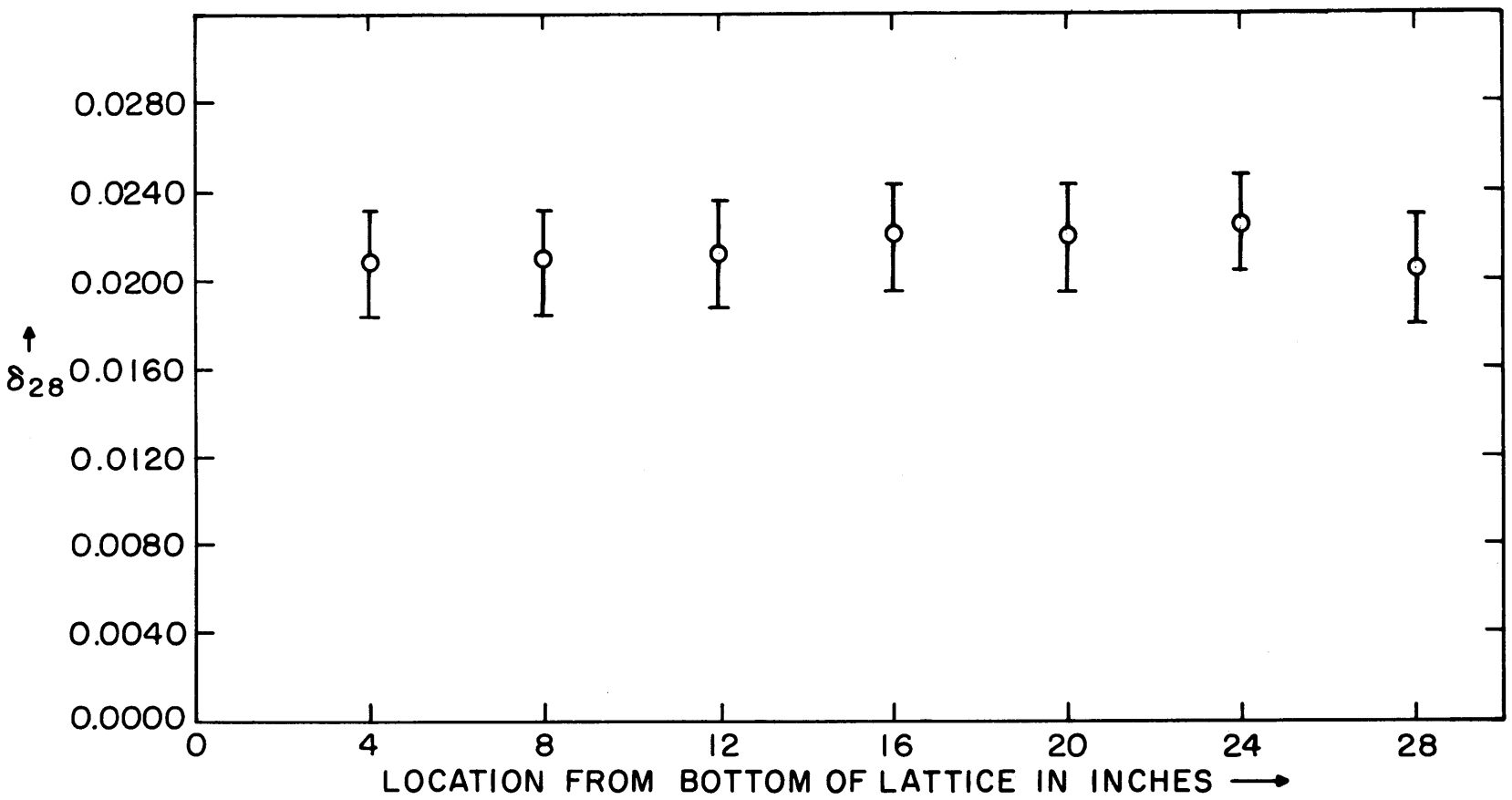

δ_{28} AS A FUNCTION OF HEIGHT
RADIAL LOCATION - 1.75 INCHES,
1.75 INCH LATTICE

FIG. 3.2.6

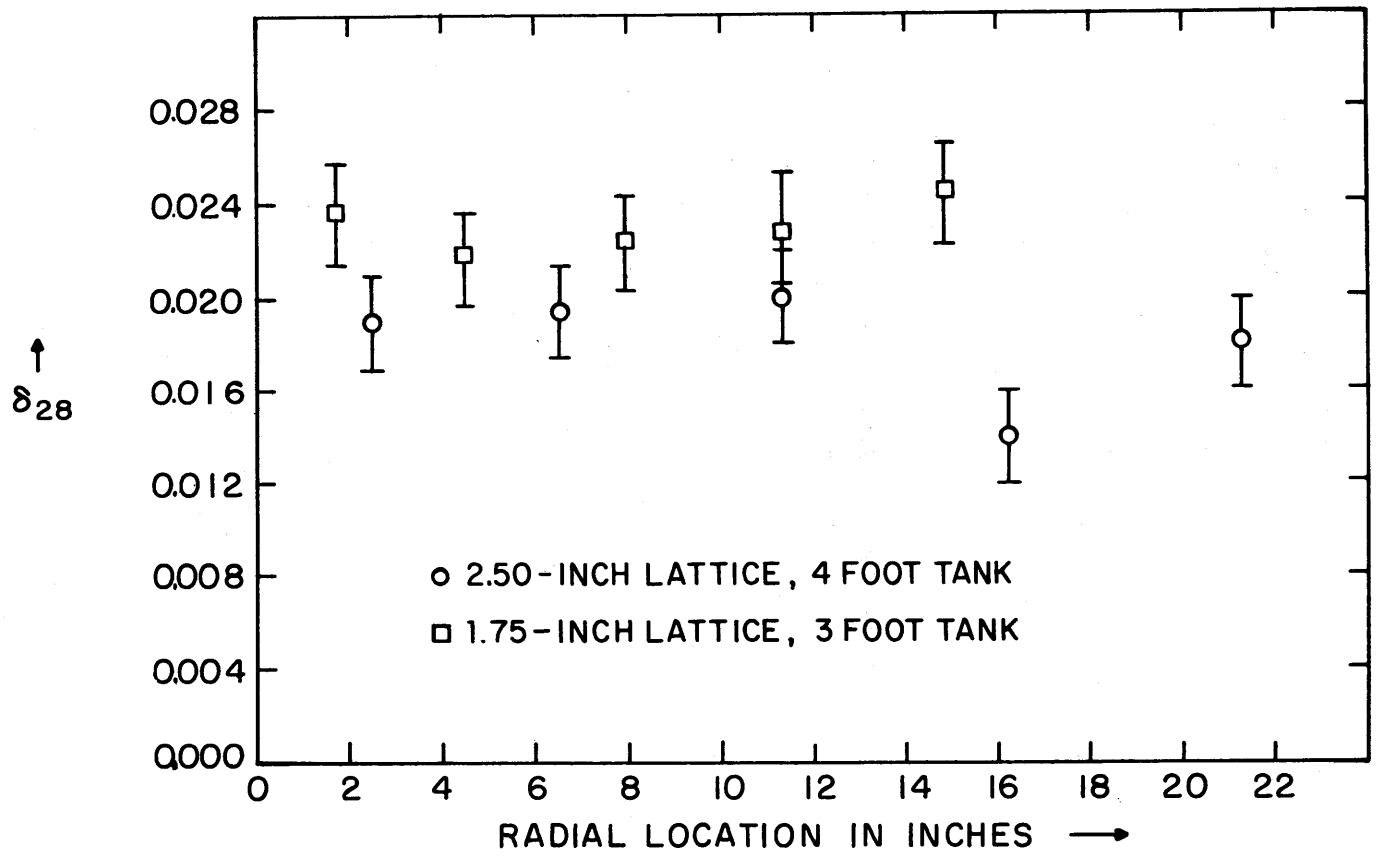

δ_{28} AS A FUNCTION OF RADIUS

FIG. 3.2.7

3.2.2 Effect of Cadmium

The use of cadmium can effect the results of the microscopic parameter measurements in three ways. First, if the bare foils are not placed far enough away from the cadmium, their activities will be decreased by the depression of the thermal flux caused by the cadmium. Second, the depression of the thermal flux will decrease the fast flux (because there will be fewer fast neutrons from thermal fission) with the result that the activity induced by fast neutrons in the cadmium-covered foils will be decreased. Finally, the effect of the decrease in the thermal flux may persist into the resonance flux; in addition, the resonance flux may be perturbed by the displacement of moderator by the external cadmium sleeve, and by the higher resonances of cadmium.

3.2.2.1 The Thermal Flux Depression

The extent of the thermal flux depression in a fuel rod caused by the use of cadmium on an adjacent rod was investigated experimentally in all three lattices studied. Axial traverses were made with bare foils inside a fuel rod adjacent to another fuel rod which had a cadmium sleeve 20 inches from the bottom of the fuel zone. The foils were spaced four inches apart with one foil at the same height as the cadmium sleeve. Each axial distribution was examined for evidence of a dip in activation at the height of the cadmium sleeve. No effect was observed within the limits of the experimental uncertainties, indicating that the presence of one cadmium sleeve did not affect the total flux in a neighboring rod.

An axial traverse with bare gold foils was made in the central fuel rod of the 1.75-inch lattice with two cadmium sleeves (one at 10 inches and one at 14 inches from the bottom of the fuel region) on the six fuel rods adjacent to the central rod. In this case, an effect was observed: the activity of the gold foil in the central rod located at a height of 12 inches (equidistant from the 12 cadmium sleeves) was decreased by 2.5%. The decrease attributable to one cadmium sleeve is about 0.2%, which is less than the estimated experimental uncertainties associated with the microscopic parameter measurements. Since the bare foils were always two rods away from a rod with a cadmium sleeve, a decrease in the activity of the bare foils of 0.2% can be considered as an upper limit.

3.2.2.2 The Fast Flux Region

The fast neutron flux was depressed within the cadmium-covered uranium detector foils so that the activities produced by fast neutrons in those foils were reduced. This reduction in the activities of the cadmium-covered foils meant that the measured microscopic parameters ρ_{28} and δ_{25} would be affected. The magnitude of the reduction in the Np^{239} activity and the U^{235} fission product activity of the cadmium-covered foils was determined from estimates of the depression of the fast flux in these foils and from calculations of the fractions of the epi-cadmium activities which were due to fast neutron captures or fissions.

An estimate of the depression of the fast flux above the fission threshold of U^{238} (about 1 Mev) was made from measurements of the ratio δ_c which is defined as follows:

$$\delta_c = \left(\frac{U^{238} \text{ fission rate in cadmium-covered fuel}}{U^{238} \text{ fission rate in bare fuel}} \right), \qquad (3.2.1)$$

or

$$\delta_c = \left(\frac{U^{238} \text{ fission product activity of a cadmium-covered uranium detector foil}}{U^{238} \text{ fission product activity of a bare uranium detector foil}} \right). \qquad (3.2.2)$$

The fractional reduction of the fast flux in the cadmium-covered foils was then $(1-\delta_c)$. The value of δ_c was calculated from the measured fission product activities of the uranium detector foils used in the measurement of δ_{25} (see Section 2.2.1.3) by means of the following relation:

$$\delta_c = \frac{D_c^{FP} - \left(\frac{\epsilon_D}{\epsilon_N}\right) N_c^{FP}}{D_b^{FP} - \left(\frac{\epsilon_D}{\epsilon_N}\right) N_b^{FP}}. \qquad (3.2.3)$$

Values of both δ_c and $(1-\delta_c)$ which are listed in Table 3.2.1 show that the U^{238} fission rate (and thus the fast flux) in the cadmium-covered uranium detector foils was reduced significantly in all three lattices studied. The reduction of the U^{238} fission rate within the cadmium-covered foils

TABLE 3.2.1

Effects of the Fast Flux Depression in the Cadmium-Covered Foils

Rod Spacing (Inches)	δ_c	$(1-\delta_c)$	Fraction of Epicadmium Np^{239} Activity Due to Fast Neutrons, F_N		Fractional Reduction of Np^{239} Activity	Fraction of Epicadmium U^{235} F.P. Activity Due to Fast Neutrons, F_F		Fractional Reduction of U^{235} F.P. Activity
			Exp.	GAM-I		Exp.	GAM-I	
1.25	0.654	0.346	0.007	0.006	0.0024	0.015	0.010	0.0053
1.75	0.459	0.541	0.011	0.012	0.0058	0.020	0.019	0.011
2.50	0.274	0.726	0.018	0.018	0.013	0.029	0.030	0.021

decreased as the rod spacing decreased because a larger fraction of the fast neutrons reaching the foils were born in neighboring fuel rods where the thermal fission rate was not appreciably depressed by the cadmium.

The fractions of the cadmium-covered foil activities which were due to fast neutron reactions were calculated both from experimental results and from analytical results. As shown in Appendix E, the fraction F_N of the N_p^{239} activity of a cadmium-covered foil due to fast neutron captures is $\frac{R_{28}}{C^*}\delta_{28}a_{28}$, and the fraction F_F of the U^{235} fission product activity of a cadmium-covered foil due to fissions by fast neutrons is $\left(\frac{1+\delta_{25}}{\delta_{25}}\right)\delta_{28}\left(\frac{\Sigma_f^{25}}{\Sigma_f^{28}}\right)_{FAST}$. Analytically, the fractions F_N and F_F were obtained directly from the output of the computer program GAM-I (see Chapter V). The reduction in the Np^{239} activity of a cadmium-covered foil is $(1-\delta_c)F_N$ and the reduction in the U^{235} fission product activity of a cadmium-covered foil is $(1-\delta_c)F_F$. The results are listed in Table 3.2.1. The reductions in Np^{239} activities and the U^{235} fission product activities are within the experimental uncertainties with one exception. The reduction of 1.3% in the Np^{239} activity of a cadmium-covered foil from the 2.50-inch lattice is more than the experimental error of 0.5% for R_{28} in that lattice (which is directly proportional to the activity of the cadmium-covered foil). For completeness, all the values of ρ_{28} and δ_{25} were adjusted to compensate for the reductions in the activities of the cadmium-covered uranium foils.

3.2.2.3 The Resonance Flux Region

Two experiments were made to determine whether the presence of cadmium perturbs the resonance flux.

First, microscopic distributions of the Np^{239} activity, induced in cadmium-covered, 0.005-inch-thick, 0.0625-inch-diameter, depleted uranium foils, were measured in the moderator between two bare rods and between a bare rod and a rod which had a cadmium sleeve. A schematic diagram of the experimental arrangement is shown in Fig. 3.2.8.

The resulting distributions were practically the same, as shown in Fig. 3.2.9.

Second, six 0.005-inch-thick, 0.250-inch-diameter, depleted uranium foils were irradiated in equivalent positions (i.e., positions of equal height and equal radius) in the lattice. The arrangement of the cadmium-covered foils, described in Chapter II and shown in Fig. 2.2.1, was used except that the natural uranium foils were omitted and the cadmium sleeve length was varied from 0.25 inch to 1.5 inches. Two types of cadmium sleeves were used, external and internal. An external sleeve is one which is placed on the outside of the fuel rod cladding as described in Section 2.2.3, and an internal sleeve is one where the cadmium sleeve replaces aluminum removed from the inside of the cladding. The results are shown in Fig. 3.2.10; the data show no significant trend compared to the experimental uncertainties. In addition, three different cadmium sleeves were used for the microscopic parameter measurements made in the 2.50-inch lattice: a 0.250-inch-long internal sleeve, a 0.500-inch-long internal sleeve, and a 1.0-inch-long external sleeve. The reproducibility error (0.6%) for the U^{238} cadmium ratio, R_{28}, in that lattice was about the same as the reproducibility errors for R_{28} in the 1.25-inch and 1.75-inch lattices in which only one type of sleeve was used. Thus the values of R_{28} obtained by using the three different cadmium sleeves were the same within the experimental errors, which indicates that the use of the three different cadmium sleeves does not introduce significant errors.

3.2.3 Effect of Foreign Materials Within the Fuel

3.2.3.1 Thermal and Resonance Flux Regions

Figure 3.2.11 shows the intracellular distributions of Np^{239} activity produced in 0.005-inch-thick, 0.0625-inch-diameter, depleted uranium foils, bare and cadmium-covered. The epicadmium activity distribution shows that the U^{238} capture rate has a steep gradient at the fuel rod surface. This steep gradient implies that at the rod surface the angular neutron flux is peaked strongly toward the center of the fuel. Hence, the epicadmium Np^{239} activation of a uranium foil placed between

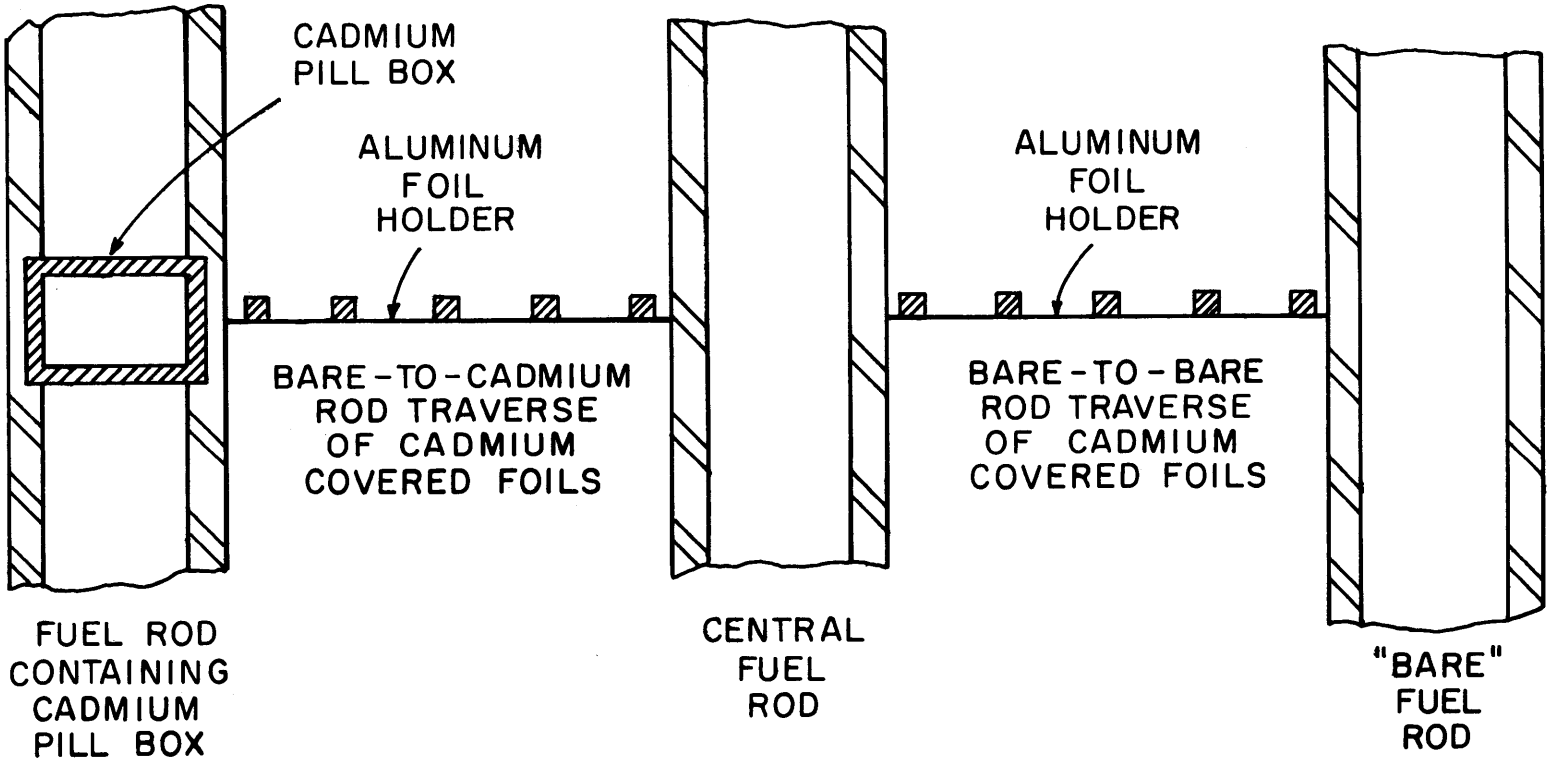

DIAGRAM OF THE EXPERIMENTAL ARRANGEMENT FOR MICROSCOPIC DISTRIBUTIONS TO STUDY EFFECT OF CADMIUM ON EPICADMIUM ACTIVITY

FIG. 3.2.8

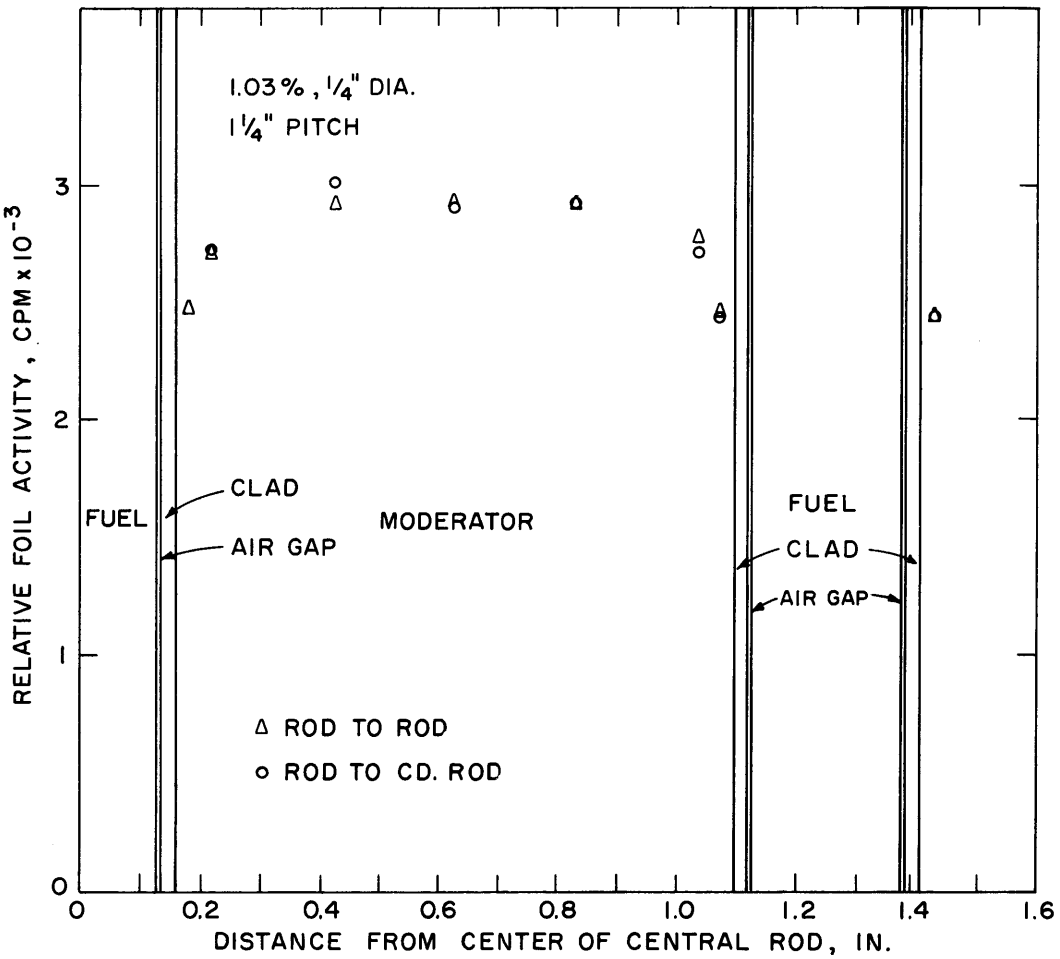

MICROSCOPIC Np^{239} ACTIVITY OF CADMIUM-COVERED DEPLETED URANIUM FOILS, 1/16 INCH DIAMETER, 0.005 INCH THICK

FIG. 3.2.9

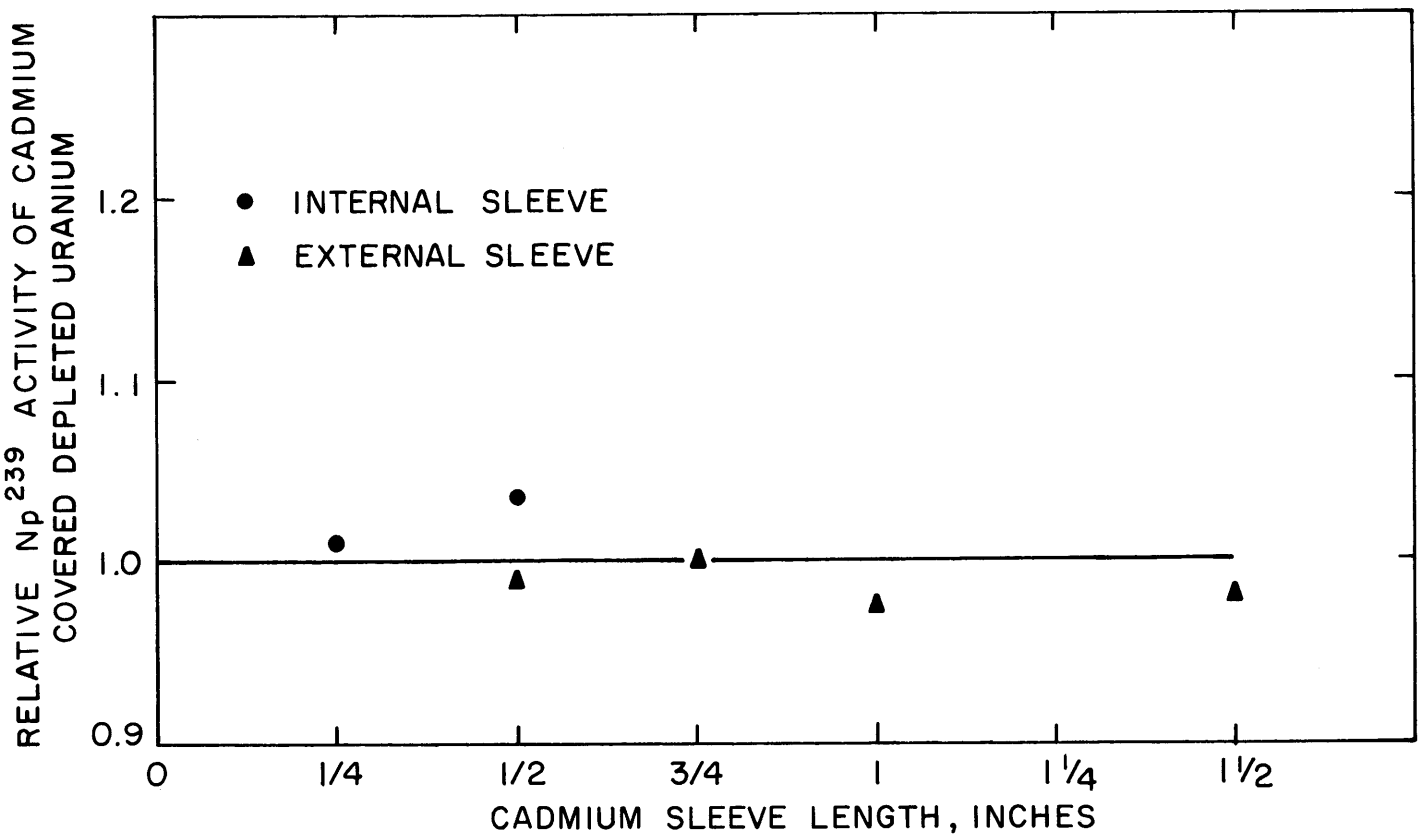

EFFECT OF CADMIUM ON CADMIUM COVERED FOIL ACTIVITY

FIG. 3.2.10

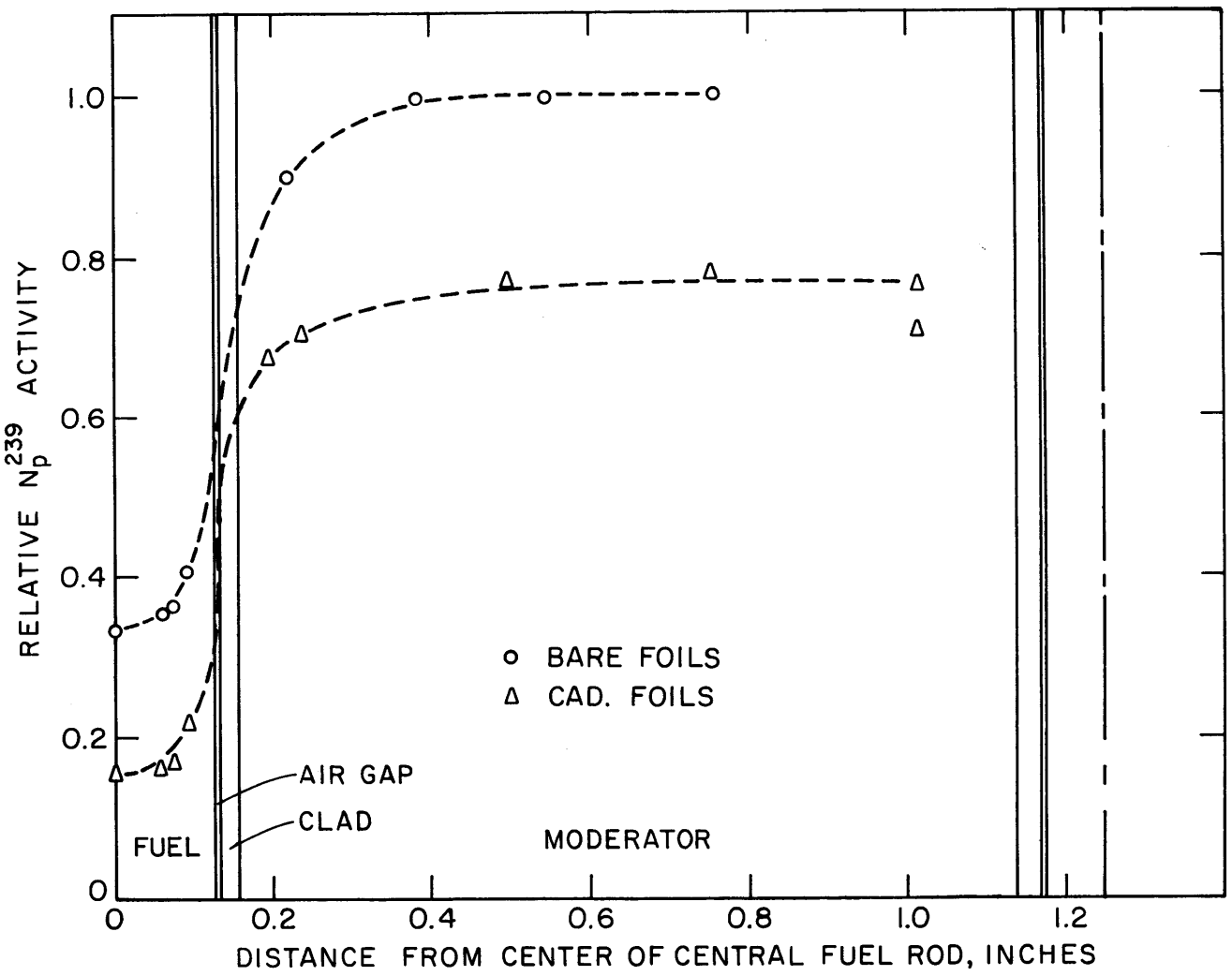

INTRACELLULAR DEPLETED URANIUM ACTIVITY DISTRIBUTION

FIG. 3.2.11

two fuel slugs in a rod may be highly sensitive to any perturbation in the rod surface. Such perturbations may include:

1. Misalignment among foils and between foils and fuel slugs;
2. Foils and fuel slugs having different diameters;
3. Burrs, chips, cracks, etc. on the edges of the foils or of the fuel slugs;
4. Gaps among the foils and between the foils and fuel slugs caused by tapered foils, crowned foils, unsquare fuel slug ends, or a uranium oxide layer on the surface of the foils or slugs;
5. Deviations due to the use of materials whose resonance cross sections depart significantly from that of the fuel; such materials are U^{235}, gold, aluminum or aluminum alloys, etc.

Special care was taken when preparing the foils and slugs to avoid the perturbations associated with the types 1 through 4; for example, Teflon sleeves were used to align the foils, and specially made foil punches were used to prepare the foils.

Several experiments were made to determine the following effects, which may be due to perturbations of type 5 above:

1. The effect of using aluminum catcher foils or aluminum alloy detector foils;
2. The effect of substituting depleted or natural uranium for fuel materials;
3. The effect on the detector foil activity due to the 0.020-inch-thick aluminum holder foils.

These experiments, made in the lattice with the 1.75-inch spacing, were:

1. Six bare, depleted uranium detector foils were irradiated in similar positions with aluminum catcher foils ranging in thickness from 0.001 inch to 0.040 inch.
2. Six cadmium-covered, depleted uranium detector foils were irradiated in similar positions with aluminum catcher foils ranging in thickness from 0.001 inch to 0.040 inch.

3. Six bare depleted uranium detector foils were irradiated in similar positions with depleted uranium catcher foils ranging in thickness from 0.005 inch to 0.030 inch.
4. Six cadmium-covered, depleted uranium foils were irradiated in similar positions with depleted uranium catcher foils ranging in thickness from 0.005 inch to 0.030 inch.
5. Six bare, depleted uranium detector foils, with 0.005-inch-thick depleted uranium catcher foils, were irradiated in similar positions with the aluminum holder foils ranging in thickness from 0.020 inch to 0.060 inch in three rods and with no aluminum present in the other three rods. Mylar tape was used instead of the Teflon sleeves for this experiment.

The results are shown in Figs. 3.2.12, 3.2.13 and 3.2.14.

Figures 3.2.12 and 3.2.13 show that the presence of aluminum catcher foils adjacent to either bare or cadmium-covered depleted uranium detector foils perturbs the Np^{239} activity induced in the detector foil; on the other hand, up to 0.030 inch of depleted uranium used as a catcher foil does not significantly affect the Np^{239} activity of either the bare or cadmium-covered detector foils. First- and second-degree curves were fitted by least squares through each set of data; all the lines had the same ordinate intercept when extrapolated to zero catcher foil thickness to within 0.9% of each other; this difference is within the experimental uncertainty.

The results show that the substitution of depleted uranium for fuel does not perturb either the thermal flux or the resonance flux. The substitution of natural uranium for fuel causes a smaller perturbation than the substitution of depleted uranium for fuel, as would be expected, because less U^{235} is removed. Hence, neither the thermal flux nor the resonance flux is perturbed by the presence of natural or depleted uranium foils and neither the U^{235} fission product activity nor the Np^{239} activity produced in these foils should be affected.

Figure 3.2.14 shows that the presence of up to 0.060 inch of aluminum with 0.065 inch of uranium separating it from the detector foil has no effect upon the Np^{239} activity of the detector foil.

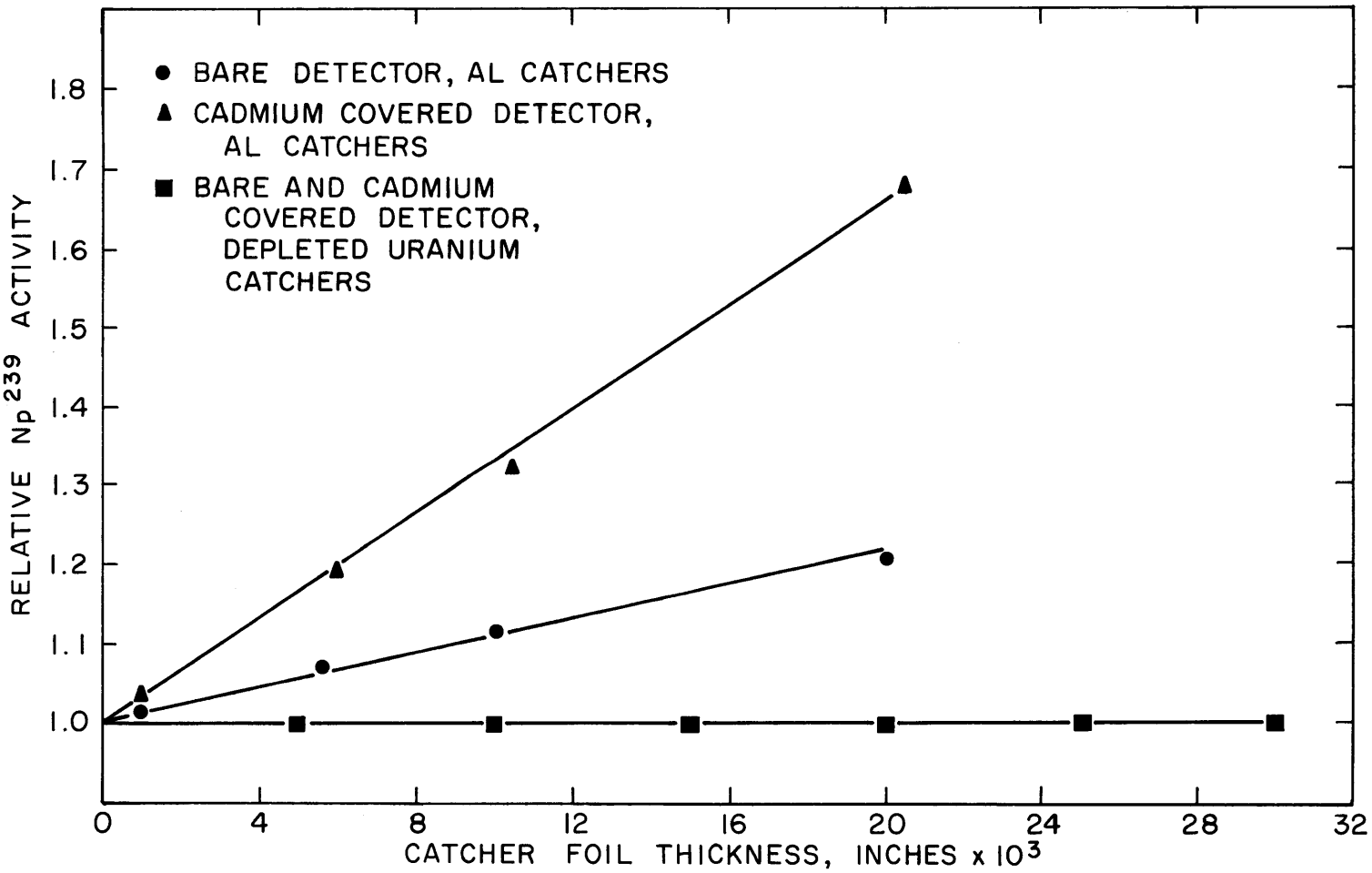

EFFECT OF CATCHER FOILS ON Np^{239} ACTIVITY OF DEPLETED URANIUM FOILS

FIG. 3.2.12

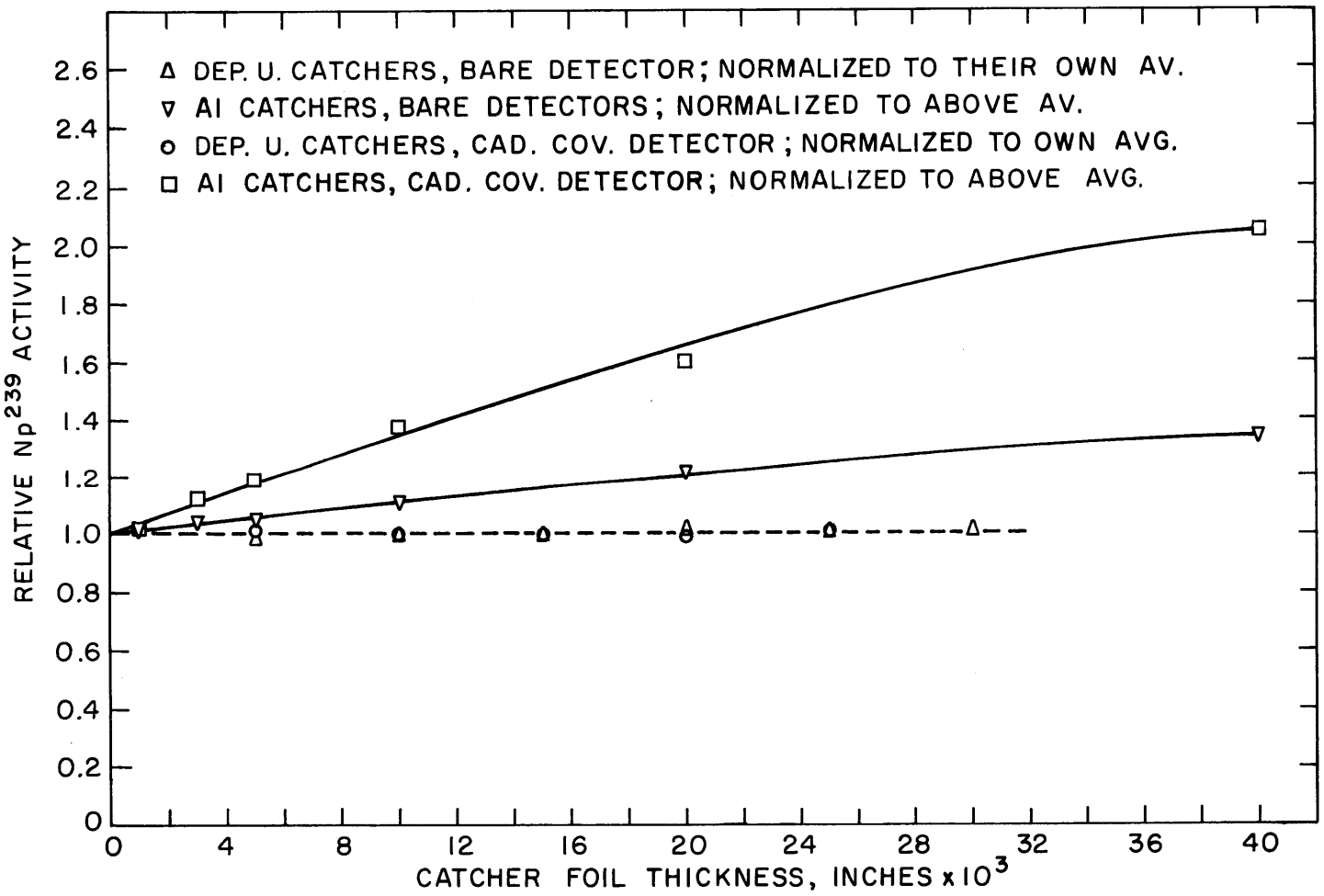

EFFECT OF CATCHER FOILS ON DEPLETED URANIUM Np^{239} ACTIVITY

FIG. 3.2.13

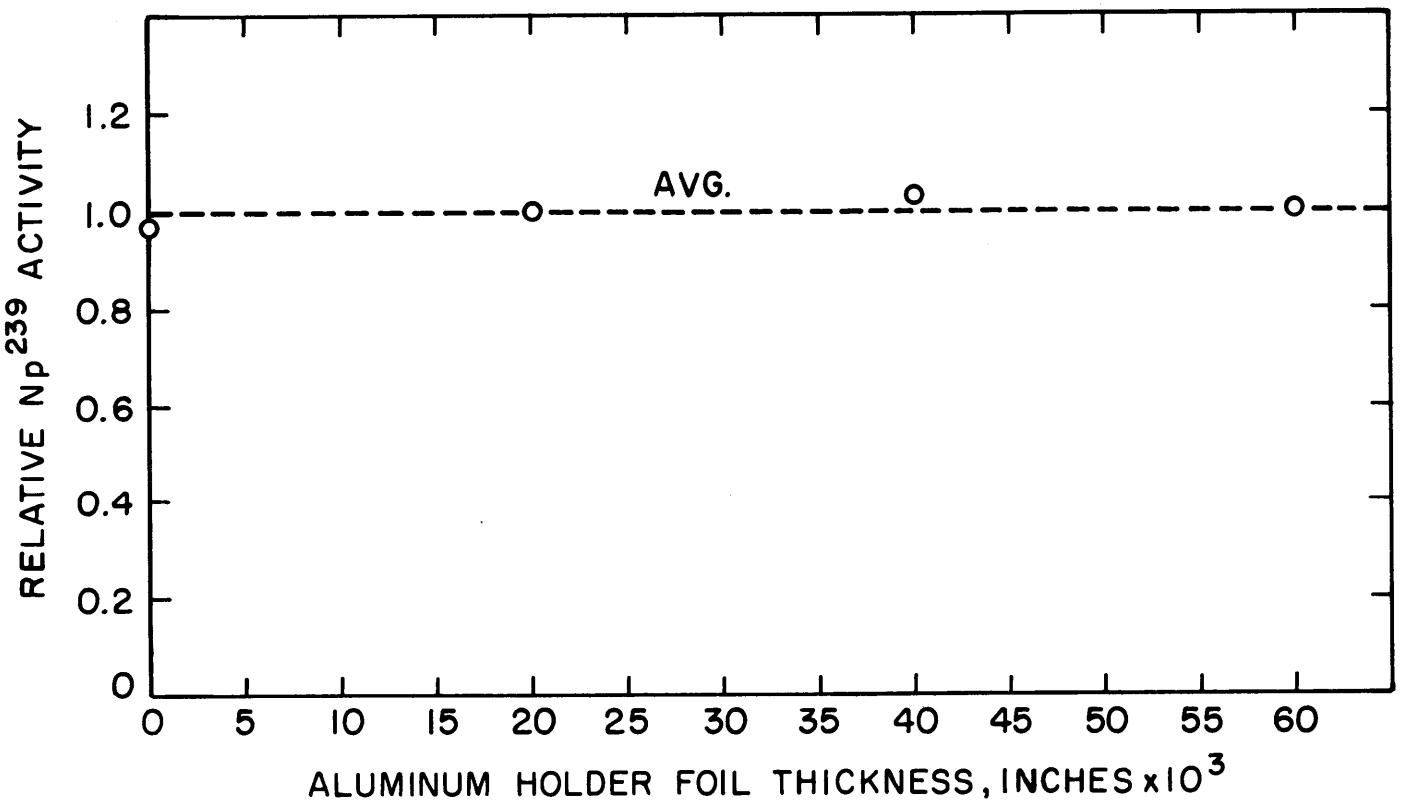

EFFECT OF ALUMINUM HOLDER FOILS ON DEPLETED URANIUM Np^{239} ACTIVITY

FIG. 3.2.14

3.2.3.2 Fast Flux Region

Replacing fuel material with aluminum, depleted uranium, or natural uranium reduces the thermal fission rate and thus the fast neutron flux. The fission neutrons born in the immediate vicinity of a foil comprise the most important source of neutrons causing fast reactions in that foil. As indicated in Section 3.2.2, a relatively large fast flux perturbation will not significantly affect the U^{235} fission product activity or the Np^{239} activity. However, U^{238} fission product activity will be affected to an extent directly proportional to any perturbation of the fast flux. Only about 3% of the fission product activity of a natural uranium foil is due to U^{238} fissions, so that the total fission product activity of a natural uranium foil will be insensitive to perturbations in the U^{238} fission rate. But more than 99% of the fission product activity of a depleted foil is due to U^{238} fissions, so that the fission product activity of a depleted foil will be affected to an extent directly proportional to the perturbation of the fast flux within the foil.

The set of experiments described in Section 3.2.3.1 was also used to investigate the effect of the presence of foreign materials within the fuel on the measured fission product activity of a depleted uranium foil. The fission product activity of each of the depleted uranium detector foils was counted as described in Section 2.2.3. This portion of the experiments was done by Mr. H. Bliss (B1). The results are plotted in Figs. 3.2.15, 3.2.16, and 3.2.17.

The fission product activity of a depleted uranium foil is significantly affected by the presence of non-fuel materials within the fuel zone. The perturbations are larger than had been anticipated, but they are of the same order of magnitude as those given by analytical formulae derived by S. A. Kushneriuk (K4) to correct fast fission measurements made at Chalk River.

As a consequence of these results, corrections to the fission product activity of the depleted foil were developed. The corrections apply only to the "single rod" portion of the activity since the fast flux due to the neutrons born in neighboring rods is not perturbed. Thus, a different correction factor is necessary for each lattice spacing. The experiments described in the preceding paragraphs were made in the 1.75-inch

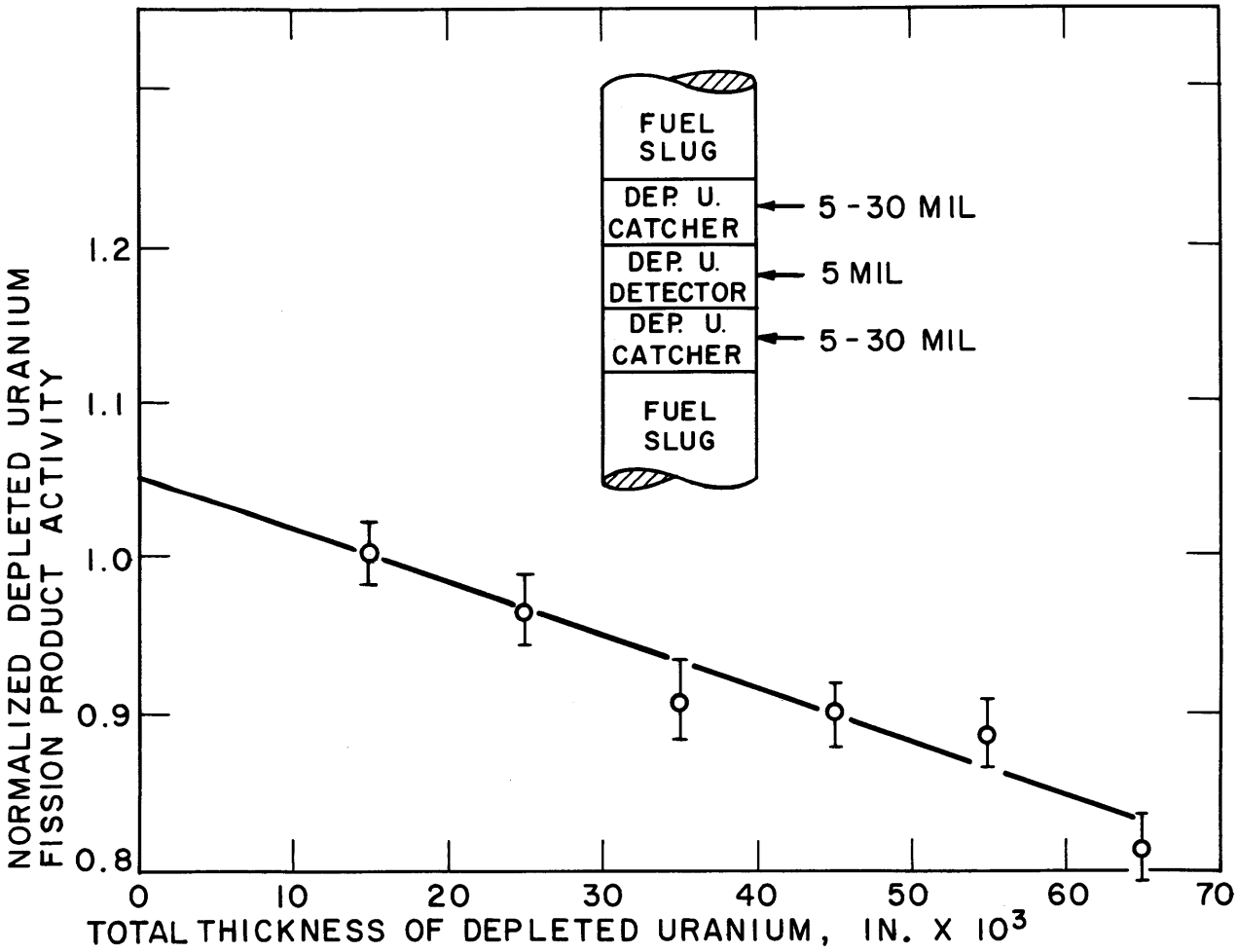

EFFECT OF DEPLETED URANIUM CATCHER FOILS ON DEPLETED URANIUM FISSION PRODUCT ACTIVITY

FIG. 3.2.15

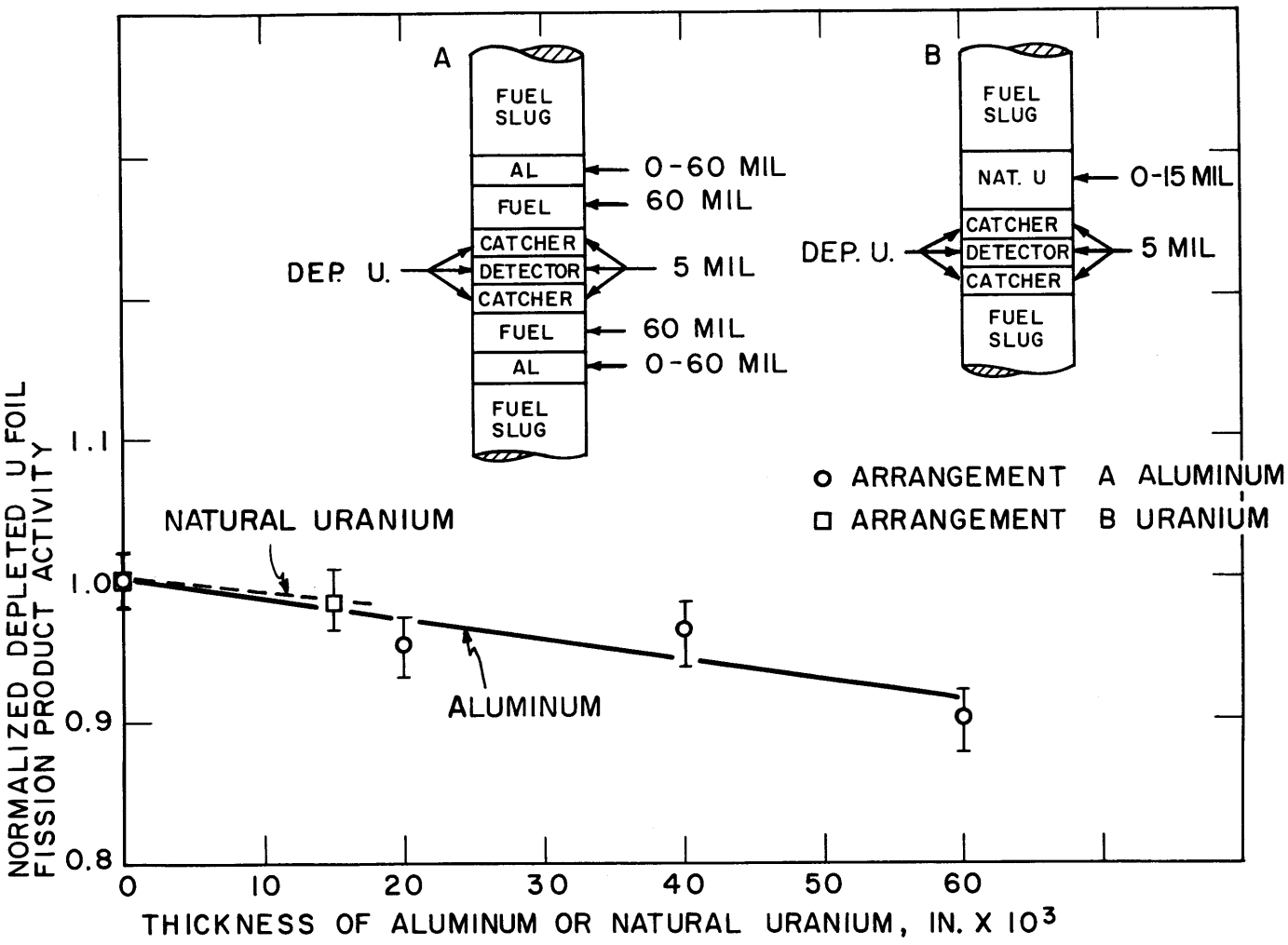

EFFECT OF ALUMINUM SLEEVE HOLDERS AND NATURAL URANIUM DETECTOR ON FISSION PRODUCT ACTIVITY OF DEPLETED URANIUM DETECTOR

FIG. 3.2.16

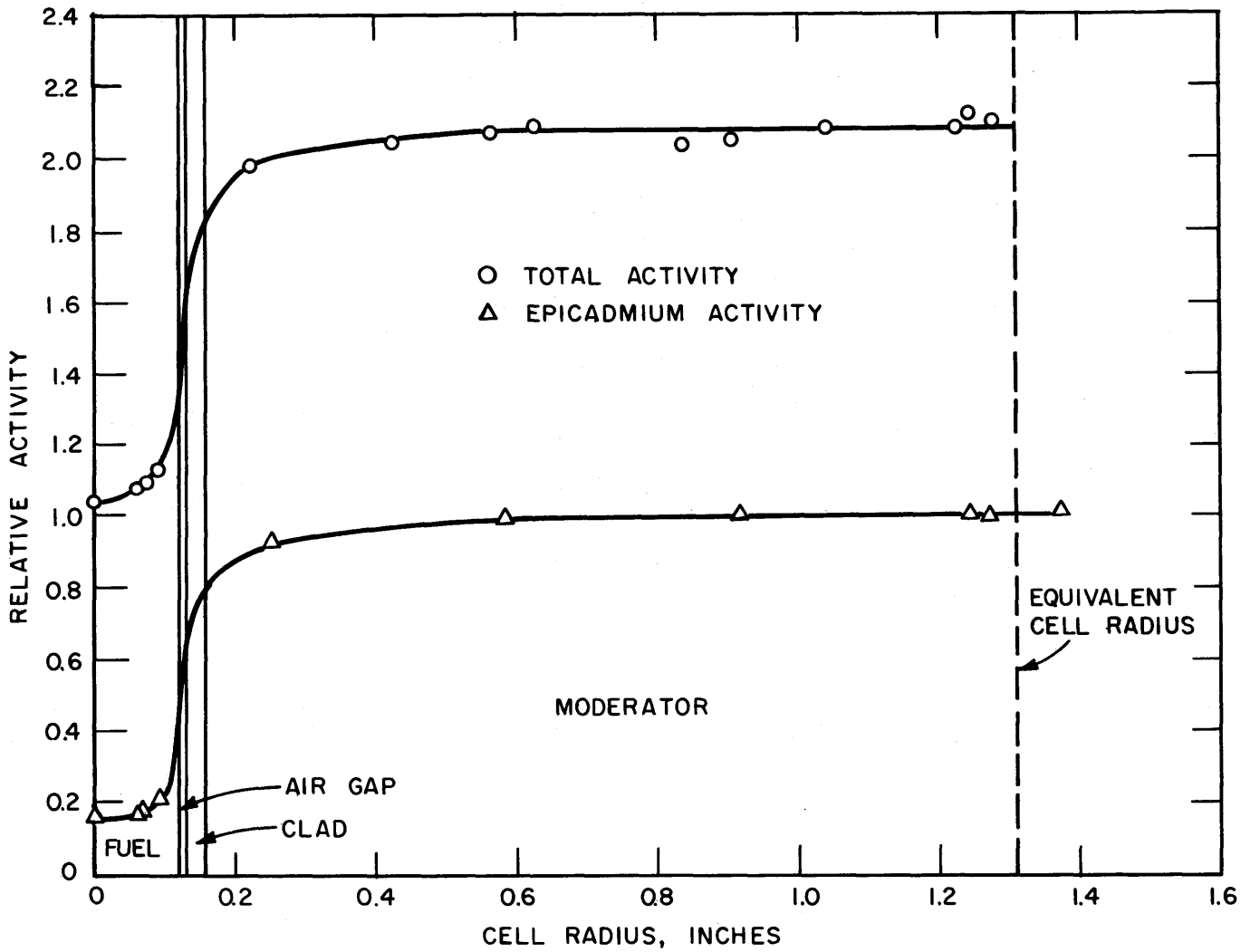

INTRACELLULAR Np^{239} ACTIVITY DISTRIBUTION FOR THE 2.50-INCH LATTICE

FIG. 4.2.5

lattice; and a correction factor to be applied to the U^{238} fission product activities of the uranium detector foils used for δ_{28} measurements in that lattice was obtained directly from Figs. 3.2.17 and 3.2.19. Correction factors, a^L, for the 1.25-inch lattice, the 2.50-inch lattice, and the single rod measurement were calculated from the correction factor, $a^{1.75}$, for the 1.75-inch lattice via the following relation, which is derived in Ref. (B1):

$$a^L = 1 + (a^{1.75}-1)\left(\frac{\gamma^{1.75}(t)}{\gamma^L(t)}\right), \qquad (3.2.4)$$

where $\gamma^{1.75}(t)$ and $\gamma^L(t)$ are the perturbed measurements of $\gamma(t)$ (as described in Chapter II) for the 1.75-inch lattice and the rod spacing corresponding to a^L, respectively. The values of the correction factors for the three lattices studied and the single rod measurement are listed in Table 3.2.2.

TABLE 3.2.2

Correction Factors for the Fission Product Activity of Depleted Uranium Foils Irradiated in the Foil Arrangement Shown in Fig. 2.2.1

Lattice Spacing	Correction Factor
1.25 inch	1.08 ± 0.02
1.75 inch	1.09 ± 0.02
2.50 inch	1.10 ± 0.02
∞	1.12 ± 0.02

3.2.4 Effect on Nonuniform Activity Distribution in the Detector Foil

As can be seen in Fig. 3.2.11, the distribution of epicadmium Np^{239} activity is strongly peaked at the surface of the fuel. The same figure shows that the distribution of the subcadmium Np^{239} activity is more nearly uniform. As a result of these two activation distributions, the over-all counting efficiency may be different for the subcadmium and epicadmium activities (A3). This difference in counting efficiency can be caused by two effects. First, for a foil centered under a NaI(Tl) crystal, a gamma ray emitted from the center of the foil will have a

higher probability of being counted than a gamma ray emitted from the foil edge. Since the subcadmium Np^{239} activity has a large fraction of its gamma rays originating near the center of the foil, the count rate due to the subcadmium Np^{239} activity will be higher relative to the count rate due to the epicadmium Np^{239} activity. Second, the Np^{239} 103-Kev gamma ray is highly self-absorbed by the uranium foil, so that gamma rays emitted through the edge of the foil will not be attenuated as much as those emitted through the top surface of the foil. Since the epicadmium Np^{239} activity is strongly peaked at the edge of the foil, a larger fraction of the gamma rays due to epicadmium Np^{239} activity will reach the crystal through the foil edge. Thus the over-all self-absorption effect will be smaller for the epicadmium Np^{239} activity. The count rate due to the epicadmium Np^{239} activity will then be higher relative to the count rate due to the subcadmium Np^{239} activity. The two effects act in opposite directions and tend to cancel each other.

To investigate the extent of these effects, three different procedures were used to determine the activities of several sets of foils. A set of foils consisted of the bare and cadmium-covered depleted uranium foils used for the ρ_{28} measurements. Two additional sets of foils were prepared, each consisting of a cadmium-covered foil irradiated in the lattice and a bare foil irradiated in the cavity sample tube, which provided a direct comparison of the counting results from two extreme activity distributions. The distribution of the Np^{239} activity of the cadmium-covered foil irradiated in the lattice was strongly peaked at the edge of the foil and the distribution of the Np^{239} activity of the bare foil irradiated in the cavity sample tube was uniform. On the other hand, the bare foils irradiated in the lattice contained both types of activity distributions, so that when their counting results were compared to the counting results for the cadmium-covered foils, any differences among the three counting procedures would not be as large.

The three different counting procedures were:

1. The distance between the NaI(Tl) crystal and the foils was varied from 0.5 inch to 2.5 inches.
2. The radiation emitted by the foils was collimated by a 5/16-inch-diameter hole through 2-inch-thick lead so that

all the gamma rays reaching the crystal would have the same detection efficiency and the solid angle permitting gammas to reach the crystal through the edge of the foil would be negligible.

3. The foils were homogenized by dissolving them in nitric acid to form identical solutions. Equal amounts (aliquots) of the solutions were then counted.

The results are listed in Table 3.2.3 and shown in Fig. 3.2.18. There is no significant difference among the results obtained with the three different procedures compared to the experimental uncertainties.

TABLE 3.2.3

Effect of the Counting Method Used on the Ratios of the Np^{239} Activity of Different Foils

Distance from NaI(Tl) Detector (Inches)	Average Value of R_{28} [a] (1.75" Lattice)
0.5	3.311 ± 0.019 (± 0.57%)
2.5	3.344 ± 0.024 (± 0.72%)
∞ (Pb collimator)	3.266 ± 0.039 (± 1.2%)
∞ (HNO_3 solu.)	3.332 ± 0.027 (± 0.81%)

[a] These values do not include flux perturbation corrections.

3.2.5 Effect of Fission Product Activity on Np^{239} Counting

The highly depleted uranium foils, containing 18 ppm U^{235}, were used so that the fission product activity produced in them would be negligible compared to the Np^{239} activity produced. This was checked experimentally. The measured activity, M, of an irradiated uranium foil can be expressed as follows:

$$M = (1-\epsilon)A^{39} + (1-\epsilon)A^{28} + \epsilon A^{25}, \qquad (3.2.5)$$

where ϵ is the U^{235} atom fraction of the uranium foil, the A's refer to the activities induced in the foil, and the superscripts 39, 28, and 25

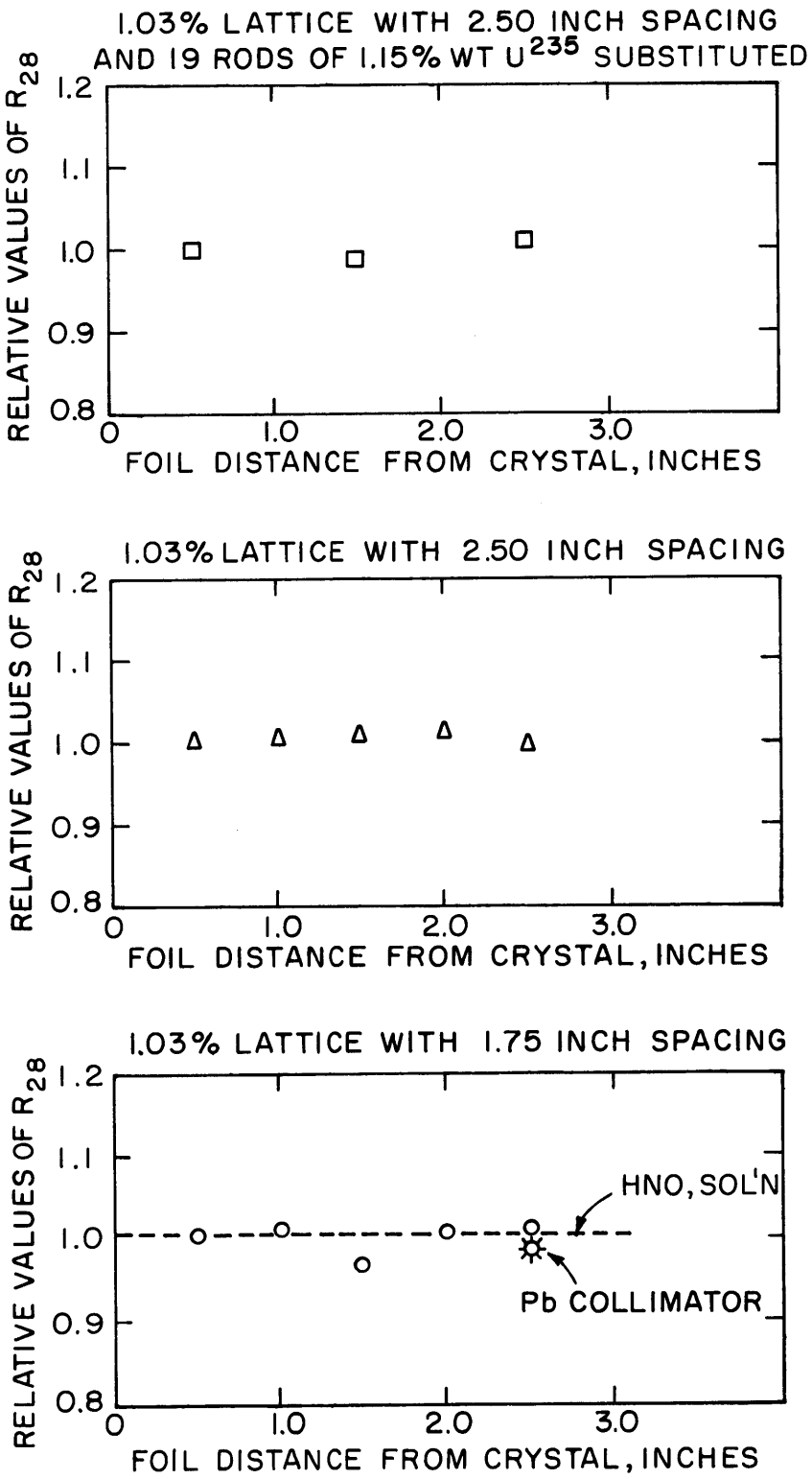

RELATIVE VALUES OF R_{28} FOR DIFFERENT COUNTING METHODS

FIG. 3.2.18

refer to Np^{239} activity, U^{238} fission product activity, and U^{235} fission product activity, respectively. If the activity of three uranium foils, each with a different but known enrichment is measured, an equation similar to Eq. 3.2.5 can be written for each foil, yielding three equations with three unknowns: A^{39}, A^{28}, and A^{25}. The fraction of any one of the constituent activities compared to the total activity of any one of the foils can then be determined. The fractions of the measured Np^{239} activity of a depleted uranium foil due to the competing activities, A^{28} and A^{25}, were calculated from the measured activities of depleted, natural, and fully (93%) enriched uranium foils. This was done for both bare and cadmium-covered foils irradiated in the 2.50-inch lattice. The results are listed in Table 3.2.4.

TABLE 3.2.4

Percentage of Depleted Foil Activity
During Np^{239} Counting Due to Fission Products

Competing Activity	Cadmium Foil	Bare Foil
U^{238} f.p.	0.1%	0.20%
U^{235} f.p.	~0	0.03%
Total f.p.	0.1%	0.2%

The results show that fraction of the measured Np^{239} activity of a depleted uranium foil due to fission product activity is negligible compared to the experimental uncertainties.

3.2.6 Effect of Variation in Foil Thickness

The 103-Kev gamma ray which is counted to measure the Np^{239} activity is highly self-absorbed in the foil with the consequence that variations in the foil thickness will affect the count rate due to the Np^{239} activity. Thus the measured Np^{239} activity of the depleted uranium foils must be corrected for differences due to the self-absorption.

The procedure used by Weitzberg et al. (W1) was followed. The average value of the transmission probability, T, of a gamma ray originating in a foil of thickness t is:

$$T = \frac{1}{\sigma t}\left(1-e^{-\sigma t}\right), \tag{3.2.6}$$

where σ is the attenuation cross section. Since the weight of each foil was found to be directly proportional to its thickness, Eq. 3.2.6 can be rewritten:

$$T = \frac{1}{\mu W}\left(1-e^{-\mu W}\right), \tag{3.2.7}$$

where μ is the mass attenuation coefficient and W is the foil weight.

The value of μ was obtained by a transmission experiment. The Np^{239} activity of an irradiated depleted uranium foil was counted as described in Section 2.2.4. The counting procedure was repeated, successively, with shields of unirradiated depleted uranium varying in thickness from 0.005 inch to 0.030 inch placed between the irradiated foil and the NaI(Tl) crystal. The measured activities were plotted against the shield thickness as shown in Fig. 3.2.19. The value of μ is given by the slope of the curve at the ordinate intercept and was found to be 0.004182 ± 0.000015 mg^{-1}.

The self-absorption correction to the Np^{239} activity of the depleted uranium foils was combined with the foil weight correction. The combined multiplicative correction factor normalized the activity of each foil to the activity of a foil with an arbitrary standard weight of 76 mg. The combined correction factor is:

$$W = \frac{0.272}{1 - e^{-\mu W}}. \tag{3.2.7}$$

The IBM 7094 of the M.I.T. Computation Center was used to compile tables of the combined correction factor for foil weights ranging from 60 mg to 80 mg.

3.3 Summary of the Results of the Investigations of Errors

An equilibrium spectrum exists axially between heights of 16 inches and 28 inches and radially out to within four inches of the lattice

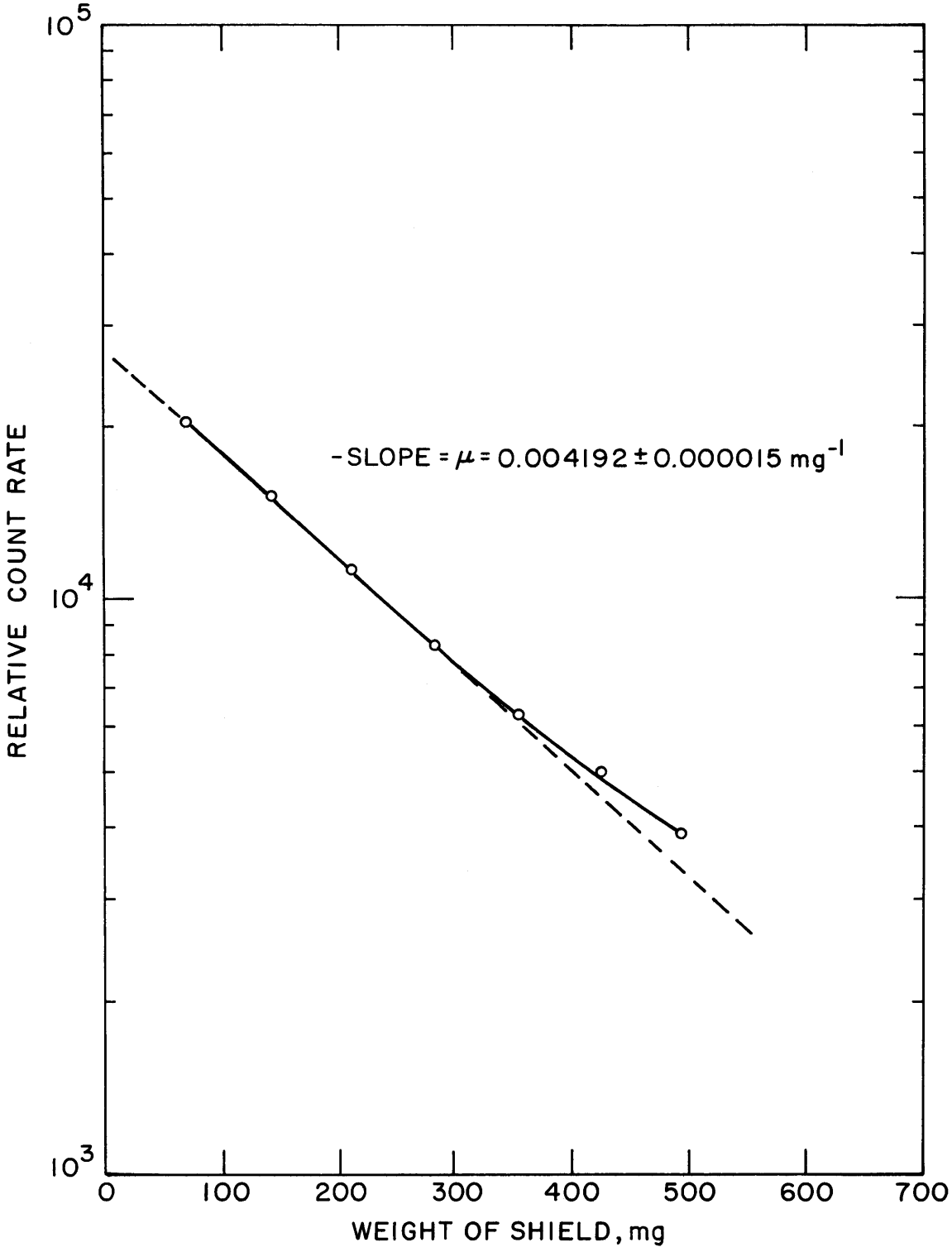

EFFECT OF GAMMA SELF ABSORPTION ON THE MEASURED Np^{239} ACTIVITY

FIG. 3.2.19

tank wall. Since all microscopic parameter measurements were made within these limits, the results should be characteristic for the lattices studied; that is, they should correspond to the results that would be obtained in critical assemblies.

The use of cadmium had no significant effects on the Np^{239} activity of the cadmium-covered foils. The thermal flux perturbation due to a single cadmium sleeve was not detectable in an adjacent fuel rod. Since the cadmium-covered foil and the bare foil were always separated by two lattice cells, the thermal flux perturbation at the bare foil was practically zero. A depression of the fast flux in the cadmium-covered foils affected a slight reduction in both δ_{25} and ρ_{28}; however, for all but one value of ρ_{28} (for the 2.50-inch lattice), the effects were within the experimental uncertainties.

The use of depleted uranium, natural uranium, and aluminum within the fuel rod as shown in Fig. 2.2.1 produces a significant perturbation only in the measurement of δ_{28}. A reduction in the fast flux caused by the displacement of fuel material depresses the fission product activity of the bare, depleted uranium foil. Corrections to be applied to the depleted foil fission product activity have been developed to compensate for this effect.

No effect due to the nonuniform Np^{239} activity distributions in the depleted foils was observed during Np^{239} counting. Also, no significant fission product activity was present during Np^{239} counting of the depleted uranium foils.

Some aspects of the methods used to measure ρ_{28}, C^*, δ_{25} and δ_{28} were a direct result of these error investigations. An attempt was made to consider all possible sources of systematic error. Those which were found to be significant were eliminated or corrections were developed to compensate for them.

CHAPTER IV
EXPERIMENTAL RESULTS

Introduction

The results given in this chapter have been corrected only for perturbations associated with the experimental method or technique. Examples of such perturbations are depression of the neutron flux by the experimental materials or reduction of the measured count rates by counter dead time. Analytical adjustments or corrections, such as corrections for neutron leakage, have not been applied; analytical corrections and interpretations are made and discussed in Chapter VI. A discussion of the methods used to reduce the raw counting data precedes the presentation of the final experimental results.

4.1 Methods of Data Reduction

Corrections for each of the following items were made, where applicable, to each count of each detector foil:

1. Room background;
2. Natural and residual activities;
3. Decay of activity between or among the foil counts to be used to calculate a ratio;
4. Decay of activity during counting;
5. Counter dead time and pulse pile-up;
6. Foil weight and thickness or intercalibration;
7. Axial and radial position in the exponential tank.

These corrections were applied to the raw counting data for the intracellular activation distributions, and to the raw counting data for the measured fission products of the uranium detector foils by means of computer programs written for the IBM 7094 of the M.I.T. Computation Center. The experiments for the intracellular activation distributions

involved a large number of foils and hence a large number of calculations; the program ANA, described in Appendix C, was therefore used to analyze the data for these experiments.

The decay of the fission product activities of the uranium detector foils is a complicated sum of exponentials, and a special technique had to be developed to correct for the decay of the activity between foil counts. A polynomial was fitted by the least squares method to the corrected foil activities as a function of the time at which the activities were measured, and then the polynomial coefficients obtained by this fitting were used to determine relative foil activities at the desired common times. The values of δ_{28} and δ_{25} were calculated by means of the computer program PEG, written by J. Wolberg and described in Ref. W3. The computer program LSQ-4D, described in Appendix C, was used to aid in the determination of values of R_F which were then used to calculate values of C^*. All the results involving fission product activities were found to be insensitive to the degree of the polynomial used, and also insensitive to the functional relation chosen for example A as a function of t, or ln A as a function of t, or ln A as a function of ln t, where A is the corrected fission product activity and t is the time at which the activity was measured.

The general method used to determine an experimental value of a ratio of foil activities was as follows:

1. A value of the ratio was determined for each set of counts for each set of foils;
2. For each foil set, the values of the ratio for each set of counts were averaged by weighting each result with its uncertainties as estimated from the counting statistics for each set of counts;
3. The values of the ratio for each foil set were averaged to obtain a final average value of the ratio. The uncertainty due to counting statistics were approximately equal; hence, the final value is taken as an unweighted average.
4. The standard deviation of the average value of the ratio was computed and is the uncertainty assigned to the values of the ratios; hence, this uncertainty includes experimental

uncertainties such as foil positioning as well as counting statistics.

4.2 Results

The values of ρ_{28}, C^*, δ_{25}, δ_{28} and ρ_{Au} obtained for the three lattices studied, containing 0.250-inch-diameter, 1.03 w/o U^{235} fuel rods, the values of ρ_{28} and ρ_{Au} for a single rod in position 13 of the MITR, and the value of δ_{28} for a single rod in the exponential tank, are listed in Table 4.2.1. In Fig. 4.2.1, the values of ρ_{28}, obtained during the present work for 1.03 w/o U^{235}, 0.25-inch-diameter fuel rods, are compared to the values of ρ_{28} for 1.14 w/o U^{235}, 0.25-inch-diameter fuel rods measured by Peak et al. (P 2) in the M.I.T. miniature lattice and to the values of ρ_{28} for 1.0-inch-diameter, natural uranium fuel rods. The three sets of results seem to show the same trends; the comparison will be discussed in more detail in Chapter VI.

Figure 4.2.2 compares the results of the C^* measurements obtained with the two different experimental methods discussed in Section 2.2:

$$C^* = C^*_{STD} \frac{R_N}{R_F}, \tag{2.2.13}$$

and

$$C^* = \left(\frac{1 + \rho_{28}}{1 + \delta_{25}}\right)\left(\frac{\Sigma_a^{28}}{\Sigma_f^{25}}\right)_{SC}. \tag{2.2.16}$$

The results differ by about two per cent. Although this discrepancy is smaller than the uncertainties associated with the values of the cross sections used in Eqs. 2.2.13 and 2.2.16, it seems to be systematic in that the results obtained from Eq. 2.2.13 are consistently lower. The difference between the two methods is in the way in which the measured activities are related to relative reaction rates; this is done by forming the ratio of the relative reaction rate of a foil as calculated by THERMOS to the measured activity of the foil. In Eq. 2.2.13, this normalization is by means of the activity of a foil irradiated in the well thermalized neutron flux in the cavity sample tube; in Eq. 2.2.16, the

TABLE 4.2.1. Measured Microscopic Parameter Data[a]

Rod Spacing (Inches)	Volume Ratio V_m/V_f	R_{28}	ρ_{28}	C^* (Equation 2.2.13)[b]	C^* (Equation 2.2.16)[c]	C^* Average	δ_{25}[d]	δ_{28}[d]	ρ_{Au}	B_m^2 cm^{-2}[e]
1.25	25.9	2.183	0.8453	0.7919	0.8137	0.8028	0.0525	0.0274	0.452	0.001195
		±0.010	±0.0071	±0.0020	±0.0075	±0.0064	±0.0100	±0.0012		±0.000023
1.75	52.4	3.287	0.4373	0.625	0.6436	0.6345	0.0310	0.0217	0.244	0.001200
		±0.016	±0.0031	±0.016	±0.0032	±0.0076	±0.0013	±0.0007		±0.000018
2.50	108.6	5.402	0.2272	0.5467	0.05544	0.5506	0.0188	0.0183	0.147	0.000907
		±0.029	±0.0014	±0.0028	±0.0018	±0.0022	±0.0023	±0.0007		±0.000020
Single Rod	∞	–	–	–	–	–	–	0.0130[g] ±0.0005	–	–
Pos. #13[f] of the MITR	∞	2.93 ±0.06	0.521 ±0.016	–	–	–	–	–	0.275	–

(a) The uncertainties are the standard deviations of the mean of two or more determinations.

(b) The value of C^*_{STD}, 0.4569, was calculated from THERMØS results for a simulated cavity.

(c) The values of $\left(\Sigma_a^{28}/\Sigma_f^{25}\right)_{SC}$ used were obtained from THERMØS results and are listed in Table 5.4.1.

(d) Results include measurements made by H. Bliss (B1).

(e) Results of Harrington (H8), Kim (K2), and F. Clikeman et al. (C2).

(f) The values quoted are an average of measurements made at heights of 14.5 inches and 21.0 inches above the bottom of the sample thimble.

(g) Preliminary results from measurements made by Olsen (O1).

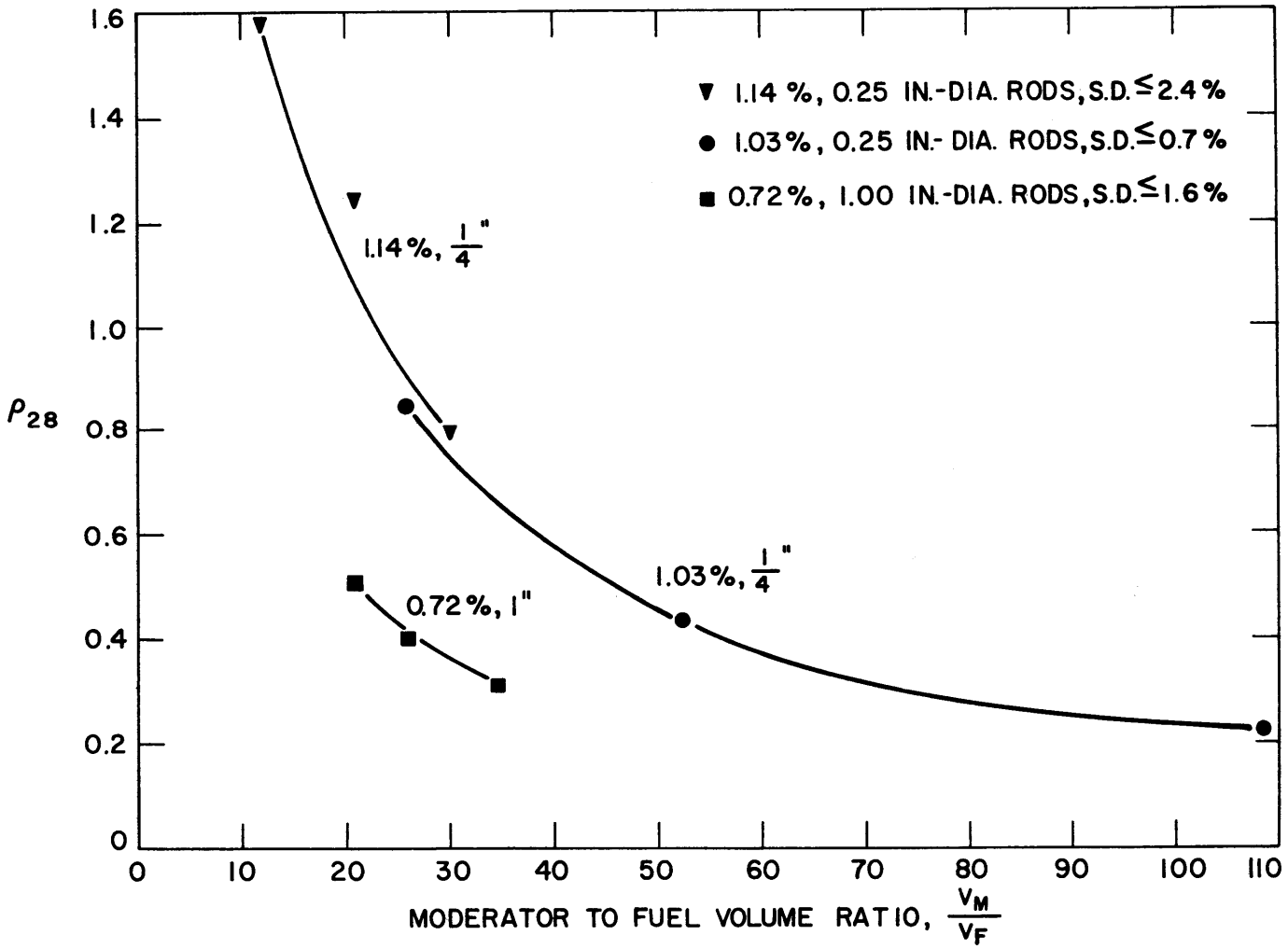

ρ_{28} VERSUS $\frac{V_M}{V_F}$

FIG. 4.2.1

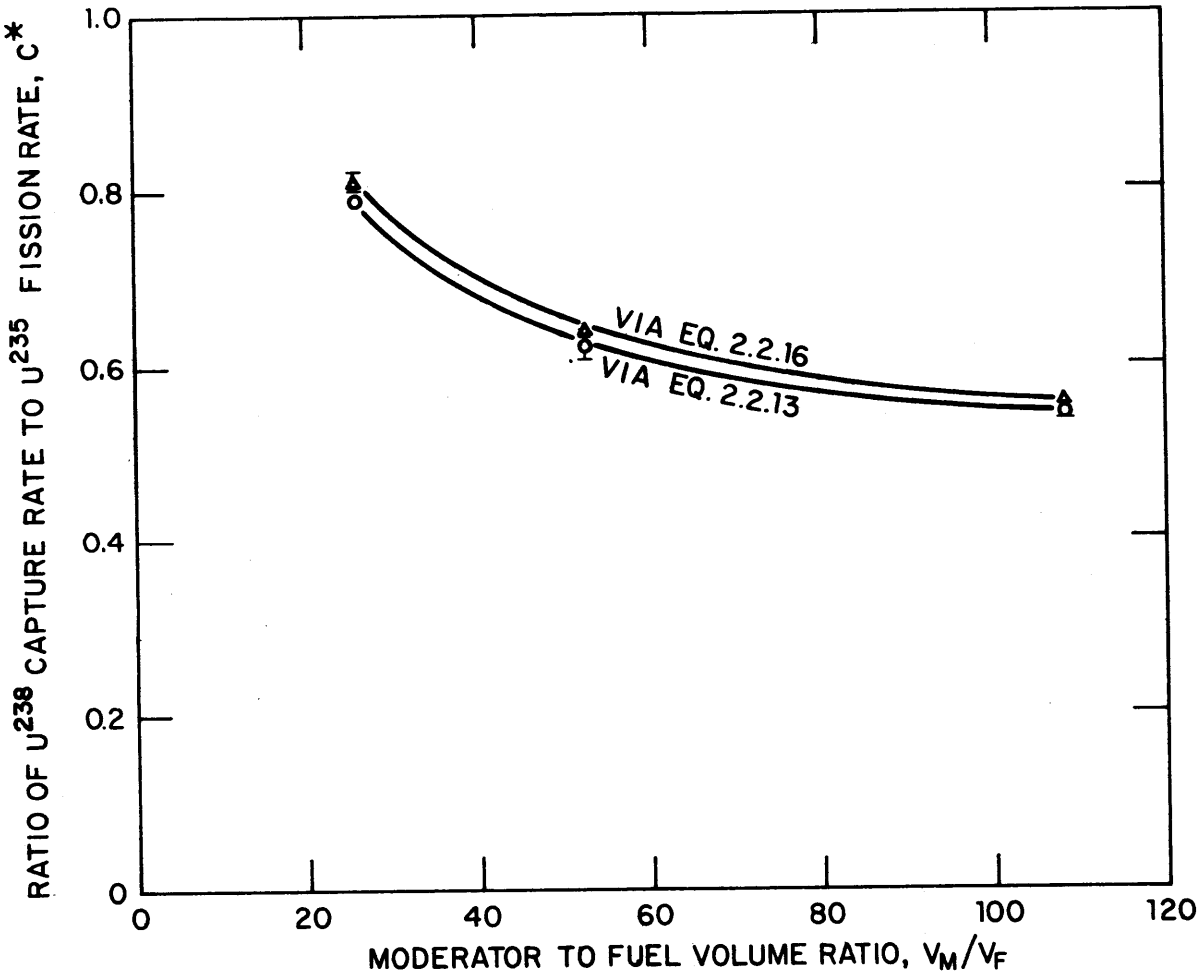

VALUES OF C^* FOR HEAVY WATER LATTICES WITH 0.25-INCH DIAMETER, 1.03 w/o U^{235} FUEL RODS

FIG. 4.2.2

normalization is by means of the subcadmium activity of a foil in the lattice. Thus, the systematic difference is probably due either to the calculated relative reaction rates obtained from THERMOS or due to a systematic error associated with the measured activities. Recent investigations of the counting systems indicate that the most likely source of error seems to be the measured U^{235} fission product activities because of the relatively high activity of the natural uranium foil irradiated in the cavity sample tube. The relatively high activity of this foil may have reduced the gain in the photomultiplier tube slightly, which would result in a lower count rate for that foil and thus a lower value of C^*. Further studies of this effect are recommended as discussed in Chapter VII.

The reproducibility errors in the values of C^* obtained by Eq. 2.2.13 decreased chronologically from 2.6% to 0.5% to 0.25% for the 1.75-, 2.50-, and 1.25-inch lattices, respectively. This increase in the precision reflects the improvements made in the technique as successive measurements were made. The uncertainty of 0.25% finally attained for this method is a large improvement over that of about 2% associated with the techniques used in earlier work (W1).

The effectiveness of the many small changes made in the experimental arrangements, technique, and procedure are also shown in the decreased scatter in the R_{28} measurements, which is about 0.5% for the results of the present work compared to about 1.0% for the results from earlier work at M.I.T. (W1).

Figures 4.2.3, 4.2.4, and 4.2.5 show the results of the intracellular Np^{239} activation distributions obtained with depleted uranium foils irradiated bare and cadmium-covered in the 1.25-, 1.75-, and 2.50-inch lattices, respectively. The epicadmium Np^{239} distributions all show the same fractional change in activity between the edge of the cell and the center of the fuel rod. This may indicate that the extent to which neighboring rods shield each other in the resonance energy region is not significant. In Figs. 4.2.6 and 4.2.7, the activation distributions obtained with bare and cadmium-covered copper foils are shown for the 1.25- and 1.75-inch lattices. The distributions obtained with bare and cadmium-covered gold foils, measured by Simms (S1) and Clikeman et

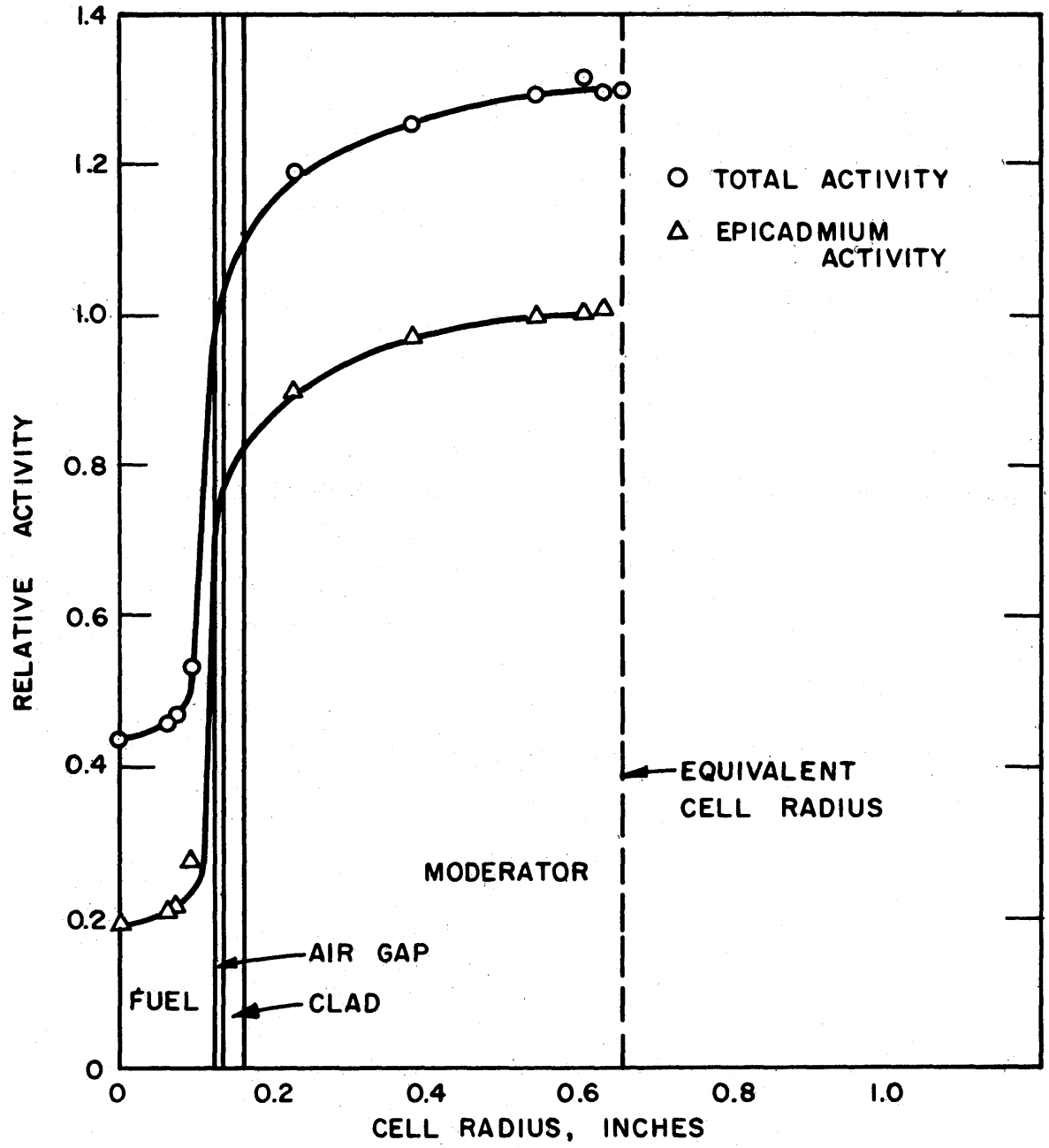

INTRACELLULAR Np^{239} ACTIVITY DISTRIBUTION FOR THE 1.25 - INCH LATTICE

FIG. 4.2.3

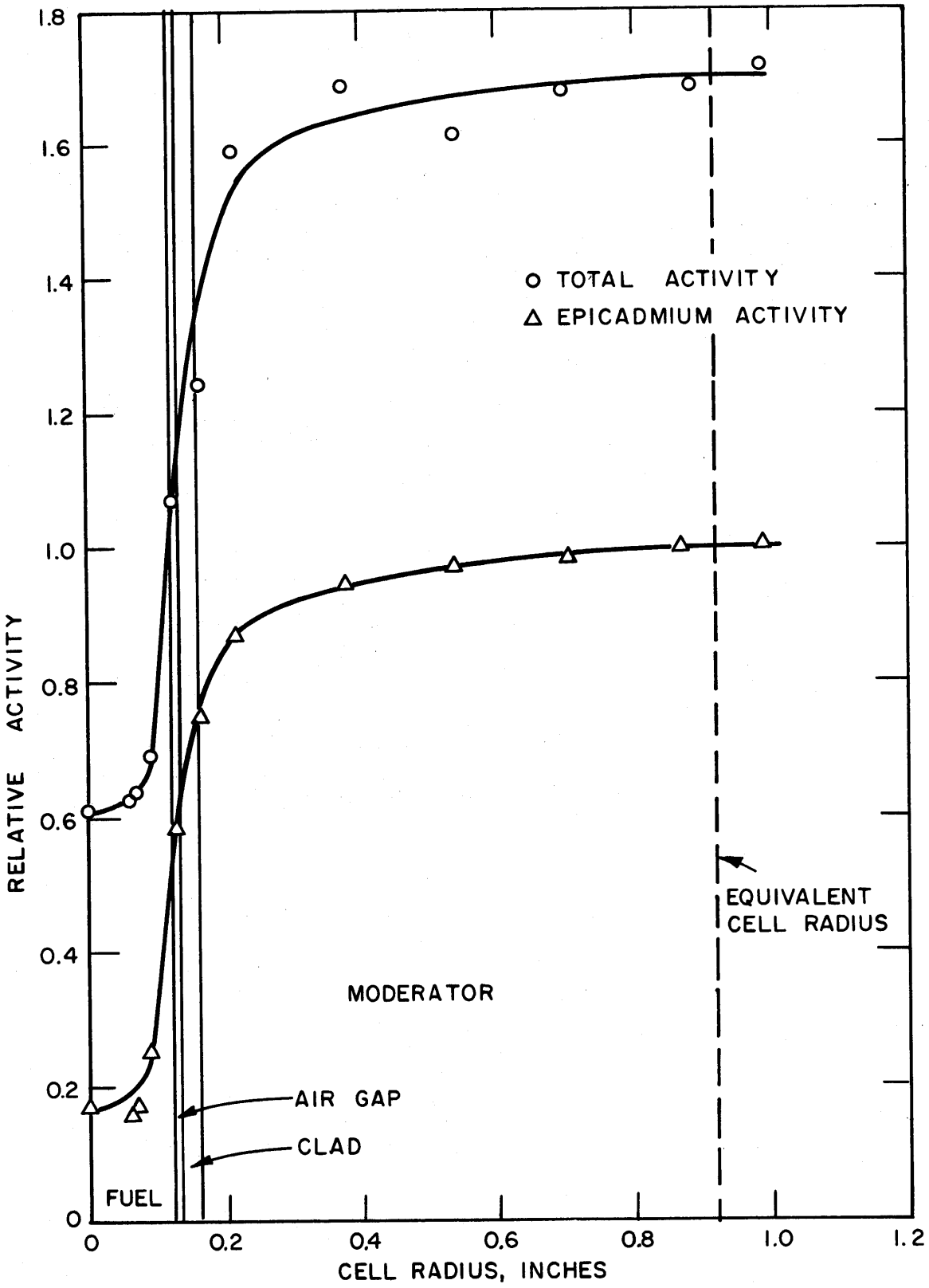

INTRACELLULAR Np^{239} ACTIVITY DISTRIBUTION FOR THE 1.75-INCH LATTICE

FIG. 4.2.4

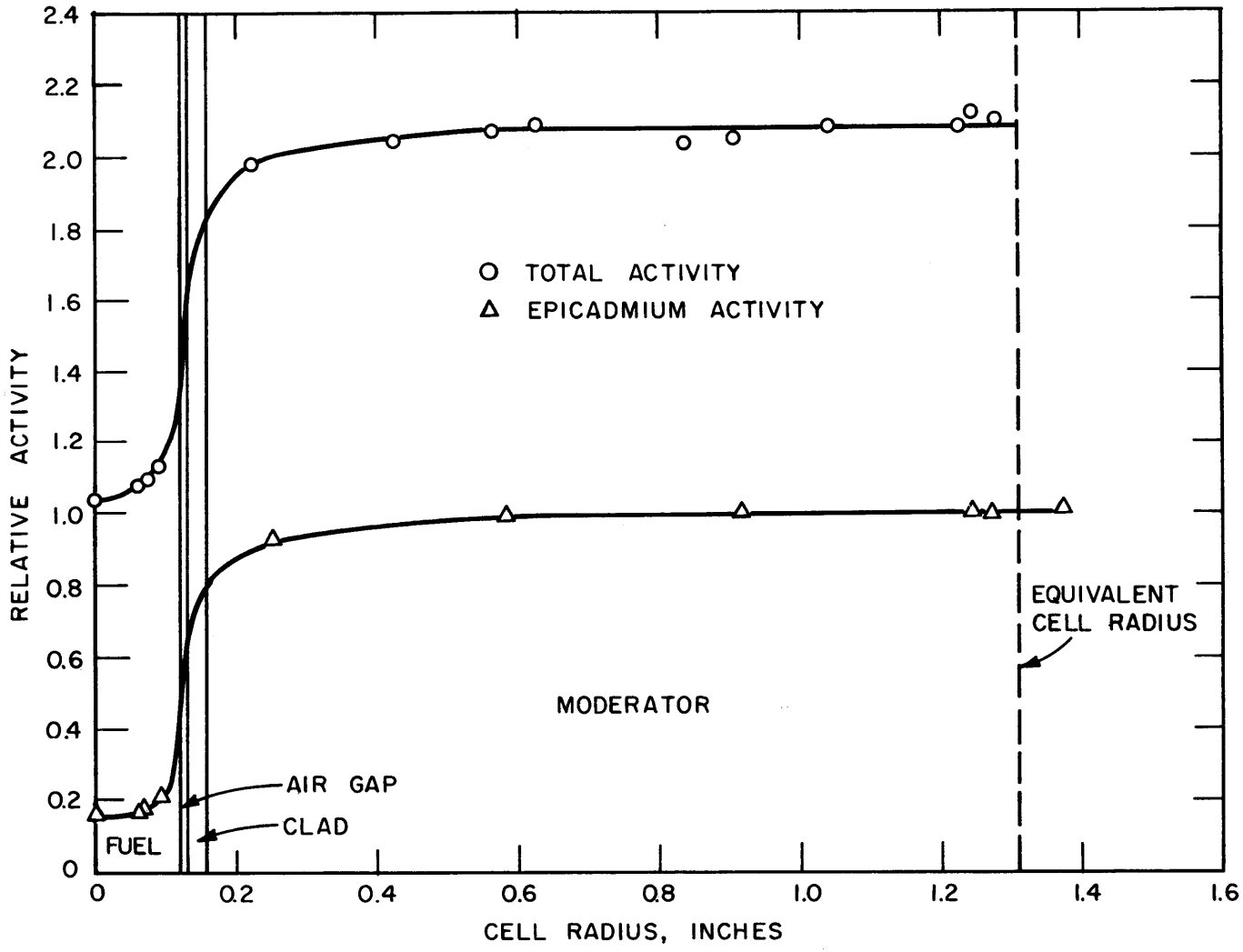

INTRACELLULAR Np^{239} ACTIVITY DISTRIBUTION FOR THE 2.50-INCH LATTICE

FIG. 4.2.5

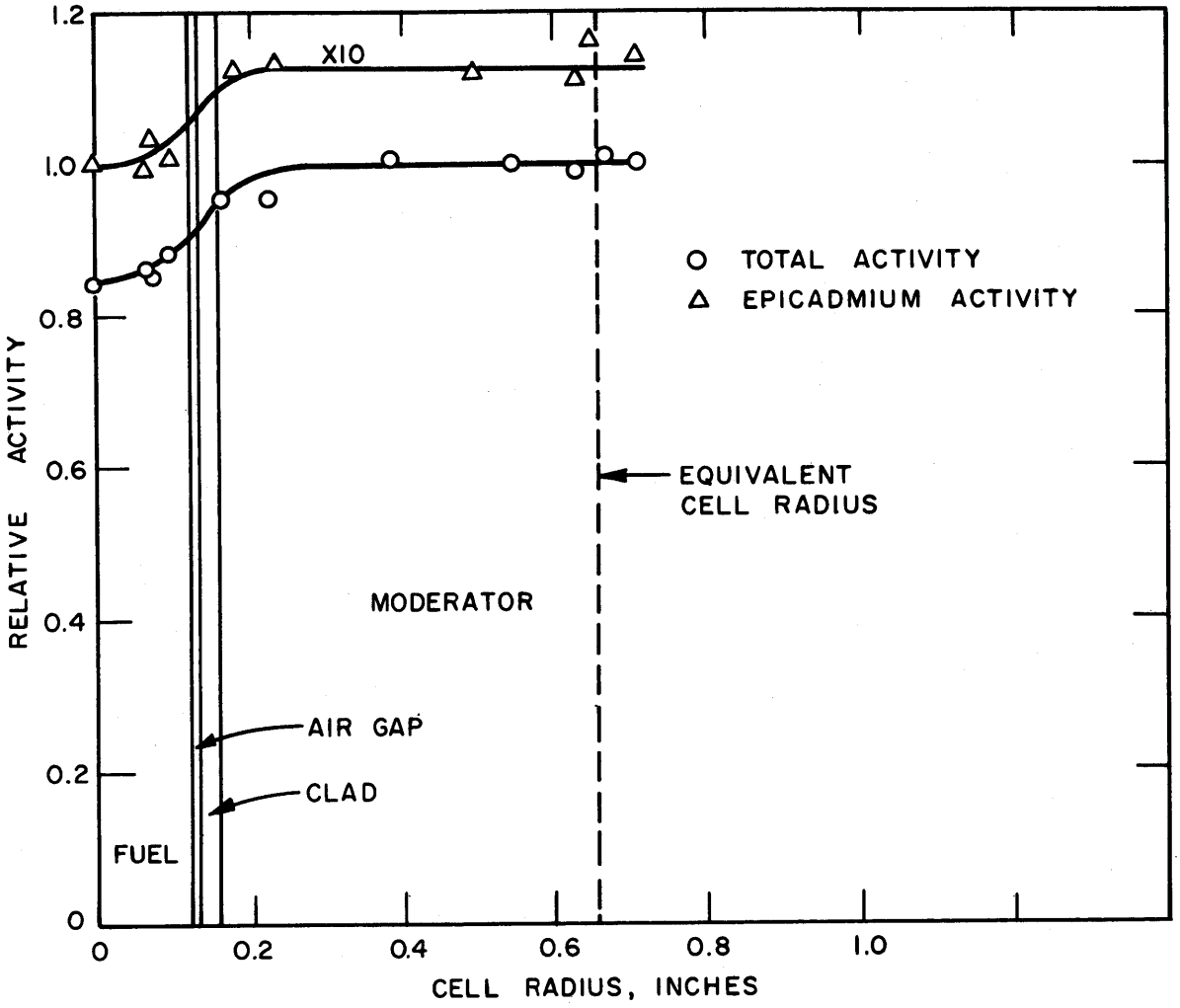

INTRACELLULAR ^{64}Cu ACTIVITY DISTRIBUTION FOR THE 1.25-INCH LATTICE

FIG. 4.2.6

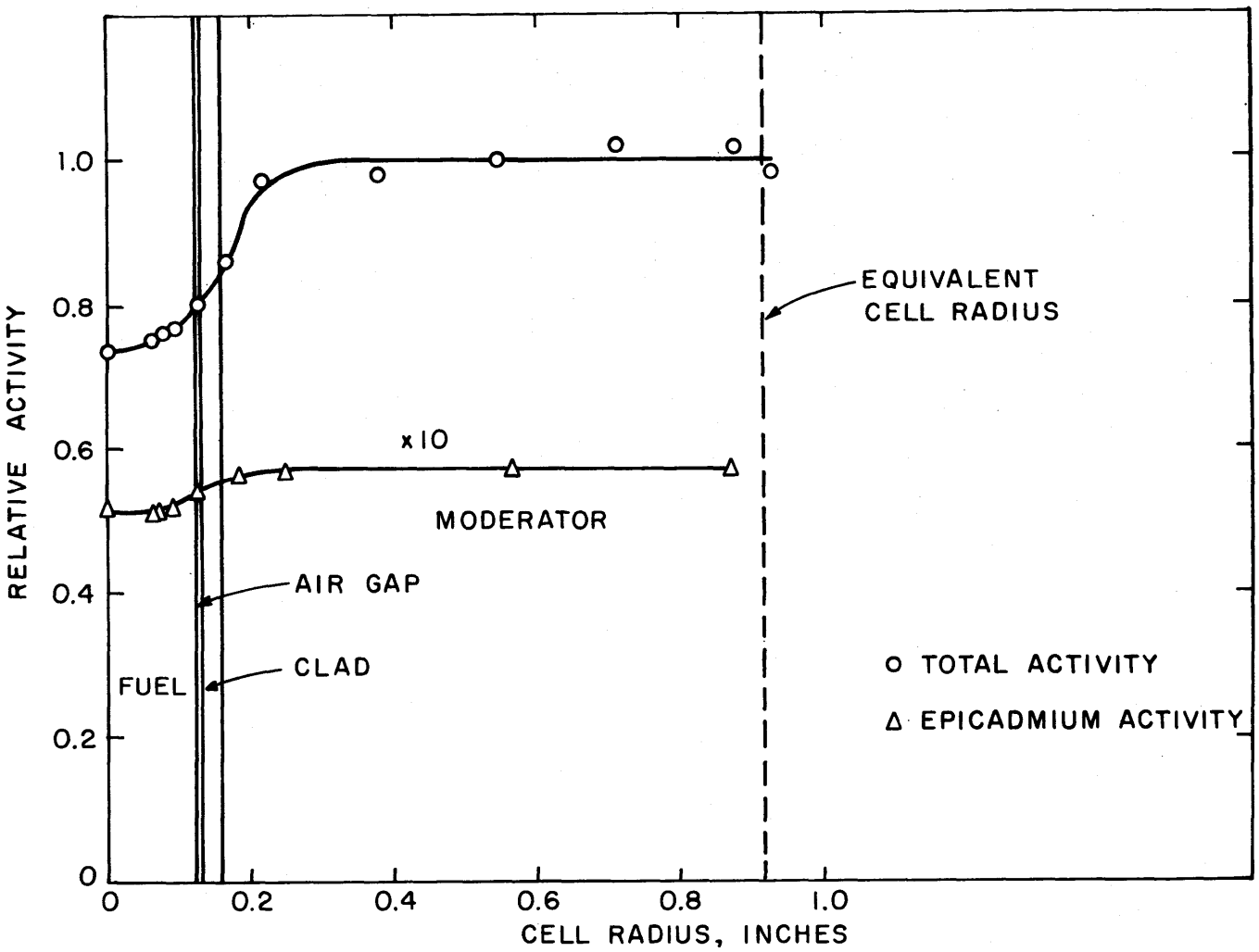

INTRACELLULAR Cu^{64} ACTIVITY DISTRIBUTION FOR THE 1.75 - INCH LATTICE

FIG. 4.2.7

al. (C2), are shown in Figs. 4.2.8, 4.2.9, and 4.2.10 for the 1.25-, 1.75-, and 2.50-inch lattices, respectively. The epicadmium copper and gold distributions are both flat in the moderator, and both distributions have about the same fractional change between the edge of the cell and the center of the fuel rod. Approximately half of the epicadmium copper activity is due to a resonance at 580 ev. In view of these observations, it seems reasonable to assume that the neutron flux in the resonance energy region is spatially flat in the moderator except at energies corresponding to the U^{238} resonances. The preliminary results of the intracellular distributions of the U^{238} fission product activity, as measured with depleted uranium foils by Woodruff (W4) in the 1.25-, 1.75-, and 2.50-inch lattices, are shown in Figs. 4.2.11, 4.2.12, and 4.2.13. Although these results are not final and will probably be corrected, their accuracy is sufficient for the purposes for which they will be used in the present work (see Chapter V). The results show that, as the rod spacing is decreased, the flux peaking in the fuel rod decreases, which is indicative of the increased interaction effect in the high energy region in the tighter lattices.

The results of the resonance activation measurements in the 1.75-inch lattice and at position 13 of the MITR are listed in Table 4.2.2. The experimental values of the resonance activation integrals were obtained by means of Eq. 2.4.20 and with the results of the measurements made in the $\frac{1}{E}$ spectrum at position 13 in the MITR; the known resonance integral of gold was used as a standard. Some of the measured resonance integrals were found to differ significantly from the values reported in the literature. Two examples are As^{75} and Ga^{71} whose resonance integrals were found to be larger than the reported values. This discrepancy cannot be due to self-shielding in the foil, because this effect would act in the opposite direction. The ratios R_F and R_N are defined in the same manner as the ratio R_b; that is, the activity of a foil irradiated bare in the lattice to the activity of a foil irradiated bare in the cavity sample tube. Hence, R_F and R_N are equal to the values of R_b for U^{238} capture in the fuel rod and U^{235} fission in the fuel rod, respectively. By means of R_F, R_N, ρ_{28}, and δ_{25}, the values of R_c for the U^{238} capture and U^{235} fission in the fuel rod were also determined. The values of R_b and R_c

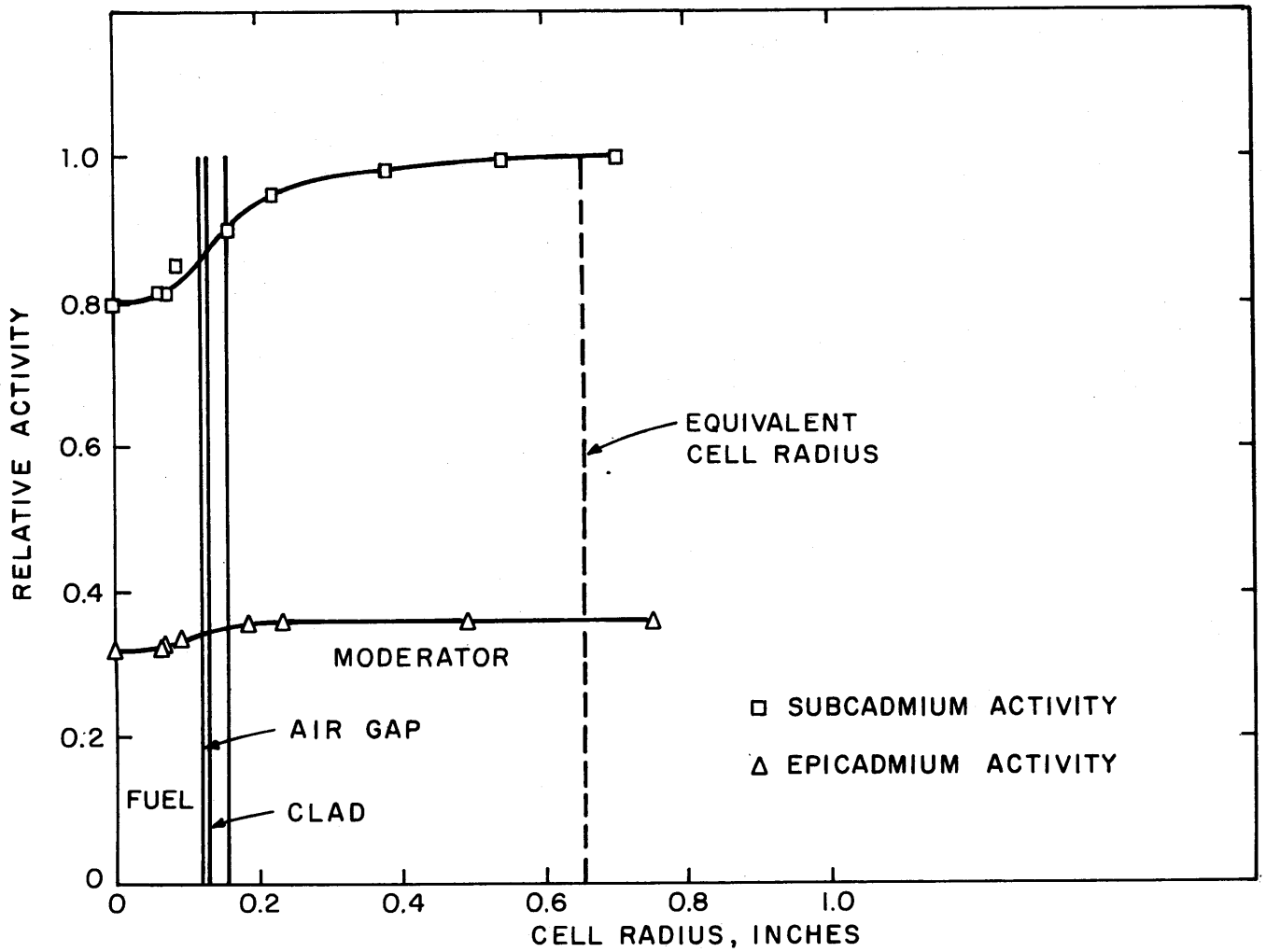

INTRACELLULAR Au^{198} ACTIVITY DISTRIBUTIONS FOR THE 1.25-INCH LATTICE

FIG. 4.2.8

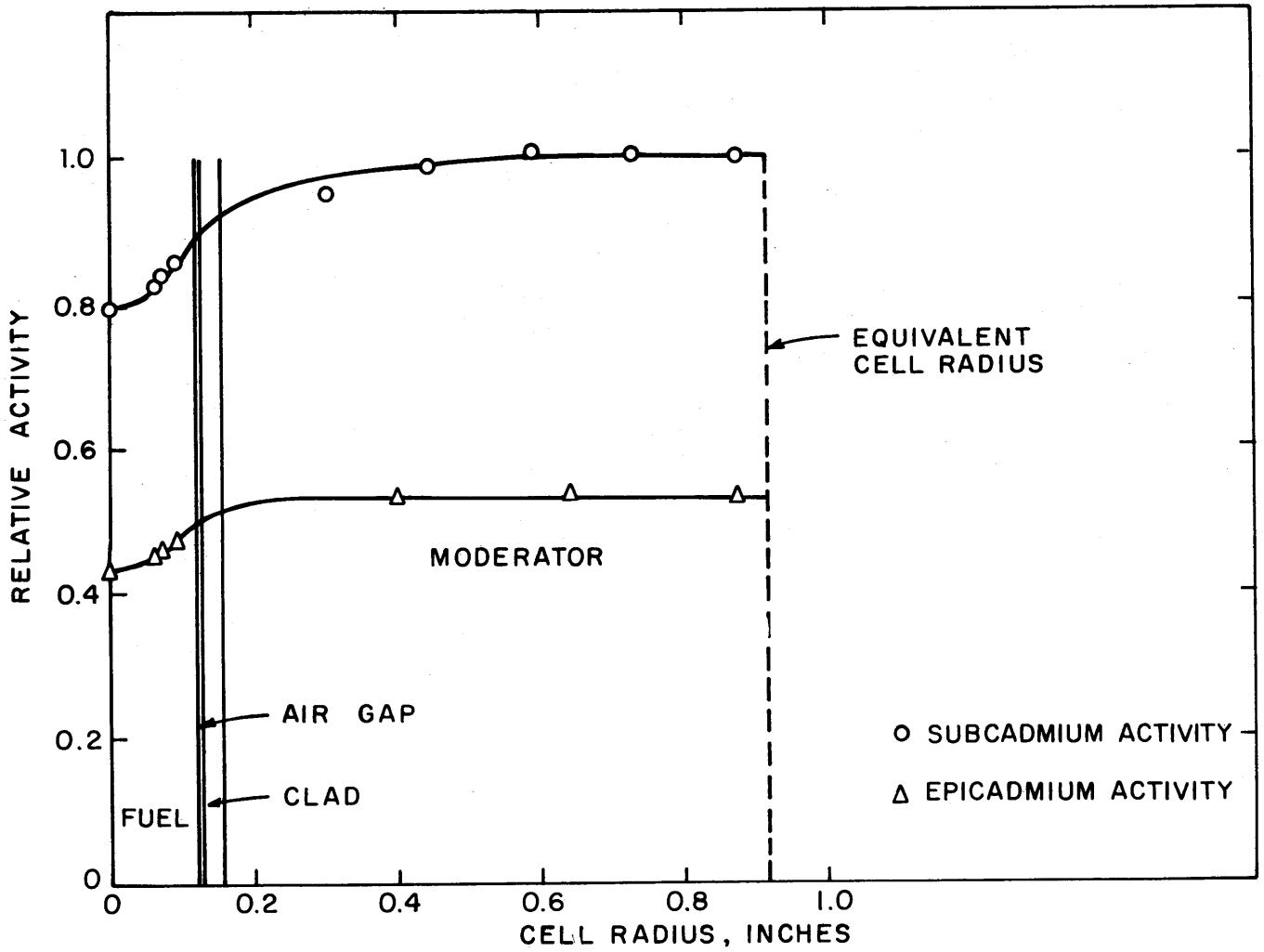

INTRACELLULAR Au^{198} ACTIVITY DISTRIBUTION FOR THE 1.75 - INCH LATTICE

FIG. 4.2.9

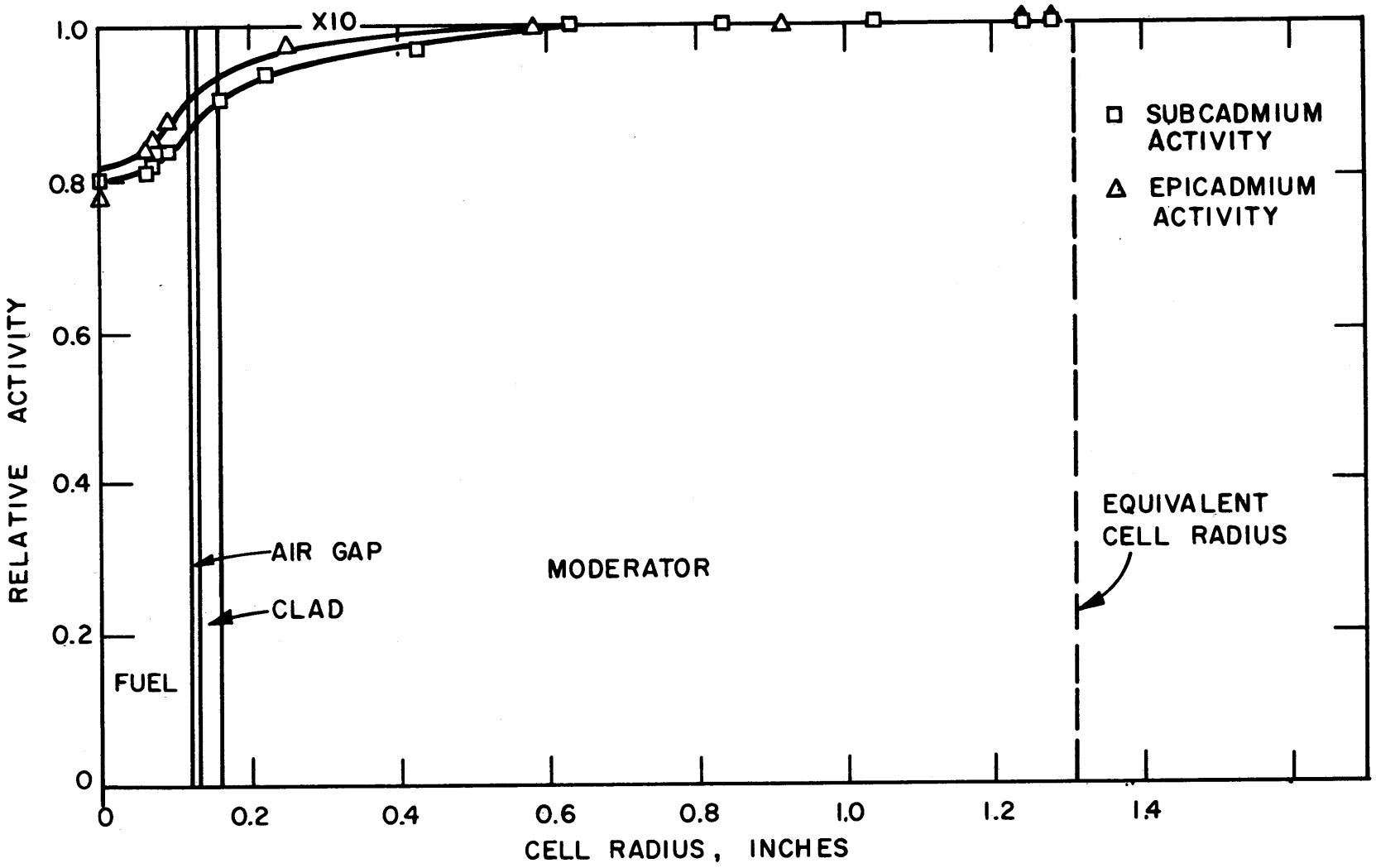

INTRACELLULAR Au^{198} ACTIVITY DISTRIBUTION FOR THE 250-INCH LATTICE

FIG. 4.2.10

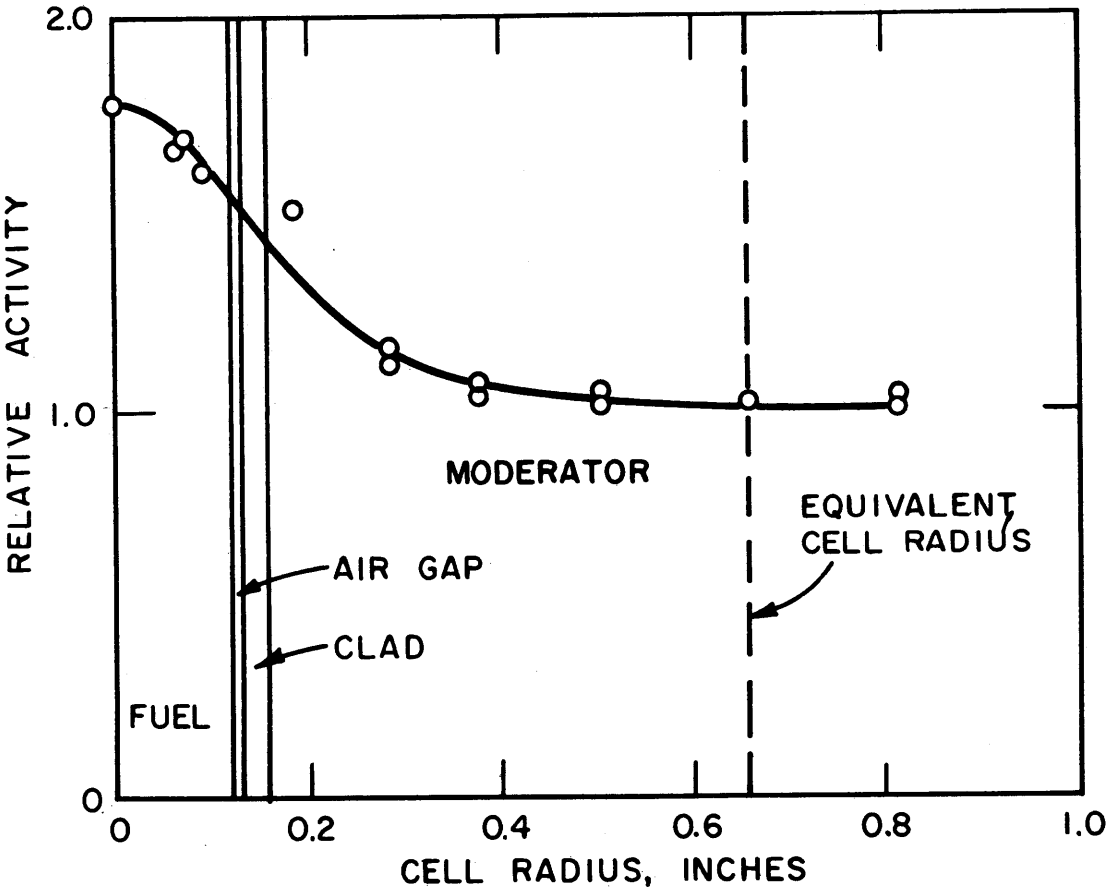

INTRACELLULAR U^{238} FISSION PRODUCT ACTIVITY DISTRIBUTION FOR THE 1.25 INCH LATTICE

FIG. 4.2.11

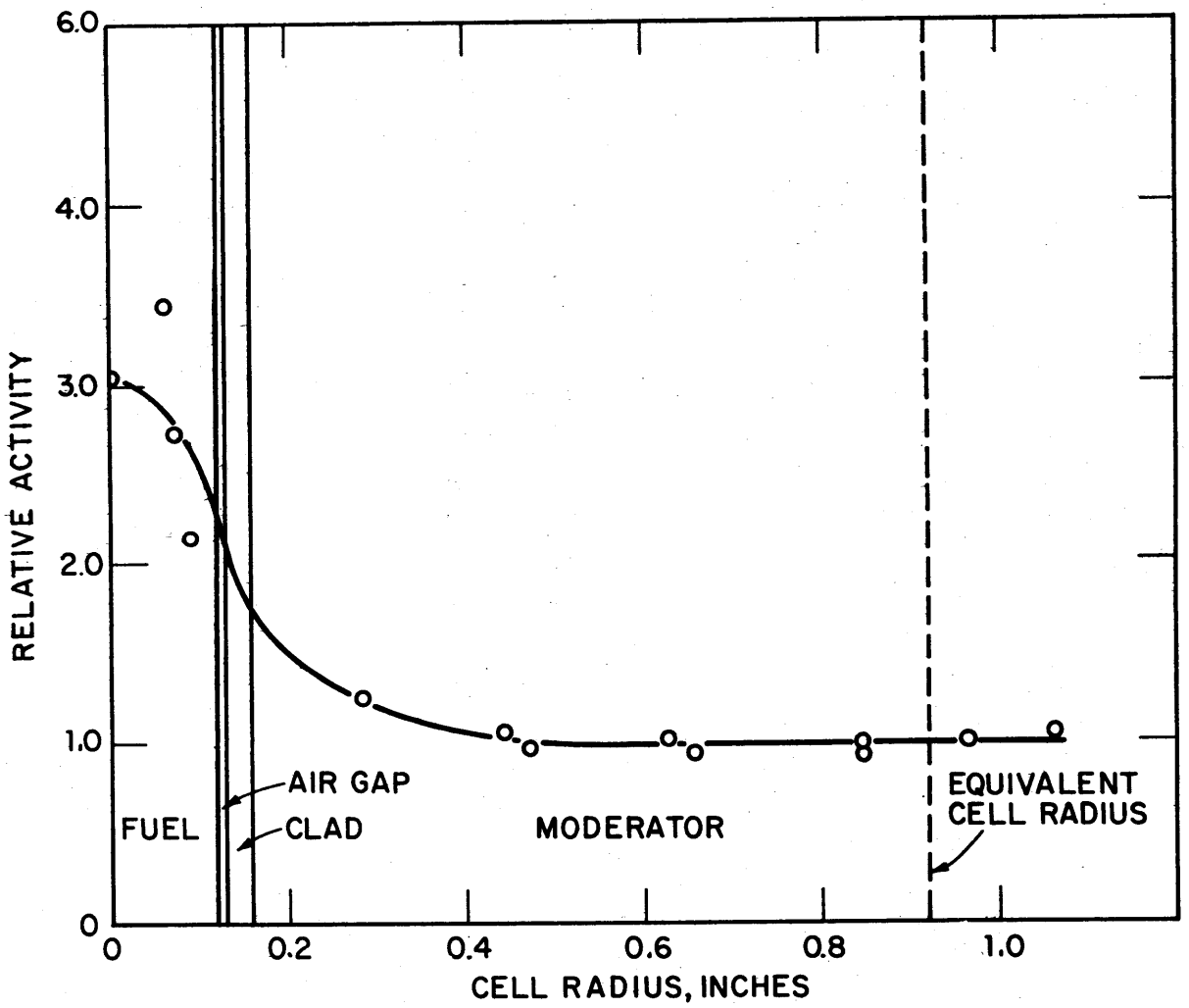

INTRACELLULAR U^{238} FISSION PRODUCT ACTIVITY DISTRIBUTION FOR THE 1.75-INCH LATTICE

FIG. 4.2.12

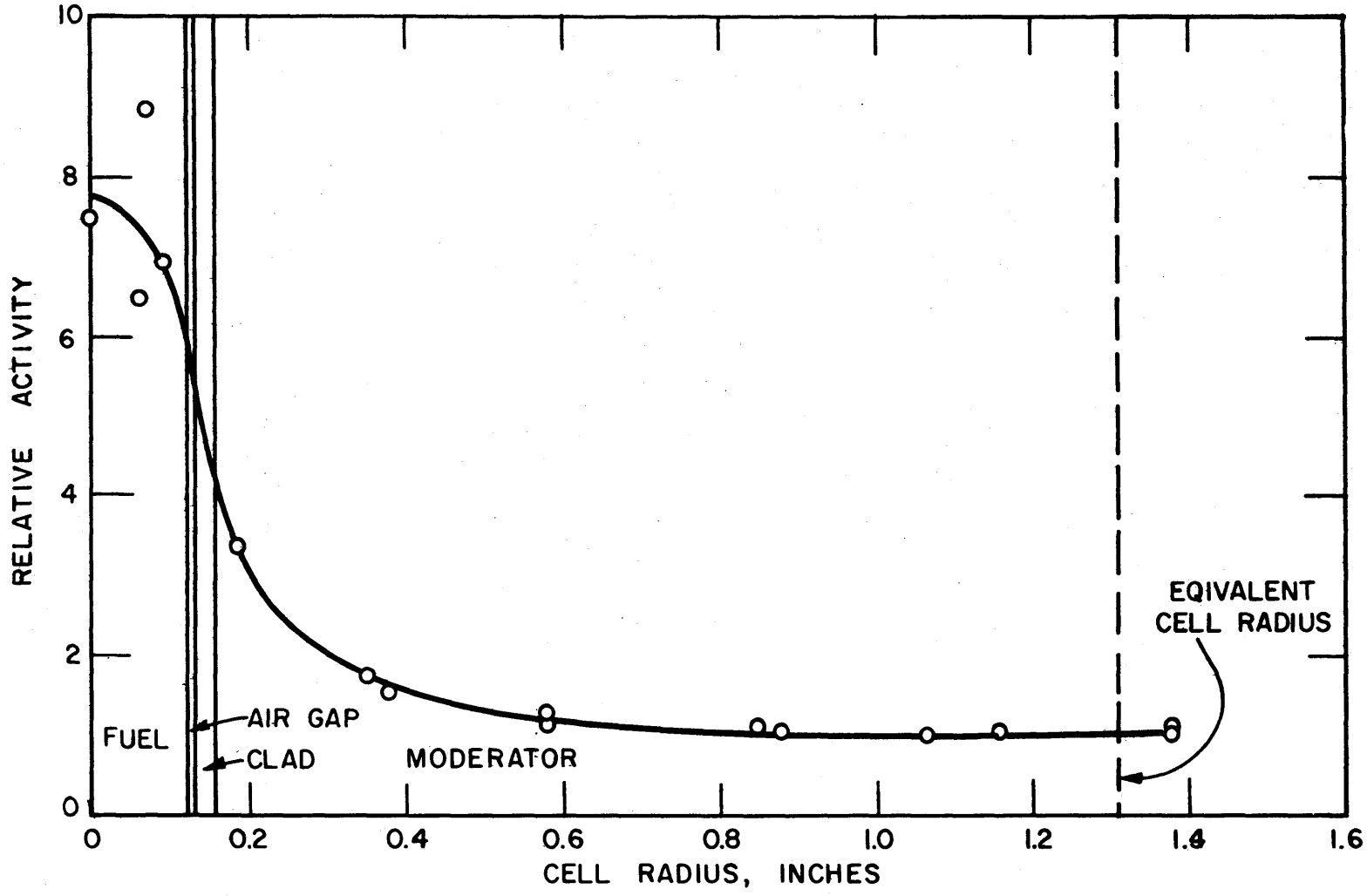

INTRACELLULAR U^{238} FISSION PRODUCT ACTIVITY DISTRIBUTION FOR THE 2.50-INCH LATTICE

FIG. 4.2.13

TABLE 4.2.2

Resonance Activation Data

Nuclide	Peak Energy of Dominant Resonance, E_o, ev	Measured Activation Ratios					Resonance Integral Ratio RI/σ_o	
		R_L	R_b (b)	R_c (b)	R_{res}	R_R (a)	Measured Value	Reported Value, Refs. (M2) and (P3)
In	1.46	2.91 ± 0.01	0.158 ± 0.003	0.0546 ± 0.0055	0.0435 ± 0.0057	6.17	8.0	12.3
Au	4.9	2.41 ± 0.09	0.228 ± 0.021	0.0944 ± 0.0047	0.0985 ± 0.0049	3.80	15.3 (assumed value)	15.3
W	18.6	2.74 ± 0.02	0.184 ± 0.013	0.0672 ± 0.0054	0.0629 ± 0.0056	4.74	11.3	9.5
As	47	2.51 ± 0.01	0.188 ± 0.006	0.0745 ± 0.0045	0.0684 ± 0.0047	4.30	12.9	8.1
Ga	95	3.52 ± 0.07	0.196 ± 0.030	0.0557 ± 0.0078	0.0634 ± 0.0080	6.21	8.0	2.4
Br	101	2.05 ± 0.02	0.246 ± 0.015	0.1202 ± 0.0084	0.1203 ± 0.0086	3.38	18.1	18.2
Mn	337	21.4 ± 4.1	0.118 ± 0.011	0.0059 ± 0.0024	0.0037 ± 0.0026	28.0	1.15	0.67
Na	2850	62 ± 19	0.123 ± 0.009	0.0022 ± 0.0004	assumed 0	95.0	assumed 0	~0
U^{238}	–	3.306 ± 0.013	0.1982 ± 0.0005	0.0600 ± 0.0003	0.0570 ± 0.0004	–	–	–
U^{235}	–	33.2 ± 1.7	0.1408 ± 0.0041	0.0042 ± 0.0002	assumed 0	–	–	–

(a) Measured at the bottom of the sample thimble at position 13 of the MITR.

(b) For foil irradiated in center lattice at height of 20 inches above the bottom of the fuel region.

listed in Table 4.2.2 have all been normalized to the values of the ratios which would be obtained if the foils in the lattice were irradiated in the central fuel rod at a height of 20 inches above the bottom of the fuel region. The values of the axial and radial bucklings, as measured by Clikeman et al. (C2), were used to correct the activities of the foils irradiated in the lattice to this standard position.

The values of the resonance activation of each nuclide, R_{res}, are the average of the values determined by means of Eqs. 2.4.13 and 2.4.16. To calculate R_{res} for the nuclides irradiated in the moderator, the sodium activation data were used as those of a $\frac{1}{v}$ detector and, in the fuel rod, the activation data from the fission of U^{235} were used as those which would be obtained for a $\frac{1}{v}$ detector.

The uncertainty of most of the resonance activation data is of the order of 5 to 10 per cent. Although this precision is only fair, it is sufficient to show the feasibility of the experimental methods described in Section 2.4 (see Section 6.3). The resonance activation measurements in the moderator have the advantage that many sources of systematic errors which are significant for foils irradiated inside the fuel rods are not present, and therefore it is expected that measurements can be made with uncertainties equivalent to or better than that found in the measurement of C^* (of about 0.25%).

CHAPTER V
THEORETICAL METHODS AND RESULTS

Introduction

This chapter treats the theoretical methods used to calculate the analytical quantities, such as spectrally averaged cross sections and relative reaction rates, necessary for the analysis and interpretation of the experimental results given in the preceding chapter. These analytical quantities were obtained from the output of two computer programs: THERMOS, which calculates the spatial and spectral thermal neutron distribution, and GAM-I, which calculates the homogeneous epithermal neutron spectrum.

5.1 THERMOS

The computer program THERMOS, developed by H. C. Honeck(H6, H7, H8), solves numerically the integral transport equation for the relative scalar neutron density as a function of position and velocity. The program also calculates spectrally averaged reaction rates and cross sections as functions of position. Up to 30 thermal velocity groups, 20 space points and 10 nuclides in five mixtures can be used in a one-dimensional slab or cylindrical arrangement with either a reflecting or vacuum boundary condition. Ten additional nuclides can be used for edit purposes. The program was used with the reflecting boundary condition to make calculations for infinite assemblies of lattice cells corresponding to the three lattices studied during the course of the present work. Simms et al. (S1) have shown that the use of the infinite-lattice THERMOS code for the finite exponential experiments introduces only negligible errors.

Two basic assumptions made in THERMOS which might affect its results are isotropic scattering and the reflection condition of the cell edge in which the angle of incidence equals the angle of reflection.

Earlier work at M.I.T. by Brown et al. (B2) and Simms et al. (S1) has shown that these assumptions can significantly affect the results. The assumption of isotropic scattering is most likely to introduce significant errors when light elements such as hydrogen or deuterium are used. A first-order correction for anisotropic scattering was made by multiplying the diagonal elements of the hydrogen and deuterium scattering kernels by $1-\bar{\mu}_o$ (B2, S1), where $\bar{\mu}_o$ is the average cosine of the scattering angle; the use of these modified scattering kernels yielded results which agreed satisfactorily with experimental results (B2, S1). The reflection condition at the cell boundary may lead to serious errors in "tight" lattices arising from the assumed cylindricalization of the unit lattice cell, as in the case of the Wigner-Seitz cell approximation. A "tight" lattice is one in which the cell dimensions are small in terms of neutron mean free paths. Modified one-dimensional THERMOS calculations, in which the usual equal-angle reflection condition at the cell boundary is replaced by an isotropic reflection condition, have been shown to give good results (H10, S1), that is, results in agreement with both experimental results and the results of two-dimensional THERMOS calculations. In the latter, the cylindrical cell approximation is not made and the actual hexagonal cell is treated.

The type of energy exchange kernel used in THERMOS is optional; the Nelkin-Honeck kernel (H9) was used for D_2O, the Nelkin kernel for H_2O (N1), and the free gas kernel was used for all other nuclides. An analytical study by Simms et al. (S1) indicated that the details of the kernel are not important for the D_2O lattices studied. A unit "$\frac{1}{E}$" slowing-down source of neutrons is assumed in THERMOS; for the three lattices studied, this assumption is valid because the calculated neutron flux spectra for the three lattices exhibit a "$\frac{1}{E}$" energy dependence in the upper velocity groups. As in earlier work at M.I.T. (P2, B2, S1), the results of the THERMOS calculations were found to be insensitive to the spatial distribution of the slowing-down source and, for simplicity, a spatially uniform source was used for all calculations. Calculations were made with the method developed by Simms et al. (S1) in which the loss of neutrons due to radial leakage was simulated; the

same technique was used to simulate the axial leakage. Neither the radial leakage nor the axial leakage had a significant effect upon the spectrally averaged relative reaction rates and cross sections. Hence, in calculations for finite assemblies, it should be valid to include the effects of thermal neutron leakage by multiplying the relative reaction rates calculated for the infinite lattice cell by the thermal nonleakage probabilities.

The good agreement between the THERMOS results and experimental results (B1, S1) indicate that the neutron distributions calculated by THERMOS are an excellent approximation of the actual distributions. The factors which limit the accuracy of the calculations are most likely the uncertainties in the input data such as the nuclide cross sections and the nuclide concentrations. The input data used for the THERMOS calculation are given in Appendix D.

5.2 GAM-I

The computer program GAM-I, developed at General Atomic and described in Ref. (J1), solves the one-dimensional, energy-dependent transport equation in either the B_1 or P_1 spherical harmonics approximation for the spatially averaged relative neutron flux and current spectra in the neutron energy range between 0.414 ev and 10 Mev. The numerical solution of the set of B_1 or consistent P_1 equations is based on a 68 lethargy group structure for this neutron energy range. The program also calculates up to 32 broad group, spectrally averaged cross sections and can optionally calculate the age of an infinite homogeneous medium by the moments method. Many approximations are associated with the solution of the equations (G1) and, although no effort will be made to evaluate all of them, a few merit comment since they affect the input data and the use of the program.

Since the solution of the GAM-I code assumes a homogeneous medium, it is necessary to homogenize the heterogeneous lattice cell. As indicated by the intracellular activation distributions presented in Chapter IV, the magnitude of the fast neutron flux is much higher in the fuel rod than in the moderator; the resonance energy flux is higher in the moderator than in the fuel rod. Obviously, this flux peaking can lead

to errors in the calculation of the relative reaction rates. To compensate for this effect, the GAM-I program has a provision for energy-dependent flux weighting factors for each nuclide. Values of these factors were calculated from the intracellular activity distributions presented in Chapter IV. The U^{238} fission products activation distributions were assumed to be proportional to the fast flux above 1 Mev, and flux weighting factors for the energy range between 1 and 10 Mev were calculated directly from these distributions. Since experimental results which would provide information for the energy range, 0.1 Mev to 1 Mev, were not available, the weighting factors for this range were set equal to one-half the magnitude of the factors for 1 to 10 Mev. This makes the transition from the fast region, where the flux peaks in the rod, to the resonance region, where the flux peaks in the moderator, more realistic. Between 1 Kev and 0.1 Mev, the factors were taken to be equal to unity; between 0.414 ev and 1 Kev, the factors were calculated directly from the Cu^{64} or Au^{198} epicadmium activation distributions. The program calculates the resonance integral for U^{238} by the methods developed by Adler et al. (A1) so that resonance energy flux weighting or "self-shielding" factors are not required for this nuclide. The flux weighting factors used for the three lattices studied are listed in Table 5.2.1. GAM-I assumes that the medium is in the form of an infinite slab and that the spatial dependence of the neutron flux is of the form $\cos BZ$ where B is the geometric buckling, assumed independent of energy. Since the medium is treated as homogeneous, there is no loss of generality with the assumption of an infinite slab; it is only required that a proper buckling, based on the total leakage from the system, should be used. Since the GAM-I calculations for the three lattices studied are to represent the characteristics or "asymptotic" spectra, the material buckling as determined by buckling measurements (H1, K2, C2) was used. Calculations with extremely small values of the buckling were also made so that the effects of neutron leakage could be estimated.

The accuracy of the GAM-I results is probably limited by a combination of the accuracy of the input data such as the cross sections and the flux weighting factors and, depending on the type of system, by the many approximations made in GAM-I. The approximations associated

TABLE 5.2.1

Flux Weighting Factors for GAM-I Input

Rod Spacing (Inches)	Energy Range	Region		
		Fuel	Clad	Moderator
1.25	1 Mev to 10 Mev	1.40	1.22	0.984
	0.1 Mev to 1 Mev	1.20	1.11	0.992
	1 Kev to 0.1 Mev	1.0	1.0	1.0
	0.414 ev to 1 Kev	0.920	0.971	1.002
1.75	1 Mev to 10 Mev	2.71	1.86	0.958
	0.1 Mev to 1 Mev	1.855	1.43	0.980
	1 Kev to 0.1 Mev	1.0	1.0	1.0
	0.414 ev to 1 Kev	0.926	0.969	1.002
2.50	1 Mev to 10 Mev	4.82	3.20	0.953
	0.1 Mev to 1 Mev	2.91	2.10	0.977
	1 Kev to 0.1 Mev	1.0	1.0	1.0
	0.414 ev to 1 Kev	0.901	0.967	1.001

with the GAM-I calculations are probably too severe due to the highly heterogeneous nature of the three lattices studied, the presence of a strong resonance absorber such as U^{238}, and the heavy water moderator; however, as will be pointed out in the next section, the GAM-I calculations are adequate for the purposes of the present work.

5.3 Normalization Between GAM-I and THERMOS

Cross sections and relative reaction rates averaged over the subcadmium portion of the neutron flux spectrum were obtained directly from the output of the THERMOS calculations and over the epicadmium portion of the spectrum from the GAM-I calculations. However, for some calculations, such as the calculation of the initial conversion ratio, C, from the experimental ratio C^* (see Chapter VI), values of cross sections or relative reaction rates averaged over the total neutron flux spectrum are required. These quantities can be obtained by combining the results of GAM-I and THERMOS because the two programs cover complimentary portions of the total flux spectrum. The lower limit of the energy range covered by GAM-I is 0.414 ev and the upper limit of the twenty-seventh velocity group in THERMOS is 0.415 ev. Since the difference between these two limits is insignificant and since these limits lie in the neighborhood of unclearly defined energy of the "cadmium-cutoff," they provide an excellent coupling point between the two programs.

The values of the cross sections and relative reaction rates averaged over the total neutron flux spectrum were calculated from the results of THERMOS and GAM-I by means of the relation:

$$\sigma_T = \frac{\langle \sigma_T \phi_T \rangle}{\phi_T} = \frac{\sigma_{SC}\phi_{SC} + \alpha\sigma_{EC}\phi_{EC}}{\phi_{SC} + \alpha\phi_{EC}} , \qquad (5.3.1)$$

where $\langle \sigma_T \phi_T \rangle$ is the spectrally averaged relative reaction rate, and the subscripts T, SC, and EC refer to the total spectrum, the subcadmium portion of the spectrum treated by THERMOS, and the epicadmium portion of the spectrum treated by GAM-I, respectively. The factor α normalizes the arbitrary magnitudes of the neutron flux of THERMOS and GAM-I and must be determined appropriately. (The relative flux calculated by THERMOS is normalized to one neutron slowing down past 0.785 ev and

the relative flux calculated by GAM-I is normalized so that the value of the integral epicadmium flux is 4.0.)

The normalization factor, a, can be determined in several ways:

1. by equating the magnitudes of the relative flux from each program at the coupling point;
2. by equating the total number of neutrons produced by fission to the total number of neutrons absorbed or lost by leakage;
3. by equating the number of neutrons slowed down out of GAM-I to the number of neutrons slowed down into THERMOS;
4. by equating the number of neutrons slowed down out of GAM-I to the total number of neutrons absorbed and lost by leakage in THERMOS.

Method 1 is sensitive to errors in the flux spectrum at the coupling point between the two programs. Method 2 involves the assumption that the neutron multiplication factor of the system described by the input data is unity which is, of course, not true for the calculations based on an infinite system. Methods 3 and 4 are equivalent because the THERMOS calculations are for a cell of an infinite system and the number of neutrons slowing down into THERMOS are equal to the total number of neutrons absorbed there. Although methods 3 or 4 might produce a discontinuity in the normalized spectrum at the coupling point, they should yield the most accurate normalization factor because they are least sensitive to inaccuracies in the input data and in the spectra calculated by GAM-I and THERMOS.

The experimental ratios, ρ_{28}, C^*, δ_{25}, and δ_{28} are compared in Table 5.3.1 to the values predicted by the combined results of THERMOS and GAM-I. The analytical values of ρ_{28}, C^*, and δ_{25} were determined by means of the calculated relative reaction rates; the analytical value of δ_{28} was determined by means of the following equation:

$$\delta_{28} = \frac{\Sigma_f^{28}}{\frac{S}{\nu} - \Sigma_f^{28}}, \qquad (5.3.2)$$

TABLE 5.3.1

Comparison of Analytical* and Experimental Results

Rod Spacing (Inches)	Ratio of Moderator Volume to Fuel Volume	ρ_{28}		δ_{25}		δ_{28}		C^*	
		Exp.	Anal.	Exp.	Anal.	Exp.	Anal.	Exp.	Anal.
1.25	25.9	0.845	0.745	0.0525	0.0630	0.0274	0.0196	0.8028	0.762
1.75	52.4	0.437	0.396	0.0310	0.0308	0.0217	0.0193	0.6345	0.625
2.50	108.6	0.227	0.195	0.0188	0.0165	0.0183	0.0167	0.5506	0.541

*The analytical results were obtained from the THERMOS and GAM-I calculations applied to a bare critical system.

where S is the number of source neutrons from fission, ν is the average number of neutrons produced per fission, and Σ_f^{28} is the spatially and spectrally averaged U^{238} fission rate. Most of the results show fair agreement, about 10% or better; however, some of the results for the 1.25-inch lattice show large differences, up to 30% in one case. As mentioned in Section 5.2, THERMOS results show good agreement with experiment and the reasonable agreement for most of the combined results indicates that the normalization method is satisfactory. The disagreement for the tight lattice is probably due to the inability of the homogenized treatment of the epithermal region used by GAM-I to take proper account of the effects of lumping the fuel and of the interaction of neutrons between fuel rods. Hellens and Honeck (H5) found that the analytical results for the BNL water-moderated lattices (K4) based on a homogeneous treatment required corrections for these effects. Honeck (H11) is presently carrying on an analysis of lattices moderated by heavy water, including the M.I.T. lattices, with an extension of the method used for water-moderated lattices; it is expected that his analysis will clarify the points raised here.

In Chapter VI, where the analytical results presented here are used to aid in the analysis of the experimental results, the effects of the errors associated with the GAM-I results are of second order. Either the analytical quantities are small and have a second-order effect on the final results, or the contribution of the GAM-I results to the analytical quantity is second order. An example of the first case is the ratio of the U^{238} capture rate in the fast region to the U^{238} fission rate, α_{28}, and an example of the second case is the value of the thermal utilization, f. In the worst case, that in which there is a 30% discrepancy between experiment and the GAM-I calculations, the estimated effect on the final results discussed in Chapter VI is less than 1.5%.

5.4 Analytical Results

The results obtained from the output of the computer programs THERMOS and GAM-I are listed in Table 5.4.1.

The thermal diffusion length L^2 was calculated from values of the macroscopic absorption cross section and the transport cross section

TABLE 5.4.1. Analytical Results from Output of THERMOS and GAM-I

Rod Spacing (Inches)	1.25	1.75	2.50	
Moderator to Fuel Volume Ratio	25.9	52.4	108.6	
L^2, cm^2	76.9	134.8	263.0	THERMOS
$\left(\frac{\Sigma_a^{28}}{\Sigma_f^{25}}\right)_{SC}$	0.464	0.462	0.460	THERMOS
ℓ_{th}	0.914	0.858	0.813	THERMOS
τ(0.4 ev) cm^2	113.3	116.4	116.8	GAM-I
ν_{28}	2.851	2.852	2.850	GAM-I
a_{28}	0.0930	0.0929	0.0926	GAM-I
F_N	0.00553	0.0101	0.0176	GAM-I
F_F	0.00955	0.0188	0.0303	GAM-I
$\left(\frac{\Sigma_f^{25}}{\Sigma_f^{28}}\right)_{FAST}$	0.0294	0.0294	0.0294	GAM-I
ℓ_{FAST}	0.973	0.971	0.979	GAM-I
ℓ_{RES}	0.964	0.888	0.920	GAM-I
$\left(\frac{\Sigma_f^{25}}{\Sigma_a^{25}}\right)_{TOT}$	0.836	0.845	0.849	THERMOS + GAM-I
η	1.475	1.481	1.485	THERMOS + GAM-I
f	0.971	0.963	0.947	THERMOS + GAM-I
G	0.258	0.264	0.278	THERMOS + GAM-I
$\left(\frac{\Sigma_a^x}{\Sigma_f^{25}}\right)_{TOT}$	0.0500	0.0626	0.0915	THERMOS + GAM-I
δ	0.0411	0.0191	0.00976	THERMOS + GAM-I
$\ell(\rho_{28})$	0.883	0.881	0.841	THERMOS + GAM-I
$\ell(\delta_{25})$	0.889	0.834	0.796	THERMOS + GAM-I
$\ell(C^*)$	0.957	0.971	0.978	THERMOS + GAM-I

spectrally averaged over the flux spectrum below 0.4 ev and spatially averaged over the unit lattice cell. The thermal nonleakage probability, ℓ_{SC}, was calculated from L^2 and B^2, the measured material bucklings (H1, K2, C2). The quantities F_F and F_N are the fractions of the epicadmium U^{235} fission rate and U^{238} capture rate due to fast neutrons. The nonleakage probabilities for the fast resonance energy regions were obtained from the calculation for a critical system by means of the relation:

$$\ell = \left(1 - \frac{\mathscr{L}}{S}\right), \tag{5.4.1}$$

where $\frac{\mathscr{L}}{S}$ is the ratio of the number of neutrons leaking from the given energy region to the number of neutrons entering that energy region. Only the $\frac{1}{v}$ portion of the U^{238} captures was included in the calculation of each of the quantities η, f, and G (the ratio of the subcadmium U^{238} capture rate to the "thermal" absorption rate in the fuel. The quantity δ, which is related to the cadmium ratio of a $\frac{1}{v}$ absorber in the fuel, was calculated from the relation:

$$\delta = \frac{\Sigma_{EC}^{H}}{\Sigma_{SC}^{28}} \left(\frac{\Sigma_o^{28}}{\Sigma_o^{H}}\right)\left(\frac{S^{28}}{S^{H}}\right), \tag{5.4.2}$$

where the S's are the weighting factors for the resonance energy flux, the Σ_o's are the macroscopic capture cross sections at 2200 m/sec, and the superscript H refers to hydrogen. The quantities $\ell_{\rho_{28}}$, $\ell_{\delta_{25}}$, and ℓ_{C^*} are the ratios of the values of the parameters ρ_{28}, δ_{28}, and C^*, respectively, calculated on the basis of an infinite system to the values of the parameters calculated on the basis of a critical system.

Some of these analytical results and some experimental results of the present work will be compared, in Chapter VI, with results obtained independently (M3) in experiments made with pulsed neutron techniques.

CHAPTER VI
ANALYSIS OF RESULTS

Introduction

In this chapter, the experimental results presented in Chapter IV are combined with the analytical results summarized in Chapter V in order to calculate quantities such as the resonance escape probability, the fast fission effect, and the multiplication factor on an infinite lattice for the three assemblies studied.

6.1 Reactor Parameters

In this section, the calculation of the resonance escape probability, the initial conversion ratio, and the fast fission effect are discussed.

6.1.1 Resonance Escape Probability

To characterize the life cycle of a neutron in a reactor, the familiar four-factor formulation of the multiplication factor k_∞ is often used:

$$k_\infty = \eta f p \epsilon = \frac{\text{"net number of neutrons produced" by fission}}{\text{"total number of absorptions"}} , \tag{6.1.1}$$

where η is the number of neutrons produced by U^{235} fission per "thermal absorption" in the fuel, the thermal utilization factor f is the number of "thermal absorptions" in the fuel per "thermal absorption" in the total system, the fast fission effect ϵ is the "net number of neutrons produced" by all fissions per neutron produced by U^{235} fission, and the resonance escape probability p is the ratio of the number of "thermal absorptions" in the total system to the "total number of absorptions" in the system. The terms thermal absorption, net number of neutrons produced, and total number of absorptions are set in

quotation marks because the specific reaction rates included in the quantities can vary, depending on the definitions used; for example, the epithermal $\frac{1}{v}$ absorptions may or may not be included in the term, thermal absorptions, and the fast absorptions may be included in the term, total net number of fast neutrons produced, rather than in the term, total number of absorptions. (The latter option affects the value of k_∞ slightly, but for the well thermalized lattices studied, the effect is of the order of only 0.1% and is negligible.)

As in earlier work at M.I.T. (W1), the following expression, derived by Kouts and Sher (K3), was used to calculate the resonance escape probability:

$$p = \frac{1 + \frac{\delta_{28}\alpha_{28}}{\nu_{25}\epsilon\ell_F}}{1 + \ell_r\ell_{th}\rho_{28}\left(\frac{1-\delta/\rho_{28}}{1+\delta}\right)fG}, \qquad (6.1.2)$$

where $\ell_F, \ell_r, \ell_{th}$ are the nonleakage probabilities for the fast, resonance and thermal energy groups, respectively; δ is defined so that the ratio δ/ρ_{28} is the fraction of the epicadmium captures in U^{238} due to the $\frac{1}{v}$ portion of the capture cross section; G is the ratio of the subcadmium U^{238} capture to the sum of the U^{235} absorptions and the $\frac{1}{v}$ U^{238} capture; ϵ is the fast fission factor; f is the thermal utilization; and δ_{28}, α_{28}, ν_{25}, and ρ_{28} have their usual meanings. If the above expression for the resonance escape probability is used, then the epicadmium $\frac{1}{v}$ capture by U^{238} is placed in the term "thermal absorptions;" the fast U^{238} capture and fission is placed into the term "net number of neutrons produced;" and corrections are included for the effects of leakage in the value of ρ_{28} which is measured in a finite system. This definition of p can be expressed as follows:

$$p = (1/v \text{ absorptions in } U^{238} + \text{all absorptions in all other materials}) \div (\text{all absorptions in all materials} - \text{fast absorptions in } U^{238}). \qquad (6.1.3)$$

As a result, we have the following definitions for η, f, and ϵ which are consistent with Eqs. 6.1.2 and 6.1.3:

$$\eta = (\text{neutrons produced by } U^{235} \text{ fission}) \div (\text{absorptions in } U^{235} + \frac{1}{v} \text{ absorptions in } U^{238}); \quad (6.1.4)$$

$$f = (\text{absorptions in } U^{235} + \frac{1}{v} \text{ absorptions in } U^{238}) \div (\frac{1}{v} \text{ absorptions in } U^{238} + \text{all other absorptions in all other materials}); \quad (6.1.5)$$

$$\epsilon = (\text{neutrons produced by all fission - fast absorptions in } U^{238}) \div (\text{neutrons produced by } U^{235} \text{ fission}). \quad (6.1.6)$$

When these definitions of the separate factors are combined, the resulting definition of k_∞ becomes:

$$k_\infty = (\text{neutrons produced by all fissions - fast absorptions in } U^{238}) \div (\text{all absorptions in all materials - fast absorptions in } U^{238}). \quad (6.1.7)$$

The values of p calculated by means of Eq. 6.1.2 are listed in Table 6.1.1 and are compared in Fig. 6.1.1 to values obtained from earlier measurements made at M.I.T. (W1, P2). The results of Peak et al. (P2) have two points which seem to be low. This apparent discrepancy will be considered in more detail later in this section.

The uncertainty associated with the value of p is difficult to estimate. The fraction of the uncertainty in p that is due to the experimental uncertainty in ρ_{28} is negligible (of the order of 0.05 per cent in p). The second term in the numerator of Eq. 6.1.2 is extremely small (~ 0.001) and the effect of uncertainties associated with that term is also negligible. Thus the uncertainty in the value of p depends on the uncertainty associated with the analytical quantities appearing in the second term of the denominator. The values of f and G depend mainly on the results of THERMOS and, as pointed out in Chapter V, their uncertainties are probably limited by the uncertainties in the input data

TABLE 6.1.1

Values of the Resonance Escape Probability, p, for Lattices with 0.25-Inch-Diameter, 1.03 w/o U^{235} Fuel Rods

Rod Spacing (Inches)	Moderator to Fuel Volume Ratio	ρ_{28} (a)	δ_{28} (a)	ϵ (b)	δ (c)	fG (c)	a_{28} (c)	ℓ_F (c)	ℓ_r (c)	ℓ_{th} (c)	p (d)
1.25	25.9	0.8453	0.0274	1.020	0.0411	0.258	0.093	0.973	0.964	0.914	0.851 ±0.007
1.75	52.4	0.4373	0.0217	1.016	0.0191	0.264	0.093	0.971	0.888	0.858	0.922 ±0.004
2.50	108.6	0.2272	0.0183	1.013	0.0098	0.0263	0.093	0.979	0.920	0.813	0.960 ±0.002

(a) From Table 4.2.1.

(b) From Table 6.1.3.

(c) From Table 5.4.1.

(d) Estimated uncertainty is ±0.5%.

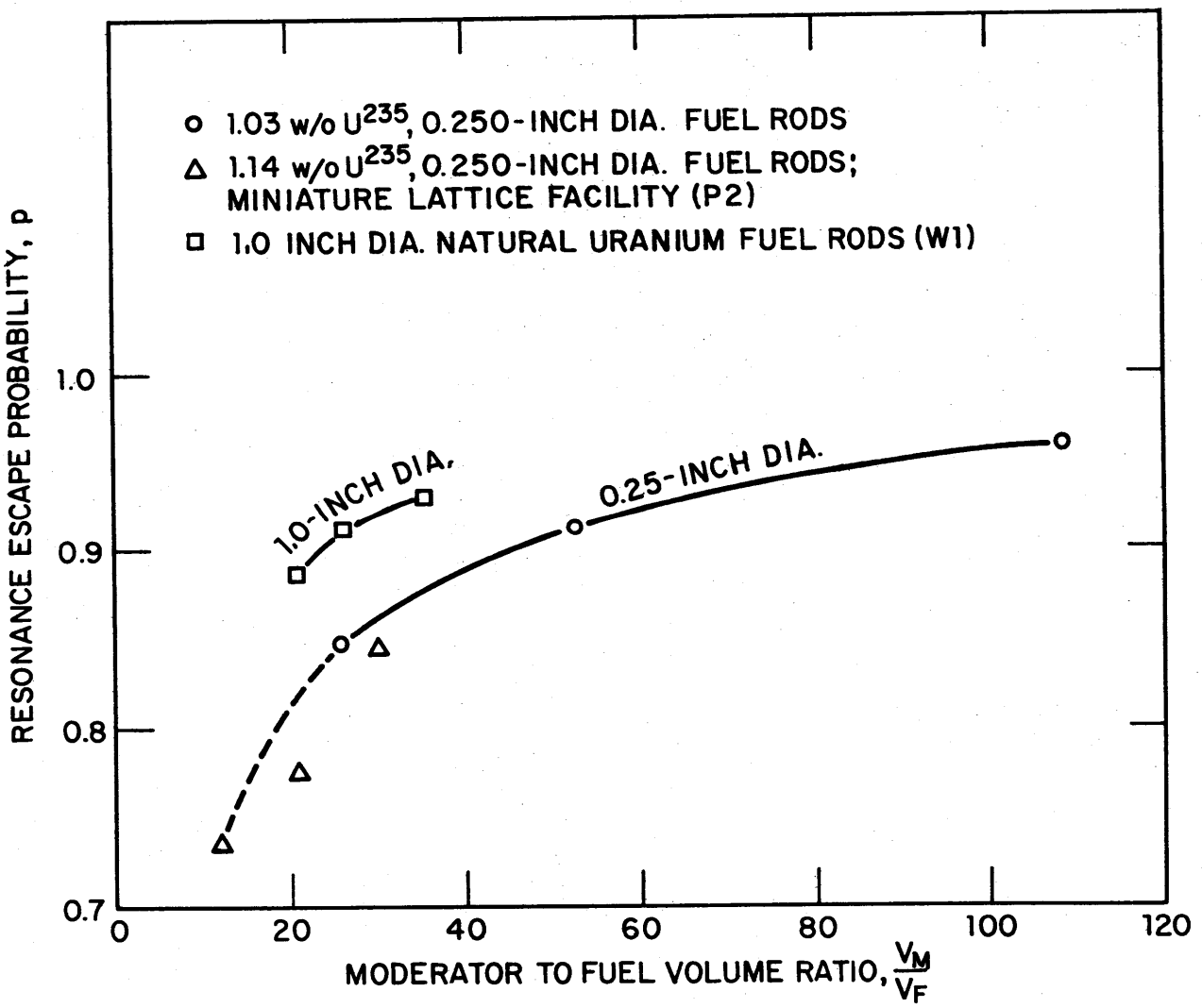

RESONANCE ESCAPE PROBABILITY VERSUS MODERATOR TO FUEL VOLUME RATIO.

FIG. 6.1.1

which are of the order of one per cent. The precision of δ is not as good but since the value of δ is less than 0.05, its contribution to the total uncertainty is small, approximately one per cent. In determining the nonleakage probabilities, the uncertainties of the input parameters (L^2, τ, B^2) are associated with one minus the nonleakage probabilities ($1-\ell$), and a 10 per cent uncertainty in the input parameters reduces to only a 1 to 2 per cent uncertainty in the nonleakage probabilities. The uncertainties associated with each of the two nonleakage probabilities are probably within five per cent. A liberal estimate of the combined uncertainty associated with these factors would be 5 per cent; however, this large error reduces to only about 0.5 per cent error in the value of p, the resonance escape probability. Therefore, the precision of the values of p, as calculated by Eq. 6.1.2, is probably of the order of 0.5%.

A simpler formula is obtained if all captures except U^{238} resonance capture above the cadmium-cutoff energy and neutron leakage are assumed negligible. Then the resonance escape probability, p, can be expressed as follows:

$$p = \frac{\text{thermal absorptions}}{\text{total absorptions}} = \frac{\text{thermal absorptions}}{\text{thermal absorptions} + U^{238}\text{ resonance absorptions}}, \tag{6.1.8}$$

or

$$p = \frac{(U^{238}\text{ thermal absorptions})(1/fG)}{(U^{238}\text{ thermal absorptions})(1/fG) + U^{238}\text{ epithermal absorptions}}, \tag{6.1.9}$$

or

$$p = \frac{1}{1 + \rho_{28} fG}, \tag{6.1.10}$$

where f and G have the same definitions as in Eq. 6.1.2. This simple relation, in spite of its severe approximations, is quite useful for making comparisons of measurements made in similar systems, such as systems which differ slightly in the U^{235} content of the fuel and, as will be seen in Section 6.3, for making comparisons of different methods of measuring p.

Another simple relation can be derived from Eq. 6.1.8: with the assumptions of only U^{238} capture above the cadmium cutoff and no leakage, Eq. 6.1.8 may be rewritten as:

$$p = \frac{\text{thermal absorptions}}{\text{total absorptions}} = \frac{\text{total absorptions - resonance absorptions}}{\text{total absorptions}}, \tag{6.1.11}$$

$$p = 1 - \frac{\text{resonance absorptions}}{\text{total absorptions}} = 1 - \frac{U^{238}\text{ resonance absorptions}}{U^{238}\text{ thermal absorptions}} \frac{G}{\eta\epsilon}, \tag{6.1.12}$$

$$p = 1 - \rho_{28} \frac{G}{\eta\epsilon}, \tag{6.1.13}$$

where the additional assumption has been made in Eq. 6.1.12 that the total number of absorptions is equal to the total number of neutrons produced. Again the approximations are severe but, as before, the expression can be useful for purposes of comparison.

The values of p obtained by means of Eq. 6.1.2 are compared to the values given by Eqs. 6.1.10 and 6.1.13 in Fig. 6.1.2. As can be seen, the values of p calculated with Eq. 6.1.13 are quite close to the more accurate values determined by means of Eq. 6.1.2.

An example of the utility of Eqs. 6.1.10 and 6.1.13 is in the comparison of the measurements of ρ_{28} made in the three lattices studied during the present work, with fuel enriched to 1.027 w/o U^{235}, and the measurements of ρ_{28} made in the M.I.T. miniature lattice by Peak et al. (P2), with 1.14 w/o U^{235} fuel. The 10% difference in the U^{235} content should not have a significant effect on the resonance energy flux spectrum and the resonance escape probability should not be affected significantly. The values of p calculated by means of Eqs. 6.1.10 and 6.1.13 for the two sets of measurements are listed in Table 6.1.2 and are compared in Fig. 6.1.3. To provide a more direct comparison of the two sets of measurements, the values $\rho_{28}fG$ and $\rho_{28}\frac{G}{\eta\epsilon}$ for the two sets of data are compared in Fig. 6.1.4. According to Hellens and Honeck (H5), the ratio of the U^{238} capture rate to the slowing-down density should vary linearly with the moderator to fuel volume ratio and should be insensitive to the U^{235} content of the fuel. Figure 6.1.5 shows

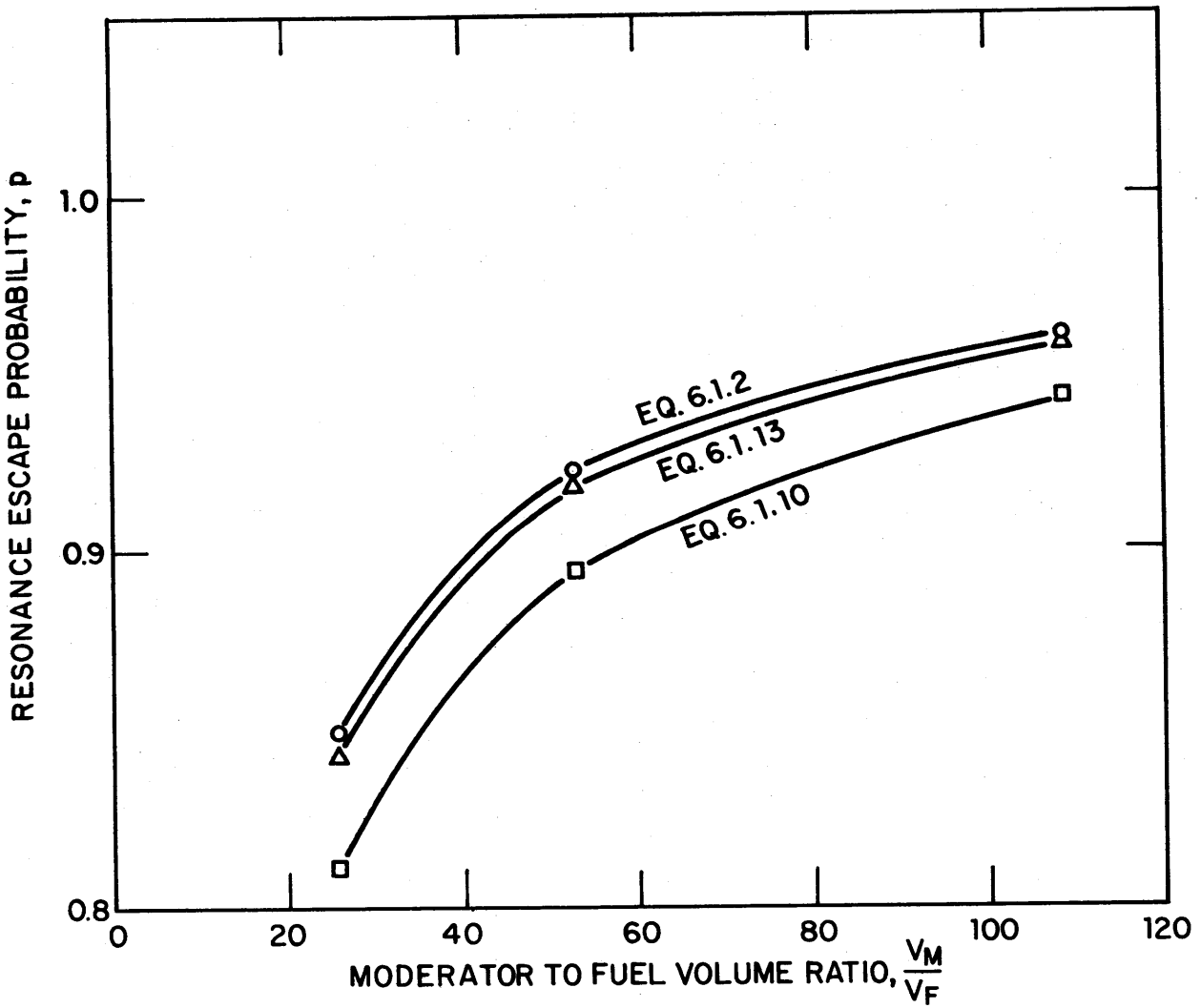

COMPARISON OF THE METHODS OF CALCULATING THE RESONANCE ESCAPE PROBABILITY

FIG. 6.1.2

TABLE 6.1.2

Values of the Resonance Escape Probability, p, Obtained by Means of Equations 6.1.10 and 6.1.13

Rod Spacing (Inches)	Moderator to Fuel Ratio	w/o U^{235}	$\rho_{28}fG$	$\rho_{28}\frac{G}{\eta\epsilon}$	Value of p		Facility
					Eq. 6.1.10	Eq. 6.1.13	
0.88	12.0	1.14	0.413	0.270	0.707	0.730	Miniature Lattice
1.128	20.8	1.14	0.323	0.213	0.755	0.787	Miniature Lattice
1.25	25.9	1.03	0.218	0.150	0.821	0.850	M.I.T. Lattice Facility
1.34	30.0	1.14	0.204	0.135	0.830	0.865	Miniature Lattice
1.75	52.4	1.03	0.115	0.080	0.897	0.920	M.I.T. Lattice Facility
2.50	108.6	1.03	0.0597	0.042	0.944	0.958	M.I.T. Lattice Facility

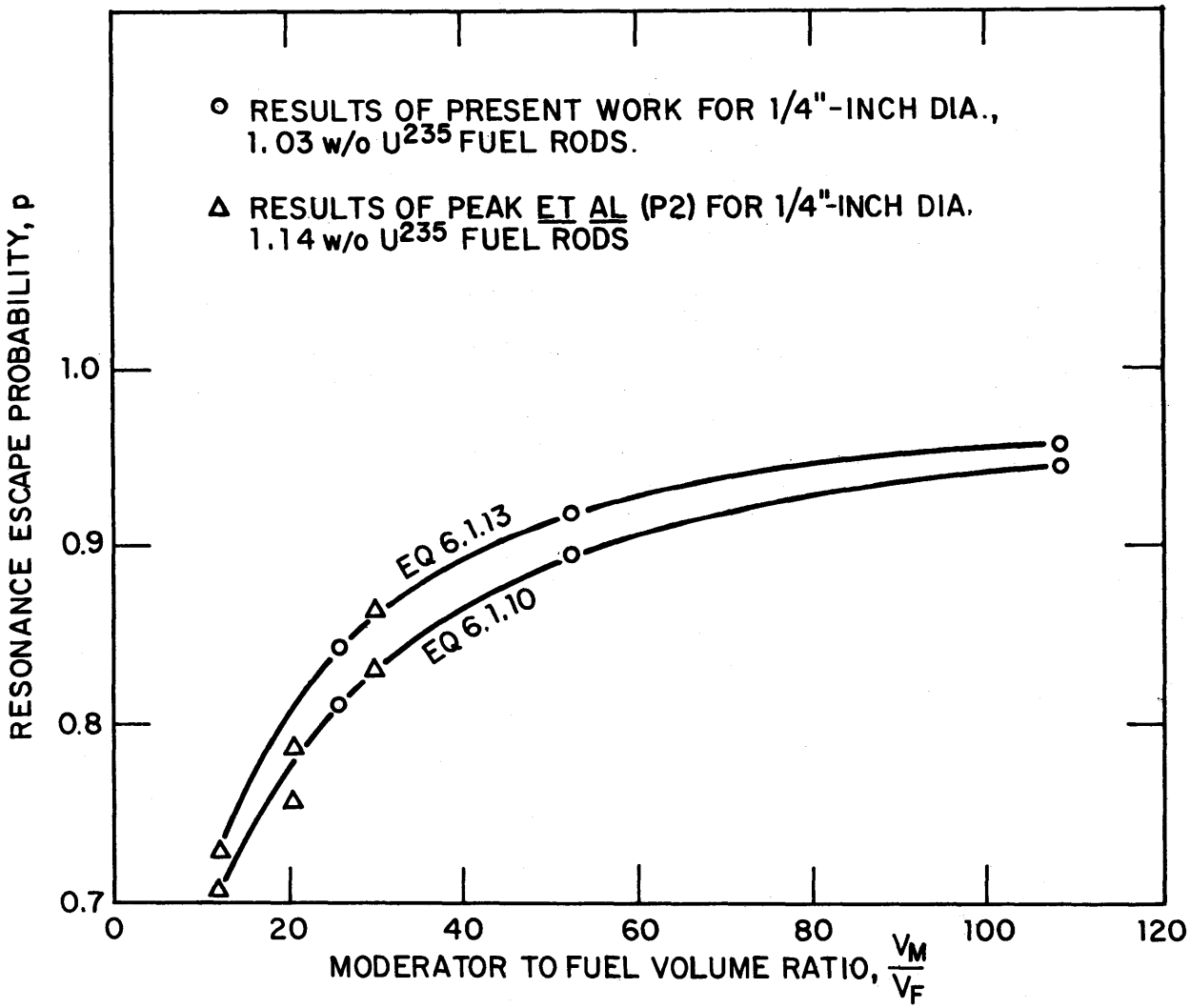

COMPARISON OF PRESENT RESULTS FOR THE RESONANCE ESCAPE PROBABILITY WITH MINIATURE LATTICE RESULTS

FIG. 6.1.3

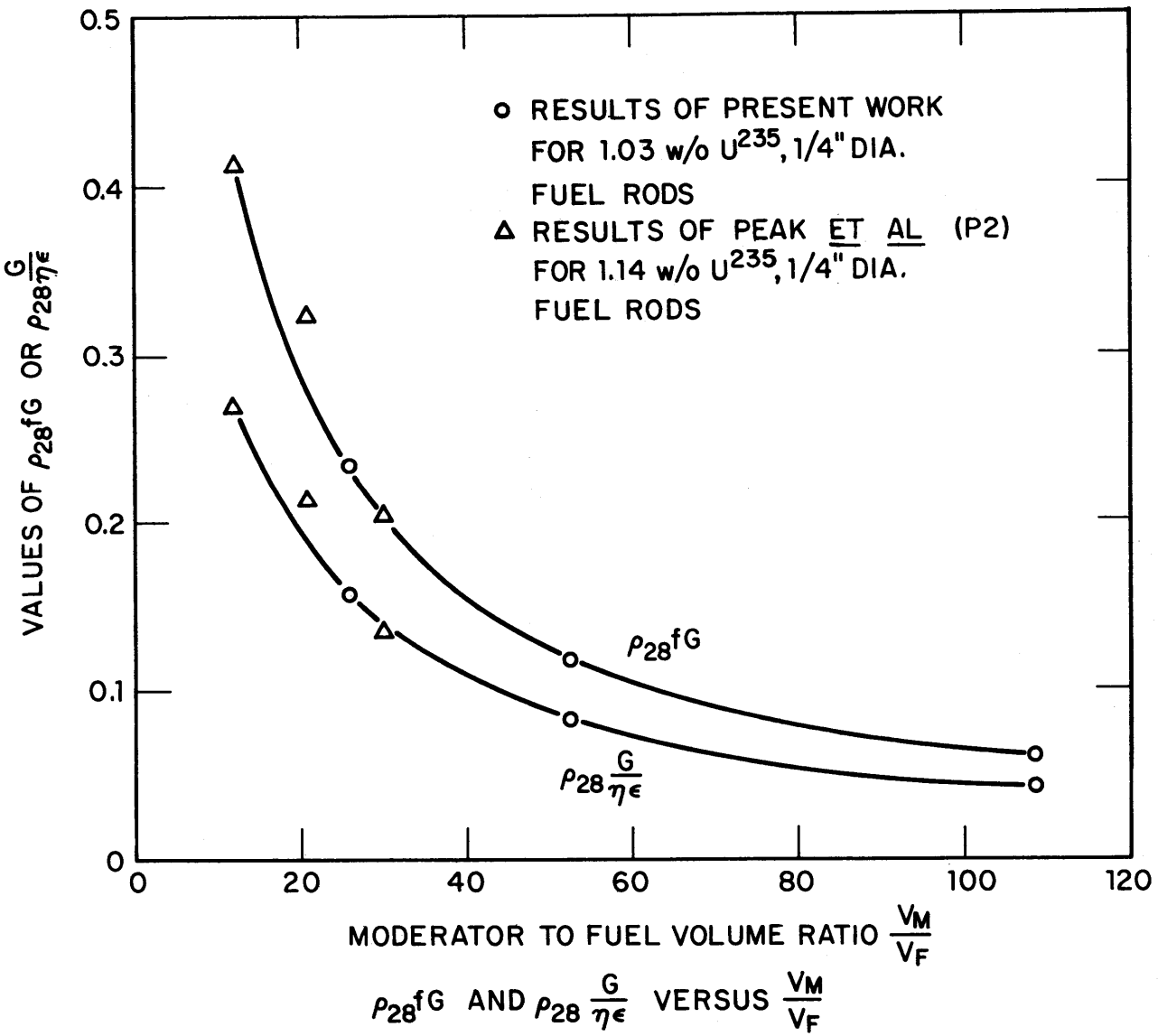

$\rho_{28}fG$ AND $\rho_{28}\frac{G}{\eta\epsilon}$ VERSUS $\frac{V_M}{V_F}$

FIG. 6.1.4

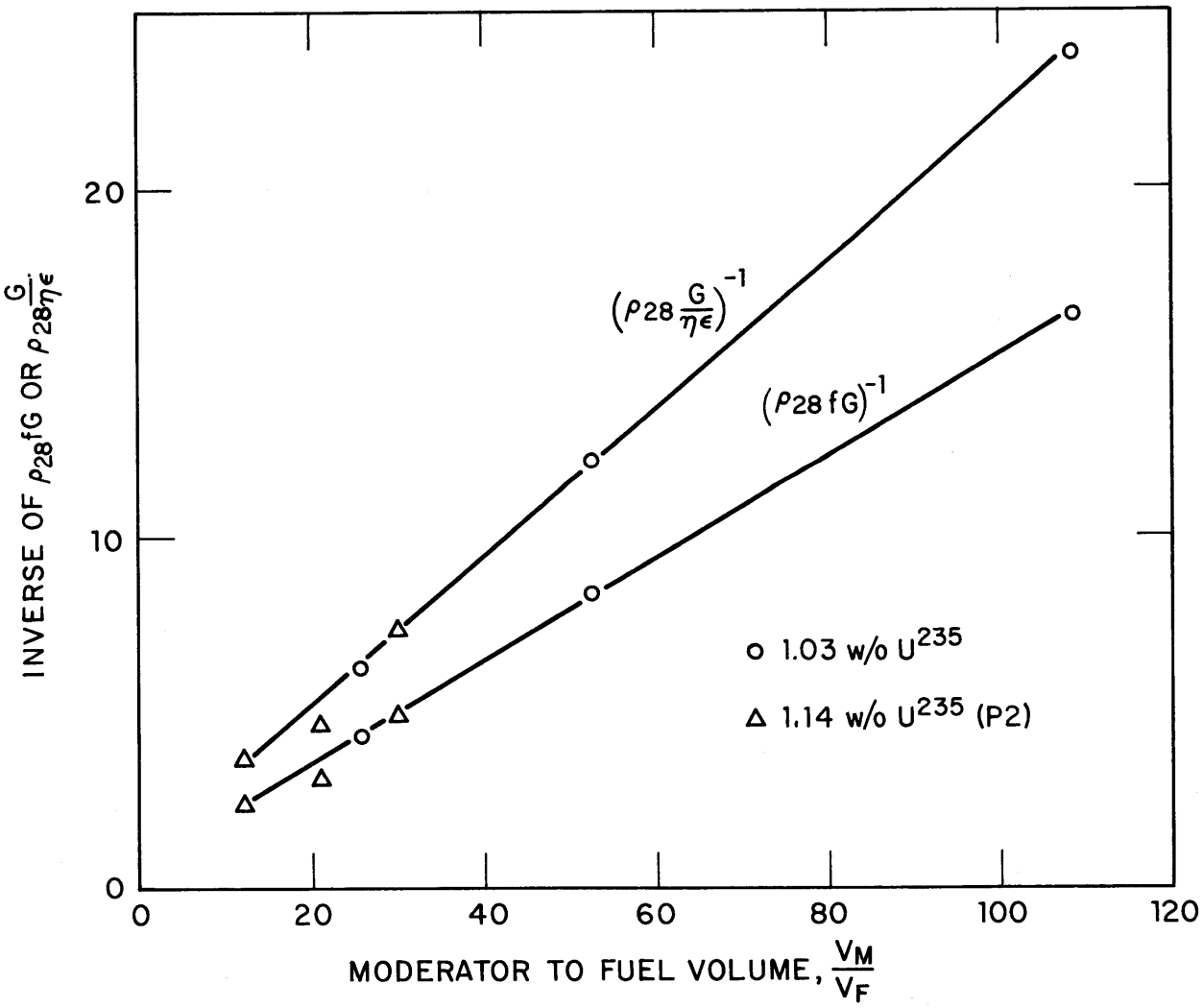

$(\rho_{28}fG)^{-1}$ AND $\left(\rho_{28}\frac{G}{\eta\epsilon}\right)^{-1}$ VERSUS $\frac{V_M}{V_F}$ FOR 0.25-INCH DIAMETER FUEL RODS

FIG. 6.1.5

that this is the case for the lattices studied by Peak et al. (P2) and in the present work.

The results of the present work and the results of Peak et al. (P2) appear to be consistent with each other with the exception of the miniature lattice measurement at a volume ratio of 20.8 as shown in Figs. 6.1.3, 6.1.4, and 6.1.5. This reasonably good agreement indicates that the apparent discrepancy noted in Fig. 6.1.1 between the results of Peak et al. (P2) and the results obtained during the present work is probably not due to an experimental error. The discrepancy is believed to be an error in the calculation of the values of p obtained from the miniature lattice measurements, probably in the calculation of the leakage factors which appear in Eq. 6.1.2. In view of the large theoretical correction (up to 25 to 30 per cent) which had to be applied to the results obtained in the miniature lattice to correct them for the effects of the non-asymptotic spectrum of that facility, the agreement with the present results obtained in the MITR Lattice Facility,indicated by the results shown in Figs. 6.1.3, 6.1.4, and 6.1.5, is reasonably good. Those theoretical corrections for the non-asymptotic spectrum were derived (P2) on the basis of age-diffusion theory, and the results here indicate that a better theoretical treatment of the corrections seems worthwhile and that satisfactory results for the measurement of ρ_{28} can be obtained from measurements in a miniature lattice.

6.1.2 Fast Fission Effect

In the last section, the fast fission factor was defined by the relation:

$$\epsilon = \frac{\text{neutrons produced by all fission - fast absorptions in } U^{238}}{\text{neutrons produced by } U^{235} \text{ fission}} . \qquad (6.1.6)$$

With this definition, ϵ is related to the measured microscopic parameter δ_{28}:

$$\epsilon = 1 + \delta_{28}\left(\frac{\nu_{28} - 1 - a_{28}}{\nu_{25}}\right), \qquad (6.1.14)$$

where ν_{28}, a_{28}, and ν_{25} have their usual meanings. The energy used to determine the lower limit for fast U^{238} capture in a_{28} is arbitrary. As noted by Bliss (B1), there is no clear preference among the several effective cutoff energies proposed; but the numerical differences in the values of ϵ, calculated by means of different formulations which use different effective cutoff energies for fast neutron capture in U^{238}, are, however, smaller than the uncertainties in ϵ, due to the uncertainties in the input data. The results of GAM-I indicated that more than 99% of the U^{238} fissions occur above 1 Mev and, since this is a convenient division point, all U^{238} capture above 1 Mev has been included in ϵ, and all U^{238} capture below 1 Mev has been included in p or f. The values of ϵ obtained with Eq. 6.1.14 are listed in Table 6.1.3. The second term in Eq. 6.1.14 is of the order of 0.01 to 0.02, and since all uncertainties are associated with this term, the uncertainty in ϵ is probably a small fraction of 1 per cent, approximately 0.1 to 0.2%, and negligible compared to the uncertainties in p, η, or f.

TABLE 6.1.3

Values of the Fast Fission Factor, ϵ, for Lattices with 0.25-Inch-Diameter, 1.03 w/o U^{235} Fuel Rods

Rod Spacing (Inches)	Moderator to Fuel Volume Ratio	δ_{28} (a)	ϵ (b)
1.25	25.9	0.0274	1.020 ± 0.002
1.75	52.4	0.0217	1.016 ± 0.002
2.50	108.6	0.0183	1.013 ± 0.001

(a) Obtained from Table 4.2.1.
(b) Values of ν_{28} and a_{28} were obtained from Table 5.4.1. The value of ν_{25} used was 2.43 ± 0.01.

In Fig. 6.1.6, the results of the measurements of the fast fission ratio δ_{28} made during the course of the present study are compared with earlier results obtained at M.I.T. by Peak et al. (P2) in the miniature lattice with 0.25-inch-diameter, 1.14 w/o U^{235} fuel rods, and with

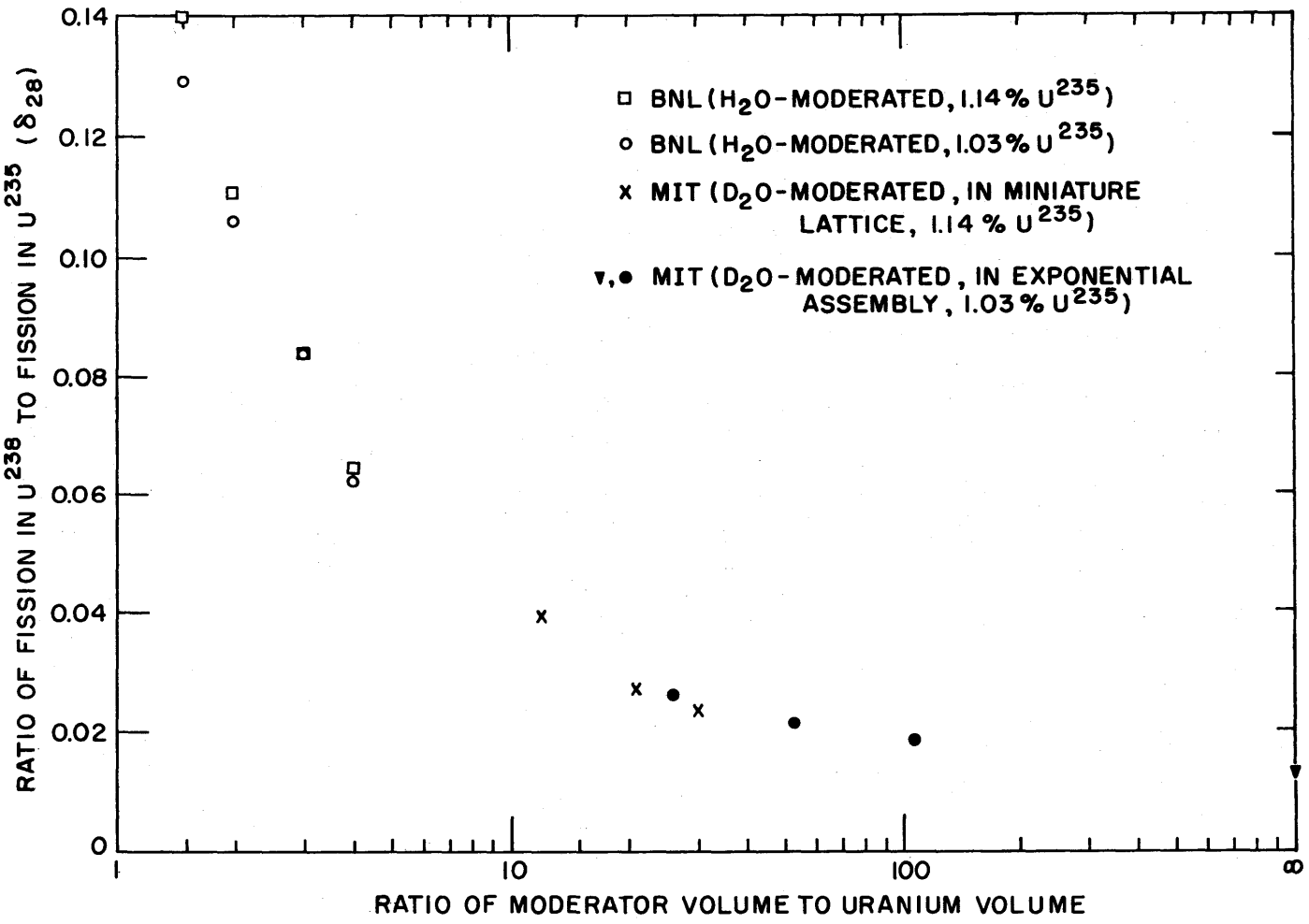

RATIO OF FISSION RATE IN U^{238} TO FISSION RATE IN U^{235}, δ_{28}, FOR URANIUM RODS, 1/4-INCH IN DIAMETER

FIG. 6.1.6

results obtained at the Brookhaven National Laboratory in water-moderated lattices with 0.25-inch-diameter, slightly enriched uranium rods (H12). The results show some discrepancies between the two M.I.T. results; however, the miniature lattice results have not been corrected for the fast flux depression associated with the measurement of δ_{28}. This flux perturbation and the correction factors developed to compensate for it are discussed in Chapter III. The application of the appropriate correction factors to compensate for this flux perturbation in the miniature lattice measurements would raise the values obtained in those measurements slightly. With this correction in mind, the results obtained in the miniature lattice and the results of the present work show fair agreement and indicate that the miniature lattice is probably satisfactory for the study of the fast fission effect; work on this problem is being continued by others. The results obtained for the heavy water lattices at M.I.T. are not consistent with those obtained in the more closely packed B.N.L. lattices, moderated with ordinary water. This difference may be due to the greater slowing-down power of ordinary water, as a result of which, a larger fraction of the fast neutrons which enter the moderator is scattered to energies below the U^{238} threshold; the interaction effect may then be relatively smaller than that in the lattices moderated by heavy water.

6.1.3 Initial Conversion Ratio

A parameter which is related to the lifetime of a reactor core is the initial conversion ratio, C, defined by the relation:

$$C = \frac{Pu^{239} \text{ produced}}{U^{235} \text{ destroyed}}$$

$$= \frac{\text{number of neutrons absorbed in } U^{238}}{\text{number of neutrons absorbed in } U^{235}} . \qquad (6.1.15)$$

The initial conversion ratio, C, is related to the measured microscopic parameter, C^*, by the relation:

$$C = C^*\left(\frac{\Sigma_f^{235}}{\Sigma_a^{235}}\right) = C^*(1+\alpha_{25})^{-1} , \qquad (6.1.16)$$

where the value of α_{25} is averaged over the entire neutron flux spectrum. The values of C for the present work are listed in Table 6.1.4 and are shown in Fig. 6.1.7 together with results of measurements made by Weitzberg et al. (W1) at M.I.T. in lattices with 1.0-inch-diameter, natural uranium fuel rods. Owing to the large differences in the fuel rod size, the two sets of results are not directly comparable; however, the two curves show similar trends, and the results seem to be consistent.

TABLE 6.1.4

Values of C for Lattices with 0.25-Inch-Diameter, 1.03 w/o U^{235} Fuel Rods

Rod Spacing (Inches)	Moderator to Fuel Volume Ratio	Av. C^* (a)	$(1+\alpha_{25})^{-1}$ (b)	C
1.25	25.9	0.803 ± 0.006	0.836	0.671 ± 0.010
1.75	52.4	0.634 ± 0.007	0.845	0.536 ± 0.008
2.50	108.6	0.551 ± 0.002	0.849	0.468 ± 0.007

(a) From Table 4.2.1.

(b) From Table 5.4.1; uncertainty assumed to be one to two per cent.

Although Peak et al. (P2) did not measure C^* in the miniature lattice, reasonable results for C^* and thus C should be obtainable in such an assembly. This can be shown by considering the following expression for C^*:

$$C^* = \left(\frac{1+\rho_{28}}{1+\delta_{25}}\right)\left(\frac{\Sigma_a^{28}}{\Sigma_f^{25}}\right)_{SC}, \qquad (2.2.16)$$

where C^* is determined from the values of the two measured ratios ρ_{28} and δ_{25}. In Section 6.1.1, it was found that measurements of ρ_{28} obtained in the present work in the exponential assembly and by Peak et al. in the miniature lattice showed good agreement. To determine if the measurements of δ_{25} are also consistent, consider the expression:

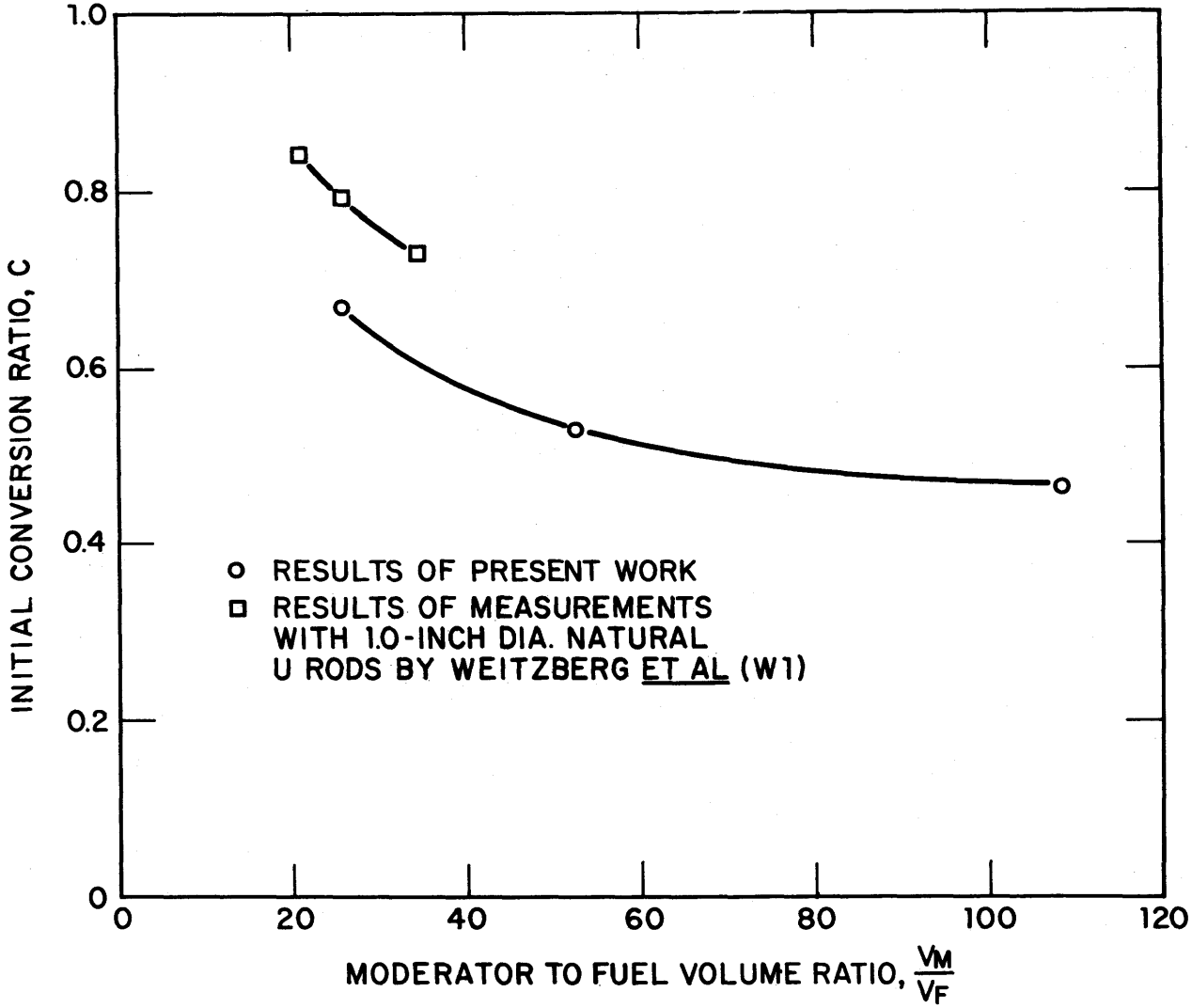

VALUES OF THE INITIAL CONVERSION RATIO FOR HEAVY WATER LATTICES

FIG. 6.1.7

$$\delta_{25} = \frac{\sigma_f^{25}\phi_{EC}}{\sigma_f^{25}\phi_{SC}} , \qquad (6.1.17)$$

where $\sigma_f^{25}\phi_{EC}$ and $\sigma_f^{25}\phi_{SC}$ are the spatially and spectrally averaged U^{235} fission rates for the epicadmium and subcadmium portions of the spectrum, respectively. From the definitions of η and f, it follows that:

$$\delta_{25}\eta f \frac{N^{25}}{N^T} = \frac{\sigma_f^{25}\phi_{EC}}{Q_o} , \qquad (6.1.18)$$

where Q_o is proportional to the slowing-down density entering the resonance region and N^{25}/N^T is the atom fraction of U^{235} in the fuel. The right side of Eq. 6.1.18 is independent of the U^{235} content and depends only on the epicadmium portion of the spectrum and the averaged microscopic U^{235} fission cross section. Thus the values of δ_{25} measured in systems with different U^{235} contents may be analyzed for consistency by comparing values of $\delta_{25}\eta f(N^{25}/N^T)$. This comparison is made in Fig. 6.1.8 for the results of the present work with 1.03 w/o U^{235} fuel and the results of Peak et al. with 1.14 w/o U^{235} fuel. The two sets of measurements again show reasonably good agreement, indicating that the miniature lattice assembly should be suitable for the measurement of δ_{25} and, therefore, also for measurements of C^*.

6.2 The Multiplication Factor for an Infinite Assembly

As noted in Section 6.1.1, the multiplication factor, k_∞, can be expressed in the familiar form:

$$k_\infty = \eta f p \epsilon \qquad (6.1.1)$$

with the definitions of k_∞ and the four factors given in Eqs. 6.1.3 to 6.1.7. Equation 6.1.1 was evaluated by using the values of η and f determined from the combined results of THERMOS and GAM-I (see Chapter V), the values of p calculated by means of Eq. 6.1.2, and the values of ϵ obtained from Eq. 6.1.14. The results are given in Table 6.2.1. The uncertainties in the values of η and f, as noted in Chapter V, are dominated by the uncertainties in the cross section data and also, in the case of η, the uncertainty in ν_{25}. The uncertainty in ν_{25} is 0.4%, and the uncertainty in

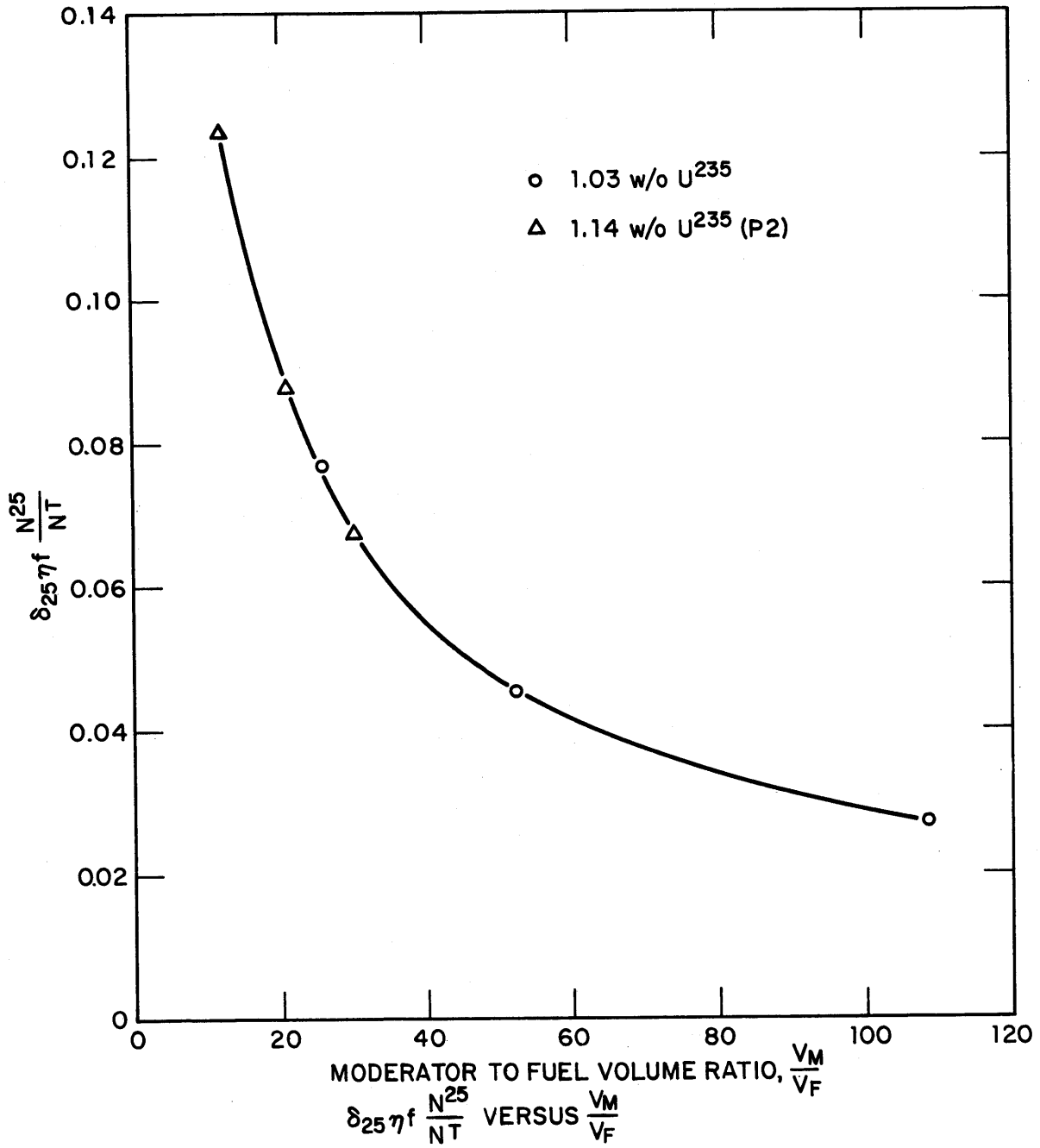

$\delta_{25}\eta f \frac{N^{25}}{NT}$ VERSUS $\frac{V_M}{V_F}$

FIG. 6.1.8

each of η and f due to the cross section uncertainties is negligible. The uncertainty associated with p, discussed in Section 6.1.1, is about 0.5%, and, as pointed out in Section 6.1.2, the uncertainty in ϵ compared to the errors in η and p is negligible. The combined effect of these uncertainties leads to an uncertainty in k_∞ as calculated by means of Eq. 6.1.1 of approximately 1.0%.

The value of k_∞ may be determined by means of a second approach. The definition of k_∞ was expressed in Section 6.1.1 as:

$$k_\infty = \frac{\text{neutrons produced by all fission} - \text{fast absorptions in } U^{238}}{\text{all absorptions of all materials} - \text{fast absorptions in } U^{238}} . \tag{6.1.7}$$

The numerator of Eq. 6.1.7 may be written:

$$\text{net production} = \left[\nu_{25}\Sigma_f^{25} + \nu_{28}\Sigma_f^{28} - \Sigma_f^{28} - \Sigma_F^{28} \right] \phi \tag{6.2.1}$$

and the denominator may be written:

$$\text{net absorption} = \left[\Sigma_a^{25} + \Sigma_c^{28} + \Sigma_a^{x} - \Sigma_F^{28} \right] \phi \tag{6.2.2}$$

where the Σ's are spectrally and spatially averaged cross sections; ϕ is the spatially and spectrally integrated flux; the subscripts f, c, a, and F refer to fission, capture, absorption, and fast capture, respectively; and the superscripts 25, 28, and x refer to U^{235}, U^{238}, and all other materials, respectively. Dividing each of the terms on the right-hand sides of Eqs. 6.2.1 and 6.2.2 by Σ_f^{25} and by using the following relations:

$$\frac{\Sigma_a^{25}}{\Sigma_f^{25}} = (1+\alpha_{25})^{-1} , \tag{6.2.3}$$

$$\frac{\Sigma_f^{28}}{\Sigma_f^{25}} = \delta_{28} , \tag{6.2.4}$$

$$\frac{\Sigma_F^{28}}{\Sigma_f^{28}} = \alpha_{28} , \tag{6.2.5}$$

$$\frac{\Sigma_a^x}{\Sigma_f^{25}} = \left(\frac{1}{f}-1\right)\left(\frac{1}{1-G}\right)\left(1+\alpha_{25}\right), \tag{6.2.6}$$

$$\frac{\Sigma_c^{28}}{\Sigma_f^{25}} = C_\infty^* = C^* \ell_{c*} , \tag{6.2.7}$$

where ℓ_{c*} is a leakage correction factor for the measured value of C^*, Eq. 6.1.7 can be rewritten as:

$$k_\infty = \frac{\nu_{25} + \delta_{28}(\nu_{28}-1-\alpha_{28})}{(1+\alpha_{25}) + C_\infty^* + \left(\frac{1}{f}-1\right)\left(\frac{1}{1-G}\right)(1+\alpha_{25}) - \delta_{28}\alpha_{28}} \tag{6.2.8}$$

All the quantities in Eq. 6.2.8 pertain to an infinite system. The measured fast fission ratio is insensitive to the effect of leakage and its effect in Eq. 6.2.8 is second order, so there will be no loss of precision if the measured value of δ_{28} is used directly. Since C^* is the ratio of two reaction rates averaged over the total spectrum and over the same region of the lattice cell (the fuel rod), the effects of leakage on each of the reaction rates will tend to cancel each other. As might be expected, the leakage corrections listed in Table 5.4.1 show that the difference between the values of C^* for a finite system and for an infinite system are small, of the order of three to four per cent. Since the leakage effect is so small, the uncertainties of the leakage correction factors for C^* are probably 1% or less. The values of k_∞ were determined by means of Eq. 6.2.8 with the values of ν_{28}, α_{28}, α_{25}, f, and G determined from the combined results of THERMOS and GAM-I which were based upon an infinite system. The uncertainty in the value of k_∞ as determined by Eq. 6.2.8 will be dominated by ν_{25} in the numerator and C^* in the denominator. The uncertainty in ν_{25} is 0.4%; in C^*, about 1%; and in the leakage correction for C^*, of the order of 1%. Thus the uncertainty in k_∞ should be of the order of 2%. The values of k_∞ obtained by means of Eq. 6.2.8 are compared in Table 6.2.1 with the values obtained from Eq. 6.1.1. No significant trend in the numerical values of k_∞ obtained by the two methods was found and the values agreed well within the uncertainties.

TABLE 6.2.1

Values of the Infinite Multiplication Factor for Heavy Water Lattices with 0.25-Inch-Diameter, 1.03 w/o U^{235} Fuel Rods

Rod Spacing (Inches)	Moderator to Fuel Volume Ratio	k_∞		(a)
		From Eq. 6.1.1	From Eq. 6.2.8	Av.
1.25	25.9	1.243	1.237	1.240 ± 0.019
1.75	52.4	1.339	1.328	1.334 ± 0.020
2.50	108.6	1.368	1.363	1.366 ± 0.021

(a) Estimated uncertainty of 1.5%.

The present results for 1.03 w/o U^{235} fuel rods are compared in Fig. 6.2.1 to the results of measurements made by Peak et al. (P2) in the M.I.T. miniature lattice for 1.14 w/o U^{235} fuel rods. As can be seen, with the exception of one point at the moderator to fuel volume ratio of 20.8 (which has already been discussed in Section 6.1.1), the miniature lattice results obtained by Peak et al. (P2) appear to be consistent with the results of the present work. Peak's results are somewhat higher, which should be expected because of the 10% difference in the U^{235} content. The values of p and ϵ should be insensitive to the change in U^{235} content, and the combination of ηf should increase slightly.

An independent experimental determination of the properties of the 1.75-inch lattice was made by Malaviya et al. (M3) by means of the pulsed neutron technique. The results of that investigation are compared in Table 6.2.2 with the results obtained during the course of the present work. The difference between the value of k_∞ obtained from the experimental results of the present work and the value of k_∞ obtained by Malaviya et al. is negligible compared to the estimated uncertainties, and the two results are in good agreement. The values of the thermal diffusion length L^2, the thermal utilization of the fuel f, and the thermal utilization of the moderator f_m, which were obtained from the analytical results discussed in Section 5.4, are also in good agreement with the results of the pulsed neutron measurements. The value of $\overline{v\Sigma_a}$, spatially

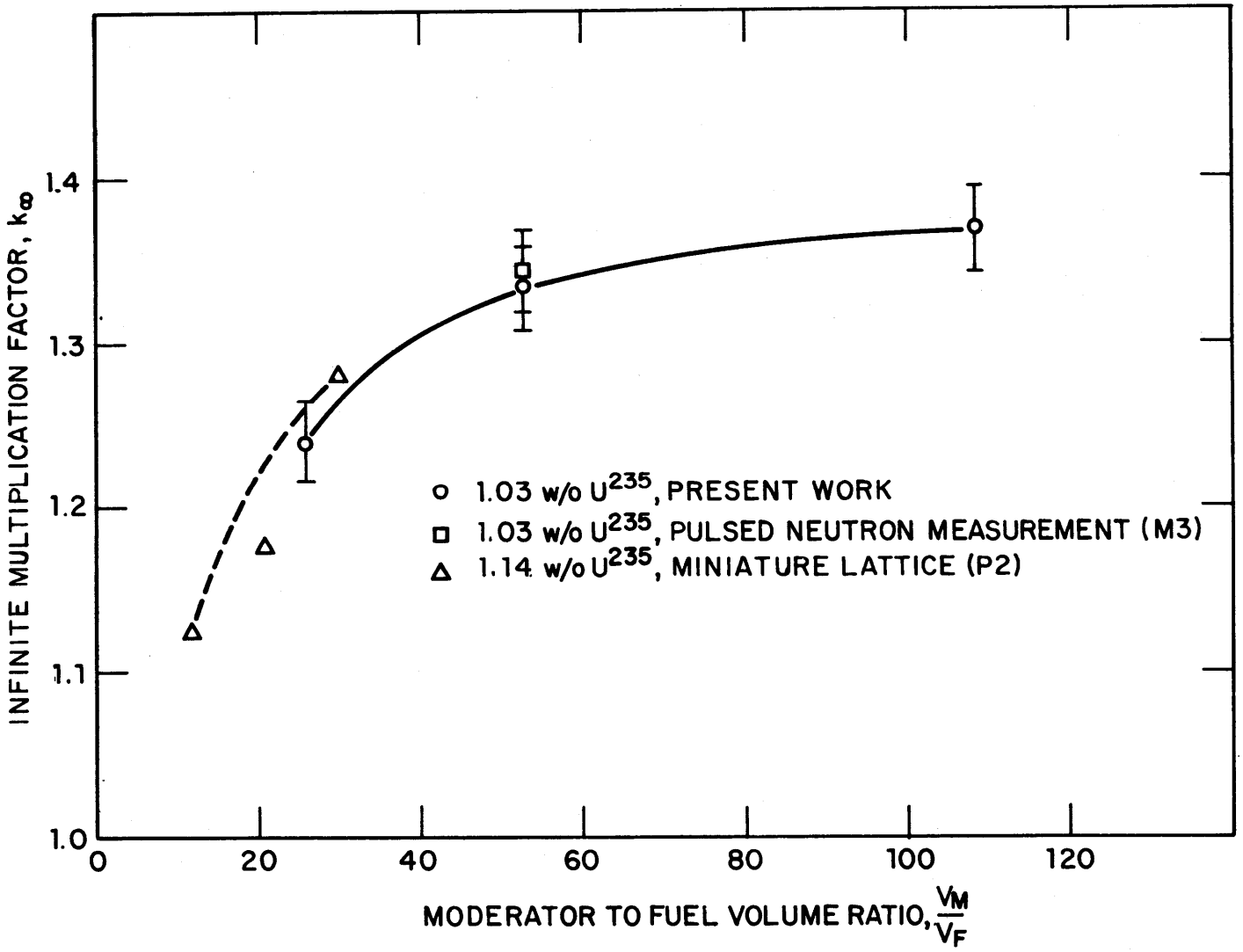

VALUES OF k_∞ FOR HEAVY WATER LATTICES WITH 0.25-INCH DIAMETER FUEL RODS

FIG. 6.2.1

TABLE 6.2.2

Comparison of Results of Present Work with Results of Pulsed Neutron Measurements

Quantity	Present Results*	Pulsed Neutron Results
k_∞	1.334 ± 0.020	1.345 ± 0.026
L^2	135 ± 3	141 ± 7
f	0.963 ± 0.009	0.966 ± 0.004
f_m	0.0215 ± 0.0009	0.0193 ± 0.0037
$\overline{\nu\Sigma_a}$	1615 ± 32	1396 ± 66

*The value of k_∞ is from Table 6.2.1; the remaining quantities are obtained from the THERMOS and GAM-I results discussed in Section 5.4.

and spectrally averaged over the lattice cell, obtained from THERMOS is only in fair agreement with the value obtained from Malaviya's pulsed neutron measurements. This discrepancy may be due to a difference between the subcadmium portion of the neutron spectrum treated by THERMOS and the effective portion of the spectrum to which the experimental value of $\overline{\nu\Sigma_a}$ pertains. Malaviya et al. (M3) suggested that this discrepancy may be due to the effects of neutron leakage (diffusion cooling effects) in the experimental results of pulsed neutron work.

6.3 Analysis of the Resonance Activation Data

The measured resonance activity of a nuclide (which is that portion of the activity of the nuclide due to neutrons captured by resonances in the activation cross section of the nuclide) can be written:

$$A_{res} = \varepsilon \int_0^\infty \sigma_{res}(u)\, \phi(u)\, du\,, \qquad (6.3.1)$$

where $\sigma_{res}(u)$ is the resonance portion of the activation cross section and ε is a proportionality factor containing such quantities as the counting efficiency, nuclei density, etc. [Note: The ε which is used in this section, Section 6.4, and Section 2.4 is a proportionality factor and should not be confused with the fast fission factor, which has the same symbol.] If $\sigma_{res}(u)$ has a single large dominant resonance (for example, Au^{197} or In^{115}) at a lethargy u_{res} (corresponding to the neutron energy E_r at which the

resonance capture occurs) and if it is assumed that over the width of the resonance $\phi(u)$ is a constant, then Eq. 6.3.1 can be rewritten:

$$A_{res} = \varepsilon \phi(u_{res}) \int_0^\infty \sigma_{res}(u)\, du \,, \tag{6.3.2}$$

or

$$A_{res} = \varepsilon \phi_{res} \int_0^\infty \sigma_{res}(E) \frac{dE}{E} = \varepsilon \phi_{res} RI \,, \tag{6.3.3}$$

where ϕ_{res} is written for $\phi(u_{res})$ and RI is the infinitely dilute resonance integral of the nuclide. From the relation:

$$q(u) = \xi \Sigma_s(u)\, \phi(u) \,, \tag{6.3.4}$$

Eq. 6.3.3 can be rewritten in terms of the slowing-down density:

$$A_{res} = \varepsilon \left(\frac{q_{res}}{\xi \Sigma_{s,res}} \right) RI \,. \tag{6.3.5}$$

Thus a study of Eqs. 6.3.3 or 6.3.5 suggests a means of measuring the relative neutron flux or the relative slowing-down density at various energies in the resonance energy region (by irradiating several nuclides which have known values of ERI for single dominant resonances at different energies for each nuclide).

The general feasibility of Eqs. 6.3.3 or 6.3.5 and the experimental techniques described in Section 2.4 can be illustrated by using Eq. 6.3.3 or 6.3.5 and the resonance activation data given in Chapter IV in a new attempt to calculate the resonance escape probability, p. If it is assumed that all epicadmium captures except U^{238} resonance captures are negligible and that neutron leakage is negligible, then the resonance escape probability as expressed in Section 6.1.1 becomes:

$$p = \frac{\text{thermal absorptions}}{\text{thermal absorptions} + U^{238} \text{ resonance absorptions in } U^{238}} \,. \tag{6.1.8}$$

Since there is no neutron leakage, we can also write:

$$\text{thermal absorptions} = Q_o \,, \tag{6.3.6}$$

where Q_o is the rate at which neutrons are slowed down into the thermal energy region. On inserting Eq. 6.3.6 in Eq. 6.1.8, we get:

$$p = \frac{1}{1 + \frac{a_{res}^{28}}{Q_o}}, \tag{6.3.7}$$

where a_{res}^{28} is the U^{238} resonance absorption rate. The term a_{res}^{28} is:

$$a_{res}^{28} = V_F N^{28} \int \sigma_{res}^{28}(u)\, \phi(u)\, du, \tag{6.3.8}$$

or

$$a_{res}^{28} = V_F N^{28} ERI^{28} \phi_{res}^{28}, \tag{6.3.9}$$

where V_F is the volume of the fuel, N^{28} is the density of the U^{238} nuclei, and

$$ERI^{28}\phi_{res}^{28} = \int \sigma_{res}^{28}(E)\, \phi(E)\, dE. \tag{6.3.10}$$

In Section 2.4, it was shown that:

$$R_{res}^{a} = \left(\frac{RI}{\sigma_o}\right)^a \frac{\phi_{res}^{a}}{\phi_H}. \tag{2.4.13}$$

The combination of Eq. 2.4.13 and Eq. 6.3.9 gives:

$$a_{res}^{28} = V_F R_{res}^{28} \Sigma_o^{28} \phi_H, \tag{6.3.11}$$

where Σ_o^{28} is written for $N^{28}\sigma_o^{28}$. If it is assumed that the contribution of the fuel and the cladding to the slowing-down density is negligible, it follows that:

$$Q_o = V_M q_o = V_M \xi^M \Sigma_s^M(u_o)\, \phi(u_o), \tag{6.3.12}$$

where V_M is the volume of the moderator, and u_o is some lethargy between the resonance region and the thermal region. The combination of Eq. 2.4.13 and Eq. 6.3.12 gives:

$$Q_o = V_M \xi_s^M \Sigma_s^M(u_o) \frac{R_{res}^{a}}{\left(\frac{RI}{\sigma_o}\right)^a} \phi_H. \tag{6.3.13}$$

The final result is derived by substituting Eqs. 6.3.11 and 6.3.13 into Eq. 6.3.7, which becomes:

$$p = \frac{1}{1 + \left(\frac{RI}{\sigma_o}\right)^a \left(\frac{\Sigma_o^{28}}{\xi^M \Sigma_s^M}\right)\left(\frac{R_{res}^{28}}{R_{res}^a}\right)\left(\frac{V_F}{V_M}\right)} . \qquad (6.3.14)$$

Values of p calculated by means of Eq. 6.3.14 are listed in Table 6.3.1. The experimental uncertainty of the resonance activation data, which was about 10%, produces an experimental uncertainty in the values of p of the order of 1 to 2%.

Since the same basic assumptions are embodied in Eqs. 6.1.10 and 6.3.14, the results of Eq. 6.3.14 may be compared directly to the results of Eq. 6.1.10. The value of p for the 1.75-inch lattice calculated by means of Eq. 6.1.10 is 0.894 and, in view of the limited experimental precision of the resonance activation data, the agreement with the results listed in Table 6.3.1 is relatively good. The fact that the measured values of (RI/σ_o) for As^{75} and Ga^{72} yield good agreement, gives support to the need for rechecking some of the data on resonance integrals reported in the literature.

Another application of Eqs. 6.3.3 and 6.3.5 is to estimate experimental values of the neutron flux and slowing-down density as a function of position and energy in order to test sophisticated theoretical calculations of the resonance energy spectrum such as the treatment developed recently at M.I.T. by Kier et al. (K1). Such a comparison is beyond the scope of this work; however, with the precision which should be attainable, as discussed in Section 4.2, and with improved resonance integral data, the basic experimental methods outlined in Section 2.4 could be useful in such a theoretically difficult region. A third application of the Eqs. 6.3.3 and 6.3.5 is to determine the effective resonance integral of U^{238}, ERI^{28}, in the fuel rods by comparing the U^{238} resonance activity of a depleted uranium foil irradiated within the fuel to the resonance activity of a nuclide irradiated in the moderator. This method is similar to the method developed by Weitzberg et al. (W1).

TABLE 6.3.1

Values of the Resonance Escape Probability, p, for the
1.75-Inch Lattice Obtained by Means of Resonance Activation Data

Resonance Detector	Peak Energy of Dominant Resonance, ev	Measured Resonance Integral Ratio, $(RI/\sigma_o)^a$ (a)	Measured Resonance Activation, R^a_{res} (a)	Value of p from Eq. 6.3.15
Br	101	18.1	0.1203	0.904
Ga	95	8.0	0.0634	0.920
As	47	12.9	0.0684	0.885
W	18.8	11.3	0.0629	0.889
Au	4.9	15.3	0.0985	0.903
In	1.5	8.0	0.0435	0.888

(a) Values of $(RI/\sigma_o)^a$ and R_{res} were obtained from Table 4.2.3. Values of other quantities used were: $V_M/V_F = 52.4$; $\Sigma_o^{28} = 0.119$; $\xi^M\Sigma_s^M = 0.178$ (calculated with effective cross sections from GAM-I output).

6.4 Effective Resonance Integral of U^{238}

The effective resonance integral of U^{238} in the fuel rods of the three lattices studied was determined by combining the results of measurements made in the epithermal flux at position 13 of the MITR. Measurements made by Anderson et al. (A3) indicate that the epithermal flux in the MITR core has a $\frac{1}{E}$ energy dependence.

The infinitely dilute resonance absorption integral of a nuclide is usually defined as follows (W5):

$$RI = \int_{E_o}^{\infty} \sigma_{res}(E) \frac{dE}{E} , \tag{6.4.1}$$

where $\sigma_{res}(E)$ is that portion of the absorption cross section of the nuclide which is due to resonances and the lower limit E_o lies above the thermal energy region and below the lowest energy resonance. The assumptions embodied in Eq. 6.4.1 are the following:

1. The neutron flux entering the resonance energy region has a $\frac{1}{E}$ dependence.
2. The scattering cross section is independent of energy.
3. The resonance absorber is uniformly distributed.
4. The absorber is infinitely dilute so that the absorption rate is negligible compared to the slowing-down density, and the neutron flux continues to have a $\frac{1}{E}$ dependence through the resonance energy region.
5. All of the resonance absorption is above the thermal energy region.

If the absorption rate becomes significant and the neutron flux no longer has a $\frac{1}{E}$ dependence, then Eq. 6.4.1 must be rewritten to include such effects. The result is called the effective resonance integral, which is usually defined as follows (W5):

$$ERI = \int_{E_o}^{\infty} \frac{\sigma_{res}(E)}{1 + \frac{\Sigma_a}{\Sigma_s}} \frac{dE}{E} , \tag{6.4.2}$$

where Σ_a and Σ_s are the total and scattering macroscopic cross sections

of the system. With the exception of the assumption 4, all the other assumptions listed above are embodied in Eq. 6.4.2. If the resonance absorber is lumped rather than uniformly distributed, as in the case of a single rod in an infinite sea of moderator, then the neutron flux inside such a single rod is depressed relative to the flux in the moderator. However, far from the rod the neutron flux in the resonance region still has a $\frac{1}{E}$ dependence. In this case, Eq. 6.4.1 must be changed, and the resultant effective resonance integral becomes:

$$ERI = \frac{1}{V_F} \int_{E_o}^{\infty} \int_{rod} \sigma_{res}(E)\, S(r,E)\, \frac{dE}{E}\, dr\,, \qquad (6.4.3)$$

where V_F is the volume of the fuel rod and $S(r,E)$ is the function which describes the spatial dependence of the neutron flux inside the fuel rod. Assumption 3 does not apply for Eq. 6.4.3, but the remaining assumptions listed after Eq. 6.4.1 are still in effect. In heterogeneous lattices such as the three studied during the course of the present work, the total number of absorber atoms present in the system is large so that the resonance absorption rate becomes significant, and the absorber is lumped so that the flux is depressed in the fuel rod. Therefore, a relation must be developed for which both assumptions 3 and 4 do not apply. To have a consistent set of definitions, the effective resonance integral of U^{238} in the fuel rods in a lattice shall be defined to include the effects of significant absorption which causes the spatially averaged neutron flux spectrum to deviate from a $\frac{1}{E}$ dependence and of lumping the absorber which depresses the neutron flux in the fuel relative to the moderator. This is done by redefining the function $S(r,E)$ in Eq. 6.4.3 so that it describes both the spectral and spatial variation of the flux in the resonance energy region.

In terms of this definition of the effective resonance integral, the resonance activation of a foil can be expressed as:

$$A_{res} = \Sigma \phi_i ERI\,, \qquad (6.4.4)$$

where ϕ_i is the value of the neutron flux per unit lethargy at energies above the energy of the resonance region.

Comparison of Eq. 6.4.4 with Eqs. 6.3.3 gives:

$$RI^a \phi^a_{res} = ERI^a \phi_i \ . \tag{6.4.5}$$

Hence, Eq. 2.4.20 may be rewritten in terms of the effective resonance integral:

$$\rho^a_{res} = \rho^a - \rho^b = \left(\frac{ERI}{\sigma_o}\right)^a \frac{\phi_i}{\phi_{1/v,sc}} \ . \tag{6.4.6}$$

If we make assumptions that δ_{25} is equal to ρ^b, that ρ_{Au} is proportional to $\phi_i/\phi_{1/v,sc}$, and that the thermal flux dip in the rod is insensitive to variations in the rod spacing, we get:

$$\frac{\left(\rho^{28}_{res}/\rho_{Au}\right)_{lat}}{\left(\rho^{28}_{res}/\rho_{Au}\right)_{13}} = \frac{ERI^{28}_{lat}}{ERI^{28}_{13}} \ , \tag{6.4.7}$$

where the subscripts, lat and 13, refer to measurements made in a lattice and in position 13 of the MITR, respectively. The value of ERI, the effective resonance integral of a single rod irradiated in an epithermal flux which has a $\frac{1}{E}$ energy spectrum, is 18.3 ± 0.9 barns (R3). Rewriting Eq. 6.4.7, we get for the effective resonance integral of U^{238} in a fuel rod in a lattice:

$$ERI^{28}_{lat} = 18.3\left(\frac{\rho^{28}_{res}}{\rho_{Au}}\right)_{lat}\left(\frac{\rho_{Au}}{\rho^{28}_{res}}\right)_{13} \quad \text{barns} \ . \tag{6.4.8}$$

Values of ERI^{28} with their estimated uncertainties for the three lattices studied are listed in Table 6.4.1. The value of ERI^{28} may then be used to calculate the resonance escape probability from the relation (W1):

$$p = \exp\left[-\frac{V_F N^{28} ERI^{28}}{V_M \xi^M \Sigma^M_s}\right] , \tag{6.4.9}$$

where N^{28} is the U^{238} concentration in the fuel rod and $\xi^M \Sigma^M_s$ is the slowing-down power of the moderator. Equation 6.4.9 is an approximate relation for the resonance probability that is derived from slowing-down theory (I1); however, the definitions of the resonance escape probability on which Eqs. 6.4.9 and 6.1.2 are based are equivalent. The values of p obtained by means of Eq. 6.4.9 are compared in Table 6.4.1 to the values of p obtained by means of Eq. 6.1.2. The results of the two methods show good agreement.

TABLE 6.4.1

Effective Resonance Integral of U^{238}

Rod Spacing (Inches)	Moderator to Fuel Volume Ratio, V_M/V_F	Effective Resonance[a] Integral of U^{238}, ERI^{28}, barns	Resonance Escape Probability	
			From Eq. 6.4.9[b]	From Eq. 6.1.2[c]
1.25	25.8	14.0 ± 1.1	0.875 ± 0.012	0.851 ± 0.007
1.75	52.4	16.2 ± 1.3	0.926 ± 0.007	0.922 ± 0.004
2.50	108.6	17.3 ± 1.4	0.962 ± 0.004	0.960 ± 0.002
∞	∞	18.3 ± 0.9[d]		

(a) Values of ρ_{28}, δ_{25}, and ρ_{Au} were obtained from Table 4.2.1.

(b) $N^{28} = 0.04375$ atom/cm^3; $\xi^M \Sigma_s^M = 0.178$ cm^{-1}.

(c) From Table 6.1.1.

(d) From Ref. (R3).

CHAPTER VII
SUMMARY, CONCLUSIONS, AND RECOMMENDATIONS

Introduction

The microscopic parameters, ρ_{28}, C^*, δ_{25}, and δ_{28}, were measured in three lattices moderated by heavy water with 1.03 w/o U^{235}, 0.25-inch-diameter fuel rods arranged in triangular arrays and spaced at 1.25-, 1.75-, and 2.50-inches. The results of these measurements are listed in Table 4.2.1. These results provide new experimental reactor physics data to which the results of theoretical treatments may be compared. Previous studies of heavy water lattices have been restricted almost entirely to large (1.0 inch in diameter or more), natural uranium fuel rods (H11). Hence, the results of the measurements reported here are particularly useful in that they extend the experimental data into the region of small, slightly enriched fuel rods, thus broadening the base against which the presently available theory may be tested. The results of an investigation of systematic errors associated with the measurements has led to many changes and adjustments in the experimental technique and procedure which have improved the general precision of the experimental results. The investigation of the resonance energy region was expanded by developing methods to measure the resonance activation of a foil which is proportional to the resonance energy neutron flux.

7.1 Cadmium Ratio Measurements

The subcadmium and epicadmium U^{235} fission product activities and the subcadmium Np^{239} activity of foils irradiated within a fuel rod were not affected by perturbations within the fuel rod such as the replacement of fuel material with aluminum catcher foils. However, because of the extremely short mean free path within the fuel of a neutron whose energy corresponds to one of the U^{238} resonances, any

perturbation in the surface of the fuel will permit neutrons to stream into the interior of the fuel rod. Hence, the measured epicadmium Np^{239} activity (which was directly proportional to the U^{238} capture rate) was found to be very sensitive to perturbations in the U^{238} concentration in the fuel rod, particularly at the rod surface (see Section 3.2.3). The use of aluminum or aluminum alloy foils within the fuel rod is an example of such a perturbation which was found to affect the measured results. The epicadmium Np^{239} activity and the epicadmium U^{235} fission product activity were found to be slightly sensitive to perturbations in the high energy neutron flux. The depression of the thermal flux caused by the use of cadmium also depresses the high energy flux in the cadmium-covered foils (see Section 3.2.2). The values of ρ_{28} and δ_{25} were corrected for this high energy flux depression. The epicadmium Np^{239} activity due to resonance energy neutrons was not found to be affected by the presence of cadmium; however, many other laboratories have reported such effects (cf. Ref. (E1)), and further study of this problem is recommended to seek the possible causes of this disagreement. In contrast to the results obtained at the Brookhaven National Laboratory (A4), no effect upon the measured Np^{239} activity due to nonuniform activity distributions was observed. Continued study of this problem is also strongly recommended. In addition, a program to compare the many methods (E1, K3, H12) of measuring the value of the U^{238} cadmium ratio should be undertaken.

7.2 The Measurement of the Ratio of Capture in U^{238} to Fission in U^{235}, C^*

A new method, described in Section 2.2.1, was developed to measure C^* which significantly reduced the experimental uncertainty associated with this quantity, eliminated some sources of systematic error inherent in the previous method, and simplified the experiment. As discussed in Section 4.2, the results of this new method and the results obtained by means of cadmium ratio measurements seemed to have a systematic discrepancy. Preliminary studies indicate that this discrepancy may be caused by the relatively high fission product activity of the natural uranium foil irradiated in the cavity sample tube. This relatively high activity may have produced a gain shift in the photomultiplier tube of the counting system.

This gain shift could be eliminated by using either a gain stabilized high voltage supply or by using zener diodes to establish the voltages for the dinodes of the photomultiplier tube. As in the measurement of ρ_{28}, the determination of C^* involves the measurement of Np^{239} activity. The precautions to be taken for the measurement of the Np^{239} activity have been discussed in Section 7.1.

7.3 The Fast Fission Ratio

The fast fission ratio was found to be highly sensitive to perturbations of the high energy neutron flux in the vicinity of the uranium detector foils used to measure this quantity (see Section 3.2.3). On the one hand, this effect is unexpected because the mean free path of a high energy neutron is large (of the order of 10 cm); but, on the other hand, this effect is quite reasonable because high energy neutrons born within, and in the immediate vicinity of, the detector foils have the highest probability of causing a U^{238} fission in those foils. The importance of these neutrons increases as the fuel rod diameter decreases and as the distance between the rods increases; hence, in the lattices which contained small fuel rods on wide spacings, a change in the U^{235} fission rate in or near the uranium detector foils significantly affected the U^{238} fission rate in those foils. The experimental methods currently used to measure the fast fission ratio require the use of two uranium foils whose U^{235} contents differ significantly; therefore, the experimental method inherently contains a source of systematic error. Correction factors were experimentally determined for the results obtained for the 1.75-inch lattice and an analytical method was developed to convert these results into the proper correction factors for other lattices. These correction factors, which are listed in Table 3.2.2, should be tested, preferably by using measurements made in single-rod experiments to maximize the perturbation.

The method used during the present work to make the fast fission measurements had the disadvantage of requiring an auxiliary experiment. The formulation of the fast fission ratio experimental values is given by the relation:

$$\delta_{28} = P(t)F(t) = \frac{\delta^*_{28}}{F^*(t)} F(t), \qquad (7.3.1)$$

where F(t) is a function of the measured relative foil activities, P(t) is a factor to convert the measured relative foil activities to relative reaction rates, t is the time after irradiation, and the superscript * refers to a reference position. The factors F(t) and P(t) are also functions of the irradiation time. This method has three disadvantages: 1) F(t) and $F^*(t)$ must be measured at different times, perhaps separated by many months; 2) F(t) and P(t) are functions of the irradiation time; and 3) F(t) and P(t) are functions of the time after irradiation. These three disadvantages could be eliminated by measuring δ^*_{28} and $F^*(t)$ in the graphite-lined cavity of the facility. Then the measurements of F(t) and $F^*(t)$ could be made simultaneously, thus eliminating all time dependence:

$$\delta_{28} = \delta^*_{28} \frac{F}{F^*} \cdot \qquad (7.3.2)$$

In Eq. 7.3.2, the value of δ^*_{28} in the cavity is assumed to be constant and not affected by the presence or absence of a lattice in the exponential tank. This independence of conditions in the exponential tank should be verified experimentally.

The value of δ^*_{28} was determined by means of the La^{140} counting technique developed by Wolberg et al. (W3) (see Section 2.2.6). It is recommended that this method be compared with the double fission chamber methods, particularly the method recently developed at the Brookhaven National Laboratory (T1). Finally, the graphite-lined cavity and the exponential tank provide excellent facilities for a study of the fast fission ratio for single rods as a function of rod size, U^{235} content, and moderator. Portions of this study are under way.

7.4 Resonance Activation Measurements

A new method of determining the resonance escape probability has been developed as described in Section 2.4. This method involves the measurement of that portion of the activity of a foil which is due to neutron captures in the resonances in the activation cross section of the foil material. The resonance escape probability was determined by using the resonance activation data to calculate the ratio of the slowing-down density in the moderator to the U^{238} resonance absorption in the fuel. This

new method has the advantage that the use of cadmium is not necessary, and the value of p determined by means of this method should be less sensitive to experimental uncertainties in systems which have a large epithermal flux relative to the thermal flux. The methods developed to determine the resonance activation of a foil are similar to methods used at other facilities (C3, B3). The resonance activation data, which is listed in Table 4.2.2, may also be used to measure the relative neutron flux or slowing-down density as functions of position at various energies in the resonance energy region, which would provide experimental data to which sophisticated theoretical treatments of this energy region could be compared. The experimental methods may also be used to determine the effective resonance integral of U^{238} in the fuel rod. It was assumed that the irradiation sample thimble at position 13 of the MITR provided a good reference position with an epithermal flux which has a $\frac{1}{E}$ energy dependence. The results of the resonance activation measurements made at that position supported this assumption. Some of the results of the measurements in the MITR indicate that some of the resonance integral data appearing in the literature may be in error. This possible discrepancy, plus the complete lack of information for many nuclides, indicates that a program to accurately measure the resonance activation integrals of various nuclides could yield some useful basic data.

7.5 Analysis and Comparison of Results

The experimental results of the measurements made during the present work show good agreement with the results of measurements by Peak et al. (P2) in the M.I.T. Miniature Lattice Facility. This agreement indicates that the miniature lattice can be used for microscopic parameter measurements. The feasibility of using the miniature lattice for other measurements is currently being studied. The value of k_∞ obtained from the results of the present work agreed within the experimental uncertainty with the value of k_∞ obtained by Malaviya et al. (M3) from pulsed neutron experiments made in the 1.75-inch lattice. The results for the values of f, f_m, L^2, and $\overline{\nu\Sigma_a}$ of Malaviya et al. also showed reasonable agreement with the results obtained from the output of the computer programs THERMOS and GAM-I. Investigations in the lattice

facility by means of the pulsed neutron technique are being continued.

The theoretical results obtained from the output of computer programs THERMOS and GAM-I were used to aid in the analysis and interpretation of the experimental results. There were some significant discrepancies between the values of the microscopic parameters calculated from the theoretical results and the experimental values of these parameters. The discrepancies are most likely due to shortcomings associated with the GAM-I calculations as applied to the present work. The effects of those discrepancies on the final analytical results given in Chapter VI are small (see Section 5.3). A more sophisticated theoretical treatment such as is being undertaken by Honeck (H11) should pinpoint the sources of errors in the theoretical treatment.

In summary, the usual microscopic lattice parameters were measured in the three lattices studied. The general precision of these measurements was improved as a result of the extra care and precautions introduced into the experimental techniques and procedures. An investigation of systematic errors was carried out and the sources of these errors were avoided or, where this was not feasible, correction factors were developed. A new method was developed to measure the ratio C^* which simplified the experiment, reduced the experimental uncertainty associated with the measurement, and avoided systematic errors inherent in the method used to measure C^* in earlier work. A new experimental method was also developed to measure the effective resonance integral of U^{238} in a fuel rod in the lattice. Methods to measure the resonance activity of a nuclide were developed, and these methods were used in a new approach for finding the value of the resonance escape probability. This new method had the advantage of avoiding the use of cadmium. The final results obtained are consistent and in good agreement with earlier work done at M.I.T.

APPENDIX A
NOMENCLATURE

Superscripts

a	denotes a quantity pertaining to nuclide a
b	denotes a quantity pertaining to $\frac{1}{v}$ absorber
FP	denotes a quantity pertaining to a measured fission product activity
25	denotes a property of U^{235}
28	denotes a property of U^{238}
39	denotes a property of Np^{239}
140	denotes a property of La^{140}

Subscripts

b	denotes a quantity pertaining to a foil irradiated bare in the lattice facility
c	denotes a quantity pertaining to a foil irradiated cadmium-covered in the lattice facility
EC	denotes a quantity pertaining to the epicadmium portion of the neutron flux spectrum
F, FAST	denotes a quantity pertaining to the high energy portion of the neutron flux spectrum
H	denotes a quantity pertaining to a foil irradiated in the cavity sample tube or "hohlraum"
Lat	denotes a quantity pertaining to the lattice
M	denotes a quantity pertaining to a Maxwellian flux
res	denotes a quantity pertaining to the resonance energy region
SC	denotes a property of or quantity pertaining to the sub-cadmium portion of the neutron flux spectrum

Subscripts (continued)

TOT	denotes a property of or quantity pertaining to the total neutron flux spectrum
$\frac{1}{v}$	denotes a property of or quantity pertaining to the $\frac{1}{v}$ portion of the activation cross section of a nuclide
13	denotes a quantity pertaining to an experiment made in position 13 of the MITR
25	denotes a property of U^{235}
28	denotes a property of U^{238}

Arabic Symbols

A	activity induced by neutron capture
B_m^2	material buckling
C	ratio of capture rate in U^{238} to absorption rate in U^{235} (initial conversion ratio)
C^*	ratio of capture rate in U^{238} to fission rate in U^{235}
C_M^*	value of C^* determined in a Maxwellian flux
C_{STD}^*	value of C^* determined at a reference position
C_∞^*	value of C^* determined in an infinite system
D	activity of depleted uranium foil
E	energy (ev)
E_{res}	peak energy of a resonance in an activation cross section
ERI	effective resonance integral
f	thermal utilization of fuel
f_m	thermal utilization of moderator
F_F	fraction of epicadmium U^{235} fission product activity caused by high energy neutrons
F_N	fraction of epicadmium Np^{239} activity caused by high energy neutrons
F(t)	ratio measured fission product activity of U^{238} to measured fission product activity of U^{235}

Arabic Symbols (continued)

G	ratio of the subcadmium capture rate in U^{238} to the sum of the absorption rate in U^{235} plus the 1/v capture rate in U^{238}
k_∞	ratio of the net neutron production rate to the net neutron consumption rate in an infinite system
L^2	thermal diffusion length
ℓ	nonleakage probability
ℓ_F	nonleakage probability in the high energy region
ℓ_r	nonleakage probability in the resonance energy region
ℓ_{th}	nonleakage probability in the thermal energy region
ℓ_{C^*}	ratio of the value of C* in an infinite system to the value of C* in a critical system
$\ell_{\delta_{25}}$	ratio of the value of δ_{25} in an infinite system to the value of δ_{25} in a critical system
$\ell_{\rho_{28}}$	ratio of the value of ρ_{28} in an infinite system to the value of ρ_{28} in a critical system
p	resonance escape probability
P(t)	ratio of the measured U^{235} fission product activity per U^{235} fission to the measured U^{238} fission product activity per U^{238} fission
Q_o	rate at which neutrons slow down into the thermal energy region
q_o	slowing-down density at upper limit of the thermal energy region
q_{res}	slowing-down density at E_{res}
q(E)	slowing-down density as a function of energy
q(u)	slowing-down density as a function of lethargy
R_{Au}	cadmium ratio of gold within the fuel rod
R_b	ratio of the activity of a foil irradiated bare in the lattice to the activity of a similar foil irradiated in the cavity sample tube
R_c	ratio of the activity of a foil irradiated cadmium-covered in the lattice to the activity of a similar foil irradiated in the cavity sample tube

Arabic Symbols (continued)

R_F	ratio of the U^{235} fission product activity of a uranium foil irradiated bare in the lattice to the U^{235} fission product activity of a uranium foil irradiated in the cavity sample tube
R_L	cadmium ratio of a nuclide in the moderator
R_N	ratio of the Np^{239} activity of a uranium foil irradiated bare in the lattice to the Np^{239} activity of a uranium foil irradiated in the cavity sample tube
R_R	cadmium ratio of a nuclide in position 13 of the MITR
R_{res}	ratio of the resonance activity of a foil irradiated in the cavity sample tube
RI	resonance integral
TRI	total resonance integral (RI plus epicadmium $\frac{1}{v}$ contribution)
u	lethargy

Greek Symbols

α_{25}	ratio of the capture rate to the fission rate in U^{235}
α_{28}	ratio of the capture rate above 1 Mev to the fission rate in U^{238}
β^{25}	yield of La^{140} from the fission of U^{235}
β^{28}	yield of La^{140} from the fission of U^{238}
Γ	ratio of La^{140} activity of a depleted uranium foil to La^{140} activity of a natural uranium foil
$\gamma(t)$	ratio of the fission product activity of a depleted uranium foil to the fission product activity of a natural uranium foil
δ	cadmium ratio of a $\frac{1}{v}$ absorber in a fuel rod
δ_c	defined by Eq. 3.2.1
δ_{25}	ratio of epicadmium U^{235} fission rate to subcadmium fission rate in a fuel rod
δ_{28}	ratio of U^{238} fission rate to U^{235} fission rate in a fuel rod
δ_{28}^*	value of δ_{28} for a reference position

Greek Symbols (continued)

ϵ	fast fission factor (defined by Eq. 6.1.6)
ε	proportionality factor (used in Sections 2.4, 6.3, and 6.4)
ϵ_D	ratio of U^{235} atom concentration to total uranium atom concentration in a depleted uranium foil
ϵ_N	ratio of U^{235} atom concentration to total uranium atom concentration in a natural uranium foil
η	multiplication factor (defined by Eq. 6.1.4)
ν_{25}	average number of neutrons produced per U^{235} fission
ν_{28}	average number of neutrons produced per U^{238} fission
ξ	average logarithmic energy loss per collision
ρ_{Au}	ratio of the epicadmium activity to the subcadmium activity of a gold foil irradiated in a fuel rod
ρ^a	ratio of the epicadmium activity to the subcadmium activity of a resonance detector
ρ^b	ratio of the epicadmium activity to the subcadmium activity of a 1/v detector
ρ_{res}	ratio of the resonance activity to the subcadmium activity of a resonance detector
ρ_{28}	ratio of the epicadmium Np^{239} activity to the subcadmium Np^{239} activity of a uranium foil irradiated in a fuel rod
σ_o	cross section at 2200 meters per second
$\sigma_{res}(E)$	resonance portion of microscopic cross section
$\sigma_{1/v}(E)$	1/v portion of microscopic cross section
Σ_a	macroscopic absorption cross section
Σ_c	macroscopic capture cross section
Σ_F	macroscopic high energy capture cross section of U^{238}
Σ_f	macroscopic fission cross section
Σ_s	macroscopic scattering cross section
τ	Fermi age of neutrons (cm^2)

ϕ	spatially and spectrally integrated neutron flux
ϕ_H	conventional neutron flux in cavity sample tube
ϕ_i	neutron flux per unit lethargy at energies above resonance absorption area
ϕ_{res}	defined such that $RI\phi_{res}$ is the resonance capture rate
$\phi_{1/v}$	defined such that $\sigma_{1/v}\phi_{1/v}$ is the $\frac{1}{v}$ capture rate
$\phi(E)$	neutron flux per unit energy
$\phi(u)$	neutron flux per unit lethargy

APPENDIX B
REFERENCES

A1 Adler, F. T., G. W. Hinman, and L. W. Nordheim, "The Quantitative Evaluation of Resonance Integrals," Proceedings of the Second United Nations Conference on Peaceful Uses of Atomic Energy, Vol. 16, 155, (1958) P/1988.

A2 Ahsan, M., Research Project, Course 22.42, M.I.T., unpublished.

A3 Anderson, C. A., "Measurement of Neutron Energy Spectra with the M.I.T.R. Fast Chopper," Ph.D. thesis, M.I.T. (1961).

A4 Arcipiani, B., D. Ricabarra, and G. H. Ricabarra, "A Note on the Measurement of the U^{238} Cadmium Ratio," Nuc. Sci. Eng., 14, 316 (1962).

B1 Bliss, H. E., "Measurements of the Fast Effect in Heavy Water Partially Enriched Uranium Lattices," M.S. thesis, M.I.T. (1964).

B2 Brown, P. S., T. J. Thompson, I. Kaplan, and A. E. Profio, "Measurements of the Spatial and Energy Distribution of Thermal Neutrons in Uranium, Heavy Water Lattices," NYO-10205 (August 1962).

B3 Bardes, R. G., J. R. Brown, M. K. Drake, P. U. Fischer, D. C. Pound, J. B. Sampson, and H. B. Stewart, "High-Temperature Gas-Cooled Reactor Critical Experiment and Its Application," GA-4496 (August 1963).

C1 Clark, L., "Prompt Activation Analysis for Boron and Lithium," M.S. thesis, M.I.T. (1963).

C2 Clikeman, F. et al., private communication.

C3 Carver, J. G. and W. R. Morgan, "Selection of a Set of Radioactivants for Investigating Slow Neutron Spectra," Proceedings of 1961 International Conference, College Sta., Texas (Dec. 15-16, 1961).

D1 Davidson, T. W., J. D. Cleary, D. Jennings, H. A. Risti, and G. H. Minton, "Multi-Region Reactor Lattice Studies," WCAP-1434 (1961).

E1 Engelder, T. C. et al., "Spectral Shift Control Reactor – Basic Physics Program – Critical Experiments on Lattices Moderated by D_2O - H_2O Mixtures," BAW-1231 (December 1961).

G1 Grimesey, R. A., F. E. Mullen, and C. J. Gannon, "Muft Revision – a Fast Neutron Spectrum Code for the IBM-650," IDO-16735 (March 1962).

H1 Harrington, J., "Measurement of the Material Buckling of a Lattice of Slightly Enriched Uranium Rods in Heavy Water, M.S. thesis, M.I.T. (July 1963).

H2 "Heavy Water Lattice Research Project Annual Report," NYO-9658 (September 1961).

H3 "Heavy Water Lattice Project Annual Report," NYO-10,208 (September 1962).

H4 "Heavy Water Lattice Project Annual Report," NYO-10,212 (September 1963).

H5 Hellens, R. L. and H. C. Honeck, "A Summary and Preliminary Analysis of the B.N.L. Slightly Enriched Uranium, Water-Moderated Lattice Measurements," Proceedings of the IAEA Conference on Light Water Lattices, Vienna (June 1962).

H6 Honeck, H. C., "THERMOS, a Thermalization Transport Theory Code for Reactor Lattice Calculations," BNL-5826 (September 1961).

H7 Honeck, H. C., and Kaplan, I., "The Distribution of Thermal Neutrons in Space and Energy in Reactor Lattices, Part I: Theory, and Part II: Comparison of Theory and Experiment," Nuc. Sci. Eng., 8, No. 3 (September 1960).

H8 Honeck, H. C., "A Method for Computing Thermal Neutron Distributions in Reactor Lattices as Functions of Space and Energy," Ph.D. thesis, M.I.T. (June 1959).

H9 Honeck, H. C., "An Incoherent Thermal Scattering Model for Heavy Water," Trans. ANS, 5, No. 1 (June 1962).

H10 Honeck, H. C., "Some Methods for Improving the Cylindrical Reflecting Boundary Condition in Cell Calculations of the Thermal Neutron Flux," Trans. Am. Nuclear Soc., 5, No. 2, 350 (1962).

H11 Honeck, H. C., private communication.

H12 Hellens, R. L. and G. A. Price, unpublished Brookhaven National Laboratory Report.

I1 Isbin, H. S., Introductory Nuclear Reactor Theory, New York: Reinhold Publishing Corporation (1963).

J1 Joanou, G. D. and J. S. Dudek, "GAM-I: A Consistent P_1 Multigroup Code for the Calculation of Fast Neutron Spectra and Multigroup Constants," GA-1850 (June 1961).

K1 Kier, P., "The Effect of a Non-Asymptotic Neutron Source on Resonance Absorption in Slab Lattices," Ph.D. thesis, M.I.T. (1963).

K2 Kim, H., "Measurement of Material Buckling of a Lattice of Enriched Uranium Rods in Heavy Water," M.S. thesis, M.I.T. (June 1963).

K3 Kours, H., and R. Sher, BNL-486 (T-111), (1957).

K4 Kushneriuk, S. A., "Progress Report," Physics Division, Chalk River, Ontario, AECL-1711 (October 1 to December 31, 1962).

L1 Larson, C. L., "Reactivity Studies of a Heavy Water Moderated, Highly Enriched Uranium Reactor," Ph.D. thesis, M.I.T. (1959).

M1 Madell, J., T. J. Thompson, A. E. Profio, and I. Kaplan, "Spatial Distribution of the Neutron Flux on the Surface of a Graphite-Lined Cavity," NYO-9657 (April 1962).

M2 McArthy, A. E., P. J. Persiani, B. I. Spinrad, and L. J. Templin, "Neutron Resonance Integral and Age Data," ANL Newsletter No. 1 (June 1961).

M3 Malaviya, B. K., I. Kaplan, T. J. Thompson, D. D. Lanning, and A. E. Profio, "Studies of Reactivity and Related Parameters in Lattices of Slightly Enriched Uranium Moderated by Heavy Water," MIT-2344-1 (1964).

N1 Nelkin, M., "Scattering of Slow Neutrons by Water," Phys. Rev., 119, 741 (1960).

N2 Nordheim, L. W., "A New Calculation of Resonance Integrals," Nuc. Sci. Eng., 12, 457 (1962).

O1 Olsen, H., private communication.

P1 Palmedo, P. F., I. Kaplan, and T. J. Thompson, "Measurements of the Material Bucklings of Lattices of Natural Uranium Rods in D_2O," NYO-9660 (January 1962).

P2 Peak, J., I. Kaplan, and T. J. Thompson, "Theory and Use of Small Subcritical Assemblies for the Measurement of Reactor Parameters," NYO-10204 (April 1962).

P3 Persiani, P. J., J. J. Kaganove, and A. E. McArthy, "Neutron Resonance Integral and Age Data," ANL Newsletter No. 10 (April 1963).

P4 Pilat, E. E., private communication.

R1 Rief, H., "An IBM 704 Monte Carlo Code to Calculate Fast Fission Effects in Homogeneous and Heterogeneous Systems," BNL 647 (T-206), (1961).

R2 Rydin, R. A., N. C. Rasmussen, and G. L. Brownell, "Fast Neutron Spectroscopy and Dosimetry of the M.I.T. Reactor Medical Therapy Facility Beam," Scientific Report No. 3, MITNE-47, AFCRL-64-404 (May 1964).

R3 "Reactor Physics Constants," ANL-5800, 485-487.

S1 Simms, R., I. Kaplan, T. J. Thompson, and D. D. Lanning, "Analytical and Experimental Investigations of the Behavior of Thermal Neutrons in Lattices of Uranium Metal Rods in Heavy Water," NYO-10,211 (October 1963).

T1 Tassan, S., "Fast Fission Factors in Slightly Enriched Uranium Light-Water-Moderated Slab Lattices," Nuc. Sci. Eng., 19, 471 (1964).

W1 Weitzberg, A., I. Kaplan, and T. J. Thompson, "Measurements of Neutron Capture in U^{238} in Lattices of Uranium Rods in Heavy Water," NYO-9659 (January 1962).

W2 Westcott, C. H., "Effective Cross Section Values for Well-Moderated Thermal Reactor Spectra," 3rd Edition corrected, AECL-1101 (November 1960).

W3 Wolberg, J. R., T. J. Thompson, and I. Kaplan, "A Study of the Fast Fission Effect in Lattices of Uranium Rods in Heavy Water," NYO-9661 (February 1962).

W4 Woodruff, E., private communication.

W5 Weinberg, A. M. and E. P. Wigner, The Physical Theory of Neutron Chain Reactors, Chicago: The University of Chicago Press (1958).

APPENDIX C
COMPUTER PROGRAMS

This appendix contains the listings of three computer programs used during the course of the present work.

The program LSQ is listed in Table C.1. This program was used to fit a polynomial by the least squares method to the measured fission product activities of uranium foils as a function of time. The raw counting data is corrected for counter dead time, room background, natural and residual activities of the foils, foil weight, and foil thickness. Polynomials ranging from second degree to tenth degree may be obtained for any combination of three functional relations: A as a function of t, ln A as a function of t, and ln A as a function of ln t, where A is the corrected fission product activity and t is the time at which the activity was measured.

The program ANA, which is listed in Table C.2, was used to aid in the reduction of the raw counting data obtained from the experiments made to measure the intracellular activation distributions. The raw counting data are corrected for counter dead time, room background, foil weight, foil thickness, decay of activity, and position in the exponential tank.

The program AVNDFL was used to calculate the spatially averaged thermal neutron flux spectrum from the punched card output of the program THERMOS. Table C.3 contains a listing of the program AVNDFL.

TABLE C.1

COMPUTER PROGRAM LSQ

```
#M2133-1657,FMS,RESULT,3,5,10000,500          W. DARDENNE      LSQ
*       XEQ
*       LIST8
*       LABEL
CLSQ-4D
*       SYMBOL TABLE
        DIMENSION YLS(100),YILS(100),CI(100),XX(100),T(100)
        DIMENSION ID(16),AN(11)
        DIMENSION X(100),Y(100),SUM(21),V(11),A(11),B(11,12),C(100),F(11,
       1100),CM(11,11),CX(11,11),COF(10,10),DCF(11),DSQ(100),FPSA(11),RSQ
       2(100),WTCO(100)
        COMMON MIN,MAX,N,MORE,NCASE,NT,NF,NTF,NP,N1,N2,N3,N4,N5,N6,N7
        COMMON X,Y,M,ID
      1 FORMAT(  16A5)
      2 READ 1,(ID(I),I=1,16)
C       ID(I) IS AN I.D. STATMENT
        PRINT 15,(ID(I),I=1,16)
        PUNCH 1,(ID(I),I=1,16)
        READ 3,MIN,MAX,N,MORE,NCASE,NT,NF,NTF,NP,N1,N2,N3,N4,N5,N6,N7
        PRINT 54
        PRINT 49,MIN,MAX,N,MORE,NCASE,NT,NF,NTF,NP,N1,N2,N3,N4,N5,N6,N7
      3 FORMAT(16I5)
      4 FORMAT(6E12.6)
C       MIN=LOWEST DEGREE EQUATION TO BE FIT TO DATA
C       MAX=HIGHEST DEGREE EQUATION TO BE FIT TO THE DATA
C       N=NUMBER OF DATA POINTS
C       MIN LESS THAN MAX LESS THAN N-1 OR 10
C       MORE=NUMBER OF SETS OF DATA FOLLOWING THIS ONE
C       NCASE=I.D. NUMBER FOR THIS SET OF DATA
C       NT=NUMBER OF T(I) POINTS TO BE READ
C       NF IS THE CONTROL FACTOR FOR THE SCALE FACTOR AND THE SHIFT TERM
C       NTF IS THE CONTROL FACTOR FOR THE TYPE OF FIT
C        NEG  LOG-LOG        ZERO  LINEAR          POS  SEMI-LOG
C       IF NP IS POS, PREP IS CALLED
C       IF N1 IS NEG, NTF=-1 FOR SECOND PASS WITH DATA SET
C        IF N1 IS POS, NTF=1 FOR SECOND PASS WITH DATA SET
C       IF N2 IS NEG AND N1 WAS POS, TWO PASSES MORE PASSES WITH DATA SET WILL BE
C        MADE WITH NTF=1 AND -1
C       N3 IS CONTROL CHARACTER FOR WEIGHTING COEFFICIENTS
C       IF N3 IS POS,WT. COEF. ARE REQUIRED, OTHERWISE WT.COEF. = 1.0
C       N4 IS CONTROL CHARACTER FOR CELL FIT, YES IF POSITIVE
        IF(NP)36,36,38
     38 CALL PREP
        IF(M)39,39,202
     36 READ INPUT TAPE 4,4,(X(I),I=1,N)
        READ INPUT TAPE 4,4,(Y(I),I=1,N)
C       X(I) IS THE INDEPENDENT VARIABLE, Y(I) IS THE DEPENDENT VARIABLE
        WRITE OUTPUT TAPE 2,50
        PRINT 44,(X(I),Y(I),I=1,N)
     39 CONTINUE
        IF(NF)10,10,11
     11 READ 4,YO,XO
```

```
C      YO IS THE SCALE FACTOR, XO IS THE SHIFT TERM
       DO 12 I=1,N
       X(I)=XO+X(I)
   12  Y(I)=YO*Y(I)
       PRINT 14
       PRINT 44,YO,XO
    7  FORMAT(12H1CASE NUMBER)
    8  FORMAT(13HOCASE NUMBER=,I6)
    9  FORMAT(17HOPOINTS TO BE FIT)
   10  IF(NT)18,19,18
   18  READ 4,(T(I),I=1,NT)
C      T(I) ARE THE NEW TIMES FOR LS VALUES
       PRINT 9
       PRINT 44,(T(I),I=1,NT)
   19  IF(NTF)25,24,25
   25  DO 27 I=1,N
   27  Y(I)=LOGF(Y(I))
       PRINT 32
       PRINT 44,(Y(I),I=1,N)
       IF(NTF)21,24,24
   21  DO 29 I=1,N
   29  X(I)=LOGF(X(I))
       PRINT 34
       PRINT 44,(X(I),I=1,N)
       IF(NT)41,24,41
   41  DO 30 I=1,NT
   30  T(I)=LOGF(T(I))
       PRINT 44,(T(I),I=1,NT)
   24  CONTINUE
       IF (N3) 610,610,600
  600  READ INPUT TAPE 4,4,(WTCO(I),I=1,N)
       WRITE OUTPUT TAPE 2,650
  650  FORMAT (23HOWEIGHTING COEFFICIENTS )
       PRINT 44,(WTCO(I),I=1,N)
       GO TO 620
  610  DO 612 I=1,N
  612  WTCO(I)=1.0
  620  IF(N4) 622,622,621
  621  READ 4,SP
       RAD = SP/2.0
       DO 700 I=1,N
       IT1=I+N
       IT2=N-I+1
       X(IT1)=2.0*RAD-X(IT2)
       WTCO(IT1)=WTCO(IT2)
  700  Y(IT1)=Y(IT2)
  622  DO 200 M=MIN,MAX
  615  IF (N4) 629,629,618
  618  N=2*N
       PRINT 715,SP
  715  FORMAT(61HOTHIS IS A CELL FIT IN POWERS OF X-SQUARE. ROD SPACING(I
      1N.) =F6.3)
  629  LS=2*M+1
       LB=M+2
       LV=M+1
       DO 5 J=1,LS
     5  SUM (J)=0.0
```

```
      DO 6 J=1,LV
    6 V(J)=0.0
      DO 16 I=1,N
      SUM(1)=SUM(1)+WTCO(I)
      P=WTCO(I)
      V(1)=V(1)+Y(I)*WTCO(I)
      DO 13 J=2,LV
      IF (N4) 818,818,813
  813 P=X(I)*X(I)*P
      GO TO 819
  818 P=X(I)*P
  819 SUM(J)=SUM(J)+P
   13 V(J)=V(J)+Y(I)*P
   14 FORMAT(28HOSCALE FACTOR AND SHIFT TERM)
   15 FORMAT(1H1,16A5)
      DO 16 J=LB,LS
      IF (N4) 828,828,823
  823 P=X(I)*X(I)*P
      GO TO 16
  828 P=X(I)*P
   16 SUM(J)=SUM(J)+P
   17 DO 20 I=1,LV
      DO 20 K=1,LV
      J=K+I
   20 B(K,I)=SUM(J-1)
      DO 22 K=1,LV
   22 B(K,LB)=V(K)
   23 DO 31 L=1,LV
      DIVB=B(L,L)
      DO 26 J=L,LB
   26 B(L,J)=B(L,J)/DIVB
      I1=L+1
      IF(I1-LB)28,33,33
   28 DO 31 I=I1,LV
      FMULTB=B(I,L)
      DO 31 J=L,LB
   31 B(I,J)=B(I,J)-B(L,J)*FMULTB
   32 FORMAT(8HOY=LN(Y))
   33 A(LV)=B(LV,LB)
   34 FORMAT(8HOX=LN(X))
      I=LV
   35 SIGMA=0.0
      DO 37 J=I,LV
   37 SIGMA = SIGMA +B(I-1,J)*A(J)
      I=I-1
      A(I)=B(I,LB)-SIGMA
   40 IF(I-1)42,42,35
   42 WRITE OUTPUT TAPE 2,43
   43 FORMAT(30H-POLYNOMIAL COEFFICIENTS, A(N))
      WRITE OUTPUT TAPE 2,44,(A(I),I=1,LV)
   44 FORMAT(1P10E12.4)
      PUNCH 45, NCASE,M
   45 FORMAT(10HCASE ID IS,I6,3X,10H,DEGREE IS,I6)
      PUNCH 43
      PUNCH 46,(A(I),I=1,LV)
   46 FORMAT(6E12.5)
      AN(1)=1.0
```

```
      DO 47 I=2,LV
   47 AN(I)=A(I)/A(1)
      PRINT 48
   48 FORMAT(10H A(N)/A(0))
   49 FORMAT(1X,16I6)
      PRINT 44,(AN(I),I=1,LV)
   50 FORMAT(9HORAW DATA)
      TT=0.0
      IF (N4) 838,838,832
  832 DO 833 K=1,N
  833 XX(K)=X(K)*X(K)
      N=N/2
      GO TO 834
  838 DO 51 K=1,N
   51 XX(K)=X(K)
  834 NN=N
   52 DO 60 K=1,NN
      P=1.0
   54 FORMAT(1H0,
     1        3X3HMIN,3X3HMAX,5X1HN,2X4HMORF,1X5HNCASE,4X2HNT,4X2HNF,3X3H
     2NTF,4X2HNP,4X2HN1,4X2HN2,4X2HN3,4X2HN4,4X2HN5,4X2HN6,4X2HN7)
C     HAVE USED STATMENT NUMBERS FROM 1 UP TO HERE    ***************************
      YLS(K)=0.0
      YILS(K)=0.0
      DO 60 I=1,LV
      YLS(K)=YLS(K)+A(I)*P
      P=P*XX(K)
   60 YILS(K)=YILS(K)+A(I)*P/FLOATF(I)
      CT=0.0
      DO 59 K=1,N
   59 CT=CT+YLS(K)
      IF(TT)61,61,77
   61 DO 62 K=1,N
      C(K)=YLS(K)
   62 CI(K)=YILS(K)
      TT=1.0
      PRINT 75
   75 FORMAT(14HOSMOOTHED DATA)
      PRINT 44,(X(I),C(I),I=1,N)
      PRINT 63,CT
   63 FORMAT(5HOSUM=,E12.5)
      PRINT 73
   73 FORMAT(26HOINTEGRAL OF SMOOTHED DATA)
      PRINT 44,(X(I),CI(I),I=1,N)
      IF(NT)74,81,74
   74 IF(N4) 835,835,837
  837 DO 839 K=1,NT
  839 XX(K)=T(K)**2.0
      GO TO 841
  835 DO 76 K=1,NT
   76 XX(K)=T(K)
  841 NN=NT
      GO TO 52
   77 PRINT 78
   78 FORMAT(13HODESIRED DATA)
      PRINT 44,(T(I),YLS(I),I=1,NT)
      PRINT 63,CT
```

```
      PRINT 79
   79 FORMAT(25H0INTEGRAL OF DESIRED DATA)
      PRINT 44,(T(I),YILS(I),I=1,NT)
   81 CONTINUE
      DO 70 K=1,N
      I=1
      FF=1.0
      F(I,K)=FF
   53 I=I+1
      FF=FF*X(K)
      F(I,K)=FF
      IF(I-M-1)53,70,70
   70 CONTINUE
      DO85 I=1,LV
      DO85 J=1,LV
      K=1
      CM(I,J)=F(I,K)*F(J,K)
   80 K=K+1
      CM(I,J)=CM(I,J)+F(I,K)*F(J,K)
      IF(K-N)80,85,85
   85 CONTINUE
      IF(NTF)141,86,141
   86 CONTINUE
      DO 140 L=1,LV
      II=1
      I=1
  103 JJ=1
      J=1
      IF(I-L)104,118,104
  104 IF(J-L)105,115,105
  105 IF(J-LV)110,110,117
  110 COF(II,JJ)=CM(I,J)
      J=J+1
      JJ=JJ+1
      GO TO 104
  115 J=J+1
      GO TO 104
  117 I=I+1
      II=II+1
      IF(I-LV)103,103,120
  118 I=I+1
      IF(I-LV)104,104,120
  120 LVV=LV-1
      CF=1.0
      MM=XDETRMF(10,LVV,COF,CF)
      DCF(L)=CF
  140 CONTINUF
      WRITE OUTPUT TAPE 2,305
  305 FORMAT(21H0DETS OF COF MATRICES)
      PRINT 44,(DCF(L),L=1,LV)
      DCM=1.0
      MM=XDETRMF(11,LV,CM,DCM)
      WRITE OUTPUT TAPE 2,300
  300 FORMAT(16H0DET OF C MATRIX)
      PRINT 44,DCM
      GO TO 149
  141 CT=0.0
```

```
      DO 142 I=1,N
      CI(I)=Y(I)
      Y(I)=EXPF(Y(I))
      C(I)=EXPF(C(I))
  142 CT=CT+C(I)
      PRINT 75
      PRINT 44,(C(I),I=1,N)
      PRINT 63,CT
      IF(NT)149,149,143
  143 CT=0.0
      DO 144 I=1,NT
      YLS(I)=EXPF(YLS(I))
  144 CT=CT+YLS(I)
      PRINT 78
      PRINT 44,(YLS(I),I=1,NT)
      PRINT 63,CT
  149 DO 150 I=1,N
  150 RSQ(I)=(C(I)-Y(I))*(C(I)-Y(I))
      IF(NTF)151,153,151
  151 DO 152 I=1,N
  152 Y(I)=CI(I)
  153 I=1
      SRSQ=RSQ(I)
  160 I=I+1
      SRSQ=SRSQ+RSQ(I)
      IF(I-N)160,170,170
  170 OM=SRSQ/FLOATF(N-M-1)
      IF(NTF)188,171,188
  171 W=OM/DCM
      DO 180 L=1,LV
      WW=DCF(L)*W
      WW=ABSF(WW)
  180 EPSA(L)=SQRTF(WW)
      WRITE OUTPUT TAPE 2,185
  185 FORMAT(32H0COEFFICIENT UNCERTAINTIES, E(N))
      WRITE OUTPUT TAPE 2,44,(EPSA(L),L=1,LV)
      DO 186 L=1,LV
  186 AN(L)=EPSA(L)/A(L)
      PRINT 187
  187 FORMAT(10H E(N)/A(N))
      PRINT 44,(AN(L),L=1,LV)
      PUNCH 185
      PUNCH 46, (EPSA(L),L=1,LV)
  188 BV=SRSQ/FLOATF(N)
      ERMS=SQRTF(BV)
      WRITE OUTPUT TAPE 2,190
  190 FORMAT(10HORMS ERROR)
      WRITE OUTPUT TAPE 2,44,ERMS
      OMEGA=SQRTF(OM)
      WRITE OUTPUT TAPE 2, 195
  195 FORMAT(11HOERMS ERROR)
      WRITE OUTPUT TAPE 2, 44, OMEGA
  200 CONTINUE
      IF(N1)201,202,203
  201 NTF=-1
      N1=0
      IF(N2)21,19,19
```

```
203 NTF=1
    N1=N2
    GO TO 19
202 CONTINUE
    IF(MORF)205,205,2
205 CALL EXIT
    END
```

```
      SUBROUTINE PREP
*     LIST8
*     LABEL
CPREP1
*     SYMBOL TABLE
      DIMENSION TC(100),CS(100),ID(16),BG(100),BT(100),CT(100),AC(100)
      DIMENSION T(100),RB(100),RT(100),CA(100)
      DIMENSION X(100),Y(100)
      DIMENSION TMCORR(100)
      COMMON MIN,MAX,N,MORE,NCASE,NT,NF,NTF,NP,N1,N2,N3,N4,N5,N6,N7
      COMMON X,Y,M,ID
    2 FORMAT(16I5)
    5 FORMAT(16A5)
      IF(N)1,3,1
    3 CALL EXIT
    1 READ 6,WT,WO,TAU,PI,DECAY,SIG
C     WT IS THE FOIL WEIGHT
C     WO IS A STANDARD FOIL WEIGHT TO WHICH ACTIVITIES ARE CORRECTED
C     TAU IS THE COUNTER DEAD TIME
C     PI IS THE COUNTER PULSE PILE UP
C     DECAY IS THE DECAY CONSTANT OF THE ACTIVITY
C     SIG IS THE WEIGHT ATTENUATION COEFFICIENT FOR THE GAMMA SELF-ABSORPTION
C     CORRECTION FACTOR
    6 FORMAT(6E12.5)
      READ 6,BA,TA,BB,TB,BS,TS
C     BA IS THE PREIRRADIATION BG OF THE FOIL
C     TA IS THE COUNT TIME FOR BA
C     BB IS THE PREIRR. BG FOR THE CONTROL BG FOIL
C     TB IS THE COUNT TIME FOR BB
C     BS IS THE PREIRR. ROOM BG
C     TS IS THE COUNT TIME FOR BS
      M=MIN
      BR=0.0
      BO=BA/TA
      GO=BB/TB
      RO=BS/TS
      IF(BO)33,34,52
   52 IF(GO)33,34,53
   53 BR=(BO-RO)/(GO-RO)
      IF(BR)33,34,35
   33 PRINT 36
   36 FORMAT(20HERROR ON DATA CARD 4)
      GO TO 3
   34 BR=1.0
   35 IF(M)27,27,28
   27 M=6
   28 DO 13 I=1,N
      BG(I)=0.0
      BT(I)=0.0
      RB(I)=0.0
      RT(I)=0.0
   13 CT(I)=0.0
      READ 6,(BG(I),I=1,M)
C     BG(I) ARE THE CONTROL BG FOIL COUNTS FOR THE I,TH COUNTING SESSION
      READ 6,(BT(I),I=1,M)
C     BT(I) ARE THE COUNT TIMES FOR BG(I)
      READ 6,(RB(I),I=1,M)
C     RB(I) ARE THE ROOM BG COUNTS FOR THE I,TH COUNTING SESSION
      READ 6,(RT(I),I=1,M)
C     RT(I) ARE THE COUNTING TIMES FOR RB(I)
      READ 6,(CT(I),I=1,M)
```

```
C      CT(I) ARE THE COUNTING TIMES FOR THE CS(I)
       IF(BT(1))51,51,54
   51  BT(1)=1.0
   54  CONTINUE
       IF(BG(1))47,47,48
   47  BG(1)=BA/TA-BS/TS+RB(1)/RT(1)
       BG(1)=BG(1)*BT(1)
   48  DO 12 I=2,N
       II=I-1
       IF(RT(I))38,37,38
   37  RT(I)=RT(II)
   38  IF(RB(I))40,39,40
   39  RB(I)=RB(II)
   40  IF(BT(I))8,7,8
    7  BT(I)=BT(II)
    8  IF(BG(I))10,9,10
    9  BG(I)=BG(II)/BT(II)-RB(II)/RT(II)+RB(I)/RT(I)
       BG(I)=BG(I)*BT(I)
   10  IF(CT(I))12,11,12
   11  CT(I)=CT(II)
   12  CONTINUE
   14  READ 6,(TC(I),CS(I),I=1,N)
C      TC(I) ARE THE TIMES THE CS(I) WERE STRATED
C      CS(I) ARE THE FOIL COUNTS FOR THE I,TH COUNTING SESSION
       M=0
       IF(SIG)21,22,21
   21  WT=(1.0-EXPF(-WT*SIG))/(WT*(1.0-EXPF(-WO*SIG)))
   22  IF(DECAY)23,26,23
   23  DO 49 I=1,N
   49  TMCORR(I)=EXPF(TC(I)*DECAY)*DECAY*CT(I)/(1.0-EXPF(-CT(I)*DECAY))
       M=1
       GO TO 30
   26  DO 50 I=1,N
       TMCORR(I)=1.0
   50  TC(I)=TC(I)+0.5*CT(I)
   30  DO 15 I=1,N
       X(I)=TC(I)
       R=RB(I)/RT(I)
       B=(BG(I)/BT(I)-R)*BR+R
       CG=CS(I)/CT(I)
       CH=CG*(1.0+TAU*CG)
       CC=CH*(1.0-PI*CH)-B
       CC=CC*TMCORR(I)
       AC(I)=CC*WO/WT
       Y(I)=AC(I)
   15  CA(I)=AC(I)*CT(I)
       IF(MAX)24,24,25
   24  MAX=4
       GO TO 25
   41  MAX=N-1
       GO TO 43
   25  IF(MAX-N)43,41,41
   43  IF(MAX-10)45,45,44
   44  MAX=10
   45  MIN=2
       PUNCH 16
   16  FORMAT(30HCORRECTED TIMES AND ACTIVITIES)
       PUNCH 6,(TC(I),AC(I),I=1,N)
       PRINT 18
   18  FORMAT(1H0,7X2HWT,12X2HWO,12X3HTAU,11X2HPI)
       PRINT 20,WT,WO,TAU,PI
```

```
      PRINT 46
   46 FORMAT(1H0,7X2HBA,12X2HTA,12X2HBB,12X2HTB,12X2HBS,12X2HTS)
      PRINT 20,BA,TA,BB,TB,BS,TS
      PRINT 19
   19 FORMAT(1H0,1X12HTIME COUNTED,1X13HCORRECTED ACT,6X8HCORR CTS,6X8HR
     1AW CTNS,1X13HCOUNTING TIME,4X10HBACKGROUND,1X13HBG COUNT TIME,7X7H
     1ROOM BG,1X13HRM BG CT TIME)
      PRINT 20,(TC(I),AC(I),CA(I),CS(I),CT(I),BG(I),BT(I),RB(I),RT(I),I=
     11,N)
   20 FORMAT(9E14.5)
      IF(DECAY)999,999,29
   29 IF(NT)999,999,17
   17 READ 6,(T(I),I=1,N)
      YT=0.0
      DO 31 I=1,N
      Y(I)=Y(I)*EXPF(-DECAY*T(I))
   31 YT=YT+Y(I)
      PRINT 42
   42 FORMAT(14H0T(I) AND Y(I))
      PRINT 6,(T(I),Y(I),I=1,N)
      PRINT 4,YT
    4 FORMAT(10H0SUM Y(I)=,E12.5)
  999 RETURN
      END
```

TABLE C.2

COMPUTER PROGRAM ANA

```
*M2133-1657,FMS,RESULT,3,5,10000,500          W. DARDENNE      ANA
*       XEQ
*       LIST8
*       LABEL
CANA-ID       PROGRAM BY W. H. DARDENNE, 9/13/63
*       SYMBOL TABLE
        DIMENSION WT(1000),ND(100),CT(100,24),SATCT(100,24),RELTM(100,24)
        DIMENSION DELAY(24),COUNTS(24),DIF(24),AVCT(100),MD(100)
        DIMENSION HOLR(16),ADENT(96),COF(100,11),X(24),Y(24),F(6),UL(100)
        DIMENSION DIV(100),RMS(100),OMEGA(100)
        DIMENSION FW(1000),WORD(4),IWD(4)
        COMMON WT,ND,CT,SATCT,RELTM,DELAY,COUNTS,DIF,AVCT,MD,HOLR,ADENT
        COMMON DKAY,LMAX,NMAX,NPASS,F,NOHITS,TMCER
      1 READ 10,NORUNS
        IF(NORUNS)100,100,102
C       A BLANK CARD TERMINATES RUN
  100   CALL EXIT
  102   CONTINUE
        CALL LIB(WT,F,ADENT)
 2010   READ18,(HOLR(I),I=1,16)
        READ 10,NOHITS
        PRINT 20
        PRINT 19,(HOLR(I),I=1,16)
        CALL CALC
        NORUNS=NORUNS-1
        IF(NORUNS)1,1,2010
   10   FORMAT(16I5)
   18   FORMAT(16A5)
   19   FORMAT(1X16A5)
   20   FORMAT(22H1ANALYSIS OF FOIL DATA)
        END
```

```
*      LIST8
*      LABEL
CLIB-1D       PROGRAM BY W. H. DARDENNE, 9/2/63
*      SYMBOL TABLE
       SUBROUTINE LIB (WT,E,ADENT)
*      SYMBOL TABLE
       DIMENSION WT(1000),E(6),ADENT(96)
       DO 2 K=1,1000
     2 WT(K)=0.0
C      PROGRAM NOW READS IN FOIL LIBRARY
       READ 18,(ADENT(I),I=1,96)
       READ 12,LMAX,(E(I),I=1,6)
       IF(LMAX)110,110,104
  104  IF(LMAX-1000)108,108,106
  106  PRINT 14
       CALL EXIT
  108  CONTINUE
       READ 16,(WT(L),L=1,LMAX)
  110  CONTINUE
       MAX=LMAX
C      NEW FOILS ADDED OR REPLACED
       READ 10,LNEW,NPRINT,NPUNCH
       NAM=LNEW
       IF(LMAX+LNEW)120,120,121
  120  PRINT 22
       CALL EXIT
  121  IF(LNEW)150,150,122
  122  IF(LNEW-1000)124,124,123
  123  PRINT 24
       CALL EXIT
  124  CONTINUE
       PRINT 26
  140  READ 28,MA,A,MB,B,MC,C,MD,D
       PRINT 30,MA,A,MB,B,MC,C,MD,D
       IF(MD)125,125,130
  125  IF(MC)126,126,132
  126  IF(MB)136,136,134
  130  WT(MD)=D
       IF(MD-MAX)132,132,131
  131  MAX=MD
  132  WT(MC)=C
       IF(MC-MAX)134,134,133
  133  MAX=MC
  134  WT(MB)=B
       IF(MB-MAX)136,136,135
  135  MAX=MB
  136  WT(MA)=A
       IF(MA-MAX)138,138,137
  137  MAX=MA
  138  CONTINUE
       NAM=NAM-4
       IF(NAM)142,142,140
  142  CONTINUE
C      MAX=MAX NO. OF FOILS TO DATE
  150  CONTINUE
       IF(MAX-1000)4,4,3
    3  PRINT51
   51  FORMAT(24H0TOTAL FOILS EXCEED 1000)
       CALL EXIT
    4  CONTINUE
       LMAX=MAX
```

```
 2000 IF(NPRINT)2001,2001,2002
 2002 CALL PRNTO(WT,MAX,ADENT)
C     PRNTO PRINTS OUT LIBRARY
 2001 CONTINUE
      IF(NPUNCH)2003,2003,2004
 2004 PUNCH 18,(ADENT(I),I=1,96)
      PUNCH 12,MAX,(F(I),I=1,6)
      PUNCH 16,(WT(I),I=1,MAX)
 2003 CONTINUE
 10   FORMAT(6I5)
   12 FORMAT(I5,6E12.5)
 14   FORMAT(27H1LIBRARY EXCEEDS 1000 FOILS)
 16   FORMAT(6E12.5)
   18 FORMAT(16A5)
 20   FORMAT(22H1ANALYSIS OF FOIL DATA)
 22   FORMAT(15H0NO FOILS GIVEN)
 24   FORMAT(24H0FOILS ADDED EXCEED 1000)
 26   FORMAT(21H0FOIL WEIGHTS CHANGED/4(4X,1HI,12X,2HWT))
 28   FORMAT(4(I5,F10.5))
 30   FORMAT(4(I5,1PE14.5))
  999 RETURN
      END
```

```
*      LIST8
*      LABEL
CPRN-1D
*      SYMBOL TABLE
C    PROGRAM PRINTS OUT AN ARRAY
       SUBROUTINE PRNTO(FW,NMAX,ADENT)
       DIMENSION FW(1000),WORD(4),IWD(4),ADENT(96)
       J=1
  200  IF(NMAX-J*200)204,204,202
  202  J=J+1
       GO TO 200
  204  NPAGE=J
       MX=NMAX-200*(NPAGE-1)
       J=1
  206  IF(MX-J*50)210,210,208
  208  J=J+1
       GO TO 206
  210  NCOLM=J
       NW=MX-50*(NCOLM-1)
C      NPAGE=NUMBER OF PAGES
C      NCOLM=NUMBER OF COLUMNS ON LAST PAGE
C      NW=NUMBER OF WORDS IN THE LAST COLUMN
       MX=0
  212  IF(NPAGE-1)230,230,214
  214  NPAGE=NPAGE-1
       PRINT 614
       PRINT 615,(ADENT(I),I=1,96)
       PRINT 616
       DO 218 M=1,50
       DO 216 J=1,4
       JX=50*(J-1)+MX+M
       WORD(J)=FW(JX)
  216  IWD(J)=JX
       PRINT 618,(IWD(J),WORD(J),J=1,4)
  218  CONTINUE
       MX=MX+200
       GO TO 212
  230  PRINT 614
       PRINT 615,(ADENT(I),I=1,96)
       PRINT 616
       DO 240 M=1,NW
       NC=NCOLM
       DO 238 J=1,NC
       JX=50*(J-1)+MX+M
       WORD(J)=FW(JX)
  238  IWD(J)=JX
       PRINT 618,(IWD(J),WORD(J),J=1,NC)
  240  CONTINUE
       NC=NCOLM-1
       IF(NC)321,321,319
  319  CONTINUE
       NW=NW+1
       IF(NW-50)10,10,20
   10  CONTINUE
       DO 242 M=NW,50
       DO 241 J=1,NC
       JX=50*(J-1)+MX+M
       WORD(J)=FW(JX)
  241  IWD(J)=JX
       PRINT 618,(IWD(J),WORD(J),J=1,NC)
  242  CONTINUE
```

```
321   CONTINUE
 20   CONTINUE
614   FORMAT(1H1,30X,12HFOIL WEIGHTS)
 615 FORMAT(1HO,16A5,/,5(1X16A5,/))
616   FORMAT(1HO,19X,4(4H NO.,4X,6HWEIGHT,10X) )
618   FORMAT(20X,4(I4,F10.3,10X))
 999 RETURN
     END
```

```
*      LIST8
*      LABEL
CCAL-1D       PROGRAM BY R. SIMMS, REVISED BY W. H. BARDENNE, 9/2/63
*      SYMBOL TABLE
C          PROGRAM ANALYZES DATA FOR CONSTANT TOTAL COUNTS
       SUBROUTINE CALC
       DIMENSION WT(1000),ND(100),CT(100,24),SATCT(100,24),RELTM(100,24)
       DIMENSION DELAY(24),COUNTS(24),DIF(24),AVCT(100),MD(100)
       DIMENSION HOLR(16),ADENT(96),COF(100,11),X(100),Y(100),E(6)
       DIMENSION DIV(100),RMS(100),OMEGA(100),NCOE(100)
       DIMENSION FW(1000),WORD(4),IWD(4)
       DIMENSION AUNC(11),ACOE(11),UNC(100,11),UL(100)
       COMMON WT,ND,CT,SATCT,RELTM,DELAY,COUNTS,DIF,AVCT,MD,HOLR,ADENT
       COMMON DKAY,LMAX,NMAX,NPASS,E,NOHITS,TMCER
       READ 10, NMAX,NPASS,ROT,BG,BG1,SEPT,SLOPE,SIG,DKAY
       READ 14,TMCER,TMIRR
       READ 62,(COUNTS(I),I=1,NPASS)
       READ 62,(DELAY(I),I=1,NPASS)
       READ 12,(ND(I),I=1,NMAX)
       DO 100 J=1,NPASS
  100  READ 14,(CT(I,J),I=1,NMAX)
       READ 5001,(UL(1))
       IF(UL(1))1,1,2
     2 READ 5002,(UL(I),I=2,NMAX)
       GO TO 3
     1 DO 3 I=1,NMAX
       UL(I)=1.0
     3 CONTINUE
       READ 5001,(DIV(1))
       IF(DIV(1))4,4,5
     5 READ 5002,(DIV(I),I=2,NMAX)
       GO TO 6
     4 DO 6 I=1,NMAX
       DIV(I)=1.0
     6 CONTINUE
  5001 FORMAT(E10.5)
  5002 FORMAT(8E10.5)
C      ND IS THE NUMBER OF THE FOIL COUNTED IN THE I-TH POSITION
C      WT= FOIL WEIGHT
C      CT=COUNTING TIME
C      ROT = ROTATION TIME OF AUTOMATIC SAMPLE CHANGER
C      RELTM=RELATIVE TIME
C      SATCT=COUNTS AT TIME ZERO
C      BACKGROUND=BG+BG1*TIME    CPM
C      DEADTIME= SEPT+SLOPE*COUNTRATE
C      DELAY= DELAY TIME BETWEEN CYCLES
C      COUNTS= TOTAL NUMBER OF COUNTS FOR THE J-TH PASS
       M=0
       MM=-5
    20 PRINT 38
       PRINT 39,(HOLR(I),I=1,16)
       CALL CLOCK(2)
       M=M+6
       MM=MM+6
       IF(NPASS-M)21,21,22
    21 M=NPASS
    22 CONTINUE
       PRINT 19,(J,J=MM,M)
       DO 23 I=1,NMAX
    23 PRINT 17,I,ND(I),(CT(I,J),J=MM,M)
       IF(NPASS-M)24,24,20
```

```
  24 RS=TMCFR
     J=1
1000 DO 110 I=1,NMAX
     M=ND(I)
     IF(SIG)101,102,101
 101 WT(M)=(1.0-EXPF(-SIG*WT(M)))/SIG
 102 RELTM(I,J)=RS
     A=COUNTS(J)/CT(I,J)
     DTIME=SEPT+SLOPE*A
     BGR=BG+BG1*RELTM(I,J)
     REALK=COUNTS(J)/(1.0-DTIME*A)-BGR*CT(I,J)
     IF(DKAY)108,109,108
 108 A=EXPF(DKAY*RELTM(I,J))
     B=1.0-EXPF(-DKAY*CT(I,J))
     SATCT(I,J)=DKAY*REALK*A/(B*WT(M))
     IF(TMIRR)111,111,107
 107 SATCT(I,J)=SATCT(I,J)/(1.0-EXPF(-DKAY*TMIRR))
     GO TO 111
 109 SATCT(I,J)=REALK/WT(M)
 111 SATCT(I,J)=SATCT(I,J)*UL(I)/DIV(I)
110  RS=RELTM(I,J)+CT(I,J)+ROT
     IF(J-NPASS)112,114,114
112  RS=RS+FLOATF(NMAX)*ROT
     IF(DELAY(J))204,204,200
200  CONTINUE
     RS=RELTM(NMAX,J)+CT(NMAX,J)+DELAY(J)
204  CONTINUE
     J=J+1
     GO TO 1000
114  CONTINUE
     M=0
     MM=-2
 115 CONTINUE
     M=M+3
     MM=MM+3
     IF(NPASS-M)300,300,301
300  M=NPASS
 301 PRINT 38
     CALL CLOCK(2)
     PRINT 60,BG,BG1,SEPT,SLOPE,DKAY,SIG
     PRINT 402,(COUNTS(J),J=MM,M)
     PRINT 40
     DO 120 I=1,NMAX
     L=ND(I)
 120 PRINT 42,I,L,WT(L),(RELTM(I,J),SATCT(I,J),J=MM,M)
     IF(NPASS-M)306,306,115
 306 CONTINUE
     DEVE=0.0
     B=0.0
     DO 308 J=1,NPASS
 308 B=B+COUNTS(J)
     IF(DKAY)403,403,307
 307 CONTINUE
     M=0
     MM=-5
 304 CONTINUE
     M=M+6
     MM=MM+6
     IF(NPASS-M)309,309,310
 309 M=NPASS
 310 PRINT 38
```

```
      PRINT 39,(HOLR(I),I=1,16)
      PRINT 80,(J,J=MM,M)
      DO92I=1,NMAX
      A=0.0
      DO 90 J=MM,M
   90 A=A+SATCT(I,J)*COUNTS(J)
      A=A/B
      AVCT(I)=A
      DO 91 J=MM,M
   91 DIF(J)=SATCT(I,J)/A-1.0
      SUMSQ=0.0
      DO 411 K=MM,M
  411 SUMSQ=SUMSQ+DIF(K)*DIF(K)*COUNTS(K)
      SUMSQ=SUMSQ/(B*FLOATF(NPASS))
      SUMSQ=SQRTF(SUMSQ)
      DEVE=DEVE+SUMSQ
   92 PRINT 81,I,ND(I),A,SUMSQ,(DIF(J),J=MM,M)
      IF(NPASS-M)311,311,304
  403 DO 408 I=1,NMAX
      DO 409 J=1,NPASS
      X(J)=RELTM(I,J)
  409 Y(J)=SATCT(I,J)
      CALL LSP(X,Y,NPASS,ACOF,NCOF,ERMS,OMEG,AUNC)
  412 NCOF=NCOF+1
      DO 401 M=1,NCOF
      COF(I,M)=ACOE(M)
  401 UNC(I,M)=AUNC(M)
      P=1.0
       Q=1.0
      AVCT(I)=0.0
      T2=RELTM(NMAX,NPASS)
      T1=RELTM(1,1)
      DO 410 K=1,NCOF
      P=P*T2
      Q=Q*T1
  410 AVCT(I)=AVCT(I)+COF(I,K)*(P-Q)
      AVCT(I)=AVCT(I)/(T2-T1)
      RMS(I)=ERMS
      OMEGA(I)=OMEG
      NCOE(I)=NCOF
  408 DEVE=DEVE+RMS(I)
  404 PRINT 38
      PRINT 39,(HOLR(I),I=1,16)
      PRINT 82
   82 FORMAT(10X,10H     I  NO.,7X,14HAVERAGE CTRATE,10H RMS ERROR,5X4HNC
     1OF)
      PRINT 83,(I,ND(I),AVCT(I),RMS(I),NCOF(I),I=1,NMAX)
   83 FORMAT(100/(10X,2I5,5X,1P2E14.5,3XI3))
  311 CONTINUE
      DEVE=100.0*DEVE/FLOATF(NPASS)
      PTDEVE=100.0/SQRTF(B)
      PRINT 85,DEVE,PTDEVE
   85 FORMAT(1H0,26X38HTHE GRAND AVERAGE OF THE DEVIATIONS IS,F9.5,9H PE
     1RCENT./27X39HTHE INVERSE SQRT OF THE TOTAL COUNTS IS,F9.5,9H PERCE
     2NT.)
   10 FORMAT(2I5,7E10.5)
   12 FORMAT(14I5)
   14 FORMAT(7E10.5)
   17 FORMAT(2I5,6F14.3)
   19 FORMAT(10H0  I ND(I),6(7X,5HCT(I,I2,1H)))
   38 FORMAT(22H1ANALYSIS OF FOIL DATA)
```

```
 39 FORMAT(1H0,16A5)
 40  FORMAT(5H0    I,5H    L,9X,5HWT(L),3(10X,4HTIME,8X,6HCTRATE))
 42  FORMAT(2I5,0PF14.5,3(0PF14.2,1PE14.5))
 60  FORMAT(18H0BACKGROUND RATE = 1PE12.5,3H + 1PE12.5, 5H*TIME/
    111H DEAD TIME=1PE12.5,3H + 1PE12.5,7H*CTRATE/
    217H DECAY CONSTANT =,1PE12.5,/30H GAMMA SELF-ABSORPTION FACTOR=,1P
    3E12.5)
 62  FORMAT(7E10.5)
  80 FORMAT(10X,10H     I  NO.,7X,14HAVERAGE CTRATE,5X,9HSUMSQ**.5,5X,6(
    13X,4HDIF(I?,1H)))
 81  FORMAT(10X,2I5,5X,1PE14.5,7X,0PF9.5,5X,0P6F10.5)
402  FORMAT(24X,3(5X,9HCOUNTS = 1PE14.5))
 405 IF(NOHITS)407,407,406
 406 CALL MICRO
 407 CONTINUE
 999 RETURN
     END
```

```
*       LIST8
*       LABEL
CLSP-1D       PROGRAM BY W. H. DARDENNE, 9/2/63
*       SYMBOL TABLE
        SUBROUTINE LSP(X,Y,N,A,M,RMS,OMEG,AUNC)
        DIMENSIONOMEGA(10),AA(100,11),X(100),Y(100),SUM(21),V(11),A(11),B(
       111,12),C(100),F(11,100),CM(11,11),CX(11,11),COF(10,10),DCF(11),DSQ
       2(100),EPSA(11,10),RSQ(100),ERMS(10),AUNC(11)
        IF(N-10)2,2,3
     2  MAX=N-1
        GO TO 12
     3  MAX=10
    12  DO 200 M=1,MAX
        LS=2*M+1
        LB=M+2
        LV=M+1
        DO 5 J=2,LS
     5   SUM (J)=0.0
        SUM(1)=N
        DO 6 J=1,LV
     6  V(J)=0.0
        DO 16 I=1,N
        P=1.0
        V(1)=V(1)+Y(I)
        DO 13 J=2,LV
        P=X(I)*P
        SUM(J)=SUM(J)+P
    13  V(J)=V(J)+Y(I)*P
        DO 16 J=LB,LS
        P=X(I)*P
    16  SUM(J)=SUM(J)+P
    17  DO 20 I=1,LV
        DO 20 K=1,LV
        J=K+I
    20  B(K,I)=SUM(J-1)
        DO 22 K=1,LV
    22  B(K,LB)=V(K)
    23  DO 31 L=1,LV
        DIVB=B(L,L)
        DO 26 J=L,LB
    26  B(L,J)=B(L,J)/DIVB
        I1=L+1
        IF(I1-LB)28,33,33
    28  DO 31 I=I1,LV
        FMULTB=B(I,L)
        DO 31 J=L,LB
    31  B(I,J)=B(I,J)-B(L,J)*FMULTB
    33  A(LV)=B(LV,LB)
        I=LV
    35  SIGMA=0.0
        DO 37 J=I,LV
    37  SIGMA = SIGMA +B(I-1,J)*A(J)
        I=I-1
        A(I)=B(I,LB)-SIGMA
    40  IF(I-1)42,42,35
    42  DO 41 I=1,LV
    41  AA(I,M)=A(I)
        DO 60 K=1,N
        I=1
        FF=1.0
        F(I,K)=FF
```

```
 55 I=I+1
    FF=FF*X(K)
    F(I,K)=FF
    IF(I-M-1)55,60,60
 60 CONTINUE
    DO 70 K=1,N
    I=1
    C(K)=A(I)*F(I,K)
 65 I=I+1
    C(K)=C(K)+A(I)*F(I,K)
    IF(I-M-1)65,70,70
 70 CONTINUE
    LV=M+1
    DO85 I=1,LV
    DO85 J=1,LV
    K=1
    CM(I,J)=F(I,K)*F(J,K)
 80 K=K+1
    CM(I,J)=CM(I,J)+F(I,K)*F(J,K)
    IF(K-N)80,85,85
 85 CONTINUE
    DO 140 L=1,LV
    II=1
    I=1
103 JJ=1
    J=1
    IF(I-L)104,118,104
104 IF(J-L)105,115,105
105 IF(J-LV)110,110,117
110 COF(II,JJ)=CM(I,J)
    J=J+1
    JJ=JJ+1
    GO TO 104
115 J=J+1
    GO TO 104
117 I=I+1
    II=II+1
    IF(I-LV)103,103,120
118 I=I+1
    IF(I-LV)104,104,120
120 LVV=LV-1
    CF=1.0
    MM=XDETRMF(10,LVV,COF,CF)
    DCF(L)=CF
140 CONTINUE
    DCM=1.0
    MM=XDETRMF(11,LV,CM,DCM)
    DO 150 I=1,N
150 RSQ(I)=(C(I)-Y(I))*(C(I)-Y(I))
    I=1
    SRSQ=RSQ(I)
160 I=I+1
    SRSQ=SRSQ+RSQ(I)
    IF(I-N)160,170,170
170 W=SRSQ/(FLOATF(N-M-1)*(DCM))
    DO 180 L=1,LV
    WW=DCF(L)*W
    WW=ABSF(WW)
180 EPSA(L,M)=SQRTF(WW)
    BV=SRSQ/FLOATF(N)
    ERMS(M)=SQRTF(BV)
```

```
      OMEGA(M)=SRSQ/FLOATF(N-M-1)
  200 CONTINUE
  189 M=2
      MM=3
  191 IF(OMEGA(MM)-OMEGA(M))192,193,193
  192 M=MM
  193 MM=MM+1
      IF(MAX-MM)194,194,191
  194 CONTINUE
      OMEG=OMEGA(M)
      RMS=ERMS(M)
      MM=M+1
      DO 198 I=1,MM
      AUNC(I)=EPSA(I,M)
  198 A(I)=AA(I,M)
  201 CONTINUE
  999 RETURN
      END
```

```
*       LIST8
*       LABEL
CMIC-1D      PROGRAM BY R. SIMMS, REVISED BY W. H. DARDENNE
*       SYMBOL TABLE
        SUBROUTINE MICRO
        DIMENSION WT(1000),ND(100),CT(100,24),SATCT(100,24),RELTM(100,24)
        DIMENSION DELAY(24),COUNTS(24),DIF(24),AVCT(100),MD(100)
        DIMENSION HOLR(16),ADENT(96),COF(100,11),X(24),Y(24),F(6),UL(100)
        DIMENSION DIV(100),RMS(100),OMEGA(100)
        DIMENSION FW(1000),WORD(4),IWD(4)
        COMMON WT,ND,CT,SATCT,RELTM,DELAY,COUNTS,DIF,AVCT,MD,HOLR,ADENT
        COMMON DKAY,LMAX,NMAX,NPASS,F,NOHITS,TMCFR
        READ 10,NCARDS
C       NCARDS IS THE NUMBER OF CARDS OF CORRECTIONS TO BE READ IN
C       TMCFR IS THE TIME CORRECTION FACTOR
        PRINT 11
        PRINT 12,(ADENT(I),I=1,96)
        PRINT 13,(HOLR(I),I=1,16)
        PRINT 14,TMCFR
        PRINT 16
        DO 200 I=1,NCARDS
        READ 18,HTFR,BJOFR,NW,(MD(J),J=1,NW)
C       HTFR IS THE HEIGHT CORRECTION FACTOR
C       BJOFR IS THE J-ZERO CORRECTION FACTOR
C       NW IS THE NUMBER OF FOILS HAVING THIS SET OF CORRECTIONS
C       MD(J) IS THE COUNTING POSITION TO WHICH THE CORRECTIONS APPLY
C       MD(J) IS THE COUNTING POSITION TO WHICH THE CORRECTIONS APPLY
C       A ZERO COUNTING POSITION SKIPS A LINE
        A=HTFR*BJOFR
        DO 140 J=1,NW
        L=MD(J)
        IF(L)105,105,110
  105   PRINT 20
        GO TO 140
  110   CONTINUE
        CTRATE = A*AVCT(L)
        PRINT 22,ND(L),AVCT(L),HTFR,BJOFR,CTRATE
  140   CONTINUE
  200   CONTINUE
  10    FORMAT(I5,E10.5)
    11  FORMAT(1H1,10X,21HANALYSIS OF FOIL DATA)
    12  FORMAT(1H0,16A5,/,5(1X16A5,/))
    13  FORMAT(1H0,16A5)
  14    FORMAT(1H0,10X,30HTHE TIME CORRECTION FACTOR IS  F10.5)
  16    FORMAT(1H0,10X,8HFOIL NO.,5X18HAVERAGE COUNT RATE,5X,9HHT FACTOR,
       15X,10HJ-0 FACTOR,5X,13HCORR. CT RATE)
  20    FORMAT(1H )
  18    FORMAT(2E10.5,10I5)
  22    FORMAT(14X,I5,9X,1PE12.5,7X,0PF9.5,5X,0PF10.5,6X,1PE12.5)
   999  RETURN
        END
```

TABLE C.3

COMPUTER PROGRAM AVNDFL

```
*M2133-1657,FMS,RESULT,3,5,10000,500          W. DARDENNE      AVNDFL
*       XEQ
*       LIST8
*       LABEL
CAVNDFL
*       SYMBOL TABLE
        DIMENSION DEN(30,20),VK(20),VI(30),A1(16),A2(16),A3(16),NK(5)
        DIMENSION VL(30,6),DV(30,6),D(30,6),F(30,6)
        DIMENSION U(30),F(30),FU(30,6)
    1   FORMAT(16A5)
    2   FORMAT(16I5)
    3   FORMAT(6E12.5)
        VI(1)=0.1
        DO 4 I=2,15
        II=I-1
    4   VI(I)=VI(II)+0.1
        VI(16)=1.605
        VI(17)=1.72
        VI(18)=1.845
        VI(19)=1.98
        VI(20)=2.1225
        VI(21)=2.2775
        VI(22)=2.455
        VI(23)=2.66
        VI(24)=2.8975
        VI(25)=3.1725
        VI(26)=3.49
        VI(27)=3.855
        VI(28)=4.2725
        VI(29)=4.7575
        VI(30)=5.285
    5   READ 1,A1
        READ 2,(NK(L),L=1,5),MORE
        NT=NK(1)+NK(2)+NK(3)+NK(4)+NK(5)
        IF(NT)19,19,6
    6   READ 1,A2
        READ 3,((DEN(I,K),I=1,30),K=1,NT)
        READ 1,A3
        READ 3,(VK(K),K=1,NT)
        DO 11 I=1,30
        E(I)=0.0253*VI(I)**2
        U(I)=9.0*LOGF(10.0)-LOGF(2.53)-2.0*LOGF(VI(I))
        DO 7 L=1,6
        VL(I,L)=0.0
        DV(I,L)=0.0
    7   D (I,L)=0.0
        K1=1
        K2=NK(1)
        DO 9 L=1,5
        DO 8 K=K1,K2
        VL(I,L)=VL(I,L)+VK(K)
    8   DV(I,L)=DV(I,L)+DEN(I,K)*VK(K)
        D(I,L)=DV(I,L)/VL(I,L)
        FU(I,L)=D(I,L)*VI(I)**2
        F(I,L)=D(I,L)*VI(I)
        K1=K1+NK(L)
```

```
      LL=L+1
    9 K2=NK(LL)
      DO 10 L=1,4
      VL(I,6)=VL(I,6)+VL(I,L)
   10 DV(I,6)=DV(I,6)+DV(I,L)
      D(I,6)=DV(I,6)/VL(I,6)
      FU(I,6)=D(I,6)*VI(I)**2
   11 F(I,6)=D(I,6)*VI(I)
      PRINT 12,A1
   12 FORMAT(1H1,16A5)
      PRINT 13
   13 FORMAT(51H-VALUES OF THE SPACIALLY AVERAGED NDEN(V) OR PHI(E))
      PRINT 14
   14 FORMAT(3H0 I,3X9HNDEN(ROD),3X9HNDEN(GAP),2X10HNDEN(CLAD),3X9HNDEN(
     1MOD),2X10HNDEN(SCAT),2X10HNDEN(CELL),8X4HV(I),8X4HE(I),8X4HU(I),/)
      PRINT 15,(I,(D(I,L),L=1,6),VI(I),E(I),U(I),I=1,30)
   15 FORMAT(I3,9F12.5)
      PRINT 12,A1
      PRINT 16
   16 FORMAT(46H-VALUES OF THE SPACIALLY AVERAGED NEUTRON FLUX)
      PRINT 17
   17 FORMAT(3H0 I,3X9HFLUX(ROD),3X9HFLUX(GAP),2X10HFLUX(CLAD),3X9HFLUX(
     1MOD),2X10HFLUX(SCAT),2X10HFLUX(CELL),8X4HV(I),8X4HE(I),8X4HU(I),/)
      PRINT 15,(I,(F(I,L),L=1,6),VI(I),E(I),U(I),I=1,30)
      PRINT 12,A1
      PRINT 20
   20 FORMAT(40H-VALUES OF THE SPACIALLY AVERAGED PHI(U))
      PRINT 21
   21 FORMAT(3H0 I,3X9HPHIU(ROD),3X9HPHIU(GAP),2X10HPHIU(CLAD),3X9HPHIU(
     1MOD),2X10HPHIU(SCAT),2X10HPHIU(CELL),8X4HV(I),8X4HE(I),8X4HU(I),/)
      PRINT 15,(I,(FU(I ,L),L=1,6),VI(I),E(I),U(I),I=1,30)
      IF(MORE)19,19,18
   18 MORE=MORE-1
      GO TO 5
   19 CALL EXIT
      END
```

APPENDIX D
INPUT DATA FOR THERMOS AND GAM-I

The computer codes THERMOS and GAM-I, which were used to obtain analytical results to aid in the analysis and interpretation of the experimental data, are described and discussed in Chapter V. The input data for THERMOS for the three lattices studied during the present work and for a simulated graphite-lined cavity calculation are listed in Tables D.1 and D.2. The GAM-I input for the three lattices studied are listed in Table D.3. Three additional GAM-I calculations were made with the values of the bucklings reduced by a factor of 10^3 to simulate an infinite system. The spatially averaged asymptotic spectrum obtained from the calculations based on a critical assembly for the 1.25-inch lattice is shown in Fig. D.1.

TABLE D.1

Input Data for THERMOS Calculations of the Three Lattices Studied

1. Nuclide Concentrations:

Region	Nuclide	Concentration $(\text{barn cm})^{-1}$
a. Fuel rods (1.027 w/o U^{235})	U^{235}	0.0004976
	U^{238}	0.04735
b. Air gap	O^{16}	0.0000538
	σ_s (for N^{14})	0.00024
	$\sigma_{a,1/v}$ (for N^{14})	0.00008
c. Clad	Al^{27}	0.060275
d. Moderator (99.6 a/o D_2O)	D^2	0.06611
	H^1	0.0002655
	O^{16}	0.033188
e. Isotropic reflector	σ_s	200.0

TABLE D.1 (continued)

2. Slowing-down source data:
   a. Spatially flat source throughout cell excluding reflector.
   b. High energy scattering cross sections:

Region	Mass of Scattering Nuclide	Concentration (barn cm)$^{-1}$	Cross Section (barns)	Reduced Temperature
1) Fuel Rod	235	0.0004976	10.0	1.0
	238	0.04735	8.5	1.0
2) Air Gap	14	0.0001	9.9	1.0
	16	0.0000538	3.75	1.0
3) Clad	27	0.060275	1.4	1.0
4) Moderator	1	0.0002655	20.4	1.0
	2	0.06611	3.4	1.0
	16	0.033188	3.75	1.0

3. Arrangement (cylindrical geometry with reflecting boundary):

Region	Space Points	Thickness (cm)
a. Fuel	3	0.318
b. Air Gap	1	0.015
c. Clad	1	0.071
d. Moderator		
1) 1.25-inch lattice	6	1.262
2) 1.75-inch lattice	6	1.928
3) 2.50-inch lattice	6	2.931
e. Isotropic Reflector	5	0.01

4. All cross section data used in the thermal energy region are tabulated in BNL 5826 (H6).

5. The Nelkin kernel for bound hydrogen was used for hydrogen (N1) and the Nelkin-Honeck kernel for bound deuterium was used for deuterium (H9). The diagonal elements of these two kernels were multiplied by $(1-\bar{\mu}_o)$ where $\bar{\mu}_o$ is the average cosine of the scattering angle (B2, S1). The free gas kernel was used for all other nuclides.

TABLE D.2

Input Data for THERMOS Calculation of
Simulated Graphite-Lined Cavity

1. Nuclide Concentrations:

Region	Nuclide	Concentration $(\text{barn cm})^{-1}$
a. Cavity	O^{16}	0.0000538
	σ_s (for N^{14})	0.00024
	$\sigma_{a,1/v}$ (for N^{14})	0.00008
b. Lining	C^{12}	0.0803
c. Source	C^{12}	0.0803

2. Slowing-down source data:
   a. Spatially flat source is source region.
   b. High energy scattering cross section:

Region	Mass of Scattering Nuclide	Concentration $(\text{barn cm})^{-1}$	Cross Section (barns)	Reduced Temperature
Thermal Column	12	0.0803	4.8	1.0

3. Arrangement (cylindrical geometry with reflecting boundary):

Region	Space Points	Thickness (cm)
a. Cavity	4	10
b. Lining	10	25
c. Source	6	15

4. All cross section data used in the thermal energy region are tabulated in BNL 5826 (H6).

5. Park's graphite kernel was used for carbon. The free gas kernel was used for all other nuclides.

TABLE D.3

Input Data for GAM-I Calculations of the Three Lattices Studied

1. Description of problem:

   a. Type of solution: B_1 approximation

   b. Neutron source: U^{235} fission spectrum

   c. Broad group structure:

Group	Energy Range (ev)
1	$10^6 - 10^7$
2	$10^5 - 10^6$
3	$10^3 - 10^5$
4	$0.414 - 10^3$

   d. Nuclide flux weighting factors are tabulated in Table 5.2.1.

2. Nuclide Concentrations:

	Concentration $(\text{barn cm})^{-1}$		
a. Nuclide	1.25-Inch Lattice	1.75-Inch Lattice	2.50-Inch Lattice
H^1	0.0002499	0.0002575	0.0002616
D^2	0.06223	0.06413	0.06514
U^{235}	0.00001807	0.000009216	0.000004516
U^{238}	0.001719	0.0008769	0.0004297
O^{16}	0.03120	0.03219	0.03270
Al^{27}	0.001137	0.0005803	0.0002843

3. Resonance Data

   a. Geometry: cylinder

   b. Resonance integral parameters: $\sigma_m = 0$; $\sigma_p = 8.5$ barns; $\sigma_m(\text{eff}) =$ 29.8 barns; lumped U^{238} atom concentration $= 0.04785\,(\text{barn cm})^{-1}$; $\bar{\ell} = 0.635$ cm; temperature = 293°K.

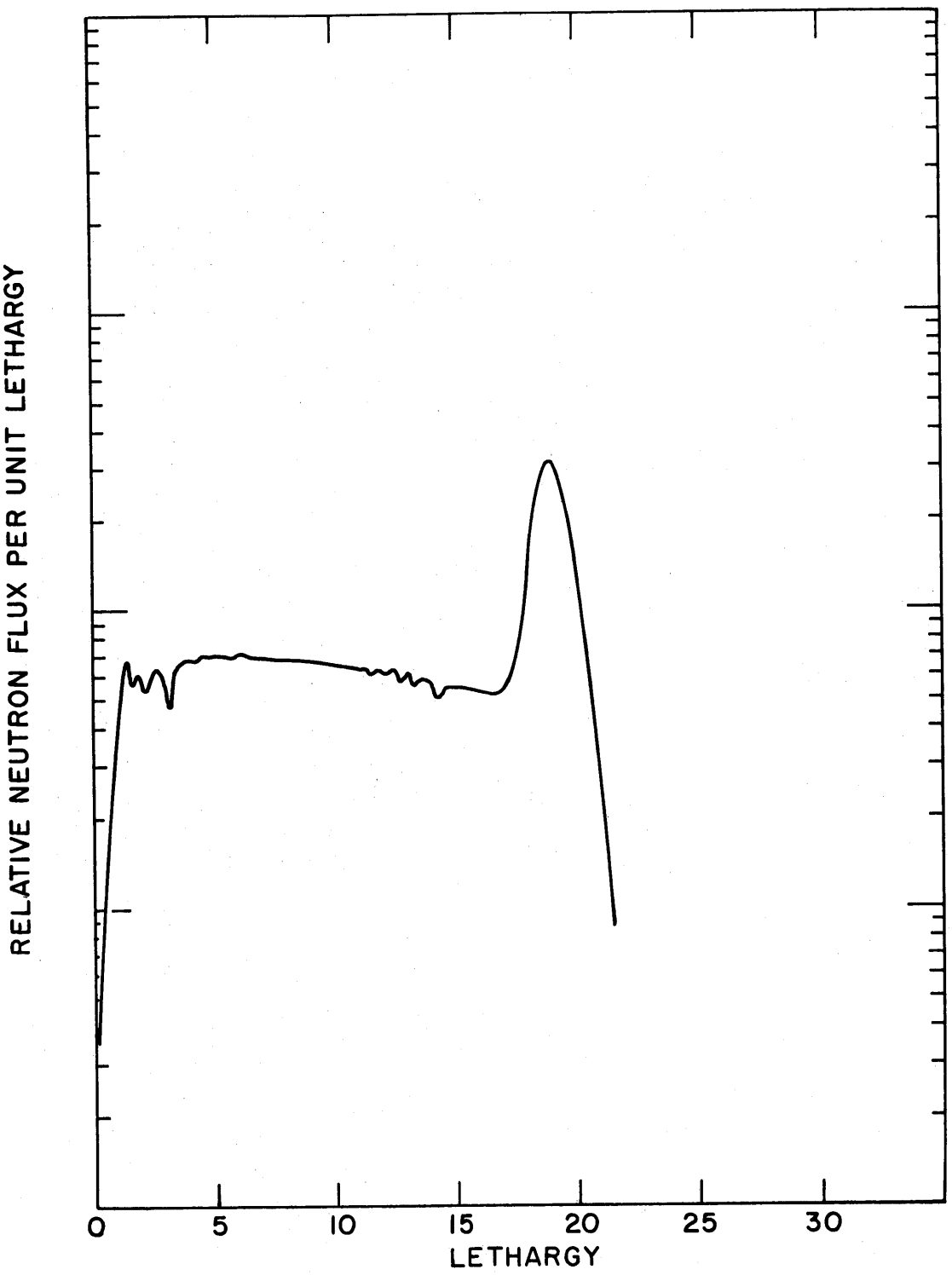

SPATIALLY AVERAGED NEUTRON FLUX SPECTRUM FOR THE 1.25 INCH LATTICE OBTAINED FROM GAM - I AND THERMOS OUTPUT

FIG. D.1

APPENDIX E

FRACTIONS OF THE ACTIVITIES OF CADMIUM-COVERED FOILS CAUSED BY FAST NEUTRON REACTIONS

Introduction

To determine the effect of the depression of the fast flux within the cadmium-covered foils on the total activities of those foils, the fraction F_N of the epicadmium Np^{239} activity and the fraction F_F of the epicadmium U^{235} fission product activity caused by fast neutron reactions were calculated. These fractions were calculated with two independent methods: the first involved the use of experimental ratios measured in the lattices studied; the second involved the use of spectrum averaged cross sections and neutron fluxes of the GAM-I output (see Chapter V). The calculation of F_N and F_F from the GAM-I output is simple and straightforward and will not be discussed further. The remainder of this appendix will be devoted to the derivation of F_N and F_F in terms of the experimental microscopic parameters.

E.1 Experimental Formulation of F_N

The fast fission factor, δ_{28}, can be expressed as follows:

$$\delta_{28} = \frac{U^{238} \text{ fission rate}}{U^{235} \text{ fission rate}} . \qquad \text{(E.1.1)}$$

The definition of α_{28} is as follows:

$$\alpha_{28} = \frac{U^{238} \text{ fast neutron capture rate}}{U^{238} \text{ fission rate}} , \qquad \text{(E.1.2)}$$

and

$$\delta_{28}\alpha_{28} = \frac{U^{238} \text{ fast capture rate}}{U^{235} \text{ fission rate}} . \qquad \text{(E.1.3)}$$

The ratios, C^* and R_{28}, can be expressed as follows:

$$\frac{1}{C^*} = \frac{\text{total } U^{235} \text{ fission rate}}{\text{total } U^{238} \text{ capture rate}}, \tag{E.1.4}$$

and

$$R_{28} = \frac{\text{total } U^{238} \text{ capture rate}}{\text{epicadmium } U^{238} \text{ capture rate}}. \tag{E.1.5}$$

Combining Eqs. E.1.3, E.1.4, and E.1.5, the result is:

$$\frac{R_{28}}{C^*}\delta_{28}\alpha_{28} = \frac{U^{238} \text{ fast neutron capture rate}}{\text{epicadmium } U^{238} \text{ capture rate}}, \tag{E.1.6}$$

which is the definition of F_N; therefore:

$$F_N = \frac{R_{28}}{C^*}\delta_{28}\alpha_{28}. \tag{E.1.7}$$

The values of F_N calculated from Eq. E.1.7 and those obtained from the output of GAM-I, which are listed in Table E.2.1, show good agreement.

E.2 Experimental Formulation of F_F

Again we start with the fast fission ratio δ_{28} (Eq. E.1.1) which we multiply by the following ratio:

$$\left(\frac{\Sigma_f^{25}}{\Sigma_f^{28}}\right)_{FAST} = \frac{U^{235} \text{ fast fission rate}}{U^{238} \text{ fission rate}}, \tag{E.2.1}$$

so that

$$\delta_{28}\left(\frac{\Sigma_f^{25}}{\Sigma_f^{28}}\right)_{FAST} = \frac{U^{235} \text{ fast fission rate}}{\text{total } U^{235} \text{ fission rate}}. \tag{E.2.2}$$

Since the ratio δ_{25} is:

$$\delta_{25} = \frac{\text{epicadmium } U^{235} \text{ fission rate}}{\text{subcadmium } U^{235} \text{ fission rate}}, \tag{E.2.3}$$

or

$$\frac{1 + \delta_{25}}{\delta_{25}} = \frac{\text{total } U^{235} \text{ fission rate}}{\text{epicadmium } U^{235} \text{ fission rate}}, \tag{E.2.4}$$

the following result is obtained:

$$\left(\frac{1+\delta_{25}}{\delta_{25}}\right)\delta_{28}\left(\frac{\Sigma_f^{25}}{\Sigma_f^{28}}\right)_{FAST} = \frac{U^{235}\text{ fast neutron fission rate}}{\text{epicadmium } U^{235}\text{ fission rate}}, \tag{E.2.5}$$

which is the definition of F_F; therefore,

$$F_F = \left(\frac{1+\delta_{25}}{\delta_{25}}\right)\delta_{28}\left(\frac{\Sigma_f^{25}}{\Sigma_f^{28}}\right)_{FAST}. \tag{E.2.6}$$

Table E.2.1 also contains values of F_F, and again the results of the analytical and experimental methods show good agreement except for the lattice with the 1.25-inch spacing. This difference is most likely due to the inability of the homogenized treatment used in GAM-I to take proper account of the effects of lumping the fuel and of the interaction of neutrons between fuel rods (see Chapter V).

TABLE E.2.1

Fractions of the Epicadmium Np^{239} and U^{235} Fission Product Activities Due to Fast Neutron Reactions

Rod Spacing (Inches)	Values of F_N		Values of F_F	
	From (a) Eq. E.1.7	From GAM-I Output	From (a) Eq. E.2.6	From GAM-I Output
1.25	0.007	0.006	0.015	0.010
1.75	0.011	0.010	0.020	0.019
2.50	0.018	0.018	0.029	0.030

(a) α_{28} and $\left(\Sigma_f^{25}/\Sigma_f^{28}\right)_{FAST}$ were calculated with the use of cross sections from the GAM-I output averaged above 1 Mev. For all three lattices, $\alpha_{28} = 0.093$ and $\left(\Sigma_f^{25}/\Sigma_f^{28}\right)_{FAST} = 0.029$.